BOSTON UNIVERSITY

GRADUATE SCHOOL OF ARTS AND SCIENCES

Dissertation

MECHANISM OF ELECTRON CAPTURE DISSOCIATION AND THE APPLICATION TO THE DIFFERENTIATION OF ISOASPARTIC AND ASPARTIC ACID RESIDUES

by

JASON JOSHUA COURNOYER

B.S., University of Rhode Island, 1996

Submitted in partial fulfillment of the

requirements for the degree of

Doctor of Philosophy

2008

Approved by

First Reader

Peter B. O'Connor, Ph.D.
Associate Professor of Biochemistry

Second Reader

Thomas Tullius, Ph.D.
Professor of Chemistry

MECHANISM OF ELECTRON CAPTURE DISSOCIATION AND THE APPLICATION TO THE DIFFERENTIATION OF ISOASPARTIC AND ASPARTIC ACID RESIDUES

(Order No.)

JASON JOSHUA COURNOYER

Boston University Graduate School of Arts and Sciences, 2008

Major Professor: Peter B. O'Connor, Associate Professor of Biochemistry

ABSTRACT

Electron Capture Dissociation (ECD) is the fragmentation of multiply protonated polypeptides caused by their reaction with electrons inside a mass spectrometer. An important hallmark of ECD compared to other dissociation techniques is the initiation of radical rearrangements that cause unique fragments. The dissociation mechanism of ECD has not been clearly established since many fragments observed cannot be accounted for by one mechanism. Another mechanism, the free radical cascade, proposes that after the initial capture, the deposited radical can migrate throughout the polypeptide via H· abstraction at C_α sites while causing additional rearrangements that generate fragments. To test this hypothesis, ECD was performed on several modified peptides. The data show that a long-lived radical intermediate exists after the initial electron capture that is composed of fragments held together by hydrogen bonding. This intermediate exists long enough for radical migration to occur and cause additional cleavages thus supporting the presence of a free radical cascade mechanism in ECD. In addition, an example of unique fragments from the ECD of peptides occurs with isoaspartic acid, which shows diagnostic fragments not found in the spectrum for the aspartyl counterpart. Deamidation of asparagine residues to a mixture of isoaspartyl and aspartyl residues is an important spontaneous modification of proteins. Isoaspartyl residues are believed to advance the inactivation, aggregation, and aging of proteins in tissue because the backbone is lengthened, and the side

chain shortened, by one methylene unit. ECD of deamidated peptides generates fragments corresponding to the loss of the aspartyl side chain from the reduced molecular ion, the aspartyl diagnostic ion, while the fragments resulting from cleavage of the C_α-C_β bond (part of the backbone for isoaspartyl residues) results in characteristic N- and C-terminal fragments indicative of the presence of isoaspartyl residues. Furthermore, the relative abundance of the two forms can be estimated by the abundance of the isoaspartyl diagnostic ions without the need for prior separation. Finally, the dissimilarity in the gas-phase structure of aspartyl and isoaspartyl peptides is determined by ECD, which shows that the shortening of the side chain affects the higher-order structure more so than the lengthening of the backbone.

Contents

List of Tables

List of Figures

List of Abbreviations

Aβ	.....	β Amyloid
AB	.....	Ammonium Bicarbonate
AdoMet	.....	S-adenosyl-L-methionine
AD	.....	Alzheimer's Disease
AH	.....	Ammonium Hydroxide
Asp	.....	Aspartic Acid
BIRD	.....	Black-Body Infrared Radiative Dissociation
CAD	.....	Collisionally Acivated Dissociation
C_α	.....	α-carbon
C_β	.....	β-carbon
D	.....	deuterium
Da	.....	Dalton
D_α	.....	Aspartic acid
D_β	.....	Isoaspartic Acid
DC	.....	Direct Current
DCM	.....	dichloromethane
DHB	.....	2,5–Dihydroxy Benzoic Acid
DMF	.....	Dimethylformamide
DR	.....	Double Resonance
ECD	.....	Electron Capture Dissociation
EE	.....	Even Electron
EI	.....	Electron Impact Ionization
ESI	.....	Electrospray Ionization
ETD	.....	Electron Transfer Dissociation
FAB	.....	Fast Atom Bombardment
FDA	.....	Food and Drug Administration
FMOC	.....	N-α-(9-fluorenylmethoxycarbonyl)
FT	.....	Fourier Transform
G_{2d}	.....	Double Deuterated Glycine
HBTU	.....	*O*-(benzotriazol-1-yl)-*N,N,N,N'*-tetramethyluronium hexafluorophosphate
H·	.....	Hydrogen Atom
HECD	.....	Hot Electron Capture Dissociation

HPLC	.....	High Performance Liquid Chromatography
ICR	.....	Ion Cyclotron Resonance
IEF	.....	Isoelectric Focusing
IR	.....	Infrared
IRMPD	.....	Infrared Multiphoton Dissociation
isoAsp	.....	Isoaspartic Acid
KI	.....	Kinetic Isotope Effect
LC	.....	Liquid Chromatography
LCMS	.....	Liquid Chromatography-Mass Spctrometry
M	.....	Molecular Mass
MS/MS	.....	Fragmentation
OE	.....	Odd Electron
PA	.....	Protective Antigen
PIMT	.....	Protein L-isoaspartyl-*O*-methyltransferase
qQq	.....	Transfer/Isolation/Trapping quadrupoles
RF	.....	Radio Frequency
rPA	.....	Recombinant Protective Antigen
RP	.....	Reversed Phase
SDS–PAGE	.....	Sodium Dodecyl Sulfate Polyacrylamide Gel Electrophoresis
SORI	.....	Sustained Off-Resonance Irradiation
SWIFT	.....	Stored Waveform Inverse Fourier Transform
TFA	.....	Trifluoroacetic Acid
TOF	.....	Time-of-Flight
UV	.....	Ultraviolet
V_{p-p}	.....	Peak-to-Peak Voltage

Chapter 1

Introduction

1.1 Introduction to the Study of Protein and Peptide Deamidation by Mass Spectrometry

Discerning the structure of proteins and peptides helps us to learn the role of these important biomolecules in the functioning of living organisms. An important result that is born from this knowledge is the understanding of the origin of the diseases that affect our everyday lives. Therefore, it becomes increasingly important for the science community to have the tools necessary to perform the structural analysis of these molecules, so that we can not only understand the pathogenesis of diseases, but to curb it within our generation. Mass spectrometry (MS) is growing into an important tool for this task because it can be used to determine the structure of proteins and peptides quickly and accurately.

MS is an analytical tool used to measure the mass of a molecule. Once used primarily to study small molecules, it is now used to study the structures of large molecules due to the advancement of the instrumentation. Determining the structure of large biomolecules relies on their fragmentation; dissociation of the large molecule into smaller units followed by systematic reconstruction gives us a better understanding of how the intact molecule is arranged. By performing such experiments, subtleties in structure can be discovered that may lead to an understanding about the function of a protein. For example, the structure of a protein at different stages of a disease changes, and MS can be used to quickly and unambiguously identify the transformation. By accelerating research in this way, MS has become an important tool in laboratories where there lies a need for understanding of structure of important biomolecules.

The focus of this thesis is the use of electron capture dissociation (ECD),[1] a fragmentation technique used in MS, to understand protein deamidation, a process believed to be one way in which a protein ages.[2–5] This chapter is divided into two sections; introduction to both MS (section 1.2) and protein deamidation (section 1.3). The first part discusses the many types of

mass spectrometers and the fragmentation techniques that can be used for structural analysis concluding with a detailed description of the actual mass spectrometer used for experiments in the proceeding chapters. The second part is a description of deamidation and the analytical techniques that can be used to study the process.

1.2 Introduction to MS

As described previously, MS is a analytical tool used to measure the mass of molecules and/or fragments thereof. There are three important components of a mass spectrometer: the ionization source, the mass analyzer and the fragmentation technique implemented. Different combinations of the three components can be combined to obtain an instrument tailored for a certain analysis. However, some components are not compatible with others, and so there are some limitations. The following discussion concludes with a detailed description of the instrument used for the experiments performed and described in the proceeding chapters.

1.2.1 Ionization Techniques

In order for the mass of a species to be measured it must be

1. ionized, either positively or negatively, and
2. vaporized,

because the weight is determined based on its mass-to-charge ratio, m/z, and trajectory in a electric and/or magnetic field within a vacuum. Several methods exist to obtain the gas-phase molecular ions and can be divided into two groups, classical and "soft" ionization methods.

The classical method refers to electron impact (EI) ionization in which molecules to be analyzed are heated and ionized with high energy electrons ($\sim$70 keV).[6,7] Bombardment causes electron stripping thus ionizing the analyte;

$$M + e^- \rightarrow M^{+\cdot} + 2e^- \tag{1.1}$$

but also causes extensive fragmentation of the molecule which can be useful for structural analysis. EI was the first ionization method for MS and is useful for non-polar, volatile molecules.

The increase in demand to analyze non-volatile molecules, such as peptides, proteins and other large molecules, helped to spawn the invention of "soft" ionization techniques that are commonly used today. These methods satisfy the two conditions mentioned previously but also allow non-volatile molecules to be analyzed, molecules that previously were unable to be analyzed by EI. In some "soft" ionization methods, such as fast atom bombardment (FAB)[8,9] and electrospray ionization (ESI) (*vide infra*),[10] analytes are ionized by charge transfer from the matrix or solution that the analyte is suspended or dissolved in, respectively. Analytes undergo either protonation (acidic modifier) or de-protonation (basic modifier) to generate the molecular ions

$$M + nAH \rightarrow (M + nH)^{n+} + nA^{-} \tag{1.2}$$

$$M + nB^{-} \rightarrow (M - nH)^{n-} + nBH \tag{1.3}$$

respectively, where n is the the number of protons (1.0072 Da), A and B represent the acid and basic modifiers and M is the species to be studied. In matrix-assisted laser desorption/ionization (MALDI),[11] the ionization mechanism is not clearly understood although the protonated/deprotonated species is detected suggesting charge transfer as the underlying method. All three methods deliver ions to the gas-phase differently, each possessing a different advantage depending on the type of analysis required, and have revolutionized the analysis of peptides and proteins by MS.

Fast Atom Bombardment (FAB)

FAB is an ionization technique wherein an ionized analyte in a matrix solution is vaporized using a high energy beam (*e.g.* ∼8 keV) of neutral atoms (*e.g.* Ar, Cs or Xe).[9,12] Samples are dissolved in a liquid matrix of low volatility (*e.g.* glycerol) that can be modified to promote ionization (*e.g.* addition of an acid or base) of the analyte. The sample matrix (∼300:1, matrix to sample) is applied to a target that is placed in a vacuum chamber and subsequently bombarded with a high-energy atom beam. Bombardment releases ionized analytes from the surface of the matrix solution that are then introduced into the mass analyzer via an applied electric field. The low-volatility requirement for the matrix allows constant recycling of the analyte to the surface of the liquid, thus supplying a constant reservoir of the ionized analyte.

A limitation to the technique is that analytes experience a low signal-to-noise ratio due charge suppression from ionized matrix clusters.

FAB revolutionized the analysis of non-volatile analytes and was the first ionization technique to ionize, fragment and determine the sequence of a peptide. In 1986, Bieman was the first to use FAB in conjunction with CAD (collisionally acivated dissociation, section 1.2.3) to sequence peptides up to 25 residues in length.[13] However, the advent of new ionization methods (*e.g.* MALDI (section 1.2.1 and ESI (section 1.2.1)) allowed scientists to surpass FAB in terms of signal-to-noise ratio and ease of sample delivery, but the technique is still an important stepping stone for the advancement of the structural analysis of biological molecules by MS.

Matrix-Assisted Laser Desorption Ionization (MALDI)

MALDI employs a pulsed laser to desorb analyte ions, initially part of a crystalline mixture of a laser absorbing matrix, which are then introduced into a mass analyzer. The technique was first used in 1987 to ionize proteins from a crystalline nicotinic acid matrix mixture using a neodymium-yttrium aluminum garnet laser (4^{th} harmonic, 266 nm) as the radiation source.[11] The function of the matrix is to be an intermediate in the energy transfer between the laser and analyte. The matrix is typically a compound that readily absorbs laser radiation (aromatic structure), contains a functional group that is a proton donor (*e.g.* carboxylic acid) and has similar solubility characteristics of the analyte to be analyzed; examples of MALDI matrices include 2,5–dihydroxy benzoic acid (DHB)[14] and cinnamic acid.[15] A mixture of the analyte and matrix are dissolved in an acidified solution of organic solvent and water and an aliquot is allowed to dry on a steel target plate which is then placed in a vacuum. The exact mechanism of ionization by MALDI is not thoroughly understood but is hypothesized to be process where (1) laser absorption and excitation of the matrix promotes vaporization of the sample to form a gaseous mixture of ionized matrix and neutral analyte (2) followed by proton transfer that results in an ionized analyte. The ion is then accelerated due to a voltage gradient created by an applied voltage to the steel target plate and entrance lens to the mass analyzer.

MALDI typically generates singly charged species (equation 1.2, where n = 1) as opposed to ESI which often generates multiply charged ion (depending on the number of available ionization sites). This feature simplifies the mass spectrum since the process of charge state deconvolution

is unnecessary. The misnamed "deconvolution" process is the mathematical transformation of a n+ to a 1+ charge state distribution so that the actual mass, and possibly identity, can be determined. However, the phenomenon often limits the ability for thorough amino acid sequencing since only one charge is available for carrying charge, and, ultimately, detection.

Electrospray Ionization (ESI)

ESI facilitates the transition of molecules from the solution to the gas-phase so that their masses can be measured inside a mass spectrometer, a technique for which the inventor John Fenn was awarded the Nobel Prize in Chemistry in 2002.[10] Analytes to be mass analyzed are typically dissolved in a solution that allows solvation but that is also easily vaporized (*e.g.* 50:50 acetonitrile:water). A small percentage of acid (∼1%, depending on the pK_a of the acid) is often also added to promote ionization of the solution (equation 1.2). The solution is loaded into a glass capillary (μm outlet diameter) and high voltage is applied to the solution ($\sim$ 1–2 kV) via an electrode that is inserted into the solution. If used in conjunction with the outlet of a liquid chromatograph (LC) system, the effluent flows over the electrode at a flow rate in the range of $\sim$ μL/min. An ion spray is produced when a counter electrode, typically the orifice leading to the vacuum system of the mass spectrometer, is held at a much lower voltage (∼50–100 V) thus creating an electric field that draws positively charged droplets from the surface of the spray tip. A gas stream is often used to aid the evaporation of the droplets. The diameter of evaporating droplet decreases thus increasing the charge density within the droplet until repulsive Coulombic forces between the charges outweigh the surface tension sustaining the droplet, *i.e.* the Rayleigh limit.[16] At this point, a "Coulombic explosion" occurs generating daughter droplets. The process continues until the potential field causes ions to desorb from the droplet surface, which are then transported to the mass analyzer via the potential and vacuum gradient inside the mass spectrometer. It should be noted that when the solution originates from a chromatography system, a heated gas stream is often used to aid evaporation of the liquid. Finally, to analyze negatively charged molecules, the polarities of the potentials applied are switched and a basic modifier (equation 1.3) is added to the solution to enhance the presence of negatively charged analytes in the solution.

ESI is often used to study peptides and proteins because they are very soluble in solvent

systems normally used and generate multiply-charged species due to their polyampholytic nature. Fragmentation of multiply-charged ions is useful for amino acid sequencing because, due to Coulombic repulsion, the charge tends to be uniformly distributed throughout the molecule, increasing the probability for detection of individual fragments. Ionized species frequently exist in a distribution of charge states (*e.g.* $(M+H)^+$, $(M+2H)^{2+}$ and $(M+3H)^{3+}$) which complicates the mass spectrum and requires the extra step of charge state deconvolution to determine the mass of the species

1.2.2 Types of Mass Analyzers

Once ions are generated, their *m/z* value is measured based on the trajectory of the ion in a electric and/or magnetic field. The trajectory can be oscillating when RF fields are used to manipulate the ions or direct when ions travel through an applied electric field. Complex vacuum systems enable mass analyzers to operate at very low pressures, thus limiting collisions with background gases that would otherwise dampen ion transmission. The differences between the mass analyzers include mass resolving power (calculated by $\Delta M/M$ where M is mass in terms of *m/z*), the types of fragmentation techniques that can be implemented, ease of use, and cost of the system.

Quadrupole Mass Analyzer

The quadrupole mass analyzer consists of four symmetrically arranged, parallel rods that allow ions with specific *m/z* values to pass through the central region based on an applied direct current (DC)/radio frequency (RF) to the rods.[6,7] Opposing rods are electrically connected and RF components on the two sets of rods are out of phase with one another. At a specific time, the electric field potential experienced by the ion beam is

$$\Phi = [U + V\cos(\omega t)]\,\frac{x^2 - y^2}{2r_0^2} \tag{1.4}$$

where U is the applied DC potential, V is the magnitude of the applied RF with angular frequency ω, x and y are the distances along the coordinate axes and r_0 is the distance from the z axis which runs in the center and parallel to the rods.

Solution to the second-order differential Mathieu equation for x and y in terms of a quadrupole

mass analyzer gives the following two equations;

$$a = \frac{8eU}{mr_0^2\omega^2} \tag{1.5}$$

$$q = \frac{4eV}{mr_0^2\omega^2} \tag{1.6}$$

where a and q are related to the DC offset potential and the magnitude of the RF. For each mass, a bounded solution to the equations results in a stability diagram (plot of a versus q,

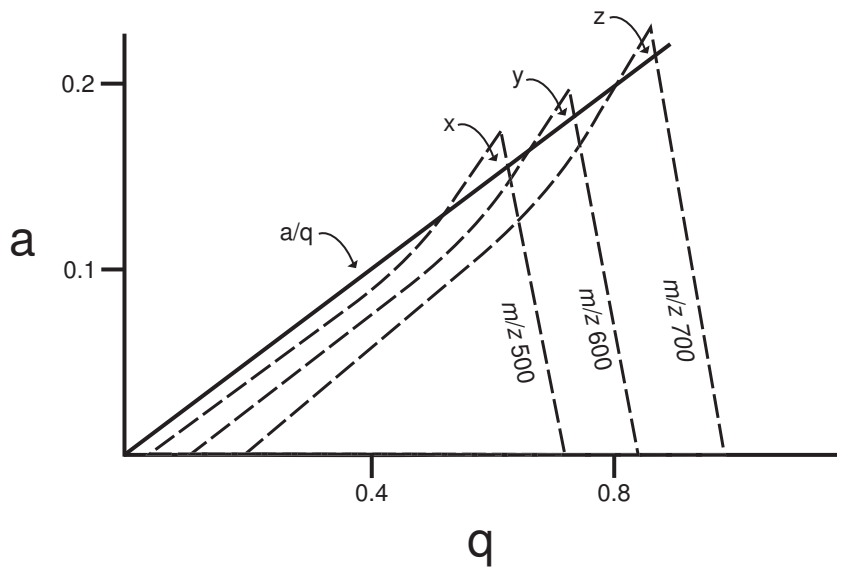

Figure 1·1: Theoretical stability diagrams (a-q plots) for three *m/z* values; bound regions (triangles) indicate regions where U and V values allow transmission of ions with *m/z* values of 500, 600 and 700. Regions x, y and z indicate stability regions (U and V values) restricted by the a/q line during a mass scan.

figure 1·1).[7,17] Therefore, specific U and V values allow ions with a certain *m/z* value to have a stable oscillation along z-axis and strike the detector. During operation, U and V values are varied (constant ω) over a range such that the ratio a/q remains constant. Such a constant a/q scan only crosses close to the vertex of the mass stability diagrams so that only a small portion of the total ions with a specific *m/z* value is transmitted. This helps improve the resolution of the transmitted ions yet decreases the sensitivity of the analysis. A mass spectrum is obtained by scanning over a range of U and V values of constant a/q values resulting in a plot of signal intensity versus a and q that can be converted to a mass-domain signal. Quadrupoles are ubiquitous mass analyzers due to their low price and ease of operation although their

inherent low sensitivity and resolution limit their use when high resolution and mass accuracy are required for analysis. A special benefit of quadrupole mass analyzers is their ability for ion isolation. This can be accomplished by adjusting the a the q values to a constant value that only allows ions with a specific *m/z* value to be transmitted to the detector. This feature is useful when the scanning quadrupole is followed by a collision cell and a subsequent mass analyzer so that isolated ions can be fragmented and their masses analyzed (MS/MS analysis, *vide infra*).

Ion Trap Mass Analyzer

The ion trap mass analyzer is three-dimensional hyperbolic extension of the quadrupole arrangement described above consisting of a ring electrode and two end-cap electrodes, thus confining ions rather than transmitting them directly to a detector.[6,7,18] The equations that govern stable oscillation of ions in an ion trap are analogous to those for quadrupole theory (1.5 and 1.6),

$$a = -\frac{16eU}{mr_0^2\omega^2} \tag{1.7}$$

$$q = -\frac{8eV}{mr_0^2\omega^2} \tag{1.8}$$

but result from derivation with respect to r_0, internal radius of the ring electrode (typically ~1 cm), and z, distance from the center of the trap to the end cap electrode, rather than than x and y for the quadrupole mass analyzer. Ions confined in the trap have stable radial and axial motion within a specific range of a and q values, and therefore U, V and ω values, thus trapping the ions.[17] In 1984 Stafford *et al.* showed that higher masses became unstable and were ejected when the amplitude of the RF was ramped low to high (*i.e.* 'mass instability mode').[19] This trend then was used to eject ions based on their unstable oscillation that then strike a detector producing a signal that changes with RF amplitude which can then be transformed to a mass spectrum. Additional improvements came about when helium gas was pulsed into the trap which helped mitigate the kinetic energy of the ions, thus driving them to the center of the trap and improving resolution and sensitivity.

The drawbacks and advantages of the ion trap mass analyzer are similar to those for a quadrupole mass analyzer, such as low resolution and low cost. However, the ion trap has

the advantage that ions can be fragmented via a gas pulse in succession; isolated ions can be fragmented and their daughter ions can be isolated and fragmented as well, and so on. This feature is described as MS^n, where n represents the number of times a resultant fragment is isolated and fragmented again. This becomes very useful for determining the structure of of complex molecules, such as peptides, but sensitivity becomes an issue as n increase since a large portion of the sample is ejected with each cycle.

Time-Of-Flight (TOF) Mass Analyzer

The time-of-flight (TOF) mass analyzer measures mass based on the flight time of an accelerated ion moving through an evacuated field-free region (drift region) to a detector.[6,7,20,21] The time it takes the ion to reach the detector is related to the mass,

$$v = \sqrt{\frac{2zeV}{m}} \tag{1.9}$$

where v is the velocity of the ion, z is the number of charges, e is the magnitude of the electric charge, V is the accelerating potential and m is the mass of the ion. Ion packets generated using an ion source are uniformly accelerated using an applied electric field and then separate in the drift region of the instrument based on their m/z value. The pressure in the drift region is in the 10^{-7} torr range so that the ions are allowed to drift with a minimum number of collisions with background gases. The time it takes to strike the detector is proportional to the mass of the individual ion thus generating a time-domain signal that can be calibrated to a mass-domain signal, or mass spectrum. Since the length of the flight region, L, remains constant, using equation 1.9, m/z can be calculated based on the flight time,

$$\frac{m}{z} = 2eV\left(\frac{t}{L}\right)^2 \tag{1.10}$$

where t is the flight time of the ion. Ion flight times typically lie in the range of 10^2 μs.

Time-lag focusing[22] and the addition of reflectrons[6] to the hardware have helped to move TOF analyzers to the forefront of structural analysis by MS. The technique of time-lag focusing facilitated the commercialization of TOF, dramatically increasing its ability to achieve high resolution. First, generated ions are allowed to convert their varying initial energy caused by ionization to spatial energy in the region just before the drift region. Then, a pulsed extraction

potential is applied that corrects for the ions' spatial diversity and drives them into the drift region with similar kinetic energies. The time lag between ionization and extraction is a critical parameter for fine tuning allowing TOF instruments to achieve high mass resolution. Also, to improve the performance of the instrument, a reflectron, or ion mirror, is used to deflect the ion beam back across the drift region, essentially doubling the path length, L. This allows ions more time to separate thus increasing resolution and increases the detectable mass range of the instrument.

Fourier Transform–Ion Cyclotron Resonance MS

First discovered by Marshall and Comisarow in the late 1960's to early 1970's, Fourier transform ion cyclotron resonance MS (FT–ICR–MS) determines the mass of trapped ions by measuring the frequency of their precession in a magnetic field (*i.e.* their cyclotron frequency).[23] Briefly, ions are trapped by an electric and magnetic field within an ICR cell in the homogeneous region of a magnetic field (figure 1·2–A).[24] Ions are excited to their particular cyclotron orbit by applying an RF to two opposed plates that are 180° out-of-phase with respect to each other (figure 1·2–B). The orbiting ions induce an alternating image charge on the remaining two plates generating a time-domain frequency signal (figure 1·2–C and –D). The spectrum is Fourier transformed to a frequency-domain spectrum (figure 1·2–E) and finally mass calibrated to produce a mass spectrum (figure 1·2–F). The advantage of FT–ICR–MS is that, once excited, ions can rotate thousands of times (∼kHz range) for several seconds which is measured constantly. This allows high precision measurements of frequencies that in turn generates high-quality mass spectra; resolving power generally reaches $\sim 10^6$. Therefore, FT–ICR–MS is mostly used for experiments that require high mass accuracy and resolution. The majority of data presented in this thesis is based on data collected from an FT–ICR–MS instrument and therefore a detailed description of the theoretical concepts of the instrumentation follows.

The Ion Cyclotron Resonance Cell. The ICR cell is a Penning trap located in the homogenous region of a strong magnetic field. The magnetic field is generated by superconducting magnets with field strengths typically ranging from 1 to 9.4 tesla. The bore of the magnet allows the insertion of the ICR cell which is suspended in a tube that is an extension of the vacuum

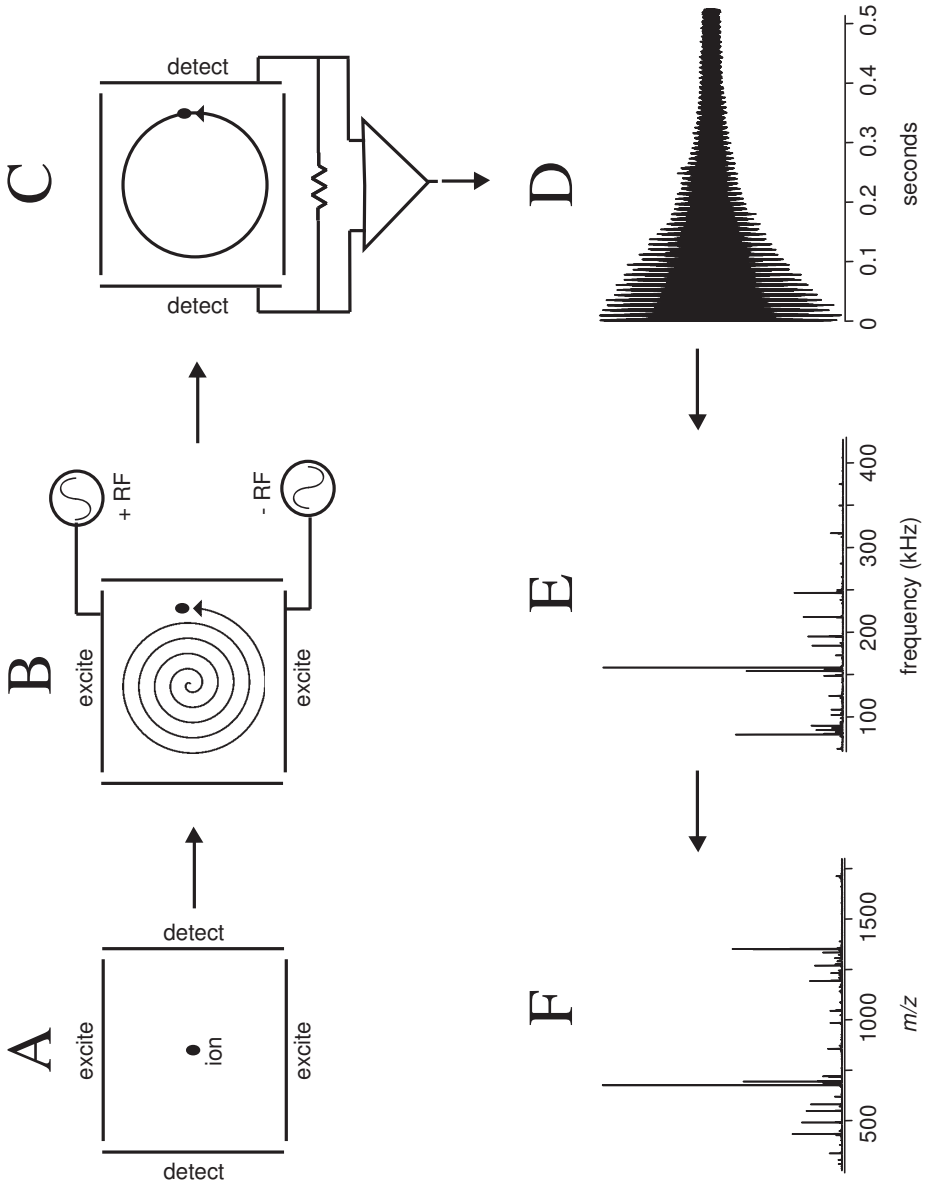

Figure 1·2: Sequence of events that takes place during a routine excite-detect cycle in an FT–ICR–MS (A–F). The ion cloud is in the center of the ICR cell (A), trapped radially by the magnetic field and in the z-direction by the electric field. Ions are excited to cyclotron orbits with enlarged radii by applying an RF to the two excite plates, 180° out of phase with each other (B). The excite event ends and the precessing ions induce a current on the two detect plates (C) . The currents are converted to voltages and differentially amplified generating a time-domain signal, or transient (D). The time-domain signal is converted to a frequency-domain spectrum (E) and calibrated to generate a mass spectrum (F).

chamber.

Several types of ICR cells exist including the cubic,[25] open-ended cubic[26], and open-ended cylindrical cells,[24] all of which consist of the basic components necessary for generating a time-domain signal; trapping, excitation and detection plates (figure 1·3). The cubic cell has the most simple configuration which is essentially a six-sided box with three sets of opposed plates used for trapping, excitation and detection that are all electrically isolated from one another (figure 1·3, top). Ions are trapped in the z-direction by applying a potential at the trapping plates and confined in the x-y plane by the magnetic field. Excitation and detection via the remaining two sets of plates (*vide infra*) occurs after trapping to generate the time-domain spectrum. The open-ended cell is different than the cubic cell such that it has two sets of four plates located on either side of the excitation/detection plates which are used to trap ions (figure 1·3, middle). The advantage of the open cell geometry is the linearization of the excitation field, optimal access for ions and the larger ion storage volume.

Linearization of the excitation field is provided by the fact that the trapping plates adjacent to excitation plates are capacitively coupled to one another.[26,27] Once the ions are trapped, the trapping potentials are lowered ($\sim$1 V) and then an RF is applied to the excitation plates. Since the plates are capacitively coupled to the adjacent plates, the ions experience an elongated, more uniformly shaped excitation field. Therefore ions with some z-motion are not ejected since fringe fields are so far removed form the center of the cell. The voltage on the coupled trapping plates (usually $\leq$1 V) helps to centralize the ions even during excitation, but must remain low to prevent space-charging that affects resolution and accuracy (*vide infra*).

A further improvement to the open-ended cell came when the shape of the plates were machined to be azimuthal so that the final arrangement of the cell is cylindrical (figure 1·3, bottom).[24] This design makes it more appropriate to fit into the bore of the magnet. Finally, trapping plates were added (no longer an 'open-ended' cell) so that ions accumulated in other regions of the instrument can be transmitted to the cell and trapped by lowering and raising voltages on one end-cap electrodes (*i.e.* gated trapping).

Ion Motion in the ICR Cell. Detection in FT–ICR–MS relies upon the phenomenon that ions in a magnetic field orbit in the plane perpendicular to the direction of the magnetic field, **B**, with

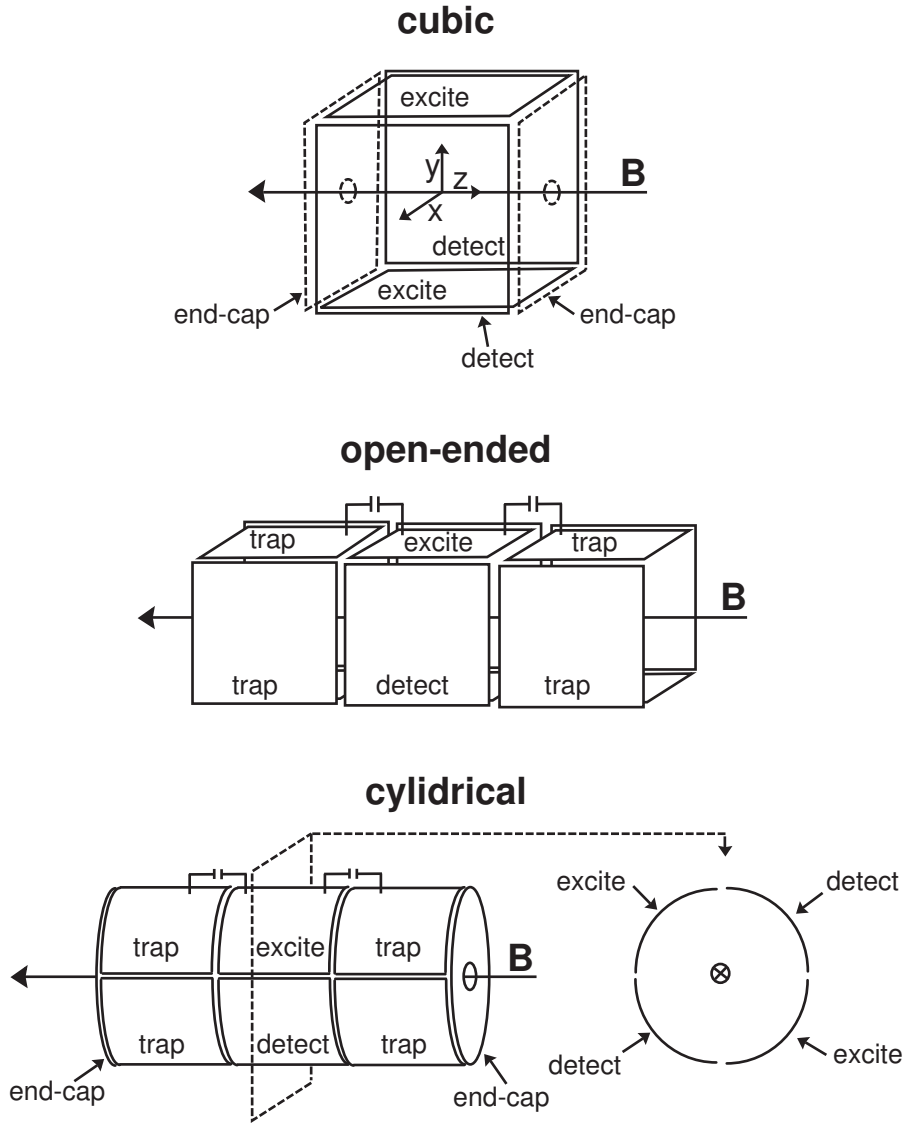

Figure 1·3: (*Top*) Cubic cell - dashed lines represent end-cap electrodes, front and back plates are detect plates, top and bottom are excite plates. (*Middle*) Open-ended cell - trap plates replace end-cap electrodes for the cubic cell and excite plates are capacitively coupled to adjacent trap plates. (*Bottom*) Cylindrical cell - similar to open-ended cell except the cylindrical shape and end-cap electrodes.

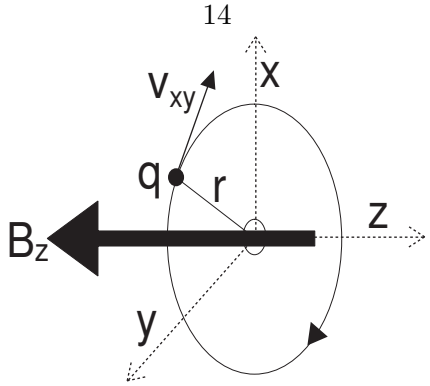

Figure 1·4: Ions undergoing cylotron motion precess with a radius r and velocity v in the x-y plane perpendicular to the magnetic field (B) or z-direction.

a mass-related frequency, or cyclotron frequency (figure 1·4).[24,28] Regarding the arrangement presented thus far, **B** is in the direction of the principal axis, z, of the ICR cell and a trapped ion with charge q, experiences an inward force, called the Lorentz force **F**, according to the equation

$$\mathbf{F} = q\mathbf{E} + q(\mathbf{v} \times \mathbf{B}) \tag{1.11}$$

where **E** is the electric field and **v** is the velocity of the ion. Ideally, ion motion is unaffected by the electric field in the center of the cell, only the magnetic field, so the equation is truncated to

$$\mathbf{F} = q(\mathbf{v} \times \mathbf{B}) \tag{1.12}$$

where **B** is the only contributing field to **F**. The inward force is in the x-y plane only since velocity from the cross product

$$\mathbf{F} = q \begin{vmatrix} \hat{i} & \hat{j} & \hat{k} \\ v_x & v_y & v_z \\ 0 & 0 & B_z \end{vmatrix} = qB_z(\hat{i}v_y - \hat{j}v_x) = qB_z v_{xy} \tag{1.13}$$

contains only x- and y-components. In order to include mass in the derivation, the general force equation in terms of mass and angular acceleration is used

$$F = ma = m\frac{v_{xy}^2}{r} \tag{1.14}$$

where where m is mass and r is the radius of the orbiting mass. Combining equation 1.13 and

1.14 gives

$$qB_z v_{xy} = m\frac{v_{xy}^2}{r} \tag{1.15}$$

and allowing ω, angular frequency, to be substituted for v/r gives

$$\omega_c = 2\pi\frac{qB_z}{m} \tag{1.16}$$

where ω_c is the cyclotron frequency for an ion of mass m in a magnetic field B_z.[24] The radius of the ions can be calculated from 1.15 giving

$$r = \frac{mv_{xy}}{qB_z} \tag{1.17}$$

where r is the radius of the cyclotron orbit.[24] For an ion with m/z of ~1000, radii range from ~0.1–0.25 mm for field strengths ranging from 9.4–3 T. Therefore, ions trapped in an ICR cell experience a precession with a small orbit of radius r with a particular frequency ω_c which is its cyclotron frequency. Next, ions must be excited to a larger radius so that its cyclotron frequency can me measured, and hence their mass.

Ion Excitation and Detection in the ICR Cell. A precessing ion is essentially a current whose frequency can be easily measured. The precessing radius becomes important because it must be large enough to be measured by the detection plates but not too large so that the ions strike the plates and are lost. To accomplish this, an RF is applied to one set of opposing plates at the center of the cell (*i.e.* excitation plates) (figure 1·2–B), each out of phase with one another generating the electric fields

$$E_1(t) = \frac{E_0}{2}(\cos\omega\mathrm{t})\hat{j} + \frac{E_0}{2}(\sin\omega\mathrm{t})\hat{i} \tag{1.18}$$

$$E_2(t) = \frac{E_0}{2}(\cos\omega\mathrm{t})\hat{j} - \frac{E_0}{2}(\sin\omega\mathrm{t})\hat{i} \tag{1.19}$$

where E_1(t) and E_2(t) are the two oscillating fields with amplitude E_0[24]. Combination of the two fields generates a linearly-polarized electric field with frequency ω. When this frequency matches, or come in 'resonance' with, the cyclotron frequency of a trapped ion, energy absorbtion occurs manifesting itself in the form of radial expansion. The enlarged radius is represented

by the equation

$$r = \frac{E_0 T}{2B_z} \tag{1.20}$$

where T (in seconds) is the length of time the resonant excitation frequency is applied.[24] The excited ion enters an orbit with radius r that is coherent with the applied oscillating excitation field (figure 1·2–C). Optimal detection of the ion is achieved when it is excited to half the radius of the ICR cell. When this is achieved, the precessing ions induce a measurable image current on the remaining two plates in the center of the cell (*i.e.* detection plates) that is converted to an alternating voltage and amplified to generate a time-domain signal (figure 1·2–D).

Generally, ions of different masses are simultaneously trapped and need to be detected. To excite all the ions, a frequency 'chirp' or 'sweep', which is a range of frequencies that includes a subset of possible cyclotron frequencies corresponding to the ions that are to be detected, is applied to the excitation plates. This excitation frequency range can also be interpreted as the 'mass range' of the experiment, since all possible ions with cyclotron frequencies in the range used should be excited and subsequently detected. The frequency sweep pulse is controlled so that the amount of time a specific frequency is applied, and its corresponding amplitude, is the same for all frequencies. Therefore, since equation 1.20 is independent of mass, all ions in terms of m/z are excited to the same radius and therefore should generate signals proportional to one another. For detection, when groups of ions with the same m/z exist in the cell and are excited, they form precessing 'ion packets' that are coherent with the applied excitation field. All of the coherently rotating ion packets, each with their own cyclotron frequency, generate a time-domain signal which is a superposition of all the precessing ion packets. This signal, also known as the transient, is Fourier transformed to a frequency-domain spectrum (figure 1·2–E) according to the equation

$$I(\omega) = 2\ re \int_0^\infty S(t) e^{\mathrm{i}\omega \mathrm{t}} \mathrm{d}t \tag{1.21}$$

where S(t) and I(ω) represent the time- and frequency-domain signals, respectively. The frequency-domain signal generated is a much more understandable summary of the detected frequencies than the time-domain signal. The frequency-domain spectrum consists of peaks corresponding to detected frequencies whose intensities correspond to the amplitude of the detected frequency, and thus is related to the number of ions in the precessing ions packets.

The theoretical cyclotron frequencies for all m/z values are known (for a specific magnetic field strength), therefore the frequency-domain spectrum can be mass calibrated to obtain the mass spectrum (figure 1·2–F) whose peak intensities are representative of distribution of the species in the analyzed sample. However, ion charge state and ionization efficiency must be taken into consideration when drawing conclusions about the distribution based on the mass spectrum. Particular to FT–ICR–MS, the charge state of an ion is proportional to the signal produced. For example, a singly charged molecule will show half the intensity of the same molecule when it is doubly charged. Also, in solution, some species are more easily charged (protonated or deprotonated) than others dependening on the pK_a of the functional groups of a molecule. Therefore, the distribution of molecules trapped in the ICR cell can be different than than those found in original sample solution.

Finally, ion excitation does not produce an everlasting signal. Loss of coherence of the oscillating ion packet causes the transient to dampen (go to zero) usually within several seconds. This occurs when the ion packets begin to disperse from cohesive groups of ions to a ring-like shape.[24] This effectively cancels out its own signal because both detection plates, which are differentially amplified, are detecting the same signal producing a net zero voltage. Loss of coherence is due to space-charge effects (*vide infra*), electric and magnetic field inhomegeneities, and collisions with background gas. Since a longer transient is important to obtaining high resolution mass spectra that is characteristic of FT–ICR–MS, several techniques can be used to mitigate loss of ion coherence, including reducing the number of ions in the cell (reduce space charge, *vide infra*), lowering the pressure (less background collisions) and changing the electric field in the ICR cell. Regarding the latter, one way is to use an electron beam that is generated down the center z-axis of the cell, passing through the orbit of the excited ions. EPIC, which stands for electron promoted ion coherence, helps to keep the ion packets in a coherent orbit so that they can be detected longer, thus improving the mass accuracy and resolution of the detected species.[29,30]

Deleterious Affects on Signal: Space Charging and Magnetron Motion. Factors that affect signal are space-charging and magnetron motion which can both can be controlled to some extent but not fully eliminated. Space-charging is a result of too many ions in the cell causing loss of peak

resolution. High ion populations result in post-excited ion packets that begin to warp in shape due to a combination of ion-ion Coulombic repulsions and affects due to the electromagnetic field.[24] The expanding ion packet results in peak broadening in the mass spectrum and therefore loss of resolution. Also, space charge can cause peak coalescence.[24,28] This occurs when two large ions packets coalesce because they have similar cyclotron frequencies (similar m/z values). Therefore, two peaks that should be separate are one peak in the mass spectrum whose mass is approximately the weighted average of the two. The most practical way to reduce space charging is to lower the ion population although increasing the magnetic field strength helps to resolve excited ion packets from one another.

Magnetron motion is an additional mode of ion motion that results from the trapping of ions in the ICR cell.[24,28] Ion motion in the z-direction is unavoidable since ions have kinetic energy from the process of being trapped and, as mentioned above, this motion can be mitigated by ramping up the trapping voltage. However, by doing so, the radial trapping field causes the ions to experience an outward force, F_r, opposite to the inward force due to cyclotron motion according to the equation

$$F_r = \frac{qV_{tr}\alpha}{a^2}r \tag{1.22}$$

where V_{tr} is the applied voltage on the trapping plates (usually ~1 V), a is the distance between the end-cap trapping plates, r is the radial position of the ion and α is a constant depending on the dimensions of the trap (*e.g.* $\alpha = \sim 2.77$ for a cubic cell).[24] The total force on the ions is due to both cyclotron motion (1.20) and from the trapping field to give

$$F_{total} = qB_z\omega r - \frac{qV_{tr}\alpha}{a^2}r \tag{1.23}$$

which is a quadratic formula with two solutions for ω, the rotational frequency of the trapped ions. These two equations for ω are

$$\omega_+ = \frac{\omega_c}{2} + \sqrt{\left(\frac{\omega_c}{2}\right)^2 - \frac{{\omega_m}^2}{2}} \tag{1.24}$$

$$\omega_- = \frac{\omega_c}{2} - \sqrt{\left(\frac{\omega_c}{2}\right)^2 - \frac{{\omega_m}^2}{2}} \tag{1.25}$$

where ω_+ and ω_- are cyclotron motion and magnetron motion, respectively, ω_c is the unper-

turbed cyclotron motion, ω_m is the frequency of the trapped ions in the z-direction. Z-axis motion ω_m is proportional to V_{tr}, so increasing the trapping potential increases ω_m and ultimately decreases ω_c. Therefore, there is a trade-off between raising the trapping plate voltages to better trap/detect the ions and perturbing the true cyclotron frequency. Although magnetron motion does distort the true cyclotron frequency, fortunately, magnetron frequency is much smaller than cyclotron motion and often remains undetected. However, an extra term that includes V_{tr} is usually added to the mass calibration equation to help correct for the affect.[31]

Ion Isolation in the ICR Cell by SWIFT. Ions of a particular *m/z* value can be isolated in the ICR cell by applying a waveform to the excitation plates, an isolation technique referred to as stored waveform inverse Fourier transform, or SWIFT.[32] The stored waveform is a frequency chirp with a sufficiently large amplitude that excites all ions out of the cell except the ions of interest. An important parameter in generating the waveform is the width of the mass window, the range of *m/z* values that includes those ions that are to be isolated. Mild excitation of the isolated ion usually occurs and increases as the window narrows around the isolated mass. This excitation may cause fragmentation, therefore careful tuning is required to properly isolate the *m/z* value of choice with minimum excitation.

1.2.3 Structural Analysis of Complex Biomolecules by MS: Fragmentation Techniques

Fragmentation in MS is the decomposition of a molecular ion so that the resulting pieces can be used to help understand the structural characteristics of the intact molecule. Fragmentation is second only in importance to measuring the mass of the intact molecule, and even more so in the case of discerning isomeric structures. Often, fragmentation techniques are referred to as 'MS/MS' methods where the first MS represents the pre-scan isolation of the parent ion and the second MS indicates mass measurement of the resultant daughter, or fragment, ions (figure 1·5).

Proteins and peptides are made of related, repeating units of small molecules with known masses called amino acid residues. Fragmentation of such structures result in pieces that are named in a systematic way based on what chemical bond is cleaved during fragmentation.

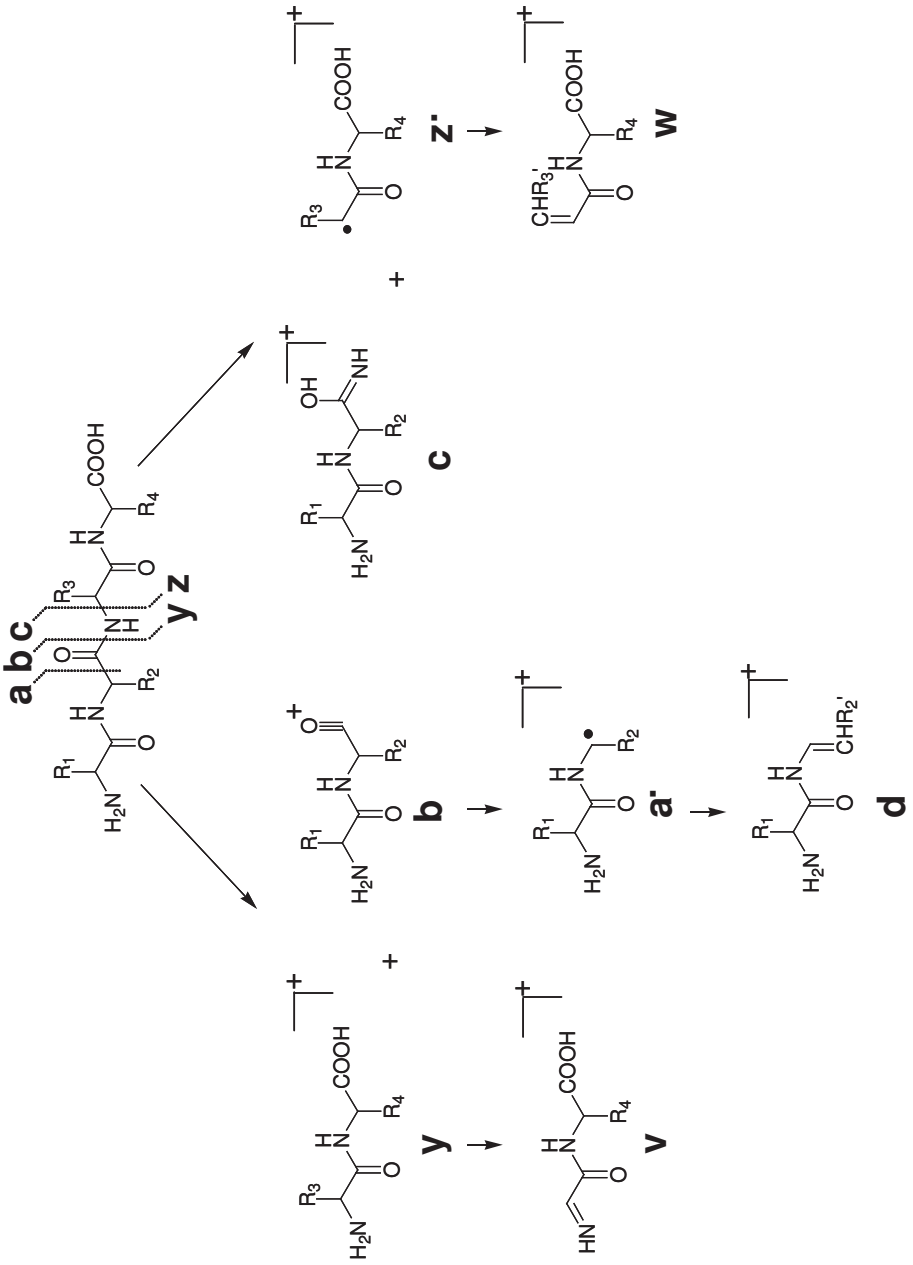

Figure 1·5: Structures of possible fragments resulting from the MS/MS of peptides and proteins. Structures represent the terminal end of the fragment chain from cleavages occurring on the C–terminal (a, b, c, d ions) side or N–terminal side (w, v, z, y ions) of a backbone bond.

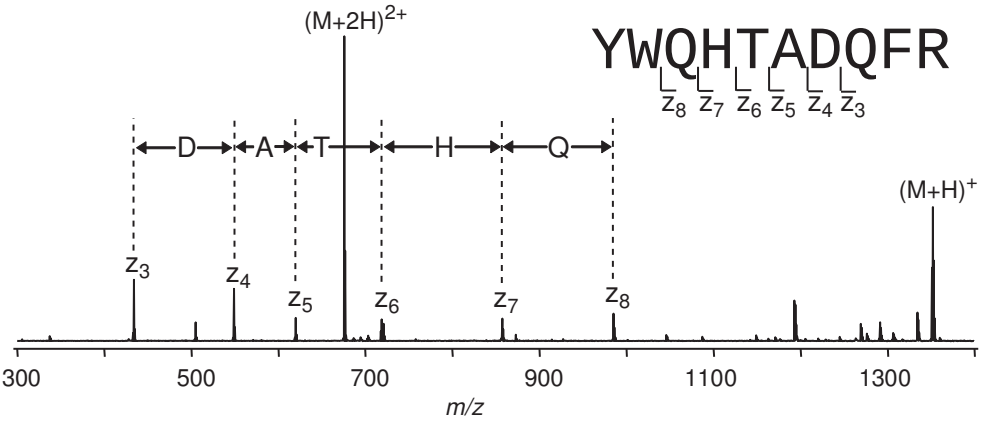

Figure 1·6: Example of sequence determination from MS/MS analysis of peptide. In this case, electron capture dissociation is used to fragment the parent ion $(M+2H)^{2+}$ at several N–C_α bonds. Mass differences between the z (C–terminal) fragment ions indicate that the peptide contains the sequence –QHTAD–.

For example, dissociation of the N–C_α bond within the peptide/protein backbone generates c– and z–type ions according to the nomenclature established in 1984 by Roepstorff (figure 1·5). [33] In this example, c and z ions contain the N– and C–terminal ends, respectively, of the dissociated peptide or protein. The subscript n is the number of the amino acid from the N–terminus for c ions and C–terminus for z ions. For example, figure 1·6 shows fragmentation of the peptide YWQHTADQFR in which several N–C_α bonds are cleaved generating a mass spectrum containing C–terminal fragment ions (z_3–z_8). The differences in masses between the fragments reveal that the peptide contains the amino acid series –QHTAD– within the sequence (in this case, the complement c ions, c_2–c_7, are not detected).

It is often important to know the sequence of the protein/peptide so that a better understanding can be made about its biological role. Typically, proteins are digested with enzymes to produces smaller peptides whose sequence can be more easily analyzed (bottom-up protein sequencing) or sometimes the intact protein can be directly fragmented and sequenced (top-down sequencing). A typical proteomics experiment involves digesting a protein into peptides using an enzyme, obtaining the fragmentation mass spectrum of the peptides and then subtracting fragment masses from one another so that the exact sequence can be determined (*de novo* sequencing, figure 1·6). However, structural discrepancies like post-translational modifications (PTMs) and three-dimensional arrangement often makes sequencing a challenge. Several methods of fragmentation exist to help navigate through the problems encountered and, often

times, the techniques provide complementary data so that a better understanding of the true structure can be made. The following sections describe several types of fragmentation methods used for the structural determination of peptides and proteins.

Collisionally Activated Dissociation (CAD)

Collisionally activated dissociation, or CAD, is the fragmentation of ions as a result of collisions with neutral gases. Early CAD techniques used high energy collisions ($\sim$ 500 eV range) between ions and gases to form fragments.[7,34] The new mass spectrometers being developed at the time could not generate the high-energy ion beam necessary for such collisions thus spawning low-energy CAD techniques (<100 eV collisions).[35–37] This energy regime is easily controlled making the technique applicable to many kinds of mass spectrometers such as triple quadrupoles and ion traps. Typical gasses used for collision (also known as 'background gas') are argon and nitrogen. Since the collision cross section increases with the radius of the interacting molecules, argon is more often used than nitrogen to enhance fragmentation.

Low-energy CAD is considered a 'slow heating' fragmentation method because ions are activated (given energy, heating via collisions) and deactivated (loose energy, cooling via collisions) simultaneously until, over time and with multiple collisions, the overall energy of the ion increases resulting in a net rise in temperature wherein dissociation occurs[37]. Excitation does not result from electronic excitation ($\sim 10^{-15}$ s) but from vibrational excitation ($\sim 10^{-6}$ s); the energy deposited on large molecules upon collision with gases excites the many degrees of vibrational freedom (3N-6 where N is the number of atoms) and increases the temperature of the target ion. The energy deposited is evenly distributed throughout the molecule so bonds with the lowest dissociation energy break first. For peptides and proteins, the amide bond dissociates first generating b_n and y_{l-n} ions (figure 1·5). The dissociation energy of the peptide bond is relatively small compared to other covalent bonds, which are typically several times stronger, and therefore dominate the CAD mass spectrum of a peptide.[35,36] Other labile bonds within peptides and proteins that dissociate easily are those involving PTMs. These include phosphorylation of the oxygen on the side chain groups of serine, threonine and tyrosine and glycosylation of side chain amide nitrogen of asparagine (*N*-glycosylation) and the side chain oxygens of serine and threonine (*O*-glycosylation). This is a general drawback to 'slow heating'

dissociation techniques since localizing PTMs at a certain residue is often important for determining the functions of a modified protein. Despite the drawbacks, CAD is the fragmentation technique of choice for the routine analysis of peptides and proteins because it is easy to use and regularly provides a thorough cleavage pattern for sequencing.

For positive mode ESI–CAD, the general mechanism of fragmentation in CAD is believed to occur via nucleophilic attack of a carbonyl oxygen of one amide group on a nearby carbonyl carbon of another amide group which is made electrophilic by protonation.[38–40] Either the amide nitrogen or the carbonyl oxygen can be protonated, although the latter is more likely because of its higher gas phase basicity. The y_{l-n} ion generated is a simple N–terminal amine while the b_n is believed to be either a acylium ion or protonated oxazolone. The possible sites of protonation along the peptide backbone account for the distribution of fragments found in the CAD spectrum of peptides.

However, an exception to this general fragmentation pathway occurs when there is an arginine residue in the peptide.[41] The high pK_a of the guanidine group of the arginine side is the most likely site of protonation in a peptide when it is positively charged. When subjected to CAD, arginine containing peptides fragment almost exclusively on the C–terminal side of acidic (*i.e.* aspartic or glutamic acid) or protonated histidine residues. Two factors are believed to contribute to this observed trend. First, the distribution of charges (protons) is skewed towards the arginine residue, leaving a dearth of protons along the peptide backbone. Second, the hydrogen of the carboxylic acid groups of acidic residues or protonated histidines are believed to be hydrogen bonded to the immediate C–terminal carbonyl oxygen. This hydrogen bond causes the carbon of the carbonyl group to be electrophilic and the most likely site for nucleophilic attack by the small population of protons remaining on the peptide. This combination makes peptide bond fragmentation competitive and therefore less diverse resulting in a large abundance of fragments from cleavage on the C–terminal side of acidic and protonated histidine residues. This can become problematic when sequencing a protein digested by trypsin since this enzyme generates peptides with C–terminal arginines.

Black-Body Infrared Radiative Dissociation (BIRD)

Similar to CAD, blackbody infrared radiative dissociation, or BIRD, is a 'slow heating' dissociation technique where ions are radiatively heated to cause fragmentation without the need for collisions with a background gas.[37,42] According to the theory of blackbody radiation, a heated object emits radiation that can be absorbed by other objects. In 1919, Perrin first postulated that molecules can undergo unimolecular dissociation via blackbody radiation absorption.[43] In the case of BIRD, the blackbody is a heated vacuum chamber that contains the trapped ions. The emitted radiation is of a large frequency range and in many directions therefore making the activation time for dissociation by BIRD quite high ($>10^1$ s)[37]; the probability of photon absorption is low. Therefore, the method is of particular use for FT–ICR–MS because ions can be trapped for long periods allowing the necessary time for radiation absorption, although the technique has also been applied to ion traps. Similar to CAD, photon absorption/emission of the ion proceeds until the distributed energy is equal to the lowest bond dissociation in the molecule resulting in fragmentation at that particular site. Therefore, for peptides[44] and proteins,[45] this is generally a backbone amide bond generating b_n and y_{l-n} ions including the loss of labile PTMs. For example, storage of the 5+ charge state of ubiquitin ($(M+5H)^{5+}$, where M is uncharged ubiquitin) for 1 minute at 417 K generated several b_n and y_{l-n} ions in an FT–ICR–MS.[45] BIRD has also been found to be useful for determining the thermodynamics of dissociation of involving noncovalent interactions between biomolecules. These types of interactions are generally weak and therefore easily probed by BIRD in the range of 20–200 °C. For example, dissociation thermodynamics and kinetics of the heme group from hemoglobin,[46] double stranded DNA,[47] and B_5 pentamers from Shiga-like toxin 1[48] have been studied by BIRD. Drawbacks to the method include long incubation time required for dissociation and the high pressures caused by having the instrument at high temperatures. However, over time, low pressures can be reached for BIRD experiments once residual gases and liquids are desorbed off the surfaces of the heated regions and pumped out via the vacuum system.

Sustained Off-Resonance Irradiated CAD (SORI–CAD)

Ions trapped in an ICR cell of an FT–MS can be fragmented by exciting the ions using an on-resonance pulse (at the cyclotron frequency of a certain *m/z*) causing the ion to undergo

collisions with a background gas that is pulsed into the instrument ($\sim 10^{-5}$ torr).[49] The kinetic energy of the ion can be calculated by rearranging equation 1.17 and substituting it into the general kinetic energy equation giving

$$kinetic\ energy = \frac{(qBr)^2}{2m} \tag{1.26}$$

where the energy is proportional to the square of the cyclotron radius. For example, an ion with $m/z = 100$ and cyclotron radius of 1 cm in a 7 T magnetic field has a kinetic energy of $\sim$2300 eV.[24] Therefore, it is easy to give the ions a large amount of translational energy for fragmentation from collisions. It is important, however, to control the energy of the ions since they can be easily be ejected from the cell. Furthermore, ions excited with an on-resonance pulse are excited away from the center of the cell and the resulting fragments are difficult to detect because location is removed from the center of the ICR cell.

These problems were addressed with the development of sustained off-resonance excitation irradiation CAD (SORI–CAD) in FT–ICR–MS.[32] In SORI–CAD ions are excited using an off-resonance pulse that causes ions to undergo acceleration and deceleration cycles while they collide with a background gas that is pulsed into the system. The advantage of SORI–CAD is that the excited ions, and their fragments, remain close to the center of the cell after the excitation pulse. Also, a lower, more controlled kinetic energy is achieved with SORI–CAD. Ions undergo many more low-energy collisions with the background gas than with on-resonance excitation resulting in fragmentation patterns similar to traditional 'slow heating' methods like CAD using triple quadrupole instruments. The magnitude of excitation is inversely proportional the difference between the applied frequency and the cyclotron frequency ($\Delta\omega$) of the target m/z. Therefore, the amplitude of the excitation pulse and $\Delta\omega$ are important parameters that control the extent of fragmentation in SORI–CAD FT–ICR–MS. Finally, both on- and off-excitation methods require the use of a gas pulse to facilitate collisions that increases the pressure inside the ICR cell. Several seconds are often needed for the pumping-out of the collision gas before the exciation/detection event so that adequate pressures are reached to obtain the high resolution and mass accuracy accompanied with FT–ICR–MS analysis.

Infrared Multi-Photon Dissociation (IRMPD)

Trapped ions can be fragmented in an FT–ICR[50,51] or ion trap[52] MS by irradiating them with ∼10 μm light via an infrared laser. Infrared multiphoton dissociation, or IRMPD, is a 'slow heating' fragmentation method similar to CAD and BIRD generating mostly b_n and y_{l-n} ions; ionized molecules absorb the low frequency radiation until the overall vibrational energy of the molecule reaches a critical energy where the weakest bonds dissociate. Dunbar *et al.* showed that ions irradiated by IR light achieve a Boltzman distribution of internal energies which can be related to temperature and varied by adjusting the intensity of the laser.[53] Therefore, most IRMPD experiments keep irradiation time constant and adjust laser intensity to achieve sufficient fragmentation. Although both methods rely on heat for dissociation, the activation energy of IRMPD ($\sim 10^{-1}$ s) can be 100 times faster than BIRD because the IR radiation is highly focused compared to black body radiation.[37] With regards to dissociation performed in an FT–ICR–MS, two advantages of IRMPD are the position of the ions after fragmentation and the pressure of the instrument. Generally, the IR laser is aligned with the center of the trap were the ion cloud resides so that, upon irradiation, fragments stay in the center of the trap for detection. Also, the pressure remains unchanged during dissociation because no collision gas is required and fragments are measured with uncompromised resolution and accuracy. The primary structure of both ubiquitin (in an FT–ICR)[51] and bee venom mellitin (in a ion trap)[54] have been analyzed by IRMPD.

Ultraviolet (UV) Photodissociation

Ultraviolet (UV) radiation can also be used to dissociate ions in MS. Implementation of the techniques is similar to IRMPD in which trapped ions (such as FT–ICR[55–58] or ion trap[59,60]) are irradiated with laser light but has also been using in other mass analyzers such as TOF.[61] However, fragmentation via electronic excitation is the basis of UV photodissociation rather than vibrational excitation. Typical wavelengths used are 193 or 157 nm resulting in cleavage of the C_α–C(O) bond of peptides and proteins generating a_n and x_{l-n} fragments ions. Formation of b_n and y_{l-n} ions have also been reported, most likely due to partial vibrational excitation during laser irradiation, as well as side chain cleavages and v– and w–type fragments.[60] In general, UV photodissociation generates a more thorough sequence coverage than CAD but

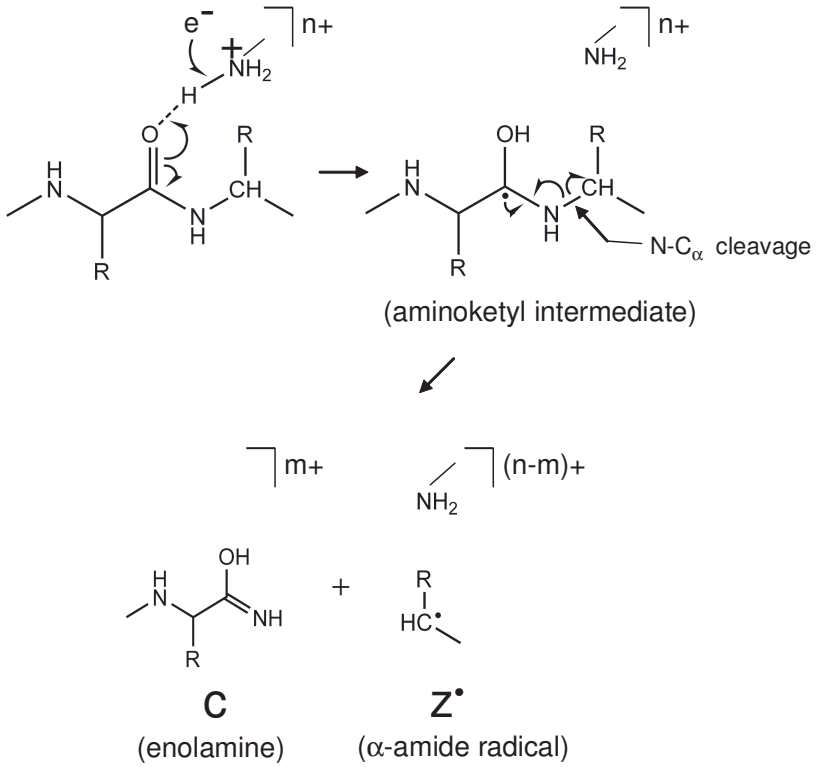

Figure 1·7: ECD fragmentation of peptide/proteins occurs at sites where protonated sites are hydrogen bonded to backbone carbonyl oxygens. Upon electron capture, H· is transferred to the carbonyl group generating a aminoketyl radical intermediate. Rearrangement causes cleavage of the N–C_α bond producing c_n and z_{l-n} fragment ions.

multiple laser pulses are necessary.[58] Despite this advantage, UV photodissociation is not used as frequently as CAD due the difficulty of implementation and optimization of the high-energy laser beam path with the ion cloud or path necessary for adequate fragmentation.

Electron Capture Dissociation (ECD)

In 1998, Zubarev *et al.* showed that gaseous proteins trapped in the cell of an FT–ICR–MS can be fragmented when irradiated with low-energy electrons (< 0.5 eV) forming c_n and z_{l-n} ions (and a_n and y_{l-n} ions but to a much smaller extent) (figure 1·7). The technique was coined electron capture dissociation, or ECD.[1] The mass of the resultant c and z ions reveal that they are even electron (EE) and odd electron (OE) species, respectively, and that the cleavage is homolytic in nature. It was proposed that the cleavage pathway occurred at sites where the protonated basic side chains are hydrogen bonded back to the peptide/protein backbone

carbonyl groups. Upon electron capture, the proton is neutralized and the hydrogen atom is transferred to the carbonyl group to form an amino-ketyl radical intermediate. Then, fast rearrangement occurs, cleaving the N–C_α bond resulting in c_n (enolamine) and $z_{l-n}\cdot$ (α-amide radical) ions. The secondary carbon is free to form a planar structure to stabilize the radical on the α-carbon of the z ion. The mechanism is believed to be non-ergodic; cleavage occurs faster than the deposited energy can be distributed throughout the molecule. It has been estimated that 5-7 eV of energy is released upon electron capture and used to cause cleavage of the N–C_α bond rather than distribute itself throughout the many vibrational modes of the target molecule.[62] This differs from the 'slow heating' methods discussed thus far in which fragments are a result of ergodic cleavages. Recently, the 'super-base' mechanism was proposed to explain the c_n and $z_{l-n}\cdot$ found in the ECD spectrum of peptides and proteins.[63] According to theoretical calculations, a protonation site in the vicinity of a backbone amide group renders it an excellent electrophile and becomes the site of electron capture. The resultant amide with delocalized radical is a super-base that can abstract a nearby by proton to a form an amino-ketyl radical intermediate that undergoes radical rearrangement cleaving the N–C_α bond resulting in c_n and $z_{l-n}\cdot$ ions. Debate continues on which mechanism is correct although the former mechanism tends to be the more accepted model for fragmentation.

ECD offers several advantages over the 'slow heating' methods of dissociation previously discussed such as beneficial cleavage patterns,[64] the preservation of PTMs[65] and noncovalent interactions,[66] and radical induced cleavages.[67] Also, there are several drawbacks including charge state restrictions, the low-efficiency of fragmentation compared to 'slow heating' techniques[64] and that ECD can only be implemented on a limited type of mass spectrometers. All these topics will be addressed below individually.

The ECD cleavage pattern. ECD generally offers a more thorough cleavage pattern that is useful for *de novo* sequencing.[64] This occurs because the probability of cleavage by ECD is less affected by the identity of amino acid residues (*e.g.* C–terminal side of acidic residues for slow-heating methods).[41] However, cleavage on the C–terminal side of proline is prohibited in ECD since cleavage of the N–C_α bond in this case is within the proline ring.

ECD and PTMs. ECD often preserves labile PTMs (*i.e* phosphorylation[68]) normally lost during 'slow heating' activation methods.[69] This occurs because of the non-ergodic nature of ECD. The energy deposited upon electron capture is not distributed mitigating vibrational excitation that would otherwise cause dissociation of labile bonds. ECD has shown the ability to localize sites of phosphorylation,[68] glycosylation,[65,70] and sulfation[71] to specific amino acids in peptides that would otherwise be lost using 'slow heating' fragmentation methods.

ECD and non-covalent interactions. Another benefit of ECD is that non-covalent interactions are retained. These interactions, such as hydrogen bonding and salt bridges, often support the higher-order structure of biomolecules.[62,66,72,73] Therefore, ECD can be used to probe the gas-phase tertiary structure of peptides and proteins, an achievement not possible with 'slow heating' methods. ECD of larger molecules, such as proteins, generates a large abundance of the reduced molecular ion ($(M+nH)^{(n-1)+\cdot}$, where n is the number of protons) that is held together by hydrogen bonding, therefore preventing the fragments from being detected. Brueker *et al.* discovered that by performing ECD and BIRD at the same time increased the number of detected c_n and $z_{l-n}\cdot$ fragments ions due to the heat-induced dissociation of the hydrogen bonding supporting the reduced molecular ion.[66] This allowed them to estimate the enthalpy of unfolding for several charge states of ubiquitin as well show some insight on the actual higher-order structure of the protein in the gas-phase.

Side chain cleavages from ECD. Since ECD is a radical mediated dissociation, other fragments in addition to c_n and $z_{l-n}\cdot$ ions can be formed that provide peptide sequence information such as side chain cleavages.[74,75] Side chain losses are detected in the region just below the mass of the reduced molecular ion as small molecule losses. For example, loss of 59.048 Da (guanidine group) from the reduced molecular ion of a peptide indicates the presence of arginine in the sequence.[74] Similar diagnostic losses can reveal the presence of lysine, histidine, aspartic acid, glutamine, asparagine and methionine.[74,75] Such losses can only reveal the presence of these amino acids and not their position in the peptide sequence but still provide a good starting point for *de novo* sequencing.

HECD and secondary fragmentation. High energy electrons (∼9 eV) (also known as hot electron

capture dissociation (HECD)) can be used to impart enough excess energy onto the primary fragment to cause them undergo additional rearrangements that result in secondary fragments.[76] The secondary fragments are typically EE w ions derived from excited z· ions and b and y ions due to energetic collisions between the high-energy electrons. a·, v and d fragment ions originating from b and y ions are also present but usually to a much lesser extent. Secondary ions are useful for sequencing and have been used to differentiate isoleucine from leucine in peptides.[77] b and y fragments are sometimes also detected in ECD spectra using low-energy electrons. They are believed to be due to the large recombination energy released between particular protonated peptides and the electron.[78] The excess energy causes vibrational excitation and cleavage of the amide bond generating b and y ions.

Free radical reaction cascade from ECD. In 2002, Leymarie *et al.* showed that ECD of three cyclic peptides initiated a free radical cascade where the radical deposited from the first electron capture undergoes more rearrangements causing additional cleavages and fragments.[67] This idea was postulated because ECD of $(M+2H)^{2+}$ (where M is the cyclic peptide) should only cause either amino acid side chain cleavages or one backbone cleavage resulting in only $(M+2H)^{+\cdot}$, which is essentially a linear peptide. As predicted, many side chain cleavages were detected but, unexpectedly, fragments were detected that were identified as portions of the cyclic peptide backbone, fragment ions that could only be generated by additional fragmentation events. However, if $(M+2H)^{2+}$ captured two electrons, no charge would remain rendering any fragments undetectable. Therefore, a secondary process, called the free radical cascade, was proposed to explain these fragments. First, the authors propose that the radical on the secondary carbon after the first electron capture can migrate along the peptide backbone via hydrogen abstraction from one C_α (secondary carbon) site to another, sites known to provide radical stability. Second, they suggest that the radical can undergo a rearrangement with neighboring regions initiating an additional cleavage that results in the fragments that were observed for the cyclic peptides. Additional experiments are underway to provide support to the free radical cascade mechanism and these experiments are the subject of chapter 2 of this dissertation.

Shortcomings of ECD. Problems encountered with ECD include the charge state restriction,

low-efficiency of fragmentation compared to 'slow heating' techniques, and that ECD can only be implemented on a limited type of mass spectrometers. First, the parent ion subjected to ECD must be at least in a 2+ charge state so that one charge remains on a fragment for detection. Peptides from proteolytic digest of a protein are usually multiply protonated although sometimes only singly protonated species of interest are detected and cannot be analyzed by ECD. This can be circumvented by digesting proteins with different types on enzymes that provide larger peptides containing the region of interest that will more likely be multiply charges during the ESI process. Furthermore, MALDI is not compatible with ECD because it only provides singly charged peptides and proteins.

ECD is typically a low-efficiency fragmentation method depending on the charge state of the species[62] and the alignment of the electron beam and ion cloud.[79] The electron capture cross section increases (and hence fragmentation efficiency) as the square of the charge of the target ion, therefore, high charge state ions are more compatible with ECD.[62] For example, ECD spectra of low charge state ions (*i.e.* 2+) are dominated by the unreacted parent ion and a small abundance of fragments. Despite the ease of capture for high-charge state ions, fragments are often held together by hydrogen bonding and remain undetected.[62,66]

Electron Transfer Dissociation (ETD)

Six years after the advent of ECD, ETD was introduced as a new way to dissociate multiply charge peptides and proteins from ESI into the homologous c– and z–type ions series fragments.[80,81] ETD is similar to ECD except that small molecule, OE anions transfer an electron to multiply charged cations to induce dissociation. The advantages of ECD also apply to fragmentation by ETD including a thorough cleavage pattern and the preservation of PTMs.[80] The technique is performed in a special linear ion trap that can simultaneously trap negative and positive ions to promote their interaction. Successful ETD depends on the anion used for electron donation, also known as the reagent ion, which must have certain properties to facilitate electron transfer.[82]

Reagent molecules, such as anthracene, are chosen based on their propensity to donate an electron versus abstracting a proton from the cation, the latter being the dominant reaction. A detailed study revealed that certain factors govern the probability of electron/proton

transfer such the electron affinity of the electron donator (must be sufficiently low) and the Franck–Codon factor between the neutral and anionic form of the reagent anion.[82] For example, azobenzene and fluoranthene have relatively low electron affinities and high Franck–Codon factors and were found to be the best electron donors compared to SF_6 and CS_2 which have opposite traits and thus promoted proton transfer.[82]

The main advantage, and also disadvantage, of ETD is that it is performed in a linear ion trap. The benefit of the linear ion trap is that it is inexpensive compared FT–ICR–MS, which requires a superconducting magnet. The drawback is the poor mass resolution associated with linear ion traps. Peptide fragmentation via electron transfer (generation of c– and z–type ions) is often very thorough producing many fragments that requires isotopic resolution so that they can be identified. Such resolution is routinely achieved with FT–ICR–MS but not linear ion traps. To help mitigate this problem, resultant ETD fragments are reacted with small gaseous molecules that promote proton transfer to reduce their charge states.[81] Reducing the charge state widens the gap betweens peaks within an isotopic cluster, diminishing the need for high resolution, and reduces the complexity of the mass spectrum by decreasing the distribution of charge states for the fragment. For example, the carboxylate anion of benzoic acid was used to reduce the charge states of fragments from ETD of histone H3 so that the N– and C–terminal regions of the protein could be sequenced.[81]

1.2.4 The ESI–qQq–FT–ICR Mass Spectrometer

The particular type of mass analyzer used for the experiments described in this thesis were performed on a home-built, hybrid ESI–qQq–FT–ICR mass spectrometer (where qQq transfer quadrupole/isolation quadrupole/trapping quadrupole).[83] The qQq region of the instrument was provided by Sciex as part of collaborative project to create the hybrid instrument. The FT–ICR–MS end of the instrument was designed and constructed at the Boston University Mass Spectrometry Resource. Software provided by Sciex (LCtune) controls the qQq portion of the instrument while Ion Spec electronics and software control the FT–ICR–MS part of the instrument, including data collection. An ESI interface at atmospheric pressure is used to produce ionized molecules that are sequentially analyzed by both a quadrupole and FT–ICR mass analyzer (figure 1·8). Briefly, ions generated at the ESI source enter the instrument

front-end where they are mass filtered and collected within the qQq region. The accumulated ions are then transferred along two sets of hexapoles to the ICR cell where their m/z values are measured. Ion transmission from the front-end to the ICR cell is facilitated by a potential gradient generated by applying deceasing voltages along the ion path. The potential gradient not only transfers ions but decreases the initial kinetic energy of the ions so that they can ultimately be trapped in the ICR cell. Also, ions are driven by the differential pumping system of the instrument that ranges from atmospheric pressure at the front-end to $\sim 10^{-10}$ in the ICR cell. Since a majority of the instrument was manufactured in the lab, each experiment requires careful tuning of the many parameters that govern ion transmission/trapping and the following section briefly describes how each region of the instrument contributes to each ESI–qQq–FT–ICR–MS experiment.

Experimental Procedure for ESI–qQq–FT–ICR MS Experiments

Ions generated by the ESI source are drawn into the orifice on the front-end of the instrument by both an applied electric field and vacuum (figure 1·8). The atmosphere/vacuum interface region of the qQq consists of several components used for the drawing in and focusing of ions into the instrument; these ion optics include the orifice plate (OR), ring (RNG) and skimmer (SK). This region is evacuated to a pressure of $\sim 10^{-3}$ torr using a turbopump backed by two rotary pumps, helping to drawn ions into the front-end. A differential electric field applied across the OR–SK region (ΔV = ~40 V) also draws the ions into the instrument while RNG is used for ion focusing. The sensitivity and fragmentation is most affected by the potential applied to SK and is often a crucial parameter for tuning. After the SK is a set of quadrupoles (*i.e.* qQq (Q0, Q1, and Q2, *vide infra*)) used for transmission and isolation that is interspersed with focusing lenses. The purpose of the first quadrupole encountered, Q0, is to focus the ions emerging from the SK region using an RF with a DC offset lower than SK. The ion beam is then focused through the lens IQ1 and past stubbies (ST), a set of mini-quadrupoles similar to Q0 in function but with a lower DC offset. The purpose of ST is to provide smooth ion transmission from Q0 to Q1 so that ions avoid fringe fields generated by the ramping DC (used to accomplish isolation) of Q1. IQ1 is also a pumping restriction providing a $\sim 10^{-5}$ vacuum past IQ1 using a turbopump and rotary pump. Ions are then mass filtered by Q1 based on

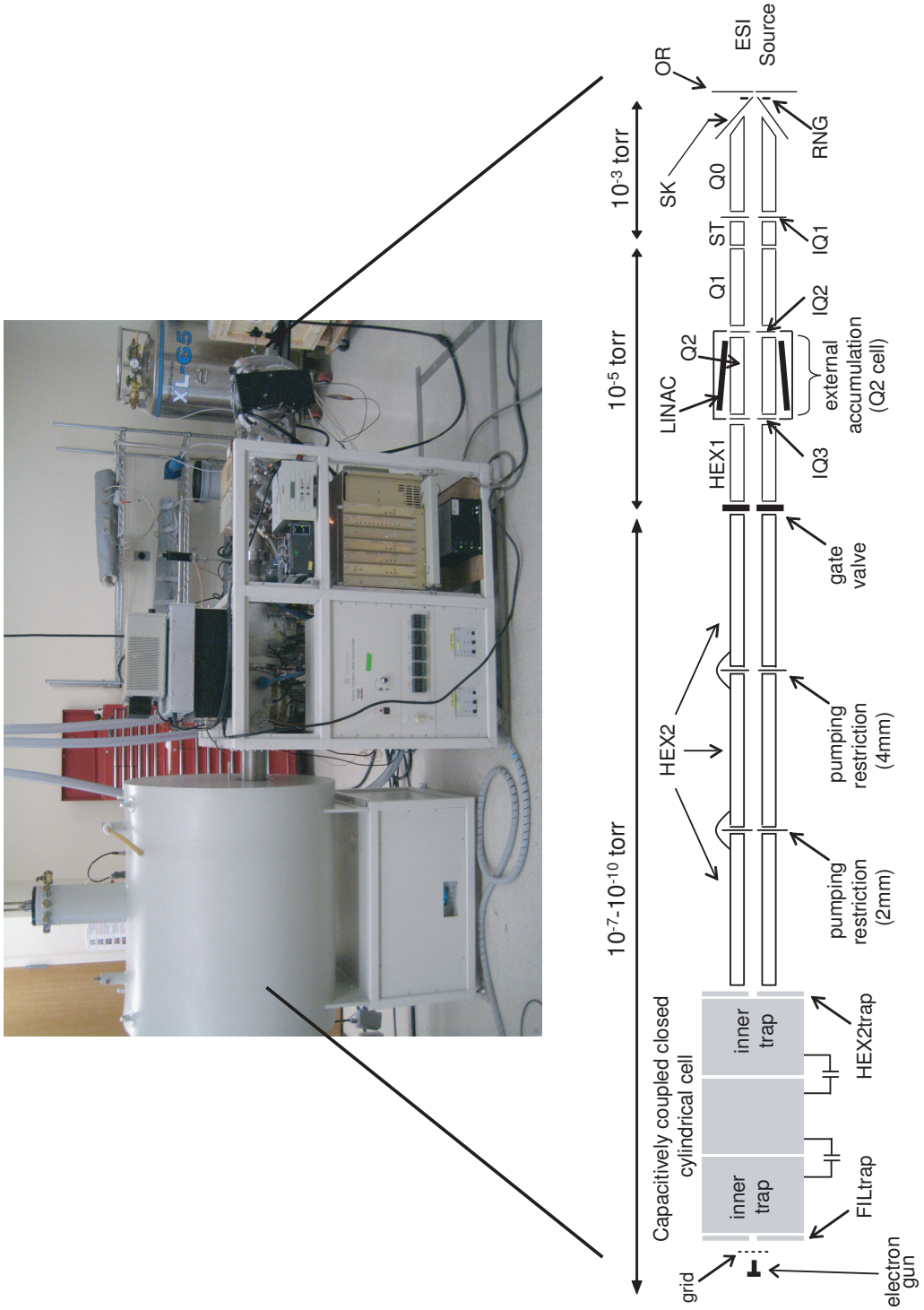

Figure 1·8: *Top* - Photo of ESI–qQq–FT–ICR–mass spectrometer scaled schematic of the major ion transmission components. *Bottom* - Detailed schematic of ion transmission components and the general pressure in their respective regions.

their m/z value and focused by IQ2 into the Q2 cell. Q2 has the function of both trapping and fragmenting ions previously selected by Q1. Ions are trapped in a potential well created by a applying a voltage to both the LINAC and IQ3 (IQ3 > IQ2). The LINAC is a set of four rods, interspersed with the Q2 quadrupoles, with a shape that produces an electric field such that the potential well is centered close to IQ3; the shape helps to prevent ions from escaping through back through IQ2 before they are transmitted. Also, the software allows the option of mildly increasing the pressure inside the cell with N_2 gas which facilitates the fragmentation of ions (*i.e.* CAD, see section 1.2.3). To accelerate the ions into the collision gas, all the offset voltage settings before IQ2 (OR, SK, RNG, Q0, IQ1, and Q1) are increased by the same amount. The difference between the original and new offset voltages are effective lab-scale energy (in eV) of the accelerated ions.

Once the desired amount of ions (fragmented or intact) are collected, IQ3 and hexapole 2 trapping plate (HEX2trap) are pulsed to negative values (HEX2trap > IQ3) to drive the ions from Q2 to the ICR cell along hexapoles 1 and 2. Ions pass along hexapole 1 through the gate valve to hexapole 2. The gate valve is used to separate the two regions of the instrument so that the front-end can be cleaned without disturbing the high vacuum region containing the ICR cell.[84] The ions are transmitted along hexapole 1 and 2 by RF and DC offsets (hexapole 1 DC > hexapole 2 DC). Hexapole 2 is a long hexapole divided into three segments by two pumping restrictions/ion lenses allowing the ICR region to reach pressures of $\sim 10^{-10}$ using two turbopumps backed by a rotary pump. The pulsing of HEX2trap and IQ3 to negative voltages occurs for ~4 ms to allow ions to reach the ICR cell which is in the homogeneous region of a 7 tesla magnetic field. Once ions are inside the cell, HEX2trap is ramped back to a positive voltage (>10 V) equal to that of the filament trapping plate (FILtrap), the other end-cap electrode of the ICR cell. A small voltage is applied (~1 V) at the inner trapping plates to create a potential well to trap the ions in the z direction while the magnetic field confines the ion cloud in the x-y direction. For excitation/detection, both the HEX2trap and FILtrap voltages are dropped to equal the inner trap voltages. The typical excitation chirp parameters are: amplitude of 60 V_{p-p} over a frequency range of ~70-400 kHz (m/z range ~250-1500) in 6 ms. Once excited, the transient is measured for times ranging from several milliseconds to a few seconds depending on the resolution desired and how long the ions remain in coherent

orbits. Ion accumulation time in Q2 and the length of time devoted to measuring the transient are the two parameters that most affect how long each experiment lasts. Typically, each scan lasts about ∼1–2 s and can be averaged over multiple scans to generate a final mass spectrum of desirable resolution and peak intensity.

ECD is the core dissociation technique for peptides in all the experiments described in this thesis. Electrons for ECD are generated using an indirectly heated cathode[85] placed outside the cell several centimeters from the the filament trapping plate (figure 1·9). A current is passed through a resistor using an external power supply heating the BaO cathode to about ∼1000 °C. At this temperature, electrons with 0 eV energy are released from the surface of the cathode (work function of the cathode). For the qQq–FT–ICR–MS, ∼8–11 W is necessary to reach the work function of the cathode; the resistor is at ∼5 V and the current is at ∼2 A on the external power supply for typical ECD experiments. The voltage bias on the gun is kept at +9 V so that the 0 eV electrons are not emitted from the surface of the cathode. In a typical ECD experiment, the multiply charged cations are trapped in the cell and the voltage bias of the gun is pulsed to a negative voltage, discharging electrons from the surface. Due to the magnetic field, the electrons beam has a diameter approximately equal to that of the cathode surface (∼0.25 cm). Also, a positive voltage is applied to a molybdenum grid placed several millimeters from the surface of the electron gun that helps to extract and focus the beam emerging from the gun. The length of the negatively-biased pulse corresponds to the electron irradiation time which can range from several to hundreds of milliseconds. The most important parameters in regards to obtaining optimal ECD fragmentation is the length and point of electron irradiation time. The length of the irradiation time should be adjusted to maximize ECD efficiency according to the equation

$$\%\ ECD = \frac{[precursor\ before\ ECD] - \sum\ [ECD fragments] - [precursor\ after\ ECD]}{[precursor\ before\ ECD]} \tag{1.27}$$

where brackets refer to the intensities of the indicated ions in the spectra. The point of irradiation time refers to the offset time between when the cations are trapped ICR cell and the ECD event. Due to magnetron motion, the ion cloud rotates in the x-y plane so the ECD irradiation event must occur at the moment that the electron beam and ion cloud overlap in the ICR cell

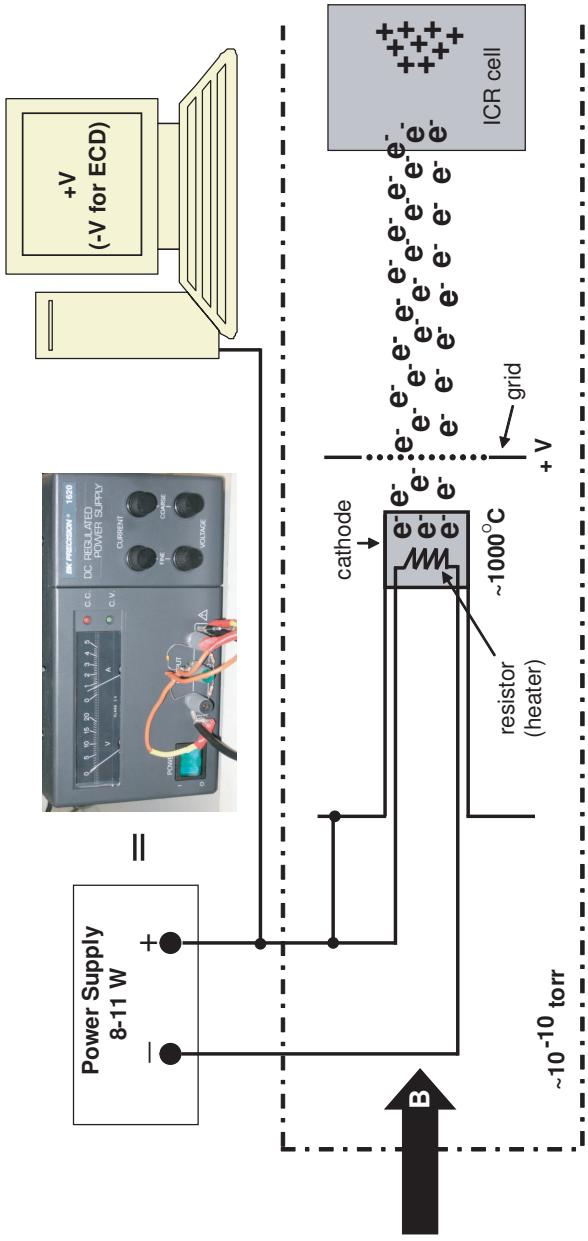

Figure 1·9: Hardware components used for ECD in the qQq–FT–ICR–MS. The cathode at the tip of the gun within the high vacuum ICR cell region is heated by an external power supply to ∼1000 °C using ∼8–11 W of power. The voltage bias is kept at a positive voltage by the computer until the ECD event wherein it is pulsed to negative voltage to emit the electron beam. The positively biased grid helps to extract the beam and focus into the ICR cell where they are captured by multiply charged cations.

('ECD resonance').[86] Magnetron frequencies were found to be ∼10 Hz for multiply protonated peptides and resonance occurs at multiples of 100 ms after the ions are trapped.

Advantages of the ESI–FT–ICR–MS Instrument

The advantage of the instrument is the routine high resolution and mass accuracy achieved in addition to the versatility of isolation methods and fragmentation techniques. Ions of certain *m/z* values can be isolated either by the Q1 or in the ICR cell by SWIFT isolation. Also, Q2 CAD, SORI-CAD, ECD, BIRD and IRMPD (and combinations thereof, IR–ECD experiments are described in chapter 6) are fragmentation techniques that can be used for the structural analysis of ionized species. The instrument is best suited for the structural analysis of complex molecules, like peptides, proteins and carbohydrates, given the multiple ways to break apart such species and having high-quality data on the resulting fragments. This allows the determination of the intact structure to be done with confidence since mass error is typically <2 ppm error of calibrated data.

1.3 Introduction to Peptide and Protein Deamidation

An important *in vivo* modification of proteins is the deamidation of asparagine and glutamine residues and isomerization of aspartyl (Asp) and glutamyl residues, through a common cyclic intermediate, to form a mixture of Asp or isoaspartyl (isoAsp) residues or glutamyl and isoglutamyl residues, respectively (figure 1·10).[2–5] Formation of the isoAsp or isoglutamyl residues is believed to be partly responsible for the inactivation, aggregation and aging of proteins in tissue because the backbone and side is lengthened and shortened, respectively, by one methylene unit (–CH_2–),[4,87–92] for isoAsp and two methylene units for isoglutamyl. Deamidation of glutamine residues is predicted to be 10-fold times slower than asparagine deamidation[93] and is therefore a more prevalent modification and will be the focus of this manuscript, although glutamine deamidation becomes important for long-lived proteins found in the lens of the eye.[94,95] In terms of analysis of deamidation by MS, the conversion of the side chain amide to acid counterparts results in a change of mass of 0.9840 Dalton (Da), a difference which, aside from isotopic interferences, can easily be distinguished in peptides and proteins by most present day mass spectrometers, but the conversion from Asp or glutamyl to isoAsp or isoglutamyl residues,

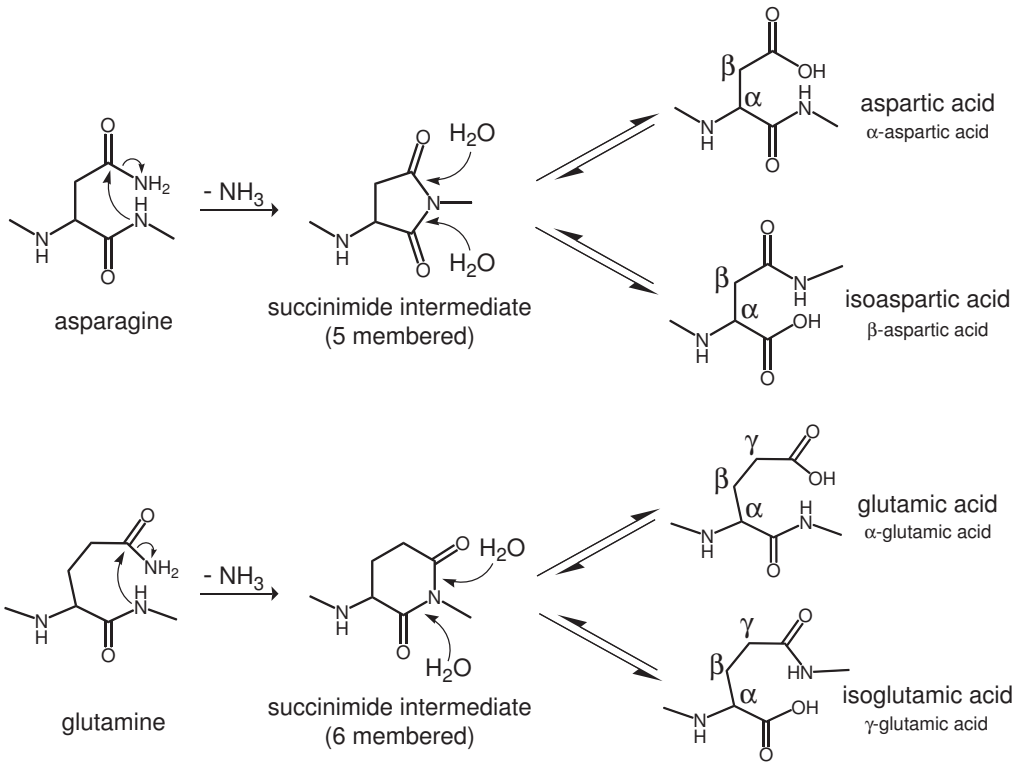

Figure 1·10: (*Top*) Isomerization of aspartic acid (α-aspartic acid) and deamidation of asparagine to isoaspartic acid (β-aspartic acid) and aspartic acid via a succinimide intermediate. (*Bottom*) Glutamine/glutamic acid can undergo a similar reaction to asparagine/aspartic acid but the intermediate is a 6-membered succinimide intermediate which is hydrolyzed to a mixture of glutamic and γ-glutamic acid.

respectively, occurs with no detectable mass change.

1.3.1 Mechanism of Deamidation in Peptides and Proteins

The common, and largely accepted, model for this non-enzymatic, post-translational modification is that it spontaneously occurs under physiological conditions through a succinimide intermediate whose rate is affected by both its amino acid sequence and three-dimensional structure.[3–5] Asparaginyl residues undergo ammonia loss (deamidation) to form the succinimide intermediate while Asp residues lose water (dehydration) to form the same intermediate at a rate approximately 40 times slower than deamidation.[96] Amino acids on the carboxyl side adjacent to either the asparaginyl or Asp residue influence the rate of succinimide formation more so than those on the amino side.[96–98] It has been shown that this rate increases for amino acids with less bulky and highly polar side chains, such as glycine and histidine, respectively.

[97] The less bulky side chain of an adjacent residue lowers the steric hindrance facilitating the nucleophilic attack of the peptide nitrogen on the γ-carbonyl of either the asparagine or Asp side chain while a more polar side chain helps stabilize the ionized transition state leading to succinimide formation.[99] The deamidation rate increases 10-fold when replacing leucine with histidine in position X of the model pentapeptide GGNXG, and 100-fold when replaced with glycine.[97]

1.3.2 The Affects of Protein Structure on Deamidation

The three dimensional structure affects both succinimide formation as well as the final products.[100–102] A dihedral ψ (psi) angle of -120° and χ (chi) angle of 120° offers the most favorable position (distance of 1.89$\mathring{A}$) for nucleophilic attack of the peptide nitrogen on the γ-carbonyl of the side chain to form the succinimide intermediate.[96] However, such configurations are uncommon in proteins suggesting that protein tertiary structure mitigates this modification by placing these residues where succinimide formation is hindered. For example, deamidation of an asparaginyl residue within the α-helix of rabbit muscle aldolase experienced a 15-fold slower half-life than that of its linear tetrapeptide model.[97] The addition of water opening the succinimide ring to form either an Asp or isoAsp residue (figure 1·10) depends on which of the amide bonds of the intermediate is hydrolyzed. This choice is partially governed by the three dimensional structure of the peptide or protein which effects the accessibility of each of the bonds to attack by water.[96,100,101,103] Typically, for linear peptides, greater than 60% of the products resulting from succinimide hydrolysis are isoAsp residues.[92,103]

1.3.3 Biological Importance of Deamidation

Formation of isoAsp residues has been correlated with protein inactivation and misfolding and whose physiological importance has been illustrated in experiments involving the repair enzyme L-isoAsp-*O*-methyltransferase (PIMT).[4,87–89,91,92,104] PIMT is a highly conserved enzyme that uses S-adenosyl-L-methionine (AdoMet) as a methyl donor to convert isoAsp to Asp residues, partially restoring the function of enzymes affected by deamidation or isomerization.[105] Methylation of the –OH group of the isoAsp side chain promotes formation of the succinimide intermediate that is then hydrolyzed. The process continues until, theoretically, only the

Asp version remain ('repaired'). The importance of the PIMT enzyme and the negative effects of the isoAsp modification have been shown in several experiments such as seizures and early death experienced by PIMT knockout mice[88] and the extension of life by 30% for *Drosphilia* with overexpression of PIMT.[106] This experimental evidence has led researchers to suspect Asp isomerization as a possible contributor to Alzheimer's disease since the isoAsp modification alters the fundamental structure of the protein structure and that the highest level of PIMT activity was located in the brain. The cerebral plaque samples of Alzheimer patients have shown evidence of Asp isomerized to isoAsp at residue positions 1, 7 and 23 of the β-amyloid peptide, where the isoAsp content was the highest at position D7 (75%)[87]. Other affected proteins include those long-lived proteins important for the structure of tooth, skin, lens of the eye and bone in humans[91]. In all, the biological motive behind deamidation so far falls into several categories including protein aging (crystallins),[94] turnover (aldolase),[107] regulation (HMAP),[92] contribution to apoptosis (Bcl-x_L),[108] and is emerging to be a common artifact during the isolation and purification of recombinant antibody therapeutics.[109,110] Whatever role is ultimately attributed to this modification, developing an analytical technique to reliably and easily differentiate Asp from isoAsp residues is critical to the biological assessment of how certain proteins aggregate, age and regulate their own activity.

1.3.4 Non-MS Based Methods for Studying Deamidation

It is important to understand methods previously used so that their shortcomings can be addressed with newer analytical techniques. The following descriptions are of techniques used to study deamidation that do not involve the use of MS. They can be categorized as chemical based (*e.g.* proteolytic digestion, antibody detection, Edman degradation, enzymatic detection) or instrumental based (chromatography, electrophoresis, nuclear magnetic resonance spectroscopy (NMR)). Like all analytical methods, each has their advantages and drawbacks which will be discussed.

Proteolytic Digestion

Kameoka used endoproteinase Asp-N and MS to detect deamidation of asparagine and isomerization of Asp residues in a protein.[111] Endoproteinase Asp-N is residue specific protease that

cleaves on the N–terminal side of an L-Asp residue and not at D-Asp or D/L-isoAsp residues. Lysozyme with an isomerized Asp and a deamidated asparagine residue were mixed separately with N^{15} labeled lysozyme, digested with Asp-N and analyzed by MALDI–TOF–MS. Modified sites were identified by the presence of new peptides (asparagine deamidation) or the lack of expected peptides (Asp isomerization) when compared to those generated from digestion of the N^{15} labeled protein. Although most mass spectrometers can detect deamidation (+0.984 Da mass shift), protein digestion with Asp-N is a useful and simple technique for detecting Asp isomerization. Also, Asp-N could be used to differentiate Asp and isoAsp peptides since one of the two forms is an acceptable substrate for the enzyme.

Other proteases have been used to detect isoAsp residues in proteins and peptides due to the uncommon peptide linkage associated with the form. The tryptic digest of the separated Asp and isoAsp forms of ribonuclease A showed differences in their HPLC peptide maps.[112,113] The differences were due to an apparent missed cleavage in the isoAsp chromatogram. The isoAsp residue, D67, was found to be adjacent to the missed cleavage site (–KDG–). Therefore, the abnormal linkage associated with the isoAsp was presumed to be the reason why the K66 site was resistant to cleavage by trypsin.

Isoaspartyl Antibody

Antibodies raised against isoAsp containing peptides using the multiple antigen peptide system procedure (MAP)[114] have been successful in identifying racemized Asp residues and deamidated asparaginyl residues in peptides and proteins, particularly for the β-Amyloid (Aβ) peptide associated with Alzheimer's Disease (AD).[89,115,116] The antibodies raised are epitope specific so each suspected isoAsp residue requires a specific antibody and thus synthetic peptide for the MAP procedure.

The antibodies raised against the synthetic peptides Aβ 1-42 (isoD7) and Aβ 1-42 (isoD23) were used to immunostain the brain tissue from six AD brains and non-AD brains that were used as control samples.[115] The Aβ 1-42 (isoD7) antibody failed to be of use because it stained both AD samples and control samples, but the Aβ 1-42 (isoD23) antibody was found to preferentially stain highly aggregated forms of Aβ 1-42 in the amyloid-bearing vessels and the core of mature plaques. Therefore, isomerized D23 was suggested to play a role in Aβ 1-42 sedimentation. In

another example, the distribution of isoAsp residues in the postmortem brain of a 65 year-old patient with cerebral amyloid angiopathy (CAA) was studied with the Aβ 1-42 (isoD7) and Aβ 1-42 (isoD23) antibodies.[116] The patient had a D23N mutation within their A sequence (Iowa-type) that was suspected to undergo deamidation to the isoD23 form more easily than D23 form, possibly triggering an early onset of fibrillogenesis in blood vessels. Tissue immunostained with anti-isoAsp detected isoD7 in vascular and parenchymal deposits but isoD23 was detected only in vascular deposits suggesting that deamidation at the mutation site could have played a part in premature deposition of the Aβ peptide in this case.

Reversed Phase High-Performance Liquid Chromatography (RP-HPLC)

Separation of the asparaginyl, Asp, and isoAsp forms of peptides can be accomplished by reversed phase high-performance liquid chromatography (RP–HPLC). Chromatography is an appealing methodology for separation because it can be used in combination with other techniques that assist in identifying the separated species. The elutant can be infused directly into a mass spectrometer or fractions can be collected so that a more detailed analysis by MS, Edman degradation or PIMT methylation can be performed. Many studies have shown that the deamidation products elute in the following order; isoAsp, Asp and then the aminosuccinyl form of the peptide.[110,117–124] This trend has been used to identify each peptide form,[110] yet subsequent analysis by other techniques provide a more dependable result.

When developing a method for separation, many factors need to be considered including the type of gradient, mobile phase composition and column selection. Typically, a linear gradient on a RP–HPLC platform equipped with a C_{18} column, and a mobile phase system that consists of an acidified aqueous phase (mobile phase A), such as 0.1 % trifluoroacetic acid (TFA), and an organic phase (mobile phase B), such as acetonitrile, is used and separation is achieved by varying the gradient. This approach was useful for measuring the deamidation rates of peptides and the enzyme kinetics and repair rates associated with the PIMT enzyme. A linear gradient of 0–40 %B in 40 minutes was adequate to separate the isoforms of the peptide VYPDGA, corresponding to residues 22–27 of deamidated adrenocorticotropin hormone, wherein the isoAsp form was discovered to be an excellent substrate for PIMT.[117] Also, the system was used to follow the repair process of WMD$_\beta$F (D$_\beta$ is isoAsp) to the Asp version by PIMT via time course

plots based on the abundance of the intermediates and by-products in the reaction mixture.[118] All five products involved in the repair process (D/L-Asp, D/L-isoAsp and succinimide versions of WMDF) were separated by a gradient 20–40 %B in 40 minutes. Both amino acid composition and length of the peptide affect the gradient necessary for separation of their isomers, each to varying degrees. For example, although the peptide GFDLDGGGVG contained twice as many residues as VYPDGA, they required the same chromatographic conditions to separate their isoforms.[117,120] Therefore, the unexpected behavior of peptides makes predicting RP–HPLC conditions almost impossible and often times results in having to develop custom gradients for every set of peptides. A general method can be developed but may require an extremely long gradient so that all possible deamidation sites are sufficiently separated. The products of three deamidation sites in a recombinant monoclonal antibody were separated on one HPLC run using a gradient of 0–65 %B in 195 minutes.[110] Other types of gradients used for separation include step and concave gradients and even isocratic conditions. Although C_{18} is a popular choice for isoAsp/Asp separations, C_8 columns can also separate the peptide isoforms although a shallower gradient may be necessary.[125] Finally, acidic modifiers such as TFA, formic acid and acetic acid provide adequate retention and peak shape, but changing the pH of the mobile phase can help shift the retention times of interfering species in the chromatogram. For example, using a mobile phase system at pH 6 helped separate four forms of a peptide that was both deamidated and isomerized.[125] Since the Asp/isoAsp forms are ionized at pH 6, the non-deamidated form is shifted to a higher retention time away from the ionized forms therefore providing a less complex chromatogram.

Ion Exchange Chromatography

Ion exchange chromatography is useful for separating species based on their ionic charge and therefore can be used to separate the native from the deamidated form of a protein since asparagine/glutamine is converted to their ionizable acid homologues. Mobile phase systems used for separation should have a pH that ensures deprotonation of the acidic group so that the overall charge of the native and deamidated forms show differential binding to the stationary phase. Bound proteins are eluted with gradual increase in concentration of a counter ion, i.e. salt. Both anionic (cation exchange) and cationic (anion exchange) interactions can be used to dif-

ferentiate the two forms. The native form of the protein binds more strongly for anion exchange chromatography therefore eluting earlier than the deamidated form, and vice versa for cation exchange analysis. Cation exchange chromatography has been used to separate the forms of a partially deamidated proteins,[126,127] including ribonuclease A[102,113,128,129] and a monoclonal antibody,[122] and anion exchange has been used for γS-crystallin[130] and protective antigen.[131] Separation of isoAsp and Asp by ion exchange is difficult, since the difference between the pK_a of the isomers is so similar.[132] The kinetics of isoAsp and Asp formation from deamidating ribonuclease A was measured using a very shallow KCl gradient on a cation exchange system.[128]

Electrophoresis

Gel electrophoresis can be used to analyze proteins affected by deamidation since both the isoelectric point and shape are altered. Isoelectric focusing (IEF) can separate based on the change in charge and native gel electrophoresis can discriminate protein forms based on the change in shape. The more traditional method, sodium dodecyl sulfate polyacrylamide gel electrophoresis (SDS-PAGE), is not used since the molecular weight resolution on gels is insufficient to discriminate between the native and deamidated forms. IEF is performed on a pH gradient gel that allows proteins to migrate based on their isoelectric point (pI) in the presence of an applied electric field. Performing separations using buffers with pH greater than the pK_a of the Asp or isoAsp side chain allows separation of the deamidated from non-deamidated forms since their respective pIs are different. The method is especially useful for separating multiple forms of a protein due to several deamidations; the multiple forms of stem cell factor,[127] protective antigen,[133] and phenylalanine hydroxylase,[134] were separated by isoelectric focusing. Native gel electrophoresis is also a useful electrophoretic technique for analyzing deamidated proteins since it can also separate the isomeric products of deamidation. The rationale for separation is that formation of Asp/isoAsp residues affects the shape of the protein when compared to the native form. For example, the three forms of partially deamidated calmodulin (N97 to isoD/D97) were separated by native gel electrophoresis.[105] The D_β97 form migrated the slowest followed by the D_α97 (D_α is Asp) and then N97 form. The larger molecular radii for D_β97 and D_α97 account for their slower migration with formation of isoAsp affecting the shape of

the protein more than the aspartyl form. Other proteins separated by native gel electrophoresis include the multiple deamidated forms of calbindin[135] and protective antigen.[131]

Nuclear Magnetic Resonance Spectroscopy

Two dimensional (2D) NMR has been used to differentiate the isoAsp from Asp residues in peptides.[136,137] Scalar coupling of the ^{1}H spin systems between the backbone nitrogen and the α-carbon (C_α), β-carbon (C_β) and amide nitrogen of the neighboring amino acid residue in NOESY 2D ^{1}H NMR spectra allows the approximate distances between these groups to be determined for large molecular structures such as proteins.[138] For normal residue linkages, the C_α-N or N-N couplings are typically strong while C_β-N tend to be weaker. However, isoAsp linkages have a methylene group inserted into the backbone that changes the magnitude of these couplings. For example, 2D ^{1}H NMR was used to detect an isoAsp residue (D_β56) within a 30-residue tryptic peptide from calbindin D_{9k} that deamidated during purification.[136] The distance between the nitrogen of the G57 and C_β of D_β56 (backbone methylene) was found to be less than 3.5 $\mathring{A}$ while the distance of C_α and N (of D_β56) from N (of G57) were 4.7 and 6 $\mathring{A}$. This trend describes spatially what is attributed to an isoAsp residue in the peptide backbone. Additionally, the data showed that the backbone region containing isoAsp residue was in a more extended helical shape compared to the Asp version. Another study used 2D 1H NMR to differentiate to the isoforms of a 15-residue peptide using the presence of the C_β-N found in the isoAsp spectrum that was not found in the Asp spectrum.[137]

The advantage of using 2D ^{1}H NMR is the additional structural information acquired that provides insight on how the presence of an isoAsp residue affects the higher order structure of the region. However, the disadvantage is that each experiment requires a large amount of sample, which may make the method inapplicable to biological experiments; the samples in the NMR studies described were in the range of 10^{-3} M, which is close to the precipitation concentration of most proteins

Edman Degradation

Edman degradation, a chemical method used to sequence N–terminal linked peptides, was found to be blocked by an isoAsp residue when Smyth *et. al* attempted to sequence residues 11–18 of

pancreatic ribonuclease.[139] For normal α-linked peptides, the addition of phenylisothiocyanate to the amino group facilitates nucleophilic attack of the carbonyl group by the thiol group ultimately resulting in cleavage of the residue and generation of a peptide with n-1 residues and a new amino terminus. When a isoAsp residue is the next residue, the carbonyl group is beyond the reach for the attacking thiol due to the inserted methylene group, and the process is interrupted.

The failure of Edman degradation at isoAsp residues has been used to detect these residues in proteolytic peptides. Furthermore, products of deamidation separated by HPLC determined to have the same masses and sequences by MS/MS or amino acid hydrolysis can be subjected to Edman degradation for differentiation. This method has been useful for experiments involving proteolytic peptides from deamidated proteins[140,141] including ribonuclease A,[112,139] calmodulin,[125] and human stem cell factor,[127] and isomerized Aβ peptide from AD brains.[87]

PIMT enzyme

The PIMT enzyme, which selectively methylates isoAsp residues, can be used for analyzing asparaginyl deamidation and Asp isomerization by detecting the resulting isoAsp residues. Analytical methods employing PIMT use radioactively labeled AdoMet (^{14}C or ^{3}H) as the methyl donor that is selectively incorporated onto the isoAsp caboxylate group. A popular technique for measuring the isoAsp content in peptides by radiolabeling with PIMT is by the vapor diffusion method. In this method, [^{14}C] or [^{3}H] methanol released by quenching the methylation reaction with a mild base is then measured by liquid scintillation.[117,142] The methylation step is carried out for 30 minutes to 1 hr and then immediately quenched with a mild base generating radiolabeled methanol. The opened reaction vial is then placed in a sealed tube containing a scintillation cocktail. The [^{14}C] or [^{3}H] methanol vapor diffuses from the reaction solution (or spotted filter paper) into the scintillation cocktail that is then counted to determine the quantity of isoAsp residues versus radiolabeled methanol standards. For proteins, the vapor diffusion method is used but precipitation of the protein using trichloroacetic acid is done after methylation and before treatment with base to remove unreacted [^{14}C] or [^{3}H] AdoMet.[143,144] Isoaspartyl residues in cell (*e. coli*,[145] erythrocytes,[146] and ooctyes[144]) and tissue homogenates (*drosophila*,[106] *c. elegans*,[147] and mice[88,148]), proteins,[104,105,105,149,150] and

peptides[87,117,120,125,126,134,151,152] have been characterized using the vapor diffusion method.

IsoAsp detection using PIMT is often used in combination with separation techniques, such as HPLC and gel electrophoresis, to localize the isoAsp residues in a mixture of proteins or peptides. The vapor diffusion method can be used with HPLC to provide two concurrent chromatograms relative to time, one based on UV absorbance and the other derived from radioactive counts of collected fractions. The peptides or proteins can be labeled after being fractionated by HPLC or before separation. Peptides from aged proteins[104,105,149] such as calmodulin[125] were analyzed using HPLC and PIMT methylation as well as a mixture of histones isolated from nuclei of mouse brain tissue.[150,153] Also, a mixture of proteins can be reacted with PIMT in the presence of radiolabeled AdoMet, separated by gel electrophoresis and then subjected to fluorography.[104,144,150,152] The fluorogram of the gel reveals which proteins, separated by molecular weight, contain isoAsp residues. The relative intensity of the spots can also provide some information of the relative amount of isoAsp formation between the proteins. Finally, the Isoquant kit developed by Promega also uses the PIMT enzyme and HPLC to detect and measure the abundance of isoAsp residues by measuring the change in UV absorbance of AdoMet before and after methylation.[154] Localization is not possible but the convenience of the kit helps to quickly and easily provide some information on isoAsp content.

1.3.5 Mass Spectrometric Methods for Studying Deamidation

The accuracy and speed associated with analysis by MS is highlighted when studying deamidation since most of the previously described methods are labor intensive techniques. Although it is not completely without some difficulty, MS experiments occur on a time scale much shorter than most chemical tests and offer comparable information. MS methods can easily detect deamidation, measure the extent of the reaction (conversion of asparagine to Asp/isoAsp residues) and help discern the two isomeric products, and each method is described below.

Measuring Deamidation by Isotopic Deconvolution and Mass Defect Methods

The isotopic deconvolution method for measuring deamidation uses the +0.984 Da shift in the mass spectrum associated with the conversion of $-NH_2$ to –OH. The corresponding peaks in the

spectrum are a combination of two overlapping species resulting in an atypical isotopic pattern. Assuming the peak intensities are additive, the pattern can be deconvolved quantitatively to its two separate forms by fitting the theoretical isotopic patterns of each contributing species to the experimental pattern. Although a considerable amount of signal averaging is advised to obtain a pattern that accurately represents the sample composition, this method is still much faster and uses less sample than use of HPLC. Robinson and Robinson efficiently performed a comprehensive analysis of the deamidation rates of asparginyl and glutamyl residues in over 700 peptides that required thousands of analyses using the isotopic deconvolution method on data obtained from a quadrupole mass spectrometer.[93,97,98] The extent of deamidation in proteins has also been determined by analyzing the proteolytic peptide mixture on a MALDI–TOF mass spectrometer. The advantage of MALDI is that ionization generates only singly charged species therefore producing a mass spectrum of minimal complexity, an important benefit considering the number of proteolytic peptides that can be obtained from a protein digest. For example, the extent of deamidation of human phenylalanine hydroxylase,[134,155] calbindin,[135] and protective antigen[133] was determined using the isotopic deconvolution method on data from a MALDI–TOF mass spectrometer. Isotopic deconvolution has also been used on high-resolution data from ESI–FT–ICR–MS analysis of deamidated ribonuclease A[156] and crystallins from human eye lenses.[157] Fragments obtained from top-down analysis of these proteins allowed the localization and extent of deamidation to be measured at several sites therefore eliminating the need for digestion.

The mass defect method for measuring deamidation relies on the ability to resolve the 19 mDa mass difference between the A+1 isotope of a non-deamidated peptide and the first isotope of the deamidated form.[158] Once resolved, the relative intensity of the two peaks corresponds to the extent of deamidation assuming the ionization and detection efficiencies of the two species is the same. FTMS can attain the high resolution necessary to resolve the two forms. For example, a resolution of 280,000 was achieved on an FT–ICR–MS in order to separate the three deamidated forms of 16–residue synthetic peptide.[158] The mass defect method can also be used on fragments generated by top-down fragmentation.[157,159] For example, mixtures of wild-type and mutant (Q162E) were mixed at known ratios and subjected to top-down fragmentation by IRMPD.[159] Both forms for fragments containing the Glu/Gln162 site were resolved from one

another and the mixture composition revealed by mass defect analysis was found to be close to the expected value.

The Diagnostic b_{n-l}+H_2O for IsoAsp Residues in CAD MS Spectra

In 1992, Papayannopoulos[13] and Carr[160] both reported a b_{n-l}+H_2O fragment ion in the CAD spectrum of peptides with an isoAsp residue (n is the position of isoAsp/Asp) that was not found in the spectrum of the Asp form of the same peptide. The fragment ion was also used to differentiate the isoAsp from Asp forms of a deamidated proteolytic peptide, separated by HPLC, from hirudin, an anticoagulant peptide.[161] The mechanism involves migration of the –OH from the isoAsp side chain to the n-1 carbonyl group via an oxazolidone intermediate that rearranges to generate the b_{n-l}+H_2O ion and an aldinine fragment. Since the isoAsp side chain resembles the C–terminus, generation of b_{n-l}+H_2O for isoAsp residues is suggested to resemble the fragmentation channel shown to occur in the low-energy MS/MS spectra of peptides wherein a C–terminal hydroxyl rearrangement generates b_{n-l}+H_2O fragment ions.[12,162] Schindler *et al.* showed evidence of the hydroxyl transfer mechanism for isoAsp residues by performing MS/MS on an ^{18}O labeled peptide.[161] The labeled peptide was synthesized by incubating the succinimide derivative of the peptide in ^{18}O water, so that upon hydrolysis, one of the equivalent oxygens of the carboxyl group of the isoAsp side chain was labeled with ^{18}O. The low energy MS/MS of the peptide showed the b_n+H_2O ion being split in a 1:1 ratio of ^{16}O:^{18}O thus proving that there is a migration of –OH from the side chain to the diagnostic fragment.

A study in 2000 by Gonzalez *et al.* showed that the b_{n-1}+H_2O fragment ion and its complement, the y_{l-n}-46 fragment ion, can be used to differentiate isoAsp from Asp residues in sets of synthetic peptides, including D7 and D23 of β-Amyloid peptides analogues, and detect isoAsp residues in deamidated tryptic peptides from recombinant proteins.[163] The data also demonstrated that the b_n+H_2O intensity is much larger if a basic amino acid or the N–terminus is on the N–terminal side of the isoAsp residue. Intermolecular interaction between the side chain of the basic and isoAsp residues is believed to facilitate rearrangement to generate the diagnostic ions. A severe limitation to using the b_n+H_2O ion to detect isoAsp residues may occur when analyzing tryptic peptides, since they should only have C–terminal basic residues

unless there is incomplete digestion or there is a histidine present within the tryptic peptide. The complement y_{l-n}-46 fragment ion can be used to detect isoAsp residues in the case of tryptic peptides, but this fragment is usually much less abundant than the b_n+H_2O fragment ion (the largest y_{l-n}-46/y_{l-n} intensity ratio reported was 0.039). Nonetheless, the isoAsp residues in two tryptic peptides were characterized by the presence of the y_{l-n}-46 ions.

Aspartyl versus isoAspartyl Fragment Ion Ratios in CAD Spectra

Lloyd and coworkers were first, in 1988, to use fragment ion abundance ratios to differentiate Asp from isoAsp residues in the MS/MS spectra of peptides using a double focusing magnetic sector mass spectrometer.[164] The MS/MS of the peptides RKDVY and DIRKF-NH_2 showed loss of CO from b_{n+1} to form a_{n+1} while the same loss was much smaller for the isoAsp versions (b_{n+1}/a_{n+1}(Asp) > b_{n+1}/a_{n+1}(isoAsp)). The authors suggest that loss of CO to form the a_{n+1}, a stable iminium ion, for the Asp form is a much more favored pathway than loss of CO from the isoAsp b_{n+1} to from a primary carbocation. Additionally, the same trend was found for a peptide containing a glutamyl residue and its isoglutamyl homologue.

A study by Lehman *et al.* in 2000 found that the intensity of fragment ions resulting from amide backbone bond cleavage (b and y ions) on either side of Asp/isoAsp showed a reproducible trend that can be used to distinguish isoAsp from Asp residues.[165] Based on the MS/MS spectra of 15 sets of isomeric peptides, the b/y intensity ratio of complementary b and y ions from cleavage on either side of the Asp/isoAsp residue were consistently larger for the Asp form than the isoAsp form. Fragmentation intensity ratios for Asp were typically less than 15 times larger than the same fragmentation for the isoAsp counterparts although some values were much larger. The trend is believed to be a result of the competition between forming the oxazolone containing the N–terminus (b ion) and direct cleavage to form an terminal amine containing the C–terminus (y ion).[166] In the ESI process, the amide nitrogen can be protonated thus weakening the C–N bond facilitating nucleophilic attack of the amide bond carbonyl on the C–terminal adjacent amino acid to form the oxazolone. When the residue is isoAsp, formation of the oxazolone is hindered. On the N–terminal side of the isoAsp residue, oxazolone formation can be hindered by a similar interaction between the isoAsp side chain and the backbone carbonyl since the carboxyl group is closer in proximity to the backbone more so than the Asp

form. On the C–terminal side, a six membered ring must be formed that contains the isoAsp residue and is kinetically less favored than the five-membered oxazolone structure. Therefore, b ion formation is hindered on both sides of the isoAsp residue and direct cleavage is favored resulting in a decreased b/y ion ratio compared to the Asp form.

Immonium Ions of Isoaspartyl Residues

The structure proposed by Lloyd for the a_1 ion found in the MS/MS spectrum of the peptide DIRKF-NH_2, missing from the spectrum for the isoAsp version, is essentially the immonium ion for an Asp residue ($m/z = 88$).[164] Immonium ions are small internal fragments containing one amino acid side chain that result from the cleavage of multiple backbone bonds and are useful for determining the amino acid composition of a peptide. Several studies since then have shown that the intensity of the Asp immonium ion found in the MS/MS spectrum of an isoAsp peptide is much smaller (or nonexistent) than that found in the Asp spectrum.[163,165]

Lehmann showed that, for 15 sets of peptides, the Asp immonium ion intensity (normalized to another immonium ion in the spectrum) was on the average 5.5 times higher for the Asp form over the isoAsp form and suggest that such a trend could be used to differentiate the two forms.[165]

Gonzalez *et al.* used the Asp and isoAsp immonium ion intensities to differentiate isomers that could not be differentiated using the b_{n-1}+H_2O and y_{l-n}-46 fragment ions.[163] In addition to the Asp immonium ion, a fragment ion at $m/z = 70$ was found in the isoAsp spectrum that was not found in the Asp spectrum. The ion was suggested to be the immonium ion for an isoAsp residue that results from a rearrangement of a primary carbocation, a structure suggested to be unstable and therefore not found in the isoAsp spectrum. Loss of water from the side chain of the carbocation yields a charged acylium structure of mass $m/z = 70$. This ion, however, cannot be used an absolute indicator for the presence of an isoAsp since it is the same mass for the proline immonium ion, which is typically a strong signal in the mass spectra of proline containing peptides.

Liquid Chromatography/Mass Spectrometry (LCMS)

LCMS methods use the RP-HPLC technique because the acid modifiers help the retention and peak shape of peptides on the LC column while assisting protonation and being volatile for MS analysis. The localization and extent of deamidation in a protein can be determined from one LCMS run of the proteolytic peptides. For example, nine deamidation sites (aspargine and glutamine) were characterized in S-crystallin from cataracts as determined from an LCMS analysis of the trypsin digest.[130] Deamidation was first determined by the isotopic deconvolution method and localization of these sites were determined by the MS/MS data, which was necessary because multiple asparagine and glutamine residues were present in many of the peptides. In another study, the carboxyl groups of tryptic peptides were methyl esterified in order to simplify the detection and measurement of two deamidation sites.[167] Detecting the 1 Da shift in an ion trap can be difficult but the +14 Da from the introduced methyl ester at the carboxyl residue (deamidation site) make recognizing deamidation much easier. Also, the methyl ester changes the hydrophobicity of peptide, shifting it away the non-deamidated form and therefore simplifying the LC chromatogram for quantitative measurements.

The relative quantification of deamidation products can also be determined by LCMS analysis, provided the LC separation is sufficient to separate the isomers. As mentioned above, the isoAsp form of a deamidated peptide typically elutes before the Asp form and this trend has been used to assign the identities of peptides found in an LC chromatogram,[110] but supportive data is often needed to unambiguously make such assignments. Analyses using synthetic peptide standards[121,168] and a mutant form of a protein[122] have been successful in confidently identifying deamidation products separated by HPLC thereby providing reliable quantitative measurements. For example, LCMS/MS was used to measure the extent of *in vivo* deamidation of a monoclonal antibody using a mutant form as a standard.[122] The antibody in question was isolated and digested in parallel with the mutant form that had an Asp residue substituted for the deamidating asparaginyl residue. The retention time of the peptide with the Asp substitution from the mutant protein had the same m/z, MS/MS profile and retention time as the Asp peptide (deamidation product) from the *in vivo* sample. The information allowed the extent of deamidation and relative quantification of the products to be determined from the LCMS/MS experiment (the identity of the isoAsp peptide was assumed based on its retention time with

respect to the Asp form). Other experiments used the retention time and MS/MS profiles of corresponding synthetic peptides (Asp, isoAsp and asparaginyl) to measure the deamidation of peptides or the natural abundance of isoAsp residues in a protein.[121,168]

1.3.6 Relative Quantitation of Deamidation Products

HPLC Combination Methods

As mentioned above, quantitating the extent of deamidation and the relative abundance of deamidation products can be done with HPLC when used in combination with techniques that can discriminate the multiple forms. Edman degradation, mass spectrometric techniques and PIMT assays can be performed on collected fractions to differentiate the peptides (Asp/isoAsp peptides) as long as the peptides are adequately separated.

CAD Methods without HPLC

The capability to quantitate the relative amounts of Asp and isoAsp residues using CAD fragments (b_n+H_2O, b/y intensity ratio and immonium ions) is possible.[165,169] The experiments illustrating this ability involve performing MS/MS analysis on mixtures of synthetic peptides that vary in isoAsp/aAsp composition, intending to represent the possible outcomes of asparaginyl deamidation or Asp isomerization. Lehman showed that both the b/y intensity ratio and immonium ions could be used to calculate the relative abundance of the two forms.[165] A plot of the b/y intensity ratio from cleavage on the N–terminal side of the peptide VQD$_{\alpha/\beta}$GLR versus aspartyl content showed an asymptotic relationship that could be used as a calibration curve. Also, MS/MS analysis of mixtures of myrGDAAAK and its isoAsp counterpart showed a linear relationship between the Asp immonium ion (normalized to the lysine immonium ion) and Asp composition. However, since these fragments ions are not diagnostic and calculation of the relative intensity the fragments are necessary, at least two points on the calibration curve are necessary and peptide standards are required to generate calibration curves. Alternatively, the b_n+H_2O fragment ion is diagnostic.[13,161,170] The relative intensity of the b_n+H_2O was shown to increase linearly with isoAsp content when compared to other backbone cleavages that were assumed to be unchanging regardless of sample composition.[169] Despite the advantage, the isoAsp peptide standard is necessary to establish the calibration plot.

1.4 Conclusion

MS is emerging as a key tool for the structural elucidation of important biomolecules including peptides and proteins. MS can quickly and accurately determine the masses of the fragments that result from protein and peptide dissociation so that one can gain an understanding of the original, intact structure. The most important components of the mass spectrometer are the ionization technique, the mass analyzer and the fragmentation method. The ionization techniques FAB and MALDI suspend the sample in a matrix that is then irradiated with a neutral atom or laser beam in order to vaporize and ionize the sample. ESI is another technique in which the sample is dissolved in a pH adjusted, semi-volatile solution which emits the ionized sample when a high voltage is applied. The heart of the mass spectrometer is the mass analyzer which is how the mass of an ionized species is measured. Quadrupole and ion traps use DC/RF fields to manipulate and isolate ions based on their mass-to-charge ratio, or m/z value, and are typically the most inexpensive mass analyzers but have the lowest mass resolving power. TOF determines the m/z value based on how long it takes the ions to strike a detector and can achieve high mass resolution than quadrupoles or ion traps. The final analyzer discussed is the FT–ICR which measures mass based on the frequency of the precessing ions in a strong magnetic field. This technique offers the highest mass resolution but is the most expensive due to the super-conducting magnet that is required. The final key component of the mass spectrometer is the fragmentation method implemented. CAD, BIRD, SORI-CAD, and IRMPD are all 'slow heating' techniques that cause cleavage of the most labile bonds including the peptide amide, PTM and non-covalent bonds found in peptides and proteins. ECD and ETD cleave the N–C_α bond via a 'non-ergodic' process, or before the energy from electron capture ($\sim$6 eV) can be distributed throughout the many vibrational modes of the molecule. ECD therefore preserves labile bonds (those normally cleaved by 'slow heating' methods) that are important for localizing PTMs and understanding the gas-phase tertiary structure of proteins and peptides. However, many aspects of ECD are still not understood. For example, the multiple cleavages observed for ECD of cyclic peptides cannot be reasoned by the primary cleavage alone and therefore a secondary mechanism, the free-radical cascade, was proposed to explain the additional cleavages. The chapter following the introduction discusses experiments

used to test the free radical cascade mechanism in ECD. These experiments were performed in order to support the free radical cascade mechanism as well as provide additional data to the general community regarding how peptide and protein dissociation occurs in ECD.

Deamidation of asparagine residues to Asp and isoAsp is a spontaneous reaction that is believed to be one way in which proteins age. Changing the side chain functionality from an amide (asparagine) to a carboxylic acid (Asp) affects protein function to some degree, but formation of isoAsp is believed to be more detrimental. It is damaging because the peptide backbone and side chain is lengthened and shortened, respectively, by one methylene unit altering the traditional peptide structure. Therefore, to evaluate the effect of deamidation, it becomes increasingly important to develop analytical tools to detect deamidation, differentiate the products and determine their relative abundance. Many chemical methods are available to perform this task such as proteolytic digestion, use of an isoAsp antibody, Edman degradation and reactivity with the PIMT enzyme. These chemical based methods tend to be very sensitive for detecting isoAsp residues but labor intensive and cannot quantify the relative abundance of the two products. Instrumental methods such as chromatography, electrophoresis and NMR can also be used but with some drawbacks. NMR can differentiate the two forms but needs a large amount of sample and the two forms must be initially separated. Electrophoresis can detect protein deamidation and separate the two isomers but cannot localize the deamidating residue. The best method to separate the two isomers in peptides is by RP-HPLC but it is difficult due to the subtle difference in their structures. Also, the two isomers cannot be differentiated unless standards are used. Finally, MS methods can be used to detect and differentiate the two forms. Isotopic deconvolution can determine the extent of deamidation while some CAD methods can be used to differentiate the two forms to some extent based on diagnostic ions which can often remain undetected or ambiguous. When CAD is used with RP–HPLC, the isomers can be differentiated to some degree and simultaneously quantitated by the chromatographic trace.

ECD has yet to be used to examine asparagine deamidation in proteins and will be the subject of chapters 3–5 and 8. Chapter 3 discusses the use of ECD to differentiate the two deamidation products in synthetic peptides using diagnostic ions particular to each isomer. Chapter 4 expands on the third chapter by illustrating the use of ECD for detecting isoAsp residues in deamidated proteins and differentiating the two isomers by RP–HPLC–ECD. Chap-

ter 5 discusses a method that can use ECD to quantitate the relative abundance of the two forms without the use for RP–HPLC or peptide standards. Chapters 6 uses information gained in chapter 2, regarding the ECD mechanism, to draw some conclusions on the kinetics of how peptides unfold/fold in the gas-phase and chapter 7 uses this information to understand how the gas-phase structure of a peptide is affected by substituting an isoAsp for an Asp residue and if the effect could be extended to the solution-phase structure. Finally, chapter 8 discusses the use of FT–ICR–MS and FT–ICR–MS–ECD to detect deamidation and isoaspartyl residues in a recombinant protein, the protective antigen used against anthrax infection.

Chapter 2

Free-Radical Cascade Mechanism in ECD

2.1 Introduction

2.1.1 Primary ECD Mechanisms

For peptides and proteins, ECD[1,69] (see section 1.2.3) cleaves more evenly along the backbone than conventional MS/MS methods (*e.g.*, CAD and IRMPD) while preserving the more labile PTMs, making it a very useful tool in the field of proteomics.[171] Such behavior has been suggested to be evidence of a nonergodic dissociation pathway, in which much of the ∼6 eV neutralization energy is utilized locally before randomization, allowing competitive cleavages of backbone bonds with significantly different dissociation energies, and preservation of more labile side chain bonds, even noncovalent interactions.[66,72] However, there is also a body of calculations that suggest that electron capture produces a long-lived aminoketyl radical species for which backbone cleavage is the lowest energy pathway, therefore eliminating the need to evoke the nonergodicity assumption.[63]

2.1.2 A Secondary ECD Fragmentation Mechanism: the Free Radical Cascade

In a previously published manuscript,[67] data were presented in which cyclic peptides were shown to undergo extensive secondary side chain and backbone fragmentation that appeared to be free-radical driven. Secondary side chain fragmentation has also been reported by other research

[1]This chapter has been partially/entirely reproduced from
P.B. O'Connor, C. Lin, J. J. Cournoyer, J. L. Pittman, M. A. Belyayev, and B. A. Budnik. Long-lived electron capture dissociation product ions experience radical migration via hydrogen abstraction. *Journal of the American Society for Mass Spectrometry*, 17(4):576-585, 2006. Copyright 2006 Elsevier

[2]This chapter has been partially/entirely reproduced from
M. A. Belyayev, J. J. Cournoyer, C. Lin, and P. B. O'Connor. The effect of radical trap moieties on electron capture dissociation spectra of substance p. *Journal of the American Society for Mass Spectrometry*, 17(10): 1428-1436, 2006. Copyright 2006 Elsevier

[3]This chapter has been partially/entirely reproduced from
C. Lin, J. J. Cournoyer, and P. B. O'Connor. Use of a double resonance electron capture dissociation experiment to probe fragment intermediate lifetimes. *Journal of the American Society for Mass Spectrometry*, 17(11): 1605-1615, 2006. Copyright 2006 Elsevier

groups,[74,76,78,172,173] and has been explored by a combined experimental and computational approach as well.[174] One significant limitation in the cyclic peptide data, however, is that it is derived from molecules for which primary backbone cleavages do not result in mass shifts and, thus, are unobservable. While these data were helpful for determining the existence of secondary backbone fragmentation in ECD, such data cannot provide information concerning which fragments are generated from primary versus secondary cleavages. The cyclic peptide data, however, did suggest a fragmentation pathway in which the expected c/z ion cleavages could arise both from a primary nonergodic fragmentation and also from a secondary ergodic pathway. The free radical cascade mechanism[67] has the following three requirements;

1. the existence of a long-lived radical intermediate after the initial electron capture,

2. radical migration is required to initiate cleavages, and

3. hydrogen atom (H·) transfer is not required for cleavages.

The first and second conditions require that the radical(s) formed from the primary fragmentation have time to migrate before the final, observed fragmentation. This is a process that is expected to occur on the nanosecond to microsecond time scale, which is much longer than the expected time frame for intramolecular vibrational redistribution (picoseconds).[175] If the free radical cascade mechanism is correct, previous calculations[176–178] suggested that it would preferentially migrate to the C_{alpha} position via hydrogen abstraction, and that there would be a preference for migration to glycine because the lack of steric hindrance would allow a radical in that position to become planar with the carbonyl. This hydrogen abstraction reaction typically proceeds via a low-energy barrier transition state and is even exothermic in some cases.[178] Hence, the C_α position is expected to be critical in most of the proposed reaction schemes.[67] Thus the first experiment described in this chapter is the ECD of a peptide that is labeled with deuterium at several amino acid C_α positions. If C_α hydrogen abstraction were occurring, deuterium scrambling would result and would be detectable in the mass spectrum as ±1.006 Da mass shifts, ±(±D–H), in the isotopic distributions of the fragment ions. This experiment would prove that radicals are migrating and this transfer is facilitated by the existence of a long-lived radical intermediate (conditions 1 and 2).

The occurrence of radical migration would indicate the existence of a long-lived radical intermediate, formed after the initial electron capture, that permits such transfers to occur, but what is the lifetime of these intermediates? To this end, the second experiment describes the use of double-resonance[179] ECD (DR–ECD) experiments to determine the lifetime of these radical intermediates. DR is the ejection of a specific ion in the ICR cell using a RF pulse corresponding to the cyclotron frequency of the species to be ejected (further explanation in given in section 2.3.2). In the experiments described, ejection of the reduced molecular ion ($(M+nH)^{(n-1)+\cdot}$, where n is the number of protons) during the ECD event should affect the distribution and abundances of fragments observed; the radical intermediates in the case of ECD are complementary (c and z$\cdot$) fragments that remain hydrogen-bonded to one another represented by the reduced molecular ion after the primary cleavage. The change in fragment abundances with the ejection should provide some information on the life-time of the bound, radical intermediate.

To further test this mechanism, the third experiment described involves the ECD peptide labeled with a coumarin radical trap. If a long-lived radical is involved in the fragmentation, a radical trap should suppress fragmentation (condition 2). Finally, a fourth experiment is done to test the hypothesis that an H$\cdot$ radical is required for the N-C_α cleavage and the free radical cascade mechanism in ECD (condition 3).[67] ECD of peptides labeled with a fixed charge tags should not generate the H$\cdot$ required for backbone cleavages according the primary mechanism, so any fragments therefore must be a result of radical-induced cleavages, *i.e.* the free radical cascade.

All four experiments successfully provide some data that supports the three requirements above and thus the presence of the the free radical cascade mechanism in ECD.

2.2 Materials and Methods

2.2.1 Sample Preparation

Cheimcals

Table 2.1 lists all the peptides analyzed by ECD. BUSM–A and –B were synthesized by Anaspec (San Jose, CA). Substance P, fibrinopeptide B, the Aβ peptides (residues 20–29 and 25–35) and all other chemicals (unless noted otherwise) were purchased from Sigma-Aldrich (St. Louis,

MO). A stock solution of each peptide was prepared in water at $\sim 10^{-3}$ M and stored at ∼20 °C.

Table 2.1: Peptides Analyzed

Peptide	Sequence	Molecular Weight
BUSM-A	RAAAGADGDGAGADAR	1400.6393
BUSM-B	$\mathrm{RAAAG}_{d,d}$[1]$\mathrm{ADG}_{d,d}\mathrm{DG}_{d,d}\mathrm{AG}_{d,d}$ADAR	1408.6895
BUSM-A1	AAAGADGDGAGADAR	1244.5382
Substance P	RPKPQQFFGLM	1346.7282
Substance P (1 tag)	^{t*}[2]RPK^{t*}PQQFFGLM	1548.7548
Substance P (2 tags)	^{t}[3]RPK^{t}PQQFFGLM	1750.7814
Aβ (20–29)	FAEDVGSNKG	1022.4669
Aβ (20–29) (1 tag)	^{t*}FAEDVGSNK^{t*}G	1127.5373
Aβ (20–29) (2 tags)	^{t}FAEDVGSNK^{t}G	1232.6077
Aβ (25–35)	GSNKGAIIGLM	1059.5747
Aβ (25–35) (1 tag)	^{t*}GSNK^{t*}GAIIGLM	1164.6451
Aβ (25–35) (2 tags)	^{t}GSNK^{t}GAIIGLM	1269.7155

Peptide Digestion

BUSM–A1 was generated by tryptic digestion of BUSM–A thus cleaving off the N–terminal arginine residue. Digestion was carried out in 0.1 M ammonium bicarbonate (AB) at 37 °C for ∼16 hours (overnight) with an enzyme:peptide ratio of 1:20 (w/w). After digestion, the sample was dried using a Speedvac with refrigerated vapor trap (Savant RVT 4104, Thermo Electron Corp., Milford, MA) and re-dissolved in water (3 cycles) to remove the AB followed by storage at ∼20 °C.

Synthesis and Isolation of Coumarin-Tagged Substance P

The coumarin tag (7-methoxycoumarin-3-carboxylic acid succinimidyl ester), purchased from Invitrogen (Carlsbad, CA), was donated by Anna Pashkova and Barry Karger from Northeastern University (figure 2·1). The coumarin based tag was chosen due to its conjugated structure

[1] d indicates deuterium
[2] t* indicates possible position of tag
[3] t indicates position of tag

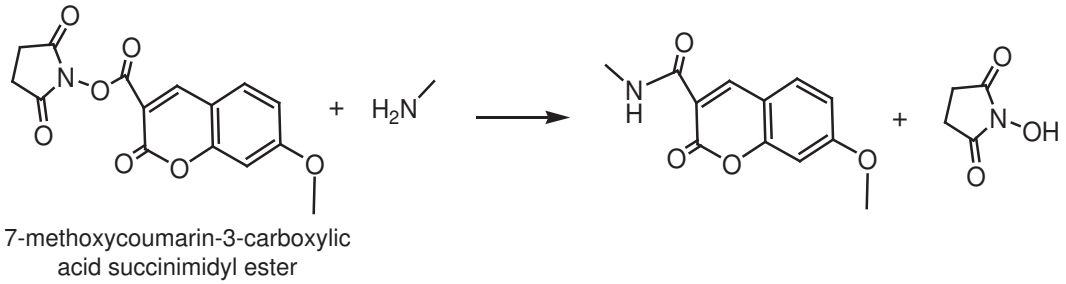

Figure 2·1: Reaction of coumarin tag (7-methoxycoumarin-3-carboxylic acid succinimidyl ester) with amines (lysine side chain and/or N–terminus).

and simple reaction mechanism with the peptide substance P utilizing N-hydroxy succinimide ester chemistry, which tags the peptide at the amine group of the N–terminus and lysine side chain.[180] The tagging reaction solution consisted of; a 10 μL aliquot of substance P stock solution ($\sim 10^{-4}$ M), 2 μL of 1 M ammonium acetate (AA) and 5 μL of tag solution (1 μg of tag per 10 μL of dimethylformamide (DMF)). The reaction was constantly rotated in a capped vial for 40 minutes. FT–ICR–MS analysis of the reaction revealed that both singly and doubly tagged substance P were generated.

Separation of the N–terminus and lysine tagged substance P was performed by RP–HPLC (solvent module 125 with detector module 166, Beckman Coulter, Fullerton, CA) equipped with a 20 μL injection loop and 4.6 x 250 mm C_{18} column (Vydak, Hesperia, CA). Mobile phase A consisted of 5:95 acetonitrile:water with 0.05% TFA and mobile phase B consisted of 80:20 acetonitrile:water with 0.035% TFA. A gradient of 0 to 40% B in 60 min was used to separate singly and doubly tagged substance P. Fractions were dried using a Speedvac with refrigerated vapor trap (Savant RVT 4104, Thermo Electron Corp., Milford, MA) and re-dissolved in water (3 cycles) to remove TFA and stored at $\sim$20 °C.

Synthesis and Isolation of Pyridinium-Tagged Aβ Peptides

The 2,4,6-trimethylpyrylium salt can react with amine group converting it to pyridinium with a fixed charge at nitrogen (figure 2·2).[181] The target amine groups in the two Aβ peptides are the N–terminus and lysine side chains. The tag solution composed of a carbonate buffer (0.1 M K_2CO_3 and 0.1 M $NaHCO_3$) with 0.05 M of 2,4,6-trimethylpyrylium tetrafluoroborate (Alfa Aesar, Ward Hill, MA). A small amount of concentrated hydrochloric acid ($\sim$10 μL) was used to

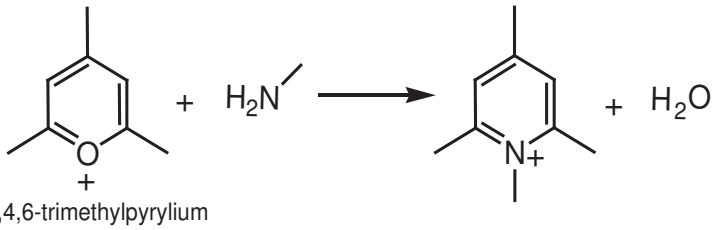

Figure 2·2: Reaction of stationary charge tag (2,4,6-trimethylpyrylium) with amines (lysine side chain and/or N–terminus).

adjust the pH of the solution to ∼9. 20 nmol of each peptide (∼20 μg) was separately dissolved in 50 μL of the tag solution, vortexed, purged with nitrogen gas and allowed to react for 18-24 hours at room temperature. The two reaction solutions were dried and the tagged peptides were purified using POROS 50 R1 (Applied Biosystems, Foster City, CA) material packed in gel-loading pipette tips. POROS 50 R1 material is essentially reverse-phase packing, similar to C_{18} material, that selectively binds the peptide using a polar solvent system (*e.g.* water). All other species are washed away (*i.e.* buffer, excess tag) and the peptide is eluted off the material by passing an less polar solvent system over the packing. In this case, the peptide is bound to the packing using acidified water (5% formic acid) and eluted with 80:20 water:methanol solvent with 5% formic acid. The eluted samples were dried using a Speedvac with refrigerated vapor trap (Savant RVT 4104, Thermo Electron Corp., Milford, MA) and re-dissolved in water (3 cycles) to remove formic acid. FT–ICR–MS analysis of these two samples showed that they are mixtures of singly and doubly tagged peptides.

Sample Preparation for MS Analysis

Immediately before use, stock solutions of all peptides were thawed and diluted to ∼1 pmol/μl in 49.5:49.5:1 H_2O:CH_3OH:formic acid. ∼5-10 μL aliquots of these solutions were pipetted into pulled glass capillary nanospray tips (made using a micropipette puller from Sutter Instruments (Novato, CA)) for MS analysis.

2.2.2 Mass Spectrometry

All experiments were carried out on a hybrid FT–ICR–MS with an ESI source as previously described in 1.2.4.[83] For ECD analysis, $(M+2H)^{2+}$ ions were isolated in Q1 and externally accumulated in the Q2 region for times ranging from several to hundreds of milliseconds, depending

on the signal intensity required to produce adequate ECD fragmentation. After accumulation, ions were then transmitted to and trapped in the cylindrical ICR cell and irradiated with electrons emitted from a dispenser cathode; the cathode heater was held at 1.2 A and the offset voltage applied to the electron gun was selected to produce ∼0.2 and ∼9.0 eV electrons while a potential of 9.0 V was applied to the grid. In double resonance-ECD (DR-ECD) experiments, the charge reduced species ($(M+2H)^{+\cdot}$) were ejected from the cell by applying a single frequency excitation with a peak-to-peak amplitude (V_{p-p}) of 5 to 40 V during the electron irradiation period. For external Q2 CAD analysis, $(M+2H)^{2+}$ ions were isolated by Q1 and accelerated into Q2 for collision with nitrogen gas. Fragment ions were accumulated for times ranging from several to hundreds of milliseconds so that a mass spectrum of sufficient intensity could be acquired. All acquired data were analyzed without apodization, with two zero-fills, and were internally calibrated based on ions $(M+2H)^{2+}$, $(M+2H)^{+\cdot}$, $(M+H)^{+}$ and their isotopes.

2.3 Experimental Results

2.3.1 ECD of a Deuterium Labeled Peptide Show the Existence of Long-Lived Radical Intermediate

ECD Spectra of Deuterium Labeled Peptide

A typical ECD spectrum of the BUSM-B peptide is shown in figure 2·3. In this case, the spectrum was obtained with low-energy (∼0.2 eV) electrons and yielded 13/16 of the possible c-ion cleavages, and ∼50% of the possible a and z ions. In almost all c_n, z_n, and a_n isotopic distributions detected, both the radical and even electron form of the assigned cleavages were observed. This resulted in a atypical isotopic pattern (figure 2·3, inset), which corresponded to (at least) three overlapped components, one for the even electron fragment (named c_n), one for the radical fragment (named $c_n\cdot$, which is 1 Da lighter), and one which is 1.0078 Da lighter than the radical fragment (named $c_n\cdot$-1). This $c_n\cdot$-1 peak appears only in the spectra of the deuterated peptides with implications discussed below. The z ions in the spectra are of very low abundance and most of the analysis described below is in regards to c ions. The two arginine residues are the most likely charge carriers, due to their high pK_a, with electron capture occurring at the C–terminal site since c ions (N–terminal fragments) are the most abundant in the fragment spectra.

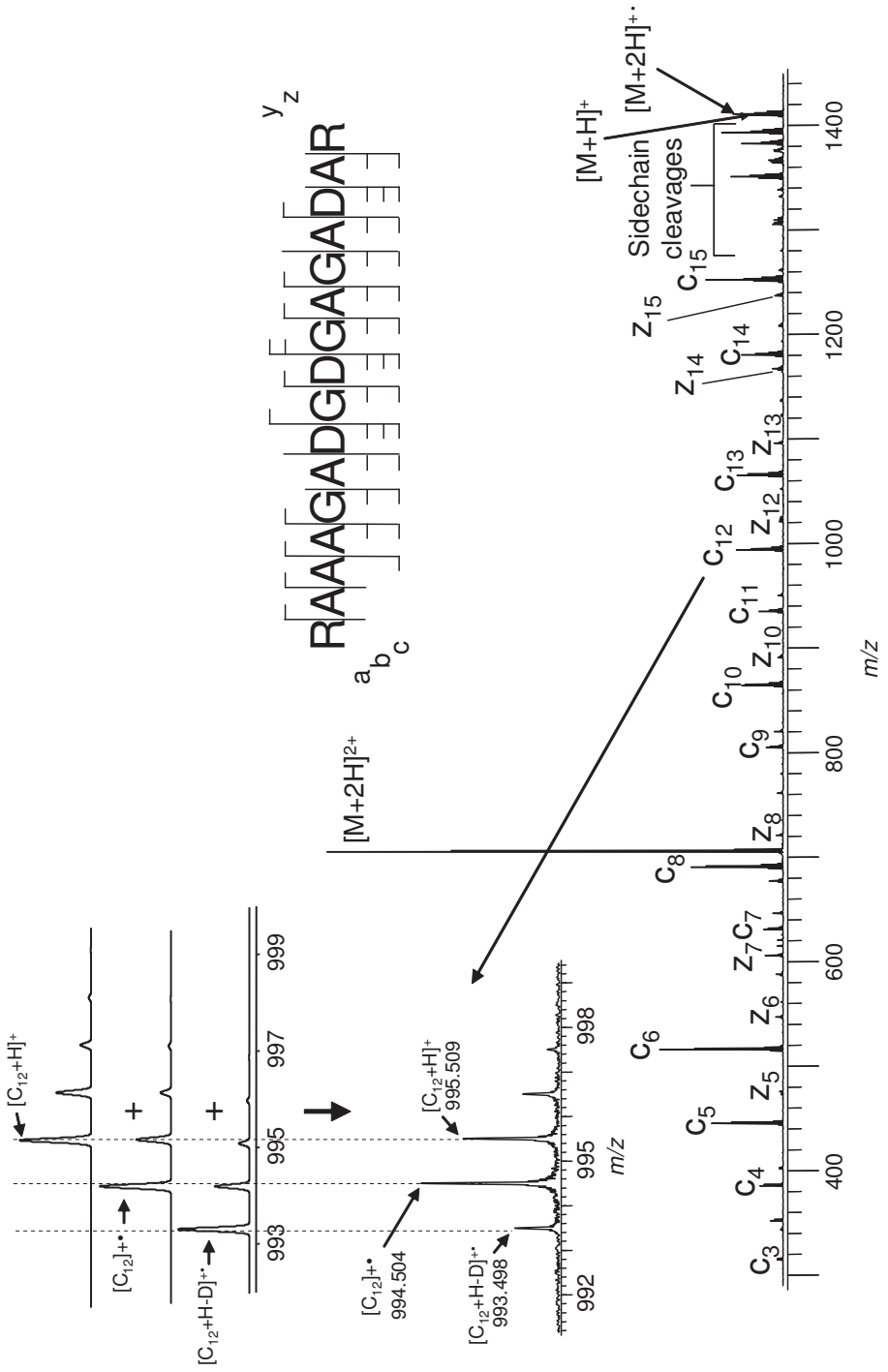

Figure 2·3: ECD mass spectra of BUSM B with ∼0.2 eV electrons. Inset, each isotopic pattern represents a convolution of three species, c_n, c_n· and c_n·-1. Shown is the example for c_{12}.

There is ∼10% under-deuteration of the precursor ion (data not shown), which is roughly evenly distributed among the eight deuterium labels as is apparent in the b_7/y_7 and b_9/y_9 ion pairs (from the initial mass spectrum without specific dissociation). The under-deuteration amount is the same for both deuterated peptides, implying a ∼97.5% purity in the d_2-glycine synthesis precursor. Thus, it is important to deduct ∼2.5% per glycine from the abundance of the deuterium-loss peak, [M + H - D], before interpretation of the data with respect to radical driven deuterium scrambling. All peptide deuterium scrambling percentages reported are ratios of the c_n·-1 to c_n· ions, and all reported deuterium scrambling ratios have been corrected for the under-deuteration as mentioned above.

To determine whether or not H/D scrambling was occurring in solution before the various MS experiments, one aliquot of the deuterium labeled peptides was simply left on the bench at pH 7 for two weeks. When the ECD spectra of these "aged" samples were run, the extent of under-deuteration was unchanged, as were the abundances of the c·-1 ion peaks. Thus, for these peptides at least, the C_{alpha} positions of glycine are not exchangeable under such conditions. Generally, as discussed above, the peptides shown were treated much more carefully with the aliquots stored in water (ice) at ∼20 °C and thawed out immediately before running the experiments.

Evidence of Deuterium Scrambling in Fragments

Figure 2·4 shows the c/c· ions series for the peptide RAAAGADGDGAGADAR and its labeled counterpart (BUSM–A and –B, respectively) from c_{15} down to c_5; c_4-c_3, while detectable, were too low in abundance to generate reliable data, and c_5 is the smallest N–terminal fragment with a glycine, and hence is the smallest fragment that can show +H-D scrambling, or presence of c_n·-1 (that is, deuterium migrating out of the fragment, and hydrogen migrating in). Most of the isotope patterns show substantial changes in the isotopic abundance distribution when comparing the non-deuterated to the deuterated peptides, but the relative isotopic abundance distributions of the ∼0.2 and ∼9 eV ECD spectra (figure 2·4 middle and bottom rows, respectively) are remarkably similar in all cases. The most marked isotopic relative abundance distribution differences are apparent in c_{14}-c_{10}, c_8 and c_6 (figure 2·4, B-F, H and J). c_9 and c_7 (figure 2·4, G and I) showed little deuterium scrambling, although the ratio of c_n to c_n· changed.

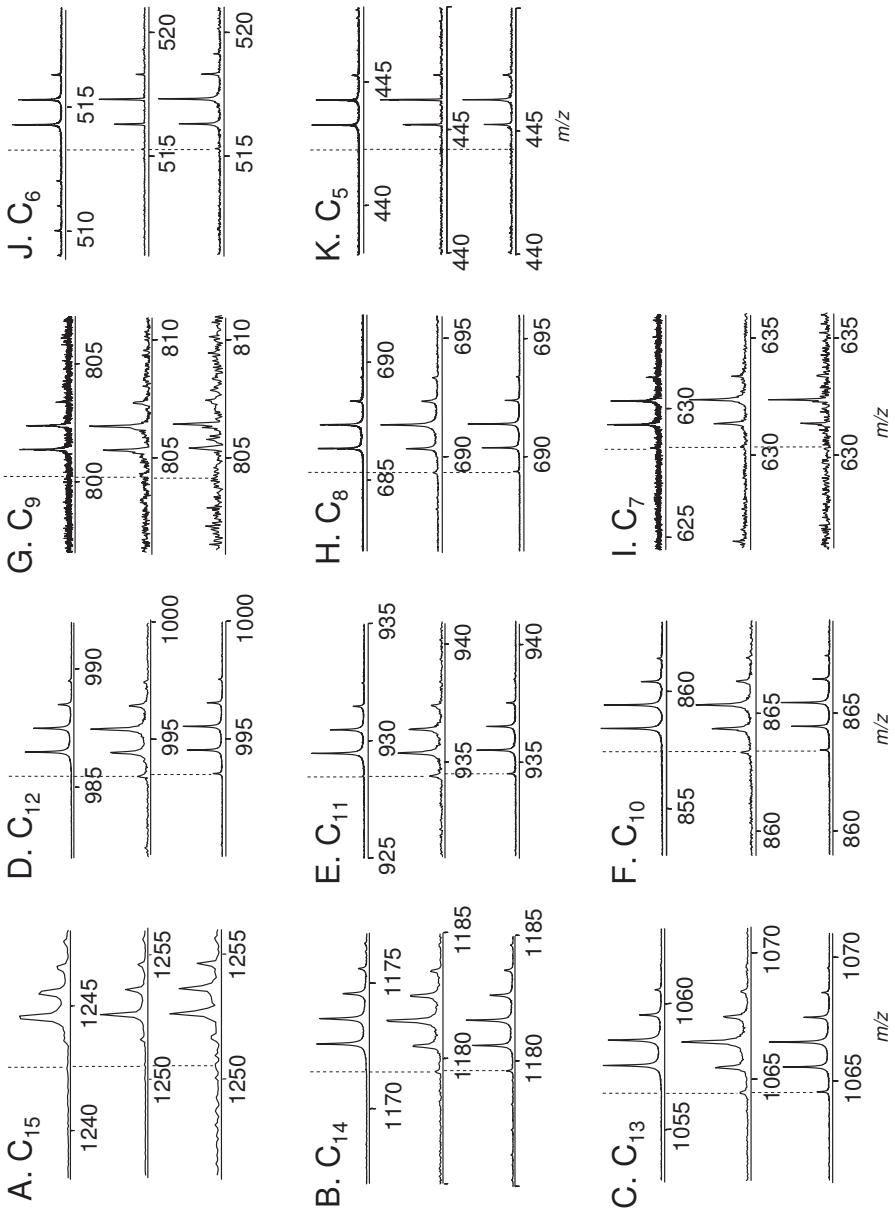

Figure 2·4: Observed c-ion regions from the ECD spectra for BUSM–A and –B. For each panel (A)-(K), top: ∼0.2 eV ECD of the undeuterated variant (BUSM–A); middle: ∼0.2 eV ECD of the deuterated variant (BUSM–B); bottom: ∼9 eV ECD of the deuterated variant (BUSM–B). Dashed lines indicates where the mass of c_n·-1 should exist.

To remove isotopic interferences, figure 2·4 was reproduced using monoisotopically isolated precursor ions by SWIFT with comparable results. These results are shown in figure 2·5, but without the additional ∼9 eV data. They also show the same trend (presence of c_n·-1) for c_{14}-c_{10}, c_8 and c_6, and lack of scrambling on c_9, c_7 and c_5.

The presence of deuterium labels on glycine has clearly caused distortion in the isotopic patterns of the fragments. The interpretation of the c_n·-1 peaks is shown in figure 2·6. In this scheme, the initial electron capture event has caused a backbone bond cleavage forming the typical c and z· ion pair that remains bound by a hydrogen bond. This complex is a long-lived radical intermediate in the electron capture dissociation mechanism. The terminal radical on the z· ion abstracts a hydrogen (or deuterium) from a more stable site, in this case the C_α of a glycine on the c fragment, thus forming a c· and z ion pair, but with the deuterium atoms scrambled. Sometime later, the hydrogen bond breaks, and the two fragments are free to be detected independently. This mechanism would be driven by the stability of the glycine C_α radical product. Figure 2·7 is essentially a variant of this same mechanism, but involves intra- rather than inter-fragment deuterium scrambling. This mechanism relies on the detection of z ions which are of very little abundance in the ECD spectra and therefore limited conclusions can be drawn from this experiment in regards to this scheme, although it is possible.

Hydrogen abstraction, and hence deuterium scrambling, is expected to be a slow reaction (microseconds) due to the need for conformational change of the gas-phase peptide ion to bring the radical close to the hydrogen before reaction. The presence of the deuterium labels resulted in substantial isotopic pattern distortions, suggesting that the radical migrates to the C_α of glycine during ECD. However the radical migration, when it occurs, is likely to occur several (or many) times before cleavage. The data, primarily in figures 2·4 and 2·5, show that H/D scrambling is occurring from the C_α positions. As discussed above, most likely interpretation of these data is that many of the observed ECD fragments are formed from a radical intermediate complex which has undergone one or more radical rearrangements via hydrogen abstraction from the C_α positions.

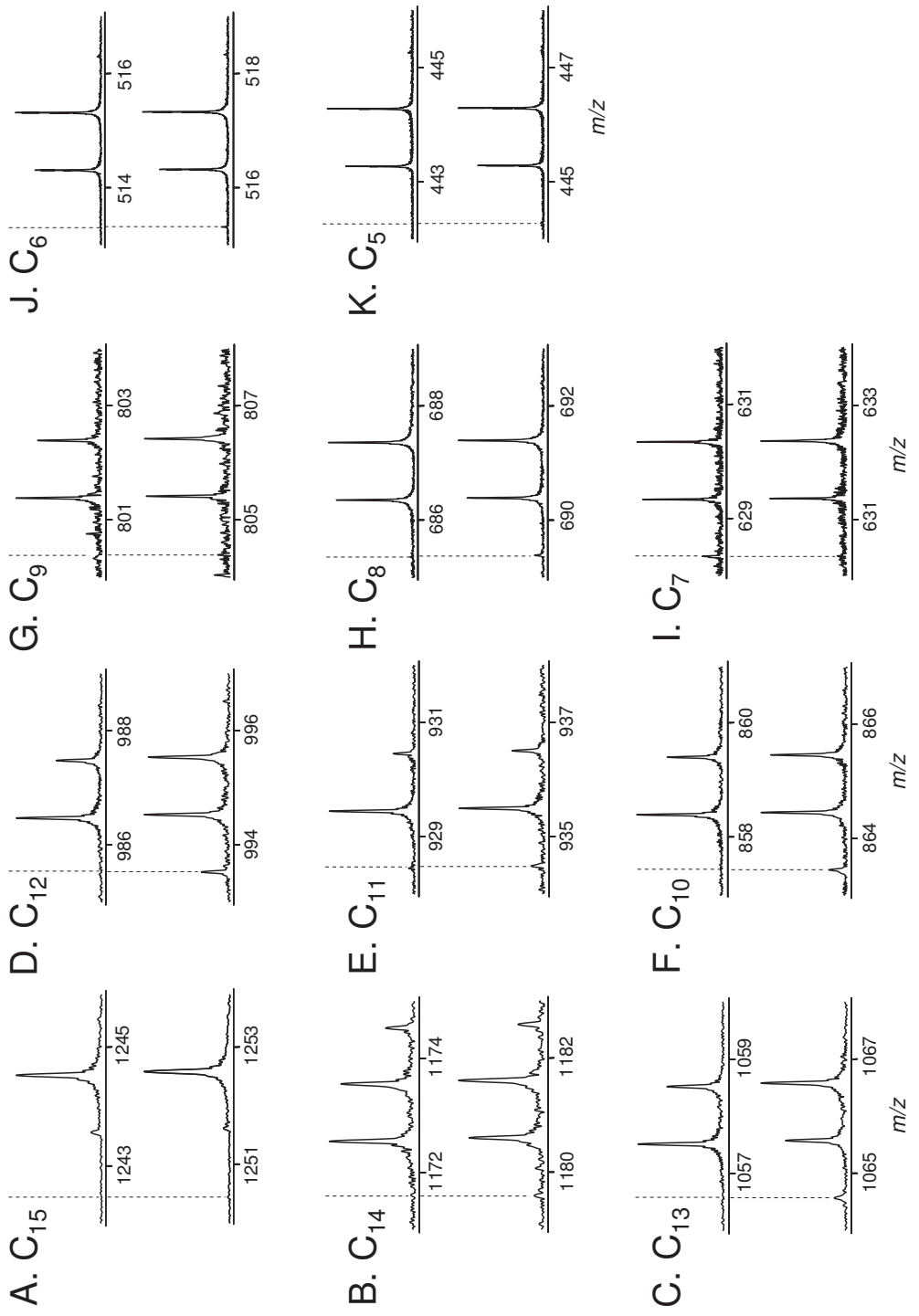

Figure 2·5: Observed c-ion regions from the ∼0.2 eV ECD spectra of BUSM–A and –B after monoisotopic isolation of the precursor ion. For each panel (A)-(K), top: the undeuterated variant (BUSM–A); bottom: the deuterated variant (BUSM–B). Dashed lines indicates where the mass of c_n·-1 should exist.

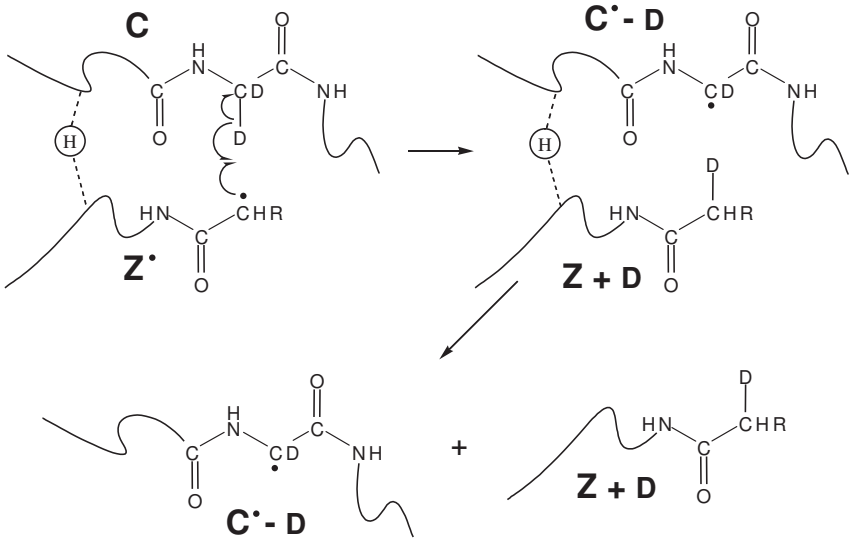

Figure 2·6: One possible mechanism (intermolecular) to describe observation of (-H+D) scrambling c· fragments.

Deuterium Scrambling in ECD versus Energetic Dissociation

CAD experiments performed in Q2 in transit to the ICR cell at ∼23 eV lab-frame collision energy was used to probe the scrambling of deuterium under ergodic fragmentation. The results are plotted in figure 2·8 and compared with the ECD data. The b and c ions are plotted together for comparison in terms of the approximate number of exchangeable hydrogens. This figure plots the ratio of the ion abundances (from figure 2·4) corrected for under-deuteration as discussed above. Deuterium scrambling of even electron molecular ions under CAD conditions is well known,[182–184] and has been explored in the same manner as was done here with deuterium located on the C_α positions.[185] Under energetic (23 eV) CAD conditions for BUSM–B (figure 2·4, black bars), scrambling occurred in most fragment ion isotopic distributions, with the notable exception of the extremely labile b_9/y_7 and b_7/y_9 complementary ion pairs. Thus, in CAD, these labile fragments undergo dissociation before scrambling, but the rest of the fragments have time for exchange before cleavage.

In spite of the greater energy available, the 23 eV CAD show much less scrambling than the ECD spectra. Furthermore, the ∼0.2 eV ECD spectra are remarkably similar to the ∼9 eV ECD spectra (figure 2·4), indicating that, in this energy range, deuterium scrambling is not highly dependent on the internal vibrational energy. Thus, for the radical cations produced by

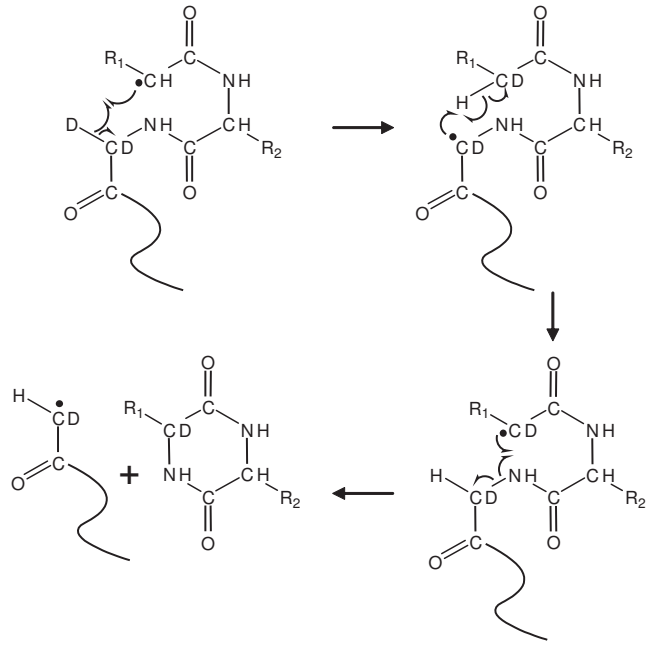

Figure 2·7: A second possible mechanism (intramolecular) to describe observation of (+H-D) scrambling in fragments.

ECD, scrambling must occur with transition-state barriers much lower than the redistributed vibrational energy of the molecule, which agrees with existing calculations in the literature.[176,177,186]

Figure 2·8 (bottom) shows the branching ratios of the c_n and $c_n\cdot$ ions. These data are plotted from the c_n and $c_n\cdot$ abundances of the ECD spectra of the monoisotopically isolated BUSM–B peptide molecular ion (figure 2·5). Except for c_{11} and c_{15}, most of the branching ratios were $\sim$1. c_{15} showed almost no $c_{15}\cdot$ formation, implying that the terminal arginine residue prefers to leave as a neutral radical species. Likewise, the c_{11} peak showed strong preference ($\sim$3-fold) for the formation of $c_{11}\cdot$. The reasons for these strong deviations from the average are unclear, but they are likely to be related to the gas-phase folding structure of these peptides.

Kinetic Isotope Effect in ECD of Deuterated Peptides

In any comparison of hydrogen versus deuterium labeled reactions, it is important to consider a kinetic isotope (KI) effect in the fragmentation. In this case, the primary isotope effect is considered; radical migration occurs via dissociation of C-D and C-H . If several reaction channels are available, and at least one of these channels involves H versus D loss or migration,

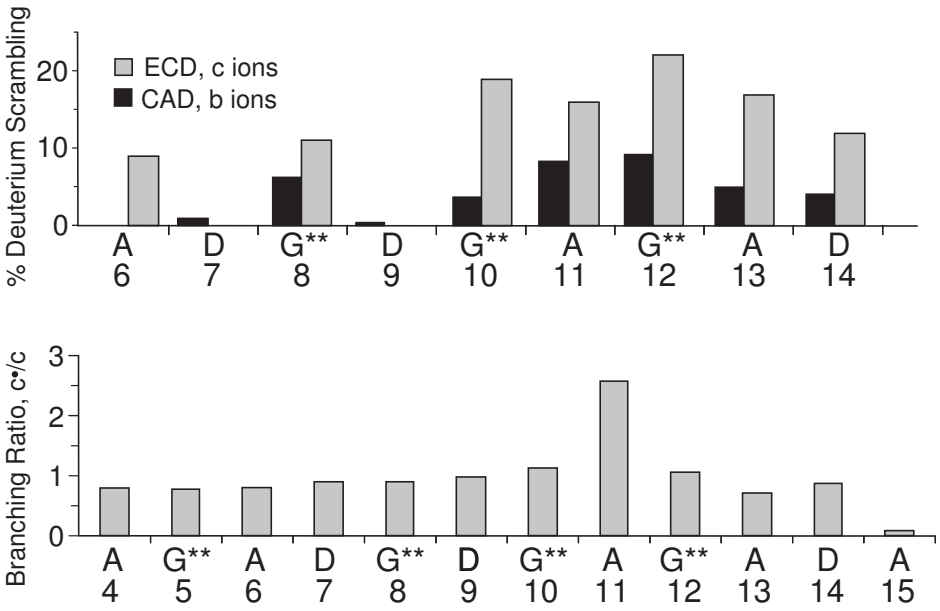

Figure 2·8: (A) Site specific (+H-D) scrambling ratios for BUSM–B, comparison of ∼0.2 eV ECD with CAD Experiment. (B) Branching ratio of c ion formation over c ion formation (from figure 2·5).

the KI effect can greatly influence the abundances of the reaction products, sometimes an order of magnitude or more in abundance.[187] In a free radical cascade, if the reaction channel quenches the radical or allows a neutral radical loss, the reaction is over. The KI effect, along with the fact that the charge sites in these peptides are protons, not deuterons, is one possible reason why H· loss is observed in the charge reduced radical cation $(M+2H)^{+\cdot}$, but D· loss is not (data not shown). However, if the reaction channel chosen does not result in the loss of a radical cleavage fragment, the radical is still present in the molecule and can initiate further reactions. For inter- or intramolecular hydrogen (deuterium) abstraction reactions (as in figures 2·6 and 2·7), this is the case. In spite of the KI effect that must be present in C_α hydrogen abstraction reactions, the long time frame of the FT–ICR–MS experiments (seconds) appears to partially overcome the effect so that deuteriums are allowed to migrate. Furthermore, if the KI effect is partially suppressing the deuterium migration relative to hydrogen migration, as would be expected, the migration percentages reported above must be considered underestimates.

2.3.2 Double Resonance–Electron Capture Dissociation (DR–ECD) of Peptides to Probe the Lifetimes of the Radical Intermediate

ECD of Fibrinopeptide B

ECD of fibrinopeptide B (EGVNDNEEGFFSAR) generated a complete z-ion series within the m/z range used (figure 2·9–A). ECD fragments are often considered as a snapshot of the

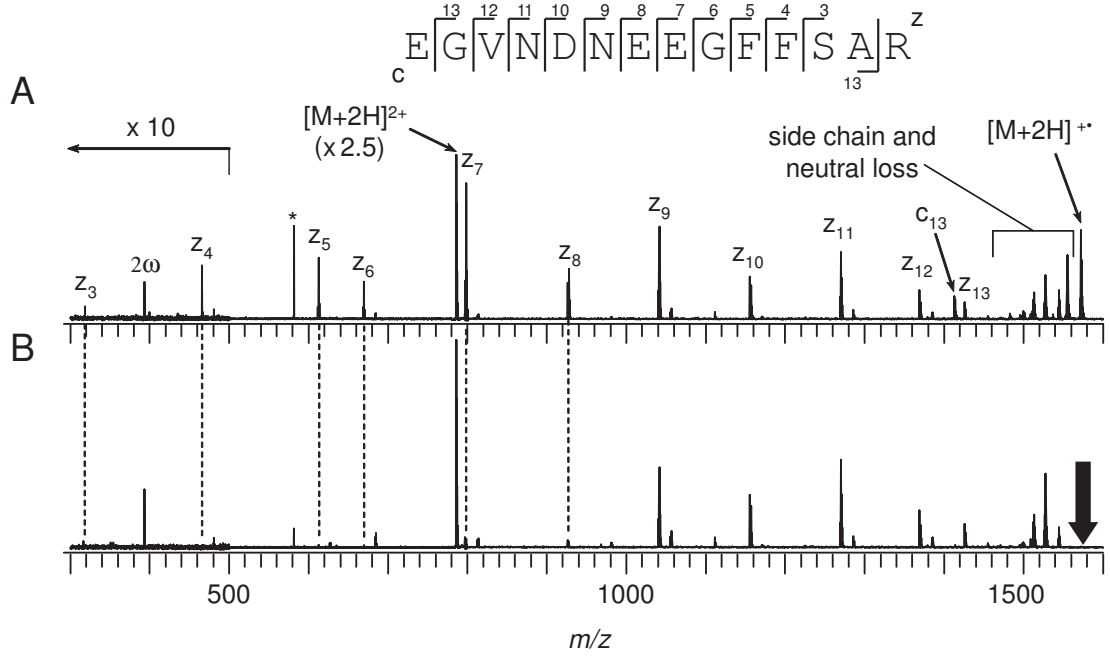

Figure 2·9: ECD spectra of fibrinopeptide B without (A) and with (B) resonant ejection of the charge reduced molecular ion. Dashed lines indicate fragment ions that significantly decrease with DR ejection of $(M+2H)^{+\cdot}$. * and 2ω represent electronic noise and the second harmonic of the $(M+2H)^{2+}$ isolated species, respectively.

ion conformations at the time of electron capture dissociation, with possible tertiary structures hindering the separation of product ions. It is tempting to claim that this peptide molecular ion has negligible tertiary structures, as all inter-residue cleavages were readily observed. However, an ECD experiment often involves a delay of at least hundreds of milliseconds (and often several seconds) between the dissociation event and the product ion excitation/detection. During this period, the noncovalent bonds holding the fragment ion pair together could well break down, possibly due to the excess energy deposited by electron capture and the Columbic repulsion of the fragment ions, or simply due to the slow heating by collisions with background gas molecules and background blackbody radiation, thus taking away conformation information

typically stored in the missing cleavages. Sometimes, the lost information can be restored by observing fragment ion abundance increase upon ion activation via heating or IR irradiation.[66,72]

DR–ECD of Fibrinopeptide B

Since ECD is initiated by capture of an electron to generate the charge reduced species, the $(M+2H)^{+\cdot}$ ion, through which all fragment ions are formed (see figure 1·7), a DR experiment with excitation at that *m/z* should provide a rough measurement of the product ion lifetimes for all fragments, which should correlate with the strength of various non-covalent interactions. DR experiments can be performed in an FT–ICR[188] or ion trap MS,[179] instruments with the ability to eject ions from the trap based on their *m/z* value. DR experiments reveal the fragmentation pathway resulting from collisions of an ion; ejection of a particular ion will eliminate all daughter fragments thereof during collisions with a neutral gas. Originally developed to identify chemically coupled ion-molecule reactions in complex mixtures in ICR studies, DR was adapted to FT–MS,[188] and other kinds of MS,[179] and was used to study the mechanisms of CAD and BIRD.[189–191] Using DR, Anicich *et al.* were able to determine the mean lifetime of the collision complex $H_2C_6N_2^+$ in the ion-molecule reaction between HC_3N^+ and HC_3N to be 180 ms.[188] Therefore, an analogous experiment to the studies mentioned can be performed with ECD with DR ejection of the reduced molecular ion ($(M+nH)^{(n-1)\cdot}$) occurring during the electron irradiation event.

The bottom of figure 2·9–B shows the ECD spectrum of fibrinopeptide B with resonant ejection of the charge reduced molecular ion (m/z = 1571.7, V_{p-p} = 40 V) during electron irradiation. The peak intensity of every z ion smaller than z_9 decreased sharply, but that of z_9 and larger ions remained roughly the same. Previous studies have shown that, after the initial N-C_α bond cleavage, the c/z· ion pair generated by ECD may still be held together by non-covalent interactions such as hydrogen bonds and salt bridges, preventing the detection of individual fragments.[72] Fibrinopeptide B has an acidic residue rich region, and the side chains of these residues could form multiple hydrogen bonds with the C–terminal arginine. When ECD cleaved any bond in or to the right (C–terminal) side of this region, the resulting c(neutral)/z·(charged) ion pair would still be held together by these hydrogen bonds, and might

have a lifetime too long to dissociate before they were ejected from the cell. It is thus of no surprise that small z fragments showed steeper drop in abundance as the complementary c neutrals have more acidic residues available to interact with the terminal arginine, either as neutral hydrogen bonds or as ionic interactions. z_9 and z_{10} ions showed only slight decreases in their peak intensities despite the presence of an Asn and Asp residue, respectively, on their complementary c neutrals. This is due to the conformation of the peptide ion that produced them. As all z ions retained charge at the C–terminal arginine side chain, the neutralized charge had to come from the N–terminal $-NH_3^+$ group. The classic picture of ECD has the N-C_α bond cleavage occurring C–terminal to the charge solvated carbonyl, thus the $z_{9/10}$ generating peptide ion should have the N–terminus hydrogen bonded to either Asn4 or Asp5, preventing Arg14 from binding there.

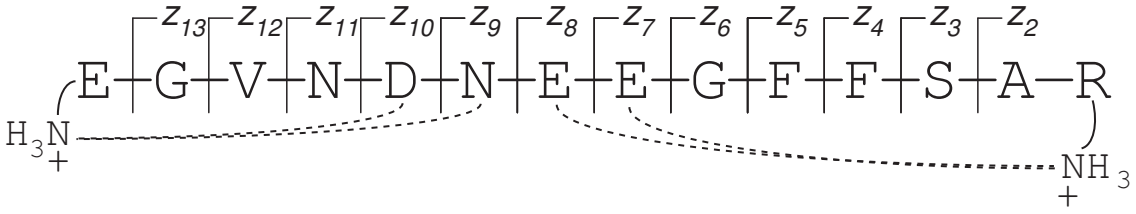

Figure 2·10: Charge solvation scheme for fibrinopeptide B. Interaction between N–terminus and Asp5 and/or Asn4 and the arginine side chain with Glu7 and Glu8 indicated by dashed lines.

Lifetime of Radical Intermediates

The lifetime of reaction intermediates can be measured using DR, provided the lifetime is within the resonance ejection time frame. Figure 2·11–A shows part of the ECD spectra of fibrinopeptide B with various ejection voltages (ejection of $(M+2H)_{+\cdot}$). The ejection time, t, relates to the excitation voltage (peak-to-peak), V_{p-p}, via the equation[188]

$$t = \frac{2drB}{V_{p-p}} \tag{2.1}$$

where d is the cell diameter, r is the ejection radius that can be approximated as d/2, and B is the magnetic field. The drop in fragment ion abundances as a function of V_{p-p} directly correlates with the number of ions ejected and, hence, the number of ions that survive for at

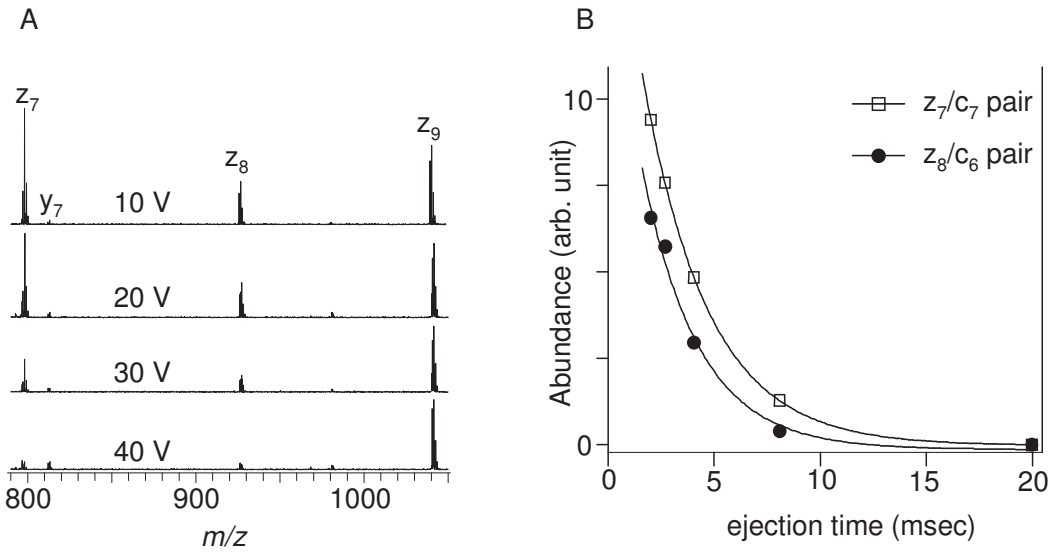

Figure 2·11: (A) Expanded region of ECD spectra of fibrinopeptide B with reduced molecular ion ejection at various ejection voltage; from top to bottom: 0, 10, 20, and 40 V. (B) First-order decay of the remaining ion pair abundance (c_7/z_7 and c_8/z_6) as a function of ejection time (as calculated from ejection voltage according to equation 2.1). Solid lines are the single exponential fits.

least time, t. Figure 2·11–B plots the abundance of "surviving" intermediates as a function of time for the z_7 and z_8 ions. Since fragmentation of the hydrogen bonded intermediate complex is a unimolecular dissociation, these values can be fit to a single exponential and the lifetimes (half-lives) were calculated to be 2.1 and 1.8 ms, respectively. This is sufficiently long to allow multiple radical rearrangements, such as those observed in the cyclic peptide experiment,[67] and the H/D scrambling experiment described above. It is important to point out that the above lifetime calculation assumes that all fragment ions produced before complete ejection of the corresponding intermediates could be detected with the same efficiency as those produced in the center of the cell. In reality, partial excitation of the ions would destroy the ion coherence for subsequent cyclotron orbit excitation, resulting in decreased detection efficiency. Strict treatment of this issue is beyond this research, but the net result is an approximately 2-fold overestimate of the intermediate lifetimes. Once we realize that the upper limit of the lifetime of these intermediates is in the millisecond range, it is easy to understand why conventional ECD failed to reveal the existence of these noncovalent interactions in small peptides, as the delay between the ECD event and fragment ion detection is often two orders of magnitude longer than what it takes for fragment ions to separate. Lastly, while the calculated lifetimes

are only approximate in absolute terms, their relative values should still give good indication of the relative strengths of the various noncovalent interactions in the molecular ion.

Fragment Ion Abundances in DR–ECD Reflect Hydrogen Bonds

The presence of a hydrogen bond between C–terminal arginine and acidic residues in fibrinopeptide B was suggested based on different behavior of z_8 and z_9 ions upon reduced ion ejection. The possibility of relating the fragment ion formation time (or the dissociation time of the corresponding intermediate) to the structure of the precursor ion is a reasonable hypothesis but required further testing. Such a test can be performed experimentally by demonstrating dissimilar behavior of a similar peptide with the acidic residues replaced by hydrophobic residues, or an isomeric analog with acidic residues at different positions.

To this end, ECD and DR-ECD experiments were carried out on a pair of peptides: BUSM–A (RAAAGADGDGAGADAR) and BUSM–A1 (AAAGADGDGAGADAR). ECD of BUSM–A produced 13 c ions of relatively high abundance and seven less-abundant z ions (figure 2·12–A). This synthetic peptide has an arginine on each end, and three acidic residues spread out in the middle, giving rise to the possibility of forming multiple hydrogen bonds throughout the molecule. Because of this, most fragment ion peaks showed steep drop in intensity upon resonance ejection of the charge reduced species (m/z ∼1402.6, figure 2·12–B). However, four c ions (c_6, c_8, c_{13}, and c_{15}), showed only moderate changes in their abundances, and all but one (c_{15}) of them resulted from cleavages N–terminal to an aspartyl residue (dashed lines in 2·12–B). As the formation of all c ions required the charge on the C–terminal arginine side chain to be neutralized while it was hydrogen bonded to the carbonyl N–terminal to the cleavage site, and the cleavage inevitably broke this hydrogen bond, the only possible noncovalent interaction that can hold the two fragment pieces together would be between the N–terminal arginine and one or more of the three aspartyl residues. The hydrogen bond between Arg16 and the carbonyl N–terminal to an aspartyl residue necessary to generate cleavages is likely to disrupt some of these interactions, thus facilitating the separation of these fragment ions once they are formed.

Lack of N–terminal arginine in BUSM–A1 peptide led to a very different ECD spectrum (figure 2·12–C) from that of BUSM–A. The predominant fragment ions were of the z type, indicating that the protonated N–terminal amine was the preferential site of charge neutralization.

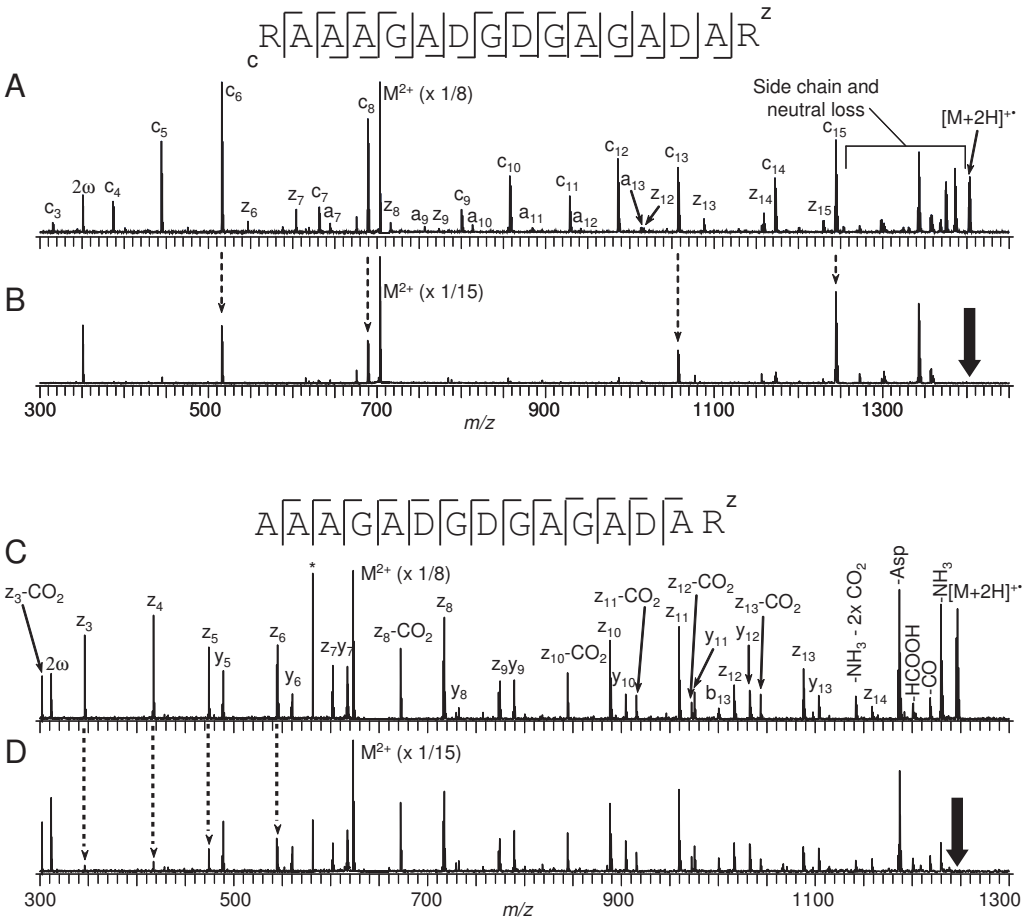

Figure 2·12: ECD (A) and DR-ECD (B) spectra of the BUSM–A peptide, and the BUSM–A1 peptide (C) and (D), respectively. Large black arrows indicate mass region where the DR pulse is applied (*i.e.* $(M+2H)^{+\cdot}$). For A and B, dashed arrows indicate fragments that do not significantly change in abundance with resonance ejection. For C and D, dashed arrows specify fragments that notably decrease in abundance with resonance ejection. * and 2ω represent electronic noise and the second harmonic of the $(M+2H)^{2+}$ isolated species, respectively.

Because no N–terminal arginine was available to form multiple hydrogen bonds with the side chains of aspartyl residues, the unique pattern of fragment ion abundance change for cleavages N–terminal to an aspartyl residue was not observed in its DR–ECD spectrum (figure 2·12–D). Instead, the DR–ECD spectrum displayed a trend similar to that observed in the fibrinopeptide B experiment, namely, larger z ions showed little abundance change, while the smaller ones (*e.g.* z_3, z_4, z_5 and z_6, indicated by dashed lines in figure 2·12–D) showed drastic drop in their abundances upon resonance ejection. The transition took place at z_8, once again, at a cleavage site one residue remote (to the C–terminal side) from the last available acidic residue (Asp6) that is capable of forming a hydrogen bond with the C–terminal arginine (Arg15). The necessity of the N–terminal $-NH_3^+$ group hydrogen bonding to the carbonyl of Gly7 to initiate the formation of z_8 ion presented a steric hindrance for Arg15 to bind the nearby Asp6, agreeing with the hypothesis set forth in the fibrinopeptide B example.

The BUSM–A peptide is known for generating unusually high abundance of odd electron c· ions (also observed in section 2.3.1). A closer look at each individual c ion peak revealed that nearly every one of them showed steeper drop in its odd electron form than in its even electron form (figure 2·13–A), which is more apparent when the survival ratios (the ratio of the ion abundance with the application of on-resonance ejection waveform to that without ion ejection) were plotted for each individual c and c· ion (figure 2·13–B). Note that the Ionspec FTMS software (Irvine, CA) does not correct for ion charge when reporting ion abundance values, even though an ICR cell has a linear response to the number of charges. However, in calculating the survival ratio, it is not necessary to correct for the charges as the ion abundance ratio is always taken for the same ion and, naturally, of the same charge state. Currently, it is believed that the initial ECD cleavage generates a c/z· ion pair, and the formation of c· ions comes from intermolecular hydrogen transfer, which can take up to ms to occur, thus making its population more susceptible to resonance ejection of the intermediates.

2.3.3 ECD of Peptides Labeled with a Radical Trap Moiety

ECD and DR–ECD Spectra of Peptides Labeled with a Radical Trap Moiety

Figure 2·14 depicts the ECD spectra of the untagged peptide (figure 2·14–A), the singly-tagged peptides (figure 2·14–B and –C), and the doubly-tagged peptide (figure 2·14–D) in which the

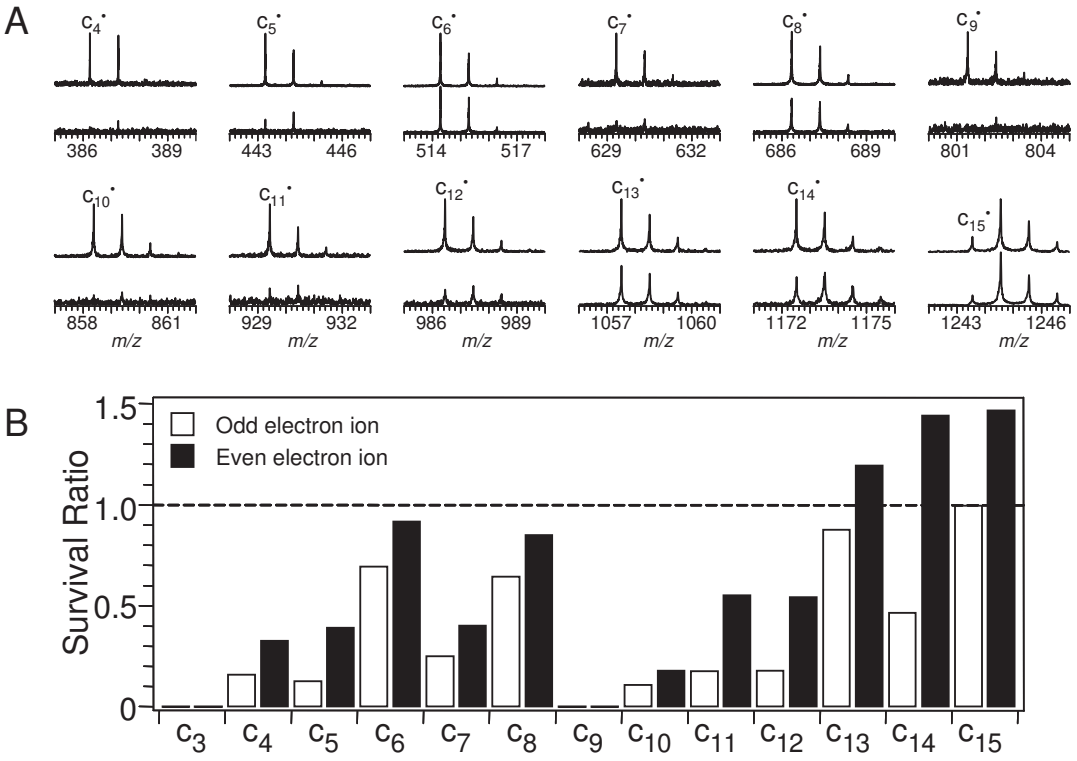

Figure 2·13: (A) Expanded regions of the ECD (top) and DR-ECD (bottom) spectra of the BUSM–A peptide (from figure 2·12, A and B); (B) the ratio of ion abundance in DR–ECD spectrum versus that in the normal ECD spectrum (named survival ratio) for all c-ions observed.

tag is a coumarin moiety (figure 2·1) (see table 2.1). The cleavages observed in these four spectra are also plotted in figures 2·16 and 2·17. The spectrum for untagged substance P (figure 2·14–A) yields seven out of eight possible backbone cleavages; the proline N–C_α cleavage cannot be observed.[62] These cleavages are primarily c-type ions (attributable to the N–terminal charge), but a fragment of low abundance corresponding to the z_9 ion (unlabeled) is visible at *m/z* 1080. Lysine-tagged substance P (figure 2·14–B) produced six backbone c-type cleavages and one a-type cleavage, but the N–terminus-tagged peptide generated only four c-type ions (figure 2·14–C). In both spectra, these backbone cleavages are reduced in intensity compared with the unlabeled peptide (figure 2·14–A). Figure 2·14–D shows the ECD spectrum of the doubly tagged substance P. This spectrum shows very few backbone cleavages at even more diminished intensities, and side chain cleavages at higher intensities. For figure 2·14–B, C, and D, the side chain cleavages usually involve multiple losses of various groups, which are summarized in the plots in figures 2·16 and 2·17. Also, figure 2·15 expands the side chain

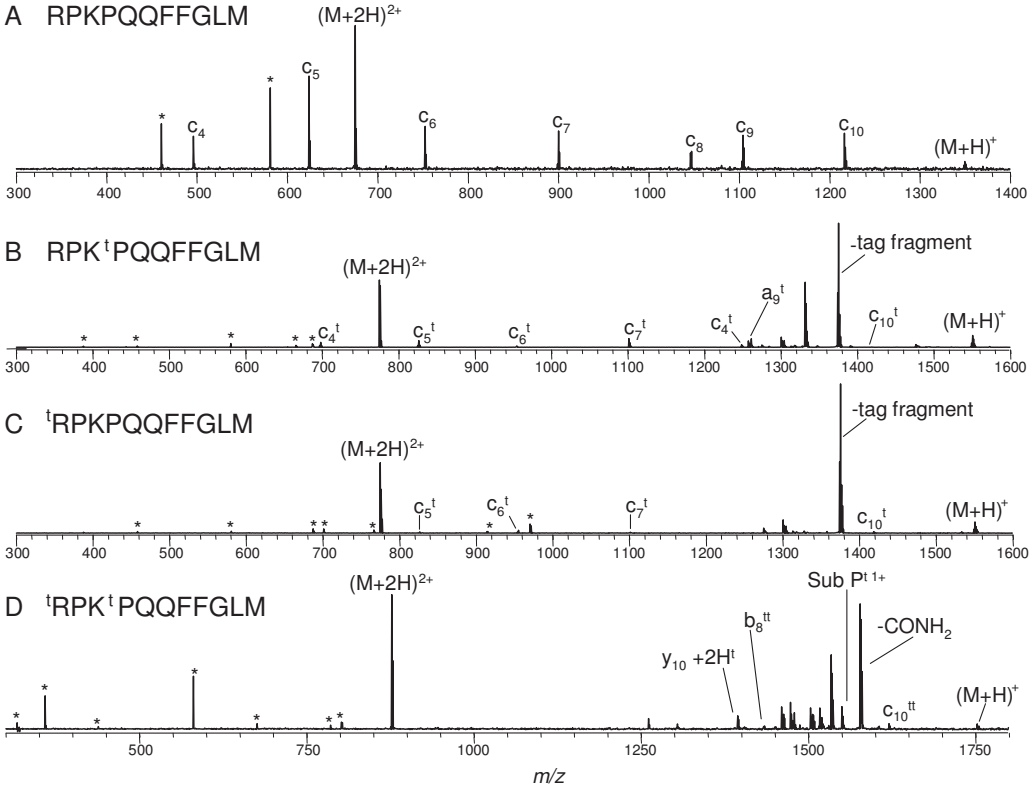

Figure 2·14: (A) ECD spectrum of substance P; (B) ECD spectrum substance P labeled with a coumarin tag on the lysine side chain; (C) ECD spectrum substance P labeled with a coumarin moiety on the N–terminal amine; (D) ECD spectrum of substance P labeled with two coumarin tags, one on lysine and one on the N–terminus. Asterisks indicate electronic noise or harmonics and "t"s represent the position of the tag in the peptide sequence and if a peak designation contains a tag.

cleavage regions from figure 2·14 and losses are tabulated in table 2.2.

Figures 2·18 and 2·19 show the results from DR-ECD experiments performed on the tagged substance P in which the charge reduced molecular ion $(M+2H)^{+\cdot}$ is continuously ejected from the ICR cell during the ECD experiment (see section 2.3.2). Figure 2·18 shows the ECD spectrum of the singly-tagged substance P with and without resonance ejection at m/z 1550, the m/z of the charge reduced molecular ion. In this case, the two variants of the singly-tagged species are not separated, so this is the ECD spectrum of the mixture of the N–terminally tagged and lysine tagged species. Figure 2·19 shows the ECD spectrum of the doubly tagged substance P with and without resonance ejection. In both DR-ECD experiments, the peaks resulting from side chain cleavages are dramatically reduced in intensity. In figure 2·18–B, the

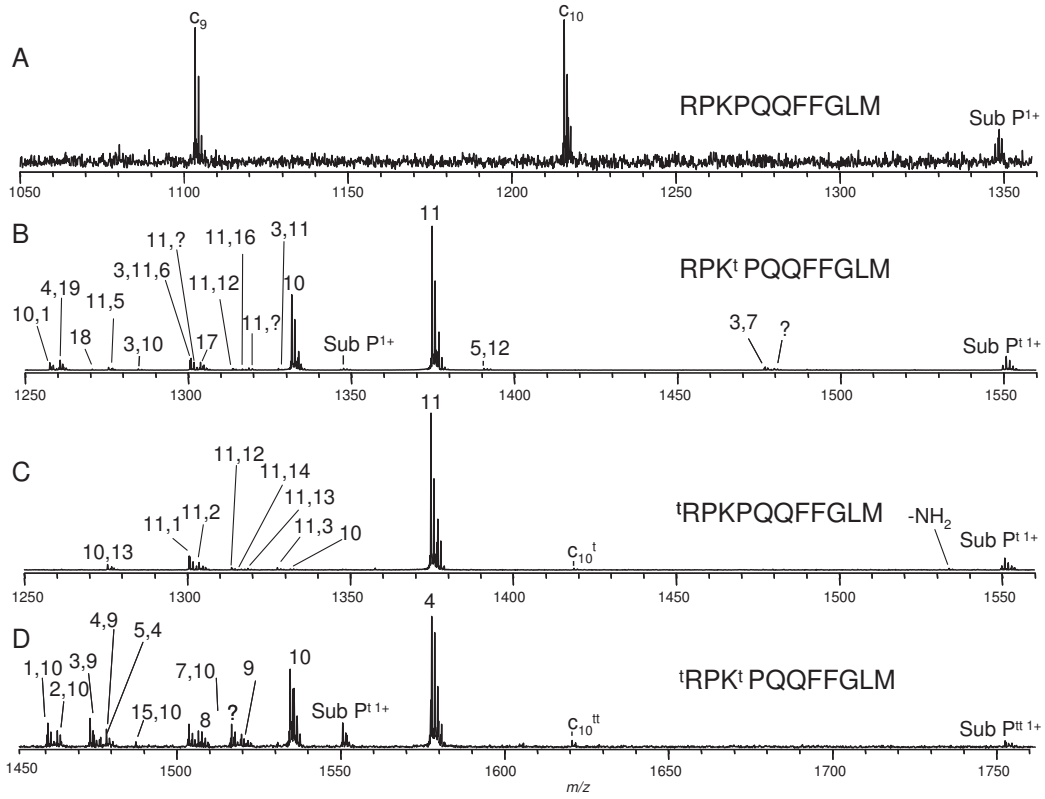

Figure 2·15: Zoomed in region of expected side chain cleavages from the ECD spectrum of (A) substance P (1050-1360 *m/z*), (B) substance P tagged on the lysine side chain (1250-1560 *m/z*), (C) substance P tagged on the N–terminus (1250-1560 *m/z*) and (D) substance P with tags on the lysine side chain and N–terminus (1450-1760 *m/z*). Peaks labeled with numbers and symbols are designated in table 2.2. "t"s represent the position of the tag in the peptide sequence and if a peak designation contains a tag

fragment ions resulting from backbone cleavages c_5 to c_{10} experience, for the most part, minimal abundance changes, but c_4 is eliminated from the spectrum. In figure 2·19–B, the side chain loss peaks around *m/z* 1500 are completely eliminated with double resonance ejection.

Effect of Coumarin Moiety on the ECD Spectra of Substance P

The addition of the coumarin tag, which contains a large sp^2 conjugated system, resulted in dramatic reduction in backbone fragments. The intensities of the backbone cleavage peaks are diminished in spectra of singly-tagged and doubly tagged species. The coumarin tags delocalized electronic structure serves as a radical trap by providing sites where a radical can be resonantly stabilized. The lower intensities of backbone fragment peaks can be attributed to

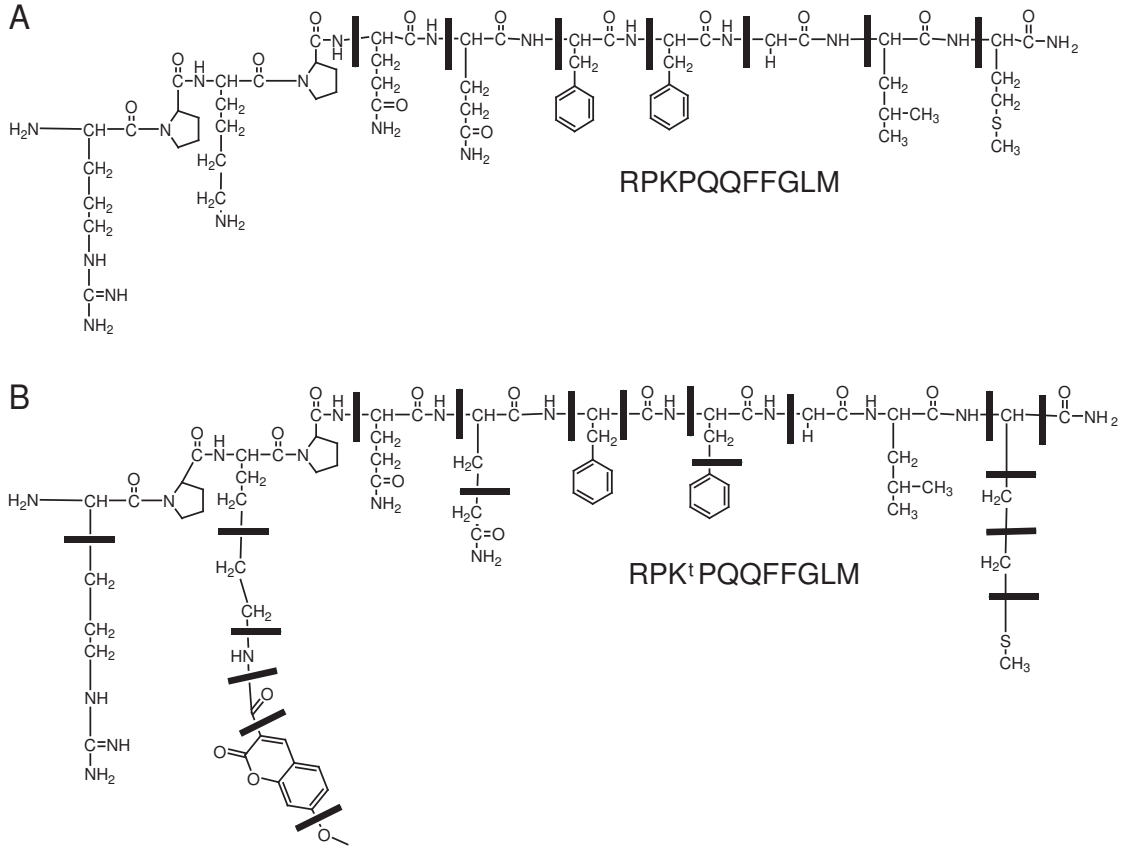

Figure 2·16: Cleavage patterns from the ECD spectrum of (A) substance P (from figure 2·14–A and 2·15–A) and (B) substance P labeled at lysine side chain with the coumarin tag (from figure 2·14–B and 2·15–B).

the electron capture in the Rydberg state followed by internal conversion to a low electronic, but vibrationally excited, state. A large conjugated system such as the coumarin tag usually involves more closely-spaced energy levels compared with a sp^3 hybridized system. Thus, internal conversion that requires resonant interaction of two states, from the Rydberg state to a low lying electronic state, within the coumarin tag is highly probable, which may account for the electron landing in the local energy minimum of the tag rather than at the charge sites. The resonance stabilization of the coumarin tag provides a local potential minimum, which stabilizes the electron and thus retains it at the coumarin site.

In singly-tagged substance P, with the tag residing either on the N–terminus or the side chain of the lysine residue, the side chain cleavages included fragments from arginine, lysine, glutamine, methionine, leucine, and phenylalanine. In particular, the $C_6H_5\cdot$ neutral loss, previously unreported, was observed from the lysine tagged species. The side chain fragmentation

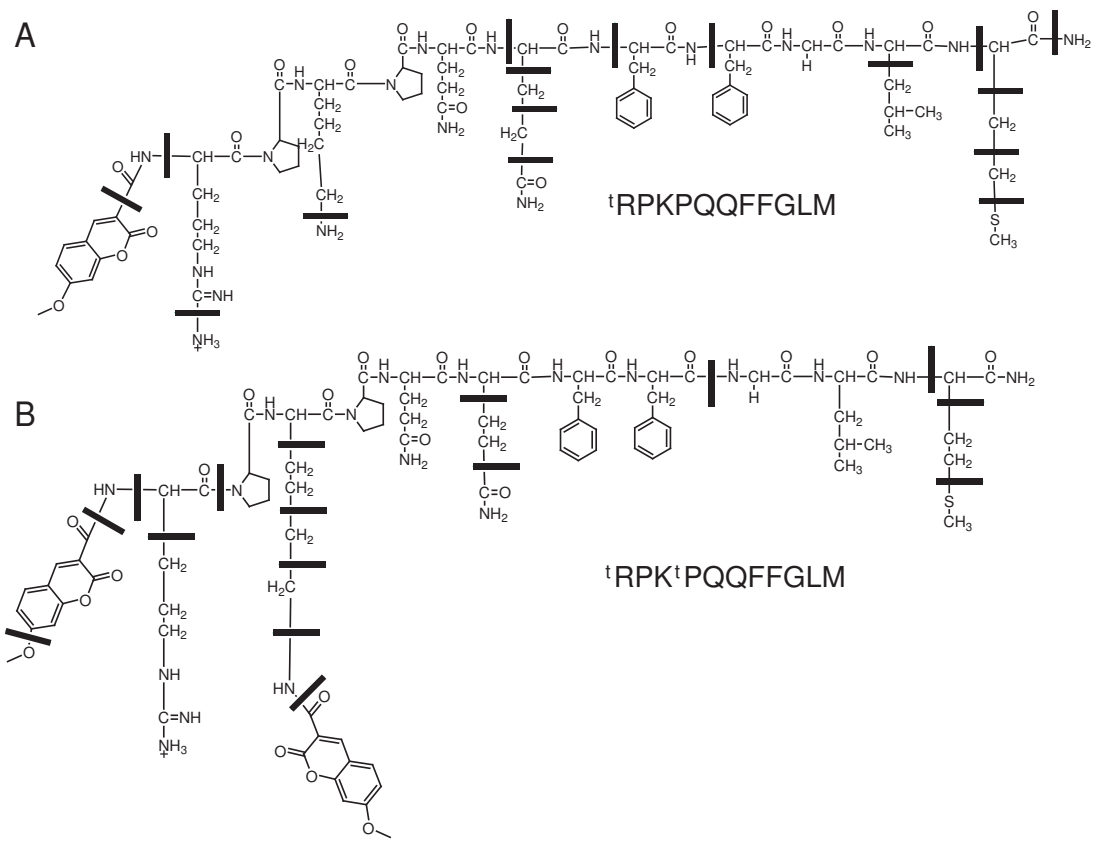

Figure 2·17: Cleavage patterns from the ECD spectrum of (A) substance P labeled at the N–terminus with the coumarin tag (from figure 2·14–C and 2·15–C) and (B) substance P labeled at both the lysine side chain and N–terminus with the coumarin tag (from figure 2·14–D and 2·15–D).

mechanisms of arginine, lysine, glutamine, and methionine are discussed by Cooper *et al.*[74] and that of leucine by Kjeldsen *et al.*.[77] The proposed mechanism of fragmentation of the phenylalanine side chain is under speculation however, the π-bonded structure of the tag offers an intriguing possibility. The conjugated systems of the tag and the two phenylalanine side chains have the potential to undergo π-stacking interactions (and would be expected to do so in solution phase). π-Stacking of the coumarin moiety and the phenylalanine side chains could enable radical transfer onto the phenylalanine side chain, to result in the loss of a phenyl radical group. However, the low abundance of the fragment resulting from this loss suggests that π-stacking in the gas phase is not a strong interaction.

Other small molecule losses from both singly-tagged peptides included carbon monoxide and ammonia losses, both of which have been previously reported and mechanisms for their

Table 2.2: Side Chain Cleavage Assignments

Designation	Assignment
1	loss of C_3H_6S (from met)
2	loss of $C_3NOH_6\cdot$ (from glu)
3	loss of CH_6S (from met)
4	loss of $CONH_2$ (from glu)
5	loss of $C_4H_9N_3$ (from arg)
6	loss of C_2H_5 (from met)
7	loss of CO from tag$\cdot$
8	loss of C_2NH_6 (from lys)
9	loss of CNH_5 (from lys)
10	loss of tag and $NH_2\cdot$
11	loss of tag fragment
12	loss of C_2H_5S (from met)
13	loss of leucine side chain
14	loss of $C_2NOH_2\cdot$ (from glu)
15	loss of CSH_5 (from met)
16	loss of C_2ONH_4 (from glu)
17	loss of C_2NH_5 (from lys)
18	loss of $C_6H_5\cdot$ (from phe)
19	loss of tag and C_2NH_4
*	electronic noise
t	contains one tag
tt	contains two tags
?	unknown

losses discussed.[74,75,192] Finally, the singly-tagged peptides contained losses of the tag as well as a tag fragment. The mixture of singly-tagged substance P was separated via HPLC and although, with ECD, no backbone cleavages were generated that could be used to differentiate between the lysine and N–terminus tagged peptides, losses of the tag attached to parts of the lysine side chain present in one spectrum and the lack of such losses in the other spectrum served as indicators to distinguish between the two species. CAD was also used to confirm this assignment (data not shown).

The doubly-tagged substance P, with coumarin groups attached at both the N–terminus and the lysine side chain, produced fragments from the side chains of arginine, glutamine, lysine, and methionine. Small molecule losses from the doubly tagged peptide included loss of CO

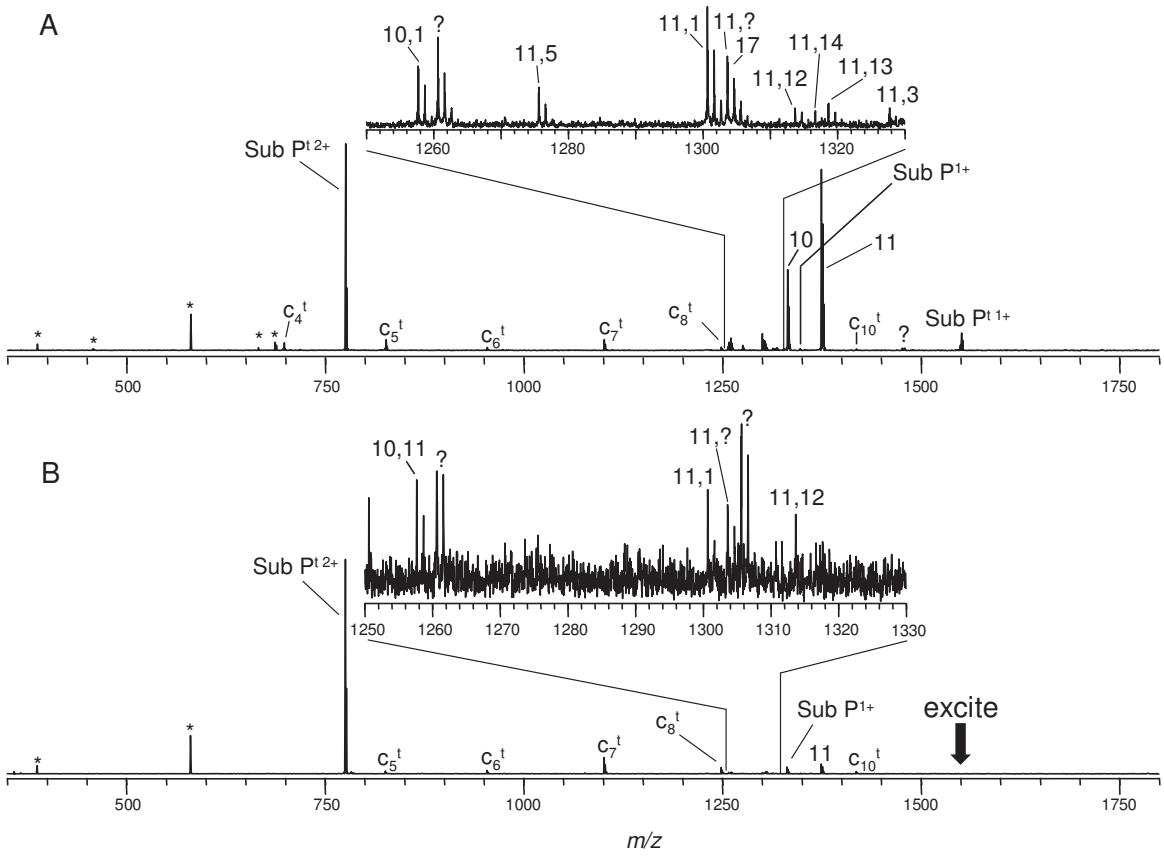

Figure 2·18: The ECD spectrum of mixed singly-tagged substance P (A) without ejection and (B) with ejection of the reduced molecular ion (m/z ∼1550). Peaks labeled with numbers and symbols are designated in table 2.2.

from a tag as well as the loss of a tag fragment and one or both tags, as previously described.

Peptides with Radical Traps and the Free-Radical Cascade Mechanism in ECD

The significant reduction of backbone cleavages apparent with the sequential addition of radical traps to substance P strongly correlates with the concept that the radical is involved in secondary cleavages, as previously suggested.[67] It is proposed that the coumarin tag uses its highly conjugated system to act as a radical trap and captures the radical, decreasing the radicals probability of interacting with the backbone carbonyl. Thus, radical trapping results in stabilization of the backbone carbonyls and the backbone cleavages are significantly reduced. At the same time, the conjugated system of the coumarin tag is able to freely rotate on the single bond connecting it to the rest of the peptide. As it bends, the amino acid side chain groups are sterically more accessible to the radical residing on the tag, creating possible pathways of

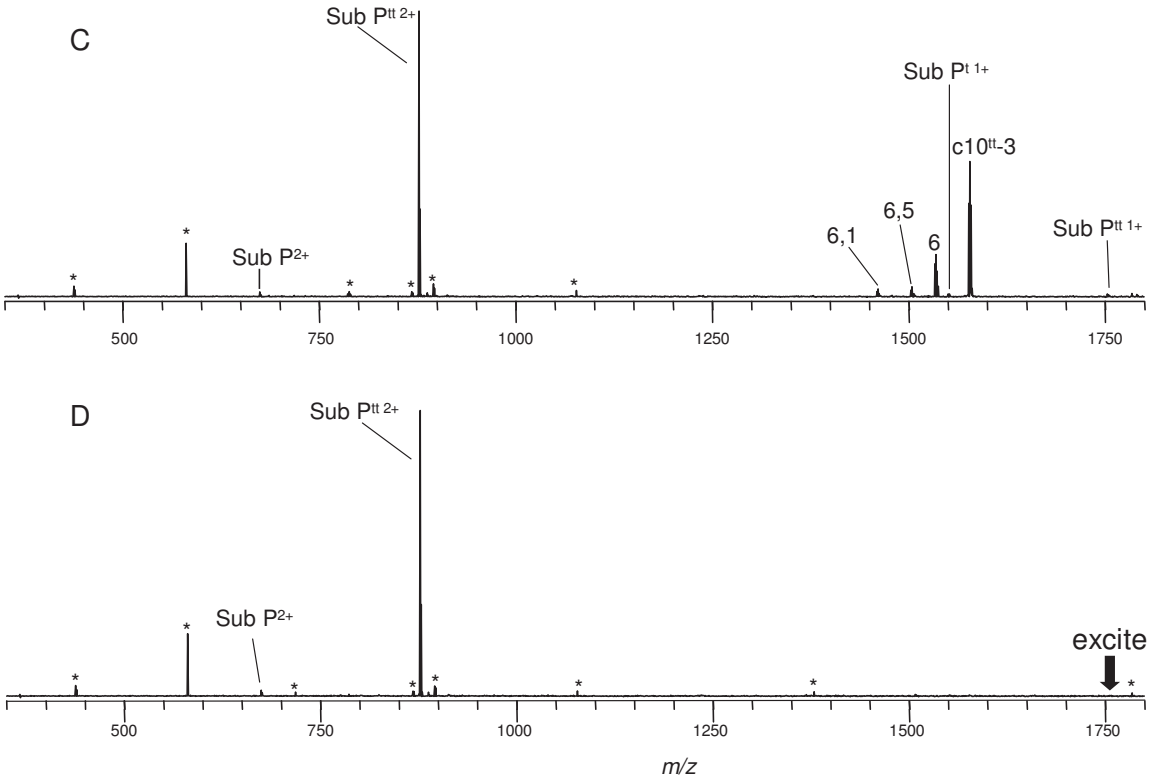

Figure 2·19: The ECD spectrum of doubly-tagged substance P (A) without ejection and (B) with ejection of the reduced molecular ion ($m/z \sim$1753). Peaks labeled with numbers and symbols are designated in table 2.2.

radical reactions on the side chains of the amino acids and, over time, inducing cleavages in the side chains.

Additional evidence of a radical cascade mechanism can be derived from the results of DR–ECD of native substance P (not shown) and the singly- and doubly-labeled peptides (figures 2·18 and 2·19). The singly-labeled substance P used for DR–ECD consisted of a mixture of lysine and N–terminus tagged substance P. The spectra of singly-tagged substance P show that most backbone cleavages were not affected by the resonant ejection, while the side chain cleavages were substantially reduced or eliminated. Reduction of these fragment ion abundances upon resonant ejection of the charge reduced molecular ion indicates that these side chain cleavages are generated on a time period greater than the time it takes to excite the intermediate to 1/2 the cell radiustypically on the order of 100 μs.

The numerous observed fragments indicate that the secondary fragments observed in ECD involve radical propagation.[67] However, the exact mechanism of cleavage is complicated by the

juxtaposition of decreasing intensities of backbone cleavages with increasing intensities of side chain cleavages (figure 2·15). If the secondary mechanism involved only radical propagation, then the amounts of all cleavages would be expected to decrease in the presence of a radical trap. Thus, the increase in abundance of slow side chain cleavages indicate the presence of another relevant mechanism. The ability of the coumarin tag groups to participate in π-stacking suggests that the flexibility of the tag is important, enabling the radical to interact with amino acid side chains and causing radical induced cleavage at these locations. Hence, the most likely mechanism of ECD involves two stages: after initial electron capture in a high Rydberg state, the electron, as it slowly drops down the potential well onto the peptide, undergoes internal conversion to a local potential minimum, which is a vibrationally excited, low-lying electronic state. When this local minimum is on the carbonyl, as in the unmodified substance P, the traditional rapid ECD c/z-type cleavages are generated via a cleavage, but for the coumarin tagged peptides, the local minimum is a stabilized radical on the distributed π–system, which prevents rapid cleavages. As this peptide then slowly explores the conformational space available, the radical interacts with the side chains enabling further odd-electron rearrangements. In this model, secondary backbone cleavages, while possible, are prevented sterically.

It is interesting to note that the observed loss of backbone fragmentation with the addition of sp^2 hybridized radical trap moieties is not dissimilar to the loss of fragmentation near the heme group in cytochrome *c*.[72] In the latter case, it is unclear if the heme is acting as a radical trap or if the iron is changing oxidation state, but the two observations may be related.

2.3.4 ECD of Peptides Labeled with Stationary Charges

ECD Spectra of Peptides Labeled with Stationary Charges

To examine the affect of a stationary charge on the ECD spectra of a peptide, two peptides derived from the Aβ peptide, residues 20–29 and 25–35, were labeled at their lysine and N-termini amino groups (figure 2·2) (table 2.1). ECD of the unlabeled peptides (figure 2·20–A and 2·21–A) generated more backbone cleavage fragments than singly labeled peptides (figures 2·20–B and 2·21–B, labeled at lysine or N–terminus). ECD of the unlabeled Aβ peptide 20–29 generated both N– and C–terminal ions because of the N–terminal amino group and the lysine group located near the C–terminus were charge carriers. The position of the tag on lys9 was

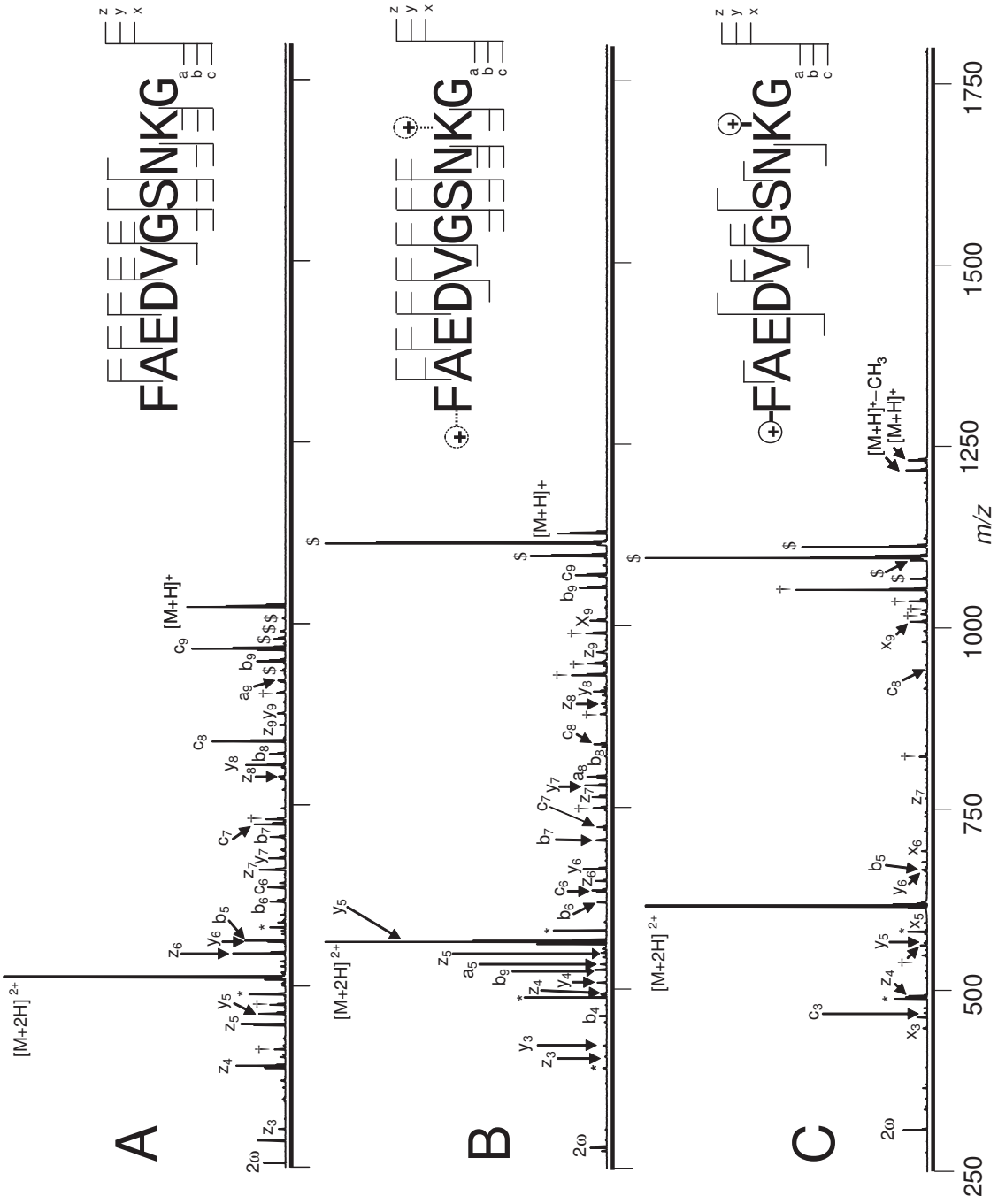

Figure 2·20: ECD spectra of $(M+2H)^{2+}$ of FAEDVGSNKG (Aβ 20-29) (A) without the fixed charge tag, (B) with one fixed charge (at either lysine or the N–terminus, indicated by dashed lines) and (C) with two tags (one at lysine and one at the N–terminus). Small molecule or side chain losses from fragments or the reduced molecular are represented by † and \$, respectively, * represents electronic noise and 2ω is the second harmonic of $(M+2H)^{2+}$.

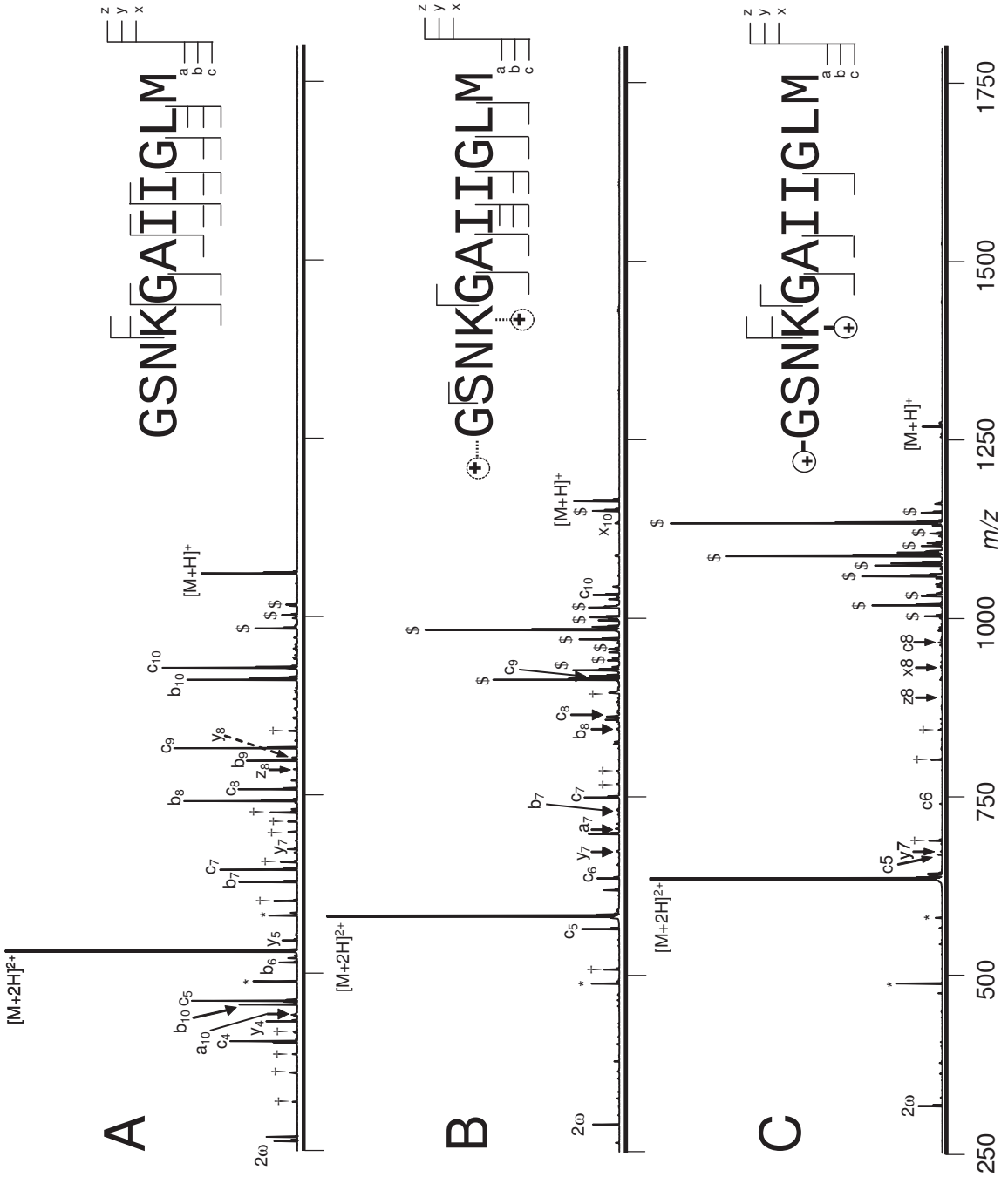

Figure 2·21: ECD spectra of $(M+2H)^{2+}$ of GSNKGAIIGLM (Aβ 25-35) (A) without the fixed charge tag, (B) with one fixed charge (at either lysine or the N–terminus, indicated by dashed lines) and (C) with two tags (one at lysine and one at the N–terminus). Small molecule or side chain losses from fragments or the reduced molecular are represented by † and \$, respectively, * represents electronic noise and 2ω is the second harmonic of $(M+2H)^{2+}$.

confirmed based on the observed c and z· ions (figure 2·20–B). The addition of a fixed charge derivative results in a decrease in backbone fragment abundance which was also observed in this experiment. The second unlabeled and singly-labeled Aβ peptide 25–35 showed N–terminal fragments (c ions) as the most abundant ions (figure 2·21–A and B), because the N–terminal amino group and the neighboring lysine group are the most likely charge carriers. Similar to first peptide, the intensities of the c ions decreased and the intensities of the side chain cleavages increased in the labeled peptide when compared to the unlabeled counterpart for Aβ peptide 25-35. Only fragment ions containing the charge or fixed charge tags could be detected indicating that the N–terminal amino group and lysine side chain ε-amino group are the preferential neutralization sites.

The ECD spectra of both doubly-labeled Aβ peptides 20–29 (figure 2·20–C) and 25–35 (figure 2·21–C), showed a diminished abundance of backbone cleavages and an increase in the intensities of sidechain cleavages compared to their singly-labeled counterparts. The two doubly-labeled peptides still showed a few ECD backbone fragment ions despite that the fixed charge tag inhibited the H· generation which is required for generation of c/z ions according to the classic ECD mechanism (figure 1·7). This data indicates that there may be other new or minor pathways in the ECD process that do not require direct H· migration. The doubly-labeled Aβ peptide 20–29 with a fixed charge located at each end of this peptide showed more backbone cleavages than the doubly-labeled Aβ peptide 25–35 with both fixed charges located at and near its N–terminus. The radical on the tag may have a preference to abstract an H· from a neighboring region; the separated radical positions for Aβ peptide 20–29 would have higher probability of generating backbone fragments after H· abstraction due to higher conformational flexibility.

Side Chain Cleavages in the ECD Spectra of Peptides Labeled with Stationary Charges

Unlabeled, singly-labeled, and doubly-labeled Aβ peptide 20–29 and 25–35 had similar side chain cleavage patterns but with increasing intensities, respectively (figure 2·20–A to C and 2·21–A to C). The singly-labeled peptides also showed an abundant methyl group loss, which may come from the ring of the tag or from the valine or alanine residue side chains, but could

not be determined from the spectra. For Aβ peptide 20–29, loss of the methyl group and tag dominated the spectra of the singly and doubly tagged species. However, loss of the methyl group and tag were accompanied with more side chain cleavages for the singly and doubly labeled ECD of Aβ peptide 25–35.

Increased side chain losses for 25–35 may be attributed to a larger energy release upon electron capture since the charges are more spatially adjacent than for 20–29 (higher Coulombic repulsion). The more energy deposited increases secondary fragmentations, such as side chain losses, which occur on a larger time-scale as demonstrated in the DR-ECD of peptides with radical traps (see section 2.3.2). This corroborates the study by Cooper *et al.* that pointed out that peptides with increased charges had increased side chain cleavages.[74]

Also, the closely located fixed charge groups for peptide 25–35 may have synergetic function that enhances side chain cleavages. This agrees with the observation that the side chain losses decreases with the increase of the distance from the radical site.[193] The intensities of the multiple side chain losses from the charge reduced species and from the fragment ions also increased in the order of unlabeled, singly-labeled, and doubly-labeled versions of the Aβ peptide 25–35; the lysine is in the center of the peptide for 25–35 while is the C–terminal residue for peptide 20-29. In summary, both the number and positions of the fixed charge tag groups in the peptides are important for ECD backbone and side chain fragmentation. More fixed charge derivatives correlate with fewer and lower abundance backbone fragments and increased side chain cleavage fragments. In addition, the closely spaced fixed charge groups result in increased multiple side chain cleavages.

Peptides with Stationary Charges and the Free-Radical Cascade Mechanism in ECD

In this study, the fixed charge tag after neutralization will block the H· generation, which is believed to be important in inducing the typical ECD backbone cleavages.[1,62,63] ECD fragments from the tagged peptides presented here could be rationalized as originating from a radical intermediate (reduced molecular ion, $(M+2H)^{+\cdot}$) that abstracts H· from its nearby neighbors to produce new pathways for the backbone and side chain cleavages, *i.e.* the free-radical cascade. In these cases, the effective increase in side chains cleavages was expected; side chain losses are

initiated by radical rearrangements and backbone cleavages should be prevented because there is no generation of H·. However, backbone fragments (c and z ions) are detected in the ECD spectra of both doubly-tagged peptides. These backbone cleavages may indicate the presence of the free radical cascade that may not be a significant pathway compared to others (*i.e.* side chain losses) since the abundance of fragments are significantly small.

2.4 Conclusions

The free radical cascade mechanism in ECD is believed to be a secondary fragmentation pathway that originates from the odd electron fragment of the primary cleavage. The radical is believed to propagate along the peptide backbone via C_α positions causing rearrangements that result in additional N– and C–temrinal fragments and amino acid side chains losses, pathways thought to occur on the millisecond time scale. To test this proposed mechanism, four experiments were conducted in attempt to support the existence of this secondary fragmentation mechanism in ECD.

In the first experiment (section 2.3.1), ECD was performed on a 16–mer peptide doubly-deuterated at the C_α positions of its four glycine residues. Deuterium scrambling via free-radical abstraction of C_α deuterium labels was observed as indicated by the presence of -1.0078 Da (+H-D) mass shifted fragments. Furthermore, although the Q2 CAD experiment, at 23 eV collision energy, provided more internal vibrational energy than the ECD spectra (with 0.2-9 eV electron kinetic energy depending on the experiment and ∼6 eV of electron-ion recombination energy), the CAD spectrum showed lower D-scrambling than did the ECD spectrum. This experiment demonstrates that many of the expected c/z ions for ECD are products of long-lived radical intermediates that migrate via the abstraction of H (or D) from the C_α of amino acid (in this case, glycine) residues.

In the second experiment (section 2.3.2), DR-ECD was performed on a peptide so that the life-time of the long-lived radical intermediates can be estimated. As shown in the example of fibrinopeptide B, the lifetime of these radical intermediates can sometimes exceed a millisecond. Multiple radical rearrangements can happen in this time, allowing processes such as free radical cascade and intramolecular hydrogen transfer to occur. The odd electron c· fragment ions in the BUSM–A peptide ECD appeared to have much smaller survival ratios than the corresponding

even electron c ions, marking their different origins, with the former likely being the result of intramolecular hydrogen transfer.

The third experiment involved ECD of substance P (section 2.3.3), a 11–mer peptide, labeled with one or two radical trap moieties. The trap used was a coumarin tag which has highly conjugated π–system and should serve an adequate radical trap. The addition of the tags served to trap the radical and resulted in decreased abundance of backbone cleavages. It also increased the abundance of side chain cleavages, which were shown to be derived from a long-lived radical intermediate with the same m/z as the charge reduced molecular ion. The enhanced presence of side chain cleavages in tagged peptides indicated that the addition of the coumarin tags not only prevents backbone cleavages, but redirects the radical to the side chains, presumably by changing the gas-phase conformation of the peptide.

The final experiment was ECD performed on peptides (oligomers of the Aβ peptide) that were labeled with stationary charges (section 2.3.4). The fixed charge tag, after neutralization, will not generate H· to facilitate the ECD process, but it can abstract H· from a through-space neighbor that can cause backbone and side chain cleavages. The addition of such a tag should inhibit formation of c/z according to the primary cleavage mechanism. However, some c and z· ions were observed in the ECD spectrum of the doubly-labeled peptides (both charge carriers are the stationary charges) which indicates that direct H· formation is not always required for backbone cleavage and could be the result of the free-radical cascade mechanism.

To conclude, the results of the four experiments provide some evidence of the free-radical cascade mechanism according to the three stipulations stated in the introduction. Briefly, the requirements include that a long-lived radical intermediate exists in ECD and that radical migration is occurring within this radical intermediate which can alone cause cleavages without the need for H·.

Chapter 3

Differentiating Isoaspartyl from Aspartyl Residues in Peptides by ECD

3.1 Introduction

3.1.1 Mechanism and Biological Significance of Asparagine Deamidation

A prevalent modification of proteins is the deamidation of asparagine residues and isomerization of Asp residues via a succinimide intermediate to form a mixture of Asp or isoAsp residues (see section 1.3).[2–5,96,97] Formation of the isoAsp residues is believed to cause the inactivation, aggregation and aging of proteins in tissue because the backbone is lengthened by one methylene unit (–CH_2–) and the side chain is shortened by the same amount.[2,4,87–92] The C–terminal side amino acid neighbor to the asparaginyl residue influences the rate of succinimide formation more so than those on the amino side.[96–98] The rate increases for amino acids with less bulky residues (e.g. glycine) and highly polar side chains (*e.g.* histidine).[97] The significant impact of isoAsp formation on protein structure and function warrants analytical techniques to differentiate deamidation products but the challenge is difficult since their structural differences are so small and their masses are identical.

3.1.2 Differentiating Aspartyl and Isoaspartyl Residues in Pepetides

Asp or isoAsp residues, resulting from the deamidation of asparaginyl and isomerization of Asp residues, are difficult to differentiate by mass spectrometric means because their masses are essentially identical. Presently, the most efficient way to detect the modification is by immunological methods,[89] PIMT assays with labeled AdoMet[92,194] and Edman degradation

[1]This chapter has been partially/entirely reproduced from
J. J. Cournoyer, J. L. Pittman, V. I. Ivleva, E. Fallows, L. Waskell, C. E. Costello, and P. B. O'Connor. Deamidation: Differentiation of aspartyl from isoaspartyl products in peptides by electron capture dissociation. *Protein Science*, 14:552-463, 2005.

(see section 1.3.4).[87,125] Other analytical techniques such as HPLC[87,125] and NMR[136,137] can be useful but both have their drawbacks. For example, HPLC can separate the two isoforms but they remain indistinguishable from one another and NMR requires more sample than can realistically be expected from most biological experiments. Several MS methods have been developed to indirectly detect the presence of isoAsp residues in peptides based on the relative abundance of fragment ions,[165] modifications to isoAsp terminal fragments[161,163] and the specific sequence of neutral loses experienced by isoAsp residues.[195] Although useful for their particular studies, these mass spectrometric methods require control samples in order to clearly differentiate between Asp and isoAsp residues in peptides and therefore may yield ambiguous results when applied to real biological samples for which there is no control sample. Data presented in this chapter demonstrates that direct differentiation of Asp from isoAsp residues in peptides can be accomplished by ECD. Under ECD conditions, peptides with Asp residues underwent neutral loss of the Asp side chains that was not observed in the isoAsp analogues. Also, the data yielded the observation of a unique fragmentation pattern that accounts for peaks observed only in the ECD spectra of peptides with isoAsp residues that do not appear in the spectra of the peptides with Asp residues. These fragments can be used to unambiguously determine the presence of isoAsp residues in biological samples without the need for control samples.

3.2 Materials and Methods

3.2.1 Sample preparation

The peptides RAAAGAD$_\alpha$GD$_\alpha$GAGAD$_\alpha$AR (BUSM1), RAAAGAD$_\beta$GD$_\beta$GAGAD$_\beta$AR (BUSM2), RAG$_{2d}$AD$_\alpha$G$_{2d}$D$_\alpha$AD$_\alpha$G$_{2d}$D$_\alpha$AG$_{2d}$D$_\alpha$AAR (BUSM3), RAGAD$_\beta$GD$_\beta$AD$_\beta$GD$_\beta$-AGAAR (BUSM4) were synthesized by AnaSpec (San Jose, CA, USA) (table 3.1). The Protein Structure Facility at the University of Michigan, directed by Dr. Henriette Remmer, synthesized the RAAD$_\alpha$FAAR (BUSM5) and RAAD$_\beta$FAAR (BUSM6) peptides. All other chemicals were purchased from Sigma-Aldrich. All peptides were dissolved to a final concentration of 1 μM in methanol, water and acetic acid (49.5:49.5:1, v/v) for FT–ICR–MS analysis.

Table 3.1: Peptides Analyzed

Peptide	Sequence	Molecular Weight
BUSM1	RAAAGAD$_\alpha$GD$_\alpha$GAGAD$_\alpha$AR	1400.6393
BUSM2	RAAAGAD$_\beta$GD$_\beta$GAGAD$_\beta$AR	1400.6393
BUSM3	RAG$_{2d}$AD$_\alpha$G$_{2d}$D$_\alpha$AD$_\alpha$G$_{2d}$D$_\alpha$AG$_{2d}$AAR	1452.6785
BUSM4	RAGAD$_\beta$GD$_\beta$AD$_\beta$GD$_\beta$AGAAR	1444.6291
BUSM5	RAAAD$_\alpha$FAAR	947.4937
BUSM6	RAAAD$_\beta$FAAR	947.4937

3.2.2 Mass Spectrometry

Although these experiments can be carried out on any mass spectrometer with ECD capability, analysis was carried out on a home built qQq–FT–ICR–MS with a nano-spray source and 7T actively shielded magnet (Cryomagnetics, Oak Ridge, TN) (see section 1.2.4). The qQq refers to a set of mass-filtering front-end quadrupoles which have the ability to select, fragment and accumulate ions which are subsequently transmitted into the FT–ICR–MS for ECD and detection. The front-end quadrupoles were controlled using the program LC2Tune 1.5 (MDS Sciex, Toronto, CA) while the data collected in the ICR cell was controlled by the program IonSpec99 (Irvine, CA, USA). A 5 μL aliquot of each peptide solution was loaded into a pulled-glass capillary tip (1 μm orifice diameter) pulled in-house with a micropipette puller (Sutter Instruments Co., Novato, CA). For ECD analysis, $(M+2H)^{2+}$ ions were isolated in Q1 and externally accumulated in the Q2 region for accumulation periods ranging from 15 to 100 ms. The collected ions were then transmitted to and trapped in the ICR cell and irradiated with electrons emitted from a dispenser cathode; the cathode heater was held at 1.2 A and the offset voltage applied to the electron gun was selected to produce ∼0.2 and ∼9.0 eV electrons while a potential of 9.0 V was applied to the grid. For external Q2 CAD analysis, $(M+2H)^{2+}$ ions were isolated by Q1 and accelerated (23 eV for BUSM1-3 and 17 eV for BUSM4) into Q2 for collision with nitrogen gas. Fragment ions were accumulated for 5 to 250 ms and transmitted to the ICR cell with subsequent cooling using a nitrogen gas pulse and detection. All data were analyzed without apodization and with two zero-fills and was internally calibrated based on ions $(M+2H)^{2+}$, $(M+2H)^{+\cdot}$, $(M+H)^{+}$ and their isotopes.

3.3 Results and Discussion

3.3.1 ECD of Isomeric Synthetic Peptides with Isoaspartyl and Aspartyl Residues

The peptides BUSM1–4 (table 3.1) were analyzed by both ECD (figure 3·1) and CAD (data not shown); BUSM1 and 3 contain Asp residues while BUSM2 and 4 are their analogues that contain isoAsp residues. All peptides from table 3.1 were designed to facilitate the detection of all possible fragment ions by incorporating arginine at both the C– and N–termini so that both ECD and CAD analysis would result in a high abundance of both N–(i.e. a, b, c) and C–(i.e. y, z) terminal fragments. The 16-residue peptides were completely sequenced by ECD at ∼0.2 eV based on c and z· ions with the radical driven fragmentation mechanism shown in figure 1·7 (all c ions down to the Nyquist limit, ∼215 Da, were present at ∼0.2 eV). CAD data (BUSM1–3, 23 eV and BUSM4, 17 eV) revealed the complete sequence based on b and y ions. The presence of b and y ions in the ∼0.2 eV ECD spectra are most likely from collisions with the gas pulse used preceding detection while these ions in the ∼9.0 eV ECD spectra are from both the cooling gas and collisions with high energy electrons. For the ECD data, both c· (OE) and z (EE) ions were detected in abundances comparable to their corresponding hydrogen-transfer fragment ions, c and z·, respectively, a trend previously observed for peptides (see section 2.3.1 and 2.3.2).[62] The neutral loss of $C_2H_4O_2$, corresponding to a loss of the Asp acid side chain,[75] from $(M+2H)^{+\cdot}$ was observed for all of the peptides containing aspartyl residues and was not observed in the peptides with isoAsp residues. Also, the neutral losses of CH_5N_3 and $C_4H_{11}N_3$ from the arginine side chains were observed in the ECD spectra of these peptides. Unexpected ions corresponding to $c_{n-1}\cdot+57$ and z_{l-n-1}-57 ions (n is the position of Asp/isoAsp and l is the total number of amino acids in the peptide) were observed in BUSM2 and 4 but not in BUSM1 and 3 therefore making these unique to the isoAsp residues (marked with asterisks for BUSM2 and BUSM6 in figure 3·1). The ion corresponding to z_3-57 for BUSM2 was not detected because its mass was not within the detection limits of the experiment. Although these ions are unresolved from other c and z ions for BUSM3 and 4, making it difficult to interpret the data, their presence is clearly indicated by changes in relative abundances of peaks when spectra of the two peptides are compared. Neither the side chain losses nor the $c_{n-1}\cdot+57$ and z_{l-n-1}-57 fragment ions were observed in the spectra from CAD analysis (BUSM1-4).

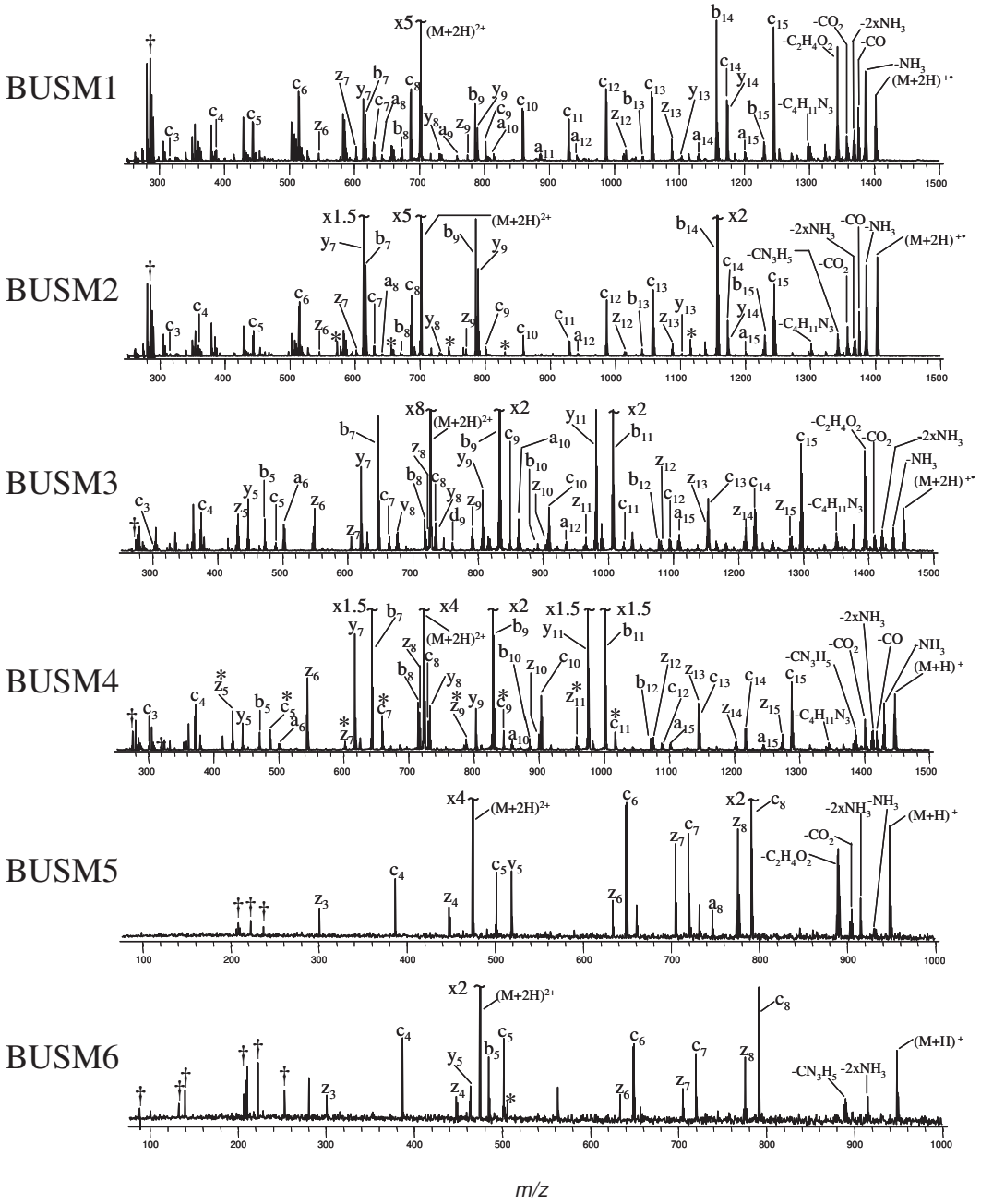

Figure 3·1: ECD spectra of the six peptides from table 3.1 (BUSM1 and 2 at ∼9 eV; BUSM3-6 at ∼0.2 eV). * signifies c_{n-1}·+57 and z_{l-n-1}-57 for BUSM2, 4 and 6, and † indicates electronic noise.

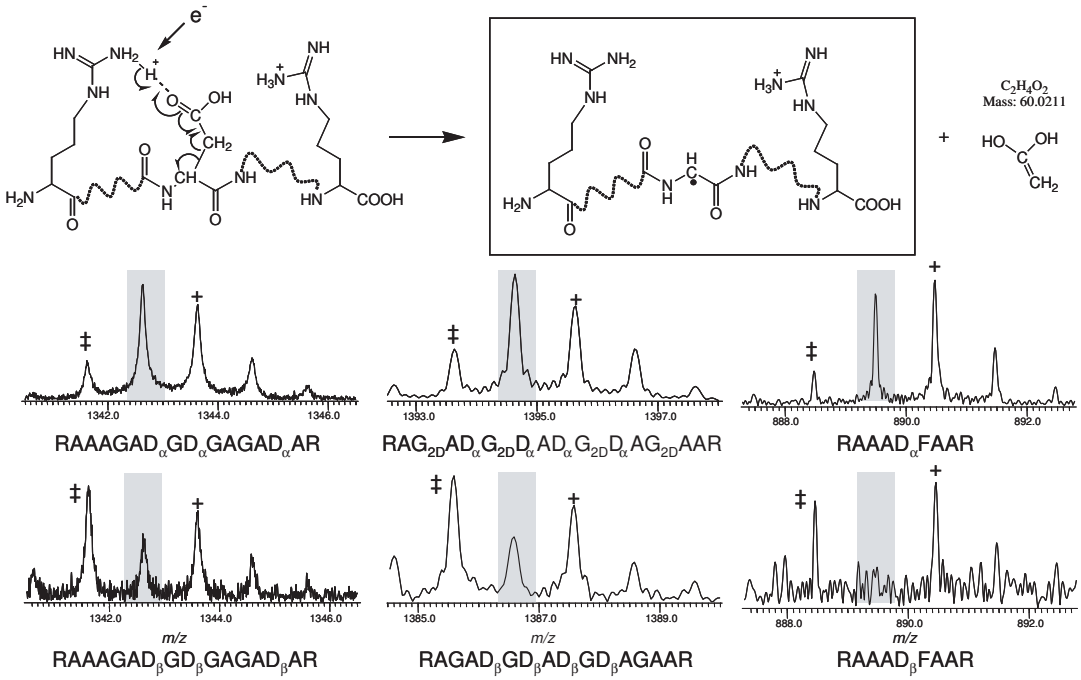

Figure 3·2: (*Top*) Proposed fragmentation scheme for the neutral loss of $C_2H_4O_2$ from Asp residues. (*Bottom*) Comparison of ECD spectra of the three peptides (Asp versions, top row, and isoAsp versions, bottom row) at ∼0.2 eV. † indicates the loss of CH_5N_3 from arginine side chain, ‡ indicates loss of NH_3 and CO_2, dotted lines represent remaining residues, and shaded regions indicate $-C_2H_4O_2$ loss peak from Asp.

Analysis by ECD at ∼0.2 eV of BUSM5 and 6 showed complete coverage based on c and z· ions (figure 3·1). Only the z_5-57 ion was observed for the isoAsp peptide (BUSM6). Also, the neutral loss of $C_2H_4O_2$ from the Asp side chain was observed for BUSM5 but not for BUSM6.

3.3.2 The Diagnostic Asp Fragment $(M+nH)^{(n-1)+\cdot}$-60

The proposed fragmentation mechanism leading to the loss of $C_2H_4O_2$ (60.0211 Da) from $(M+2H)^{+\cdot}$ is shown in the top portion of figure 3·2, and the resulting MS peaks are shown below in the shaded regions for Asp (top) and isoAsp (bottom). Upon electron capture by the positively charged arginine side chain, an O–H bond is formed between the neutralized proton (H·) and the carbonyl oxygen of the Asp acid side chain. This bond formation promotes the cleavage of the C_α-C_β bond of the Asp residue, resulting in the loss of acetic acid and leaving behind what is essentially a glycine residue with a C_α-radical. This C_α-radical amino acid has been reported to be the most stable of all C_α-radical amino acid residues.[186,196] Its sta-

bility is reflected in its substantial abundance in all of the ECD spectra for peptides with Asp residues. This type of cleavage has been previously reported but without a proposed fragmentation mechanism.[75] All three aspartyl versions of the peptides (BUSM1, 3 and 5) experienced the loss of $C_2H_4O_2$ (bottom portion of figure 3·2, top row), which was not observed in the spectra for isoAsp peptides (bottom row of figure 3·2). A peak corresponding to the possible loss of $C_2H_4O_2$ in the isoAsp peptides could be observed in these spectra, but this signal is most likely due to the A+1 isotope, the second isotopic peak (*i.e.* $^{13}C_1$),[197] of the peak corresponding to the loss of both CO_2 and NH_3 from these peptides (loss of 61.0164 Da). The A+1 isotope peak should have 50% or greater abundance relative to its adjacent monoisotopic peak; its appearance in the spectra with an abundance appropriate for the A+1 ion argues against the interpretation as the loss of $C_2H_4O_2$ from the isoAsp peptides.

3.3.3 The Diagnostic isoAsp c_{n-1}·+57 and z_{l-n-1}-57 Fragments

IsoAsp residues generated peaks corresponding to c_{n-1}·+57 and z_{l-n-1}-57 (numbers represent Daltons) that were observed for BUSM2 and not for BUSM1, as indicated in the bottom of figure 3·3 and 3·4. Again, the relevant monoisotopic peaks are highlighted in the mass spectra for the Asp (BUSM1, left) and isoAsp (BUSM2, right) containing peptides along with the theoretical masses of these fragment ions (center). These ions are present in the ECD spectra for the isoAsp peptides at ∼0.2 eV and with increasing abundance at ∼9 eV but completely absent at both energies for the Asp peptide. The proposed mechanism for the formation of these ions is shown in the top portion of figure 3·3 and 3·4 illustrating the homolytic cleavage of isoAsp residue at the N-C_β bond. Although usual Roepstorff nomenclature[33] breaks down for isoAsp acid, because the fragments result from ECD, the c and z notation is used to describe them. Upon electron capture, the electron neutralizes the protonation site forming an O–H bond with the backbone carbonyl oxygen adjacent to the isoAsp residue. The formation of the O–H bond induces an electronic rearrangement in which a double bond between the C_β and carbon of the reduced carbonyl group is formed (z_{l-n-1}-57). This results in the cleavage of the C_α-C_β bond, now part of the backbone for isoAsp residues, and a complementary radical product (c_{n-1}·+57).

Although in lower abundance compared to c_n and z_{l-n} ions, the c_{n-1}·+57 and z_{l-n-1}-

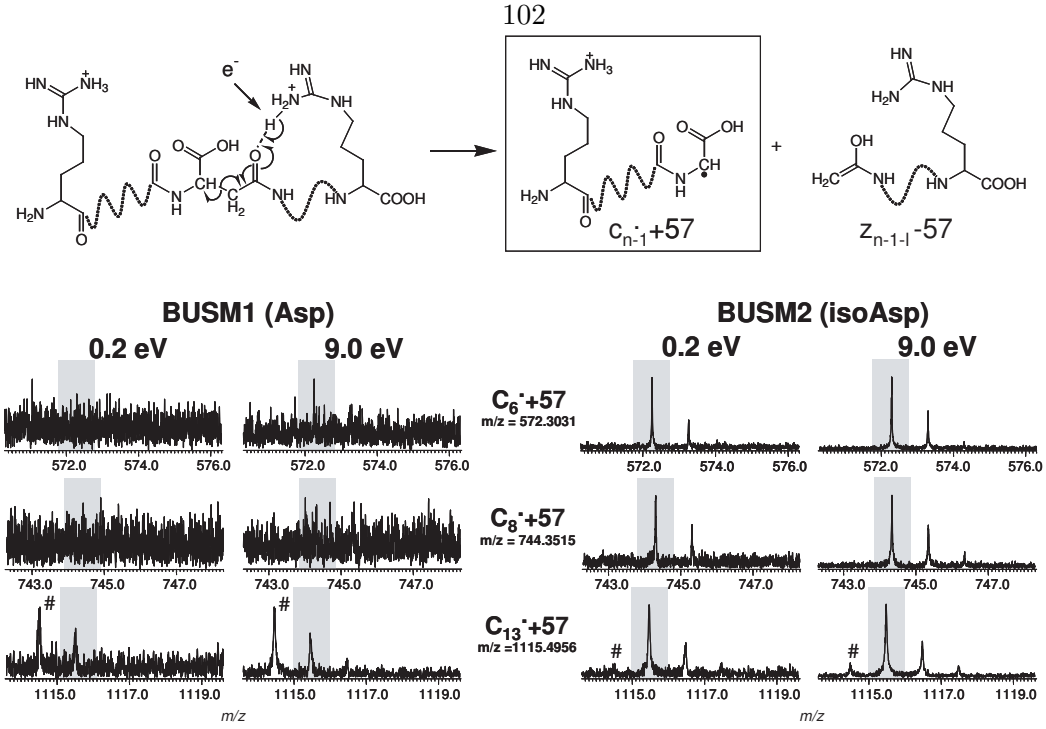

Figure 3·3: (*Top*) Proposed fragmentation scheme for the formation of c_{n-1}·+57 ions from ECD of peptides with isoAsp residues. (*Bottom*) Expanded views of ECD spectra of BUSM1 and BUSM2 at ∼0.2 and ∼9.0 eV. # indicates an interfering secondary fragment ion due to loss of NH_3 and CHON from y_{14} (found in the spectra of both peptides), dotted lines represent remaining residues, and shaded regions indicate the monoisotopic peak of interest.

57 fragment ions are quite stable as indicated by their significant abundance in the spectra. The z_{l-n-1}-57 ion, similar to one of the products from a McLafferty rearrangement (figure 3·3 and 3·4),[197] is stabilized by resonance (H_3C–C(=O)–R ⇔ H_2C=C(–OH)–R). The c_{n-1}·+57 ion has a C–terminal glycine residue with a C_α radical which is known to be a relatively stable radical position due to the captodative effect.[186,196] Recently, theoretical calculations have shown that dissociation of the C_α-C_β bond generating the isoAsp diagnostic ions is energetically possible.[198] However, the pathway producing the classical c and z ions is lower in energy which may explain why the diagnostic isoAsp fragment ions are of relatively lower abundance in the mass spectrum.

The one Dalton difference between a fragment containing a glycyl residue and the odd electron c_{n-1}·+57 fragment is easily resolved on an FT–ICR–MS eliminating any possibility of incorrectly assigning one fragment for the other. Also, the complementary z_{l-n-1}-57 fragment ion can provide additional supporting proof to the presence of an isoAsp residue.

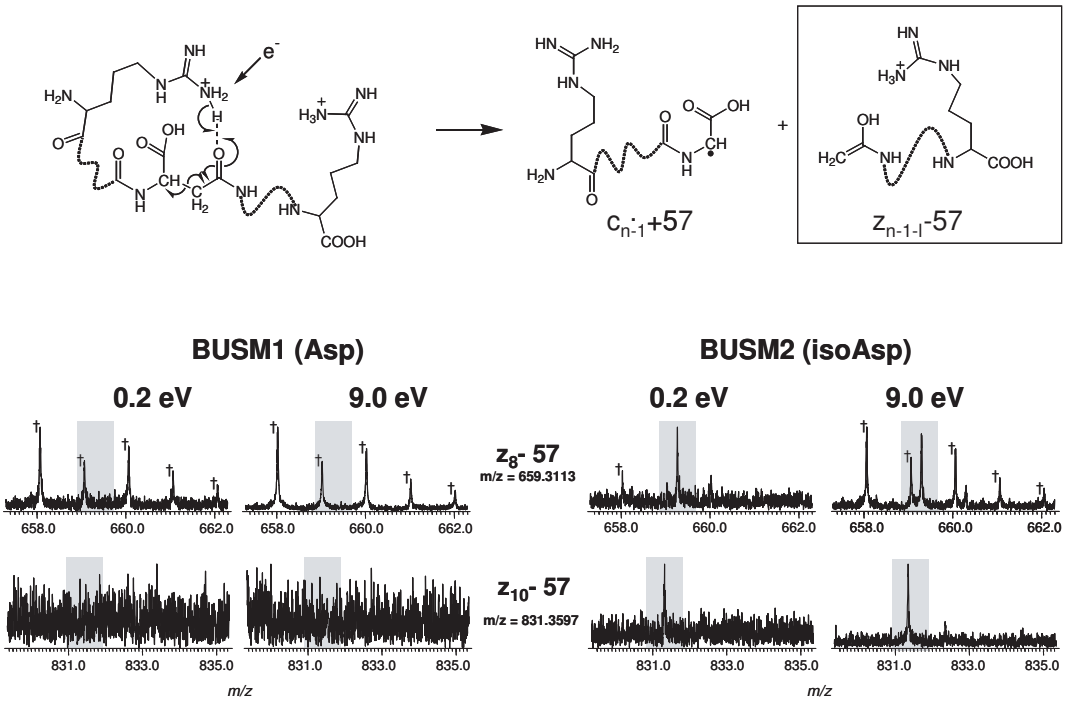

Figure 3·4: (*Top*) Proposed fragmentation scheme for the formation of z_{l-n-1}-57 ions from ECD of peptides with isoAsp residues. (*Bottom*) Expanded views of ECD spectra of BUSM1 and BUSM2 at ∼0.2 and ∼9.0 eV. † indicates noise, dotted lines represent remaining residues, and shaded regions indicate the monoisotopic peak of interest.

Peptides BUSM3 and 4 showed the c_{n-1}·+57 and z_{l-n-1}-57 fragment ions as well but could not be resolved from other c and z ions present in the spectra (data not shown). The presence of the c_{n-1}·+57 and z_{l-n-1}-57 ions is revealed upon examination of changes in isotopic abundances between the spectra of the two peptides. The difference in masses between the fragments was 0.0126 Da and were not resolved from each other under experimental conditions used. Peaks corresponding to both the isoAsp fragments and interfering c and z ions were higher in relative abundance for BUSM4 than for BUSM3 relative to adjacent peaks that were assumed to be of constant abundance in the two peptides. All overlying regions where the diagnostic isoAsp peak should appear showed the same trend except for c_{10}·+58 that experienced interference from y_{11}-H_20. Therefore, the isoAsp residue must be responsible for this trend since that is the only difference between the peptides.

Analysis of BUSM5 and 6 by ECD at ∼0.2 eV (figure 3·1) showed similar trends to those found for BUSM1–4. Neutral loss of $C_2H_4O_2$ was experienced only by BUSM5 while the z_5-57

peak ($m/z = 506.2727$) was found only for the isoaspartyl peptide but its complementary c_4·+58 ion was not detected. The deficiency of the c_4·+58 ion in the isoAsp spectrum may be due to steric hindrance from the neighboring phenylalanine residue such that the charged C–terminal arginine residue upon electron capture is unable to facilitate the O–H bond formation to the isoAsp backbone carbonyl because of interference from the bulky phenyl group adjacent to the isoAsp residue (see bottom of figure 3·1).

3.3.4 CAD versus ECD Analysis of Asp and IsoAsp Peptides

Using the CAD data collected for BUSM1–4 (data not shown), comparisons were made to previous studies that differentiated Asp from isoAsp residues in peptides. Studies by Lehmann *et al.*,[165] using low energy CAD and ESI-MS/MS, showed that the b_n/y_{l-n} (n is position of the Asp/isoAsp residue and l is the length of the peptide) abundance ratio for peptides with Asp residues is larger than those of their counterpart peptides with isoAsp residues. The b_n ion abundances are thought to be diminished in isoAsp peptides due to interference from the carboxylic acid side chain upon ion formation, which occurs via an oxazolone intermediate,[166] while y ions are considered to be of constant abundance between the two peptides because they are formed by direct cleavage during bombardment with collision gas (see section 1.3.5). The same ratios were calculated using b and y fragment ion abundances from CAD data for BUSM1–4 and shown in tables 3.2 and 3.3 for the cleavage of Xxx-(Asp/isoAsp) and (Asp/isoAsp)-Xxx

Table 3.2: Xxx–(α/β)Asp

Peptide	b_n/y_{16-n}	α	β	α/β
RAAAGADGDGAGADAR	b_6/y_{10}	0.23	4.45	0.05
RAGADGDADGDAGAAR	b_8/y_8	3.33	1.09	3.04

bonds (Xxx is adjacent residue). Only two ions (b_8/y_8 and y_5/y_{11} for BUSM4) showed an increase in their b/y ratio upon substitution of Asp with isoAsp residues while all the other calculated ratios showed an opposite trend. The data shows no correlation to the trend found in the previous study; however, the authors noted that their results were probably highly sensitive to instrument parameters, which probably explains the discrepancy. However, some b and y fragments were not detected (too low an abundance or out of mass range) so a full comparison of trends could not be made. These data suggest that, although the side chain is shorter by

Table 3.3: (α/β)Asp–Xxx

Peptide	b_n/y_{16-n}	α	β	α/β
RAAAGADGDGAGADAR	b_7/y_9	2.67	6.47	0.41
RAAAGADGDGAGADAR	b_9/y_7	1.95	3.51	0.56
RAGADGDADGDAGAAR	b_5/y_{11}	1.68	0.01	261.76
RAGADGDADGDAGAAR	b_7/y_9	1.75	8.3	0.21
RAGADGDADGDAGAAR	b_9/y_7	1.21	3.29	0.37
RAGADGDADGDAGAAR	b_{11}/y_5	1.49	36.23	0.04

one methylene unit, the acidic hydrogen of the hydroxyl group of an isoAsp residue can still participate in the preferential C–terminal bond cleavage attributed to Asp residues.

Another method to distinguish aspartyl from isoAsp residues using ESI-MS/MS and low energy CAD used the diagnostic b_{n-1}+H_2O and y_{l-n+1}-46 ions (n is position of the Asp/isoAsp residue and l is the length of the peptide) found in the spectra of peptides with isoAsp residues to distinguish it from the analogous peptides with Asp residues,[161,163] The fragmentation mechanism to support these ions as indicators proposes that formation of a 5-membered heterocyclic intermediate, resulting from the attack of the hydroxyl oxygen on the carbon of the adjacent carbonyl group (n-1 position) of an isoAsp, is more stable than a 6-membered intermediate involving an Asp side chain. The b_{n-1}+H_2O and y_{l-n+1}-46 ions resulting from rearrangement should be of higher abundance for isoAsp than that of Asp because of the relative stability of their intermediates. Upon examination of the CAD data for BUSM2, the three b_{n-1}+H_2O peaks were detected in the isoAsp peptide (data not shown). However, all three peaks were also detected in BUSM1, albeit showing a significantly lower abundance that could be accounted for in two ways. First, these peaks could correspond to b_{n-1}+H_2O ions for Asp residues, which are possible but unlikely. Second, and more likely, these peaks could be the A+1 isotopes for the c_6, c_8 and c_{13} ions, which occur at low abundances in the CAD spectra. The y_{l-n+1}-46 ions were not detected for BUSM2 but are suggested by the authors to be only prevalent with tryptic peptides. The b_{n-1}+H_2O ions for BUSM4 and BUSM3 could not be resolved from interfering fragment ions so no conclusions could be drawn for these peptides.

3.3.5 Advantages of Using the ESI–qQq–FTMS to Differentiate Deamidation Products

The ESI–qQq–FT–ICR–MS with ECD capability used in the study makes both ECD and CAD possible in order establish a method to distinguish isoAsp from Asp residues in model peptides which can be applied to real biological samples. The instrument has the capability for application of the top-down approach[199,200] to protein analysis by selecting and fragmenting selected charge states of the intact protein then isolating fragments in the ICR cell for subsequent ECD analysis. Proteins with suspected deamidated asparagine residues could be fragmented and the fragments containing the asparagine residues of interest can be isolated for detection (with possible SORI-CAD analysis) in order to determine if there is indeed a 1 Da mass shift from the theoretical value. If the mass shift is present, the fragment can be subjected to ECD analysis to determine if the result of the modification is either an Asp or isoAsp residue indicated by the diagnostic ions or side chain fragmentation discussed above. Likewise, fragments believed to have isomerized Asp residues can also be subjected to ECD by applying the method used in this study. The instrumentation used here could facilitate the determination of the modification, either the deamidation of asparagine or the isomerization of Asp residues at the picomole ($\sim\mu$g for a 20 kDa protein) or lower sensitivity levels, without the need for chemical tests such as the PIMT assay and Edman degradation as well as control samples. Differentiating Asp from isoAsp residues in digested peptides by ECD could be complicated by the need for multiply charged states and favorably situated basic residues required for the production of $c_{n-1}\cdot$+57 and z_{l-n-1}-57 ions. For example, trypsin, the most common protease used for sequencing proteins, cleaves on the C–terminal sides of arginine and lysine residues and results in mostly tryptic peptides with N–terminal basic residues. If such peptides were suspected to have isoAsp residues, ECD analysis would yield only z_{l-n-1}-57 ions. Furthermore, efficient protease activity might only produce tryptic peptides of a single charge state that would be worthless for analysis by ECD. Therefore, partial digestion procedures (shorter reactions times, less enzyme) would have to be developed to produce tryptic peptides that can be multiply charged under ESI conditions and different enzymes could be used, such as chymotrypsin or Glu-C, to yield peptides that meet the needed specifications.

3.4 Conclusions

The ability to distinguish Asp from its isomeric form, isoAsp, in peptides was successfully demonstrated via ECD experiments in which several fragmentation trends were detected that clearly characterize this amino acid modification. Six peptides, three with Asp residues and their equivalent peptides with isoAsp residues, were subjected to analysis by ECD. The isoAsp peptides showed a cleavage pattern corresponding to formation of $c_{n-1}\cdot$+57 and z_{l-n-1}-57 ions ions that were not found in the Asp peptides. The proposed mechanism involves cleavage of the C_α–C_β bond producing two fragments unique to isoAsp residues. The isoAsp residue is essentially split; the odd electron c fragment contains a radical glycine structure while the even electron z ion contains the remaining methylene group (C_β). The side chain loss of $C_2H_4O_2$ from Asp was found only in the ECD spectra of peptides with Asp residues; this observation could also help to distinguish the isomers in peptides and proteins, although the appearance of this fragment is more uncertain than the $c_{n1-}\cdot$+57 and z_{l-n-1}-57 ions due to interfering isotopes of fragments from parallel fragmentation channels. The CAD data obtained for peptides 1–4 were used to compare other methods to detect isoAsp residues in peptides using low energy CAD and ESI-MS/MS. The data showed no correlation to the report of the increase in b_n/y_{l-n} ratio for Asp as compared to isoAsp residues in peptides, but the authors had suggested this trend may be sequence and instrument dependent. However, the CAD data for BUSM1 and 2 agreed well with several other studies that show the formation of b_{n-1}+H_2O is enhanced by the presence of isoAsp acid in peptides, as opposed to Asp. The advantage of the ECD method developed here relies not on the relative abundance of fragment ions, but on the appearance of specific diagnostic ions, $(M+nH)^{(n-1)+\cdot}$–$C_2H_4O_2$ for Asp and $c_{n-1}\cdot$+57/z_{l-n-1}-57 for isoAsp, which makes determination of the Asp versus isoAsp residues unambiguous. Furthermore, this method provides the potential for the Asp/isoAsp assignment without synthetic control samples. Using ECD, observation of the two combined fragmentation trends could prove to be a powerful means for efficiently detecting this ubiquitous protein modification via one mass spectrometric experiment.

Chapter 4

Detecting and Differentiating Deamidation Products in Proteins

4.1 Introduction

4.1.1 Analyzing Deamidation in Proteins

Deamidation of peptides and proteins[2–5,96,97] produces isomers and therefore distinguishing between the two can be analytically challenging (see section 1.3). Dependable, yet lengthy, methods of detection thus far used include HPLC,[87,125] Edman degradation,[87,125] immunological methods,[89] and, more recently, a commercially available radiolabeling kit employing the PIMT enzyme (see section 1.3.4).[194] MS can easily detect the ∼1 Da mass shift caused by conversion of the amine to the hydroxyl group but cannot resolve the isomeric products. Attempts with CAD have been made that show shifts in b ion intensities upon substitution with either form, but these methods rely on comparisons with control peptides.[163,165]

ECD[1] in an FT–ICR–MS has demonstrated the ability to distinguish the two forms based on diagnostic ions particular to each form of aspartic acid in a set of synthetic peptides (see section 1.2.3). A relatively new dissociation technique, ECD involves the gas phase reaction of low energy electrons with multiply charged peptide and protein ions produced by ESI.[1] Primarily, electron capture is believed to occur at sites where basic side chains are hydrogen bonded to the protein or peptide backbone resulting in inter-residue cleavages represented by N– and C–terminal fragment ions labeled c- and z-type ions (figure 1·7),[33] respectively, although secondary radical rearrangements also occur.[67,78] Also, a- and y-type ions occur but to a much lower extent. The low-energy fragmentation pathway of ECD allows retention of labile PTMs compared to CAD where loss of PTMs is the primary fragmentation pathway.[65,68,71,201]

[1] This chapter has been partially/entirely reproduced from
J. J. Cournoyer, C. Lin, and P. B. O'Connor. Detecting deamidation products in proteins by electron capture dissociation. *Analytical Chemistry*, 78: 1264-1271, 2006. Copyright 2006 American Chemical Society

Additionally, ECD generates a more uniform cleavage pattern between amino acids than CAD, [202] generates some useful side chain cleavages, [74,75] and has shown the ability to differentiate isomeric amino acid residues such as isoleucine from leucine in peptides. [77] In chapter 3, ECD of synthetic peptides with isoAsp residues show fragment ions corresponding to cleavages on either side of the residue as well as the $c_{n-1}\cdot+57/z_{l-n-1}$-57 complement fragment ions (n is the position

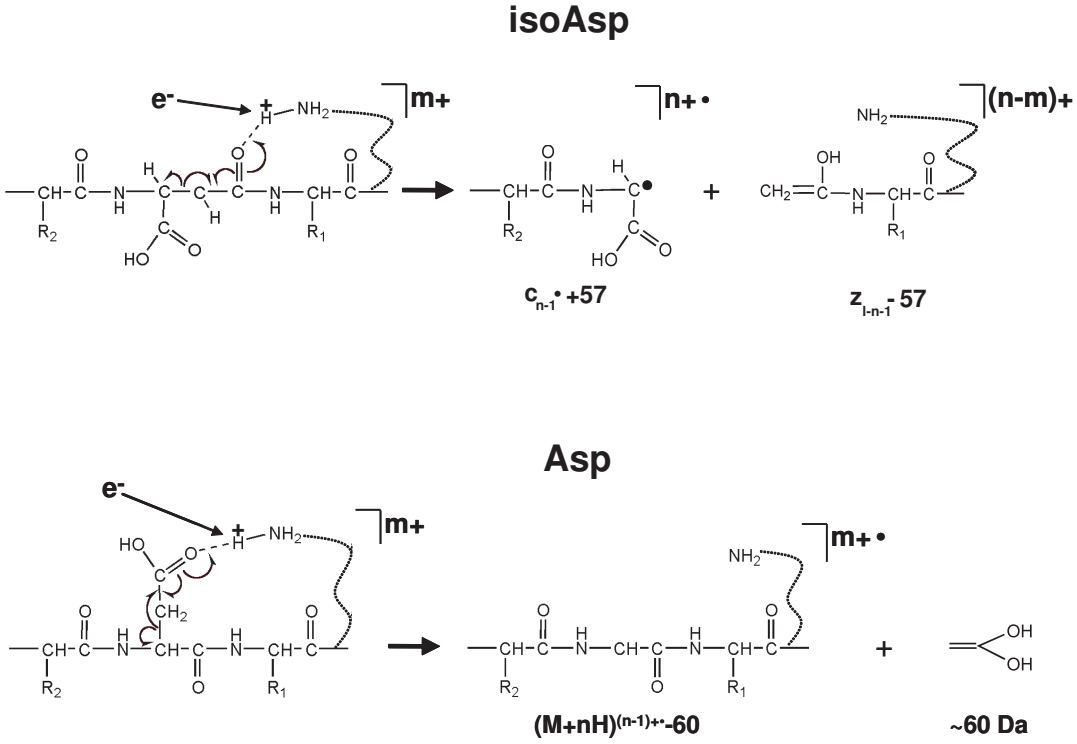

Figure 4·1: Proposed ECD fragmentation mechanisms for the formation of (*top*) isoaspartyl ($c_{n-1}\cdot+57/z_{l-n-1}$-57) and (*bottom*) aspartyl ($(M+nH)^{(n-1)+\cdot}$-60) diagnostic fragment ions

of the Asp/isoAsp residue, l is the length of the peptide and numbers represent nominal mass shifts, in Daltons) (figure 4·1, top). When compared to the ECD spectra of the same peptide with Asp residues, $c_{n-1}\cdot+57/z_{l-n-1}$-57 are unique to the isoAsp form. Also, loss of the Asp side chain from the reduced molecular ions ($(M+nH)^{(n-1)+\cdot}$-60) (figure 4·1, bottom), where n is number of protons) was found to be unique to the Asp containing peptide and considered diagnostic of the presence of an Asp residue. However, this method was developed based on synthetic peptides and is therefore critical to determine if it can also be used in deamidated proteins.

The purpose of this chapter is to show experimental results testing the hypothesis previously

reported that the isoAsp/Asp diagnostic ions could be used to differentiate the two forms in whole proteins. These experiments use natural peptides from proteins that have been deamidated to a mixture of Asp and isoAsp residues; a deamidated tryptic peptide, a tryptic peptide from an unfolded deamidated protein, and a tryptic peptide from a protein deamidated in its native state. ECD spectra of peptides with deamidated residues containing the isoAsp/Asp diagnostic ions show the applicability of this method for determining which of the isomeric forms of aspartic acid is present in a deamidated protein.

4.2 Materials and Methods

4.2.1 Protein digestion

All chemicals and proteins were purchased from Sigma (St. Louis, MO). Trypsin was purchased from Roche Applied Science (Indianapolis, IN). Bovine cytochrome *c* was digested with trypsin at 1:50 (w/w) in 100 mM AB (pH 8.3) for 5 hours at 37°C. Calmodulin was digested with trypsin at 1:20 (w/w, enzyme:substrate) in 50 mM tris buffer (pH 8.3) for 30 minutes at 37°C. The four disulfide bonds in ribonuclease A were reduced in 6 M urea/100 mM AB with 10-fold molar excess of dithiothreitol over disulfide bonds and incubated for 1 hour at 37°C. Iodoacetamide was then added in 5-fold molar excess over cysteine residues and incubated for 1 hour in the dark at room temperature. Reduced and alkylated ribonuclease A was then aged as described below and digested with trypsin at 1:50 (w/w) in 50 mM tris buffer (pH 8.3) for 5 hours at 37°C.

4.2.2 Deamidation of Peptides and Proteins

The tryptic peptides of cytochrome *c* were incubated (∼2 mg/ml) at 37°C in 20 mM 3-(cyclohexylamino)-1-propanesulfonic acid buffer, adjusted to pH 11 with ammonium hydroxide (AH), for 12 days to promote deamidation. Calmodulin was incubated (∼2 mg/ml) at 37°C for 3 weeks in 50 mM tris buffer (pH 7.4) to replicate native state deamidation prior to digestion. Reduced and alkylated ribonuclease A was incubated (∼1 mg/ml) in 50 mM tris buffer (pH 7.9) for 4 days prior to digestion.

4.2.3 HPLC of Deamidated Tryptic Peptides of Cytochrome *c*

Separation of the incubated tryptic peptides was performed by RP–HPLC (solvent module 125 with detector module 166, Beckman Coulter, Fullerton, CA) equipped with a 20 μL injection loop and 4.6 x 250 mm C18 column (Vydak, Hesperia, CA). Mobile phase A consisted of 5:95 acetonitrile:water with 0.05% TFA and mobile phase B consisted of 80:20 acetonitrile:water with 0.035% TFA. A gradient of 0–35 %B in 60 minutes was used to separate the tryptic peptide mixture (based on 100 μg of cytochrome *c*) and isolate the deamidated peptide, which was a mixture of the isoAsp and Asp forms (^{28}TGP(D$_\alpha$/D$_\beta$)LHGLFGR$_{38}$). A second gradient of 15-19 %B in 60 minutes was used to separate the isoAsp from the Asp containing peptides. All collected peaks were evaporated using a speedvac with refrigerated vapor trap (Savant RVT 4104, Thermo Electron Corp., Milford, MA) several times in water to remove TFA for FT–ICR–MS analysis.

4.2.4 Mass Spectrometry

All ECD experiments were performed on a home-built FT–ICR–MS previously described (see section 1.2.4).[83] All peptides were cleaned prior to MS analysis using POROS 50 R1 material (Applied Biosystems, Foster City, CA) (method described in section 2.2.1) and electrosprayed in a 49.5:49.5:1 solution of methanol/water/formic acid at ~10 μM. Before ECD, multiply charged peptides of interest were isolated by one of two different methods; by front-end quadrupole (Q1) isolation followed by external accumulation in the CAD cell (Q2) or isolation in the ICR cell by a stored waveform (SWIFT)[203] after external accumulation in Q2. Gated trapping was used to trap the transmitted ions in the cell that were then irradiated with low energy electrons (~0.2 eV) for time periods ranging from 50 to 300 ms to generate ECD fragments. Fragment ions were detected by a conventional FTT–ICR–MS excitation/detection sequence with signal averaging ranging from 20-200 scans. All ECD spectra were internally calibrated on the precursor ion, charged reduced precursor ions and their higher isotopes.

4.3 Experimental Results

4.3.1 ECD of a Deamidated Tryptic Peptide from Cytochrome *c*

The first experiment was intended to determine the presence of isoAsp/Asp diagnostic ions in the ECD spectrum of a peptide from a protein as opposed to a synthetic peptide. A tryptic peptide, (^{28}TGPNLHGLFGR$_{38}$) (m/z = 584.815, 2+), of cytochrome *c* was shown to deamidate

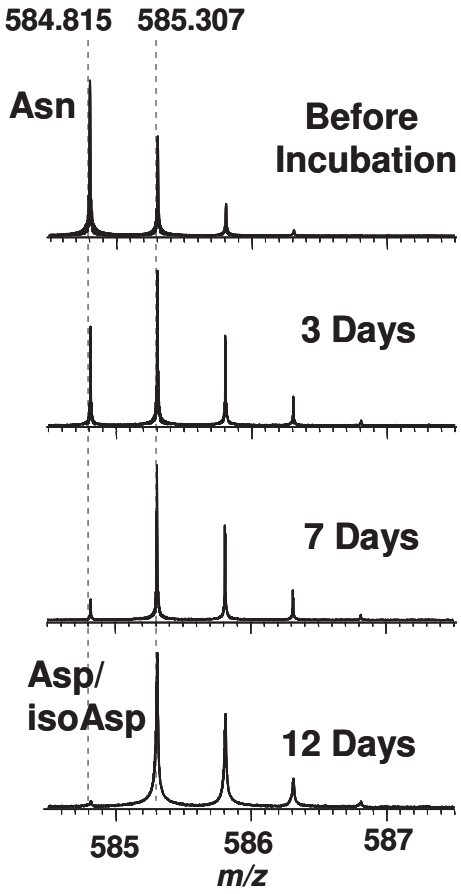

Figure 4·2: ESI–FT–ICR–MS spectra of the deamidation of the tryptic peptide ^{28}TGPNLHGLFGR$_{38}$ ((M+2H)$^{2+}$) from cytochrome *c* at 37 °C and pH 11 for 12 days. The ∼+0.5 Da mass shift corresponds to deamidation of N31 to D$_\alpha$/D$_\beta$31.

over ∼12 days at 37°C and pH 11 as indicated by the decrease and near disappearance of intensity at $m/z = 584.815$ with concomitant increase in intensity at $m/z = 585.307$ (figure 4·2). The deamidation conditions used were found to dramatically increase the deamidation rate while mitigating overall sample degradation in contrast to harsher conditions that used both elevated pH and temperature (data not shown). The ECD spectrum of the deamidated peptide showed

nearly complete sequence coverage proving that the peptide is the product of deamidation (figure 4·3). In addition to c, z and y ions, low energy radical rearrangements such as z·-C_4H_8 (loss of the leucine side chain)[77] and u (γ-lactone formation originating from the leucine side chain)[204] fragment ions were observed. A peak corresponding to z_8-57 was detected (841.468 Da) within 1 ppm indicating the presence and position of an isoAsp residue (figure 4·3, inset). Overlap with z_8·-C_4H_8 was readily resolved. No c_3·+58 was detected probably because it is a tryptic peptide and most of the charge resides at the C–terminal arginine residue, although larger c ions were detected with histidine as the most likely charge carrier. Loss of 60 Da from the reduced molecular ion was observed indicating the presence of the peptide with an Asp residue (figure 4·3, inset). Only a small abundance of the $(M+nH)^{(n-1)+\cdot}$-59.048 Da, corresponding to the loss of the arginine side chain, was detected compared to previously reported ECD spectra of synthetic peptides showing a large abundance of arginine side chain loss (section 3.3.2). However, the synthetic peptides contained two arginine residues as opposed to a single arginine residue in the tryptic peptide from cytochrome *c*. The presence of diagnostic ions particular to each form of aspartic acid show that the peptide isolated is a mixture of the two forms.

4.3.2 ECD of HPLC Separated isoAsp and Asp Containing Peptides

In order to check that the diagnostic ions are unique to each form, the peptides were separated by HPLC prior to ECD analysis. Initial separation of the incubated tryptic peptides of cytochrome *c* by RP–HPLC (0–35 %B in 60 minutes) could not separate the coeluting peptide mixture ^{28}TGP(D_α/D_β)LHGLFGR$_{38}$ (data not shown). However, use of a shallower gradient (15–19 %B in 60 minutes) helped to achieve baseline resolution that enabled separate collection of the two isomeric peptides (figure 4·4). ESI–FT–ICR–MS of both fractions showed a doubly charged species with molecular weight corresponding to the deamidated form of ^{28}TGPNLHGLFGR$_{38}$ and front-end isolation with ECD confirmed that both species were the deamidated peptides of interest. Upon comparison of the ECD spectra, the HPLC peak at 27.2 minutes showed the z_8-57 while the peak at 29.4 minutes did not. Also, the peak at 29.4 minutes showed a much larger abundance of $(M+2H)^{+\cdot}$-60 fragment ion than the HPLC peak at 27.2 minutes (figure 4·4). These differences clearly indicate that the first peak is the peptide with an isoAsp residue while the second peak contains none of the isoAsp form of the peptide and must be the

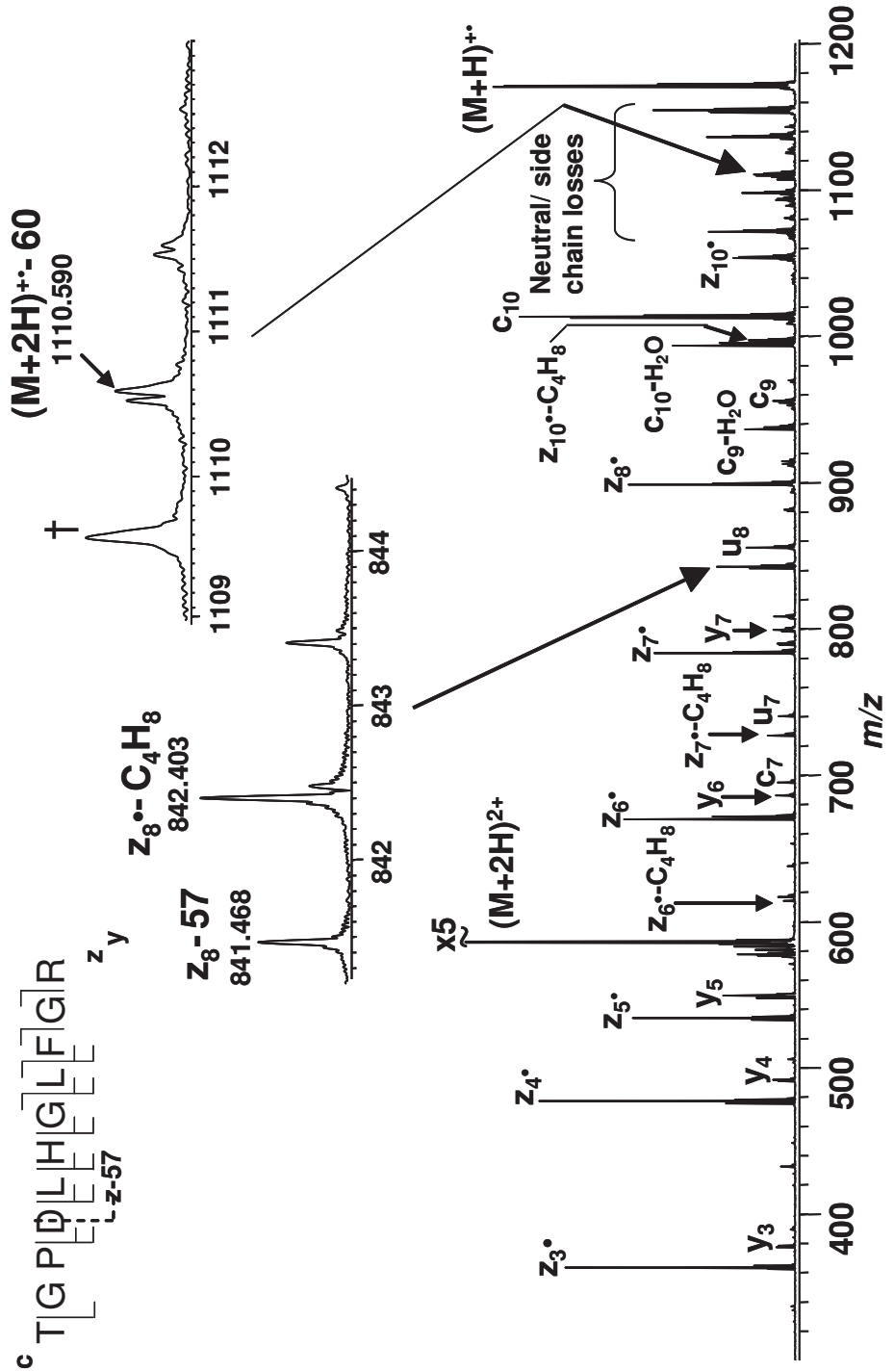

Figure 4·3: ECD spectrum of ^{28}TGP(D_α/D_β)LHGLFGR$_{38}$. Insets are zoomed in mass ranges where the z_8-57 and $(M+2H)^{+\cdot}$-60 fragments ions are found. † indicates loss of NH_3 and CO_2 from $(M+2H)^{+\cdot}$.

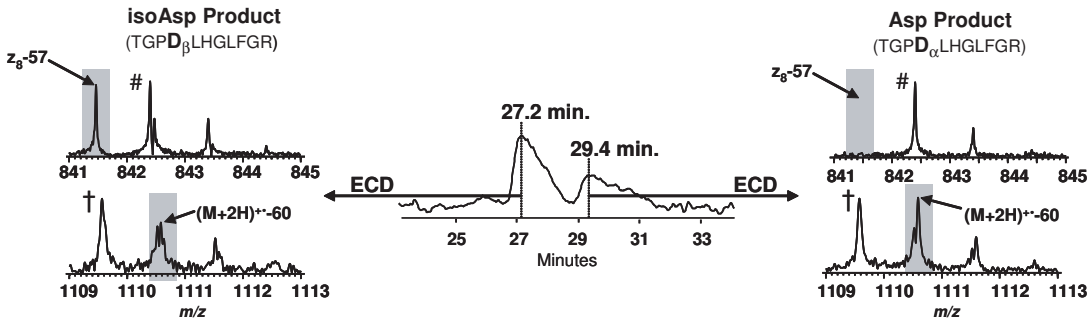

Figure 4·4: ECD spectra of HPLC separated ^{28}TGP(D_α/D_β)LHGLFGR$_{38}$. Middle, zoomed in trace of the HPLC separation of the two isoforms using a shallow gradient. Zoomed in ECD spectra on left and right are of the HPLC fractions at 27.2 and 29.4 minutes, respectively. These mass regions are where the z_8-57 (top) and $(M+2H)^{+\cdot}$-60 (bottom) would occur. † indicates loss of NH_3 and CO_2 from $(M+2H)^{+\cdot}$, and # is z_8·-leucine side chain (C_4H_8, 56.063 Da).

Asp form. The abundance of the second HPLC peak is about 1/3 that of the first peak, which roughly agrees with other studies that show deamidation of Asn residues in a peptide often produces a 1:3 mixture in favor of the isoAsp form. The $(M+2H)^{+\cdot}$-60 Da peak was present in both spectra but was unquestionably higher in abundance in the second HPLC fraction, which has two possible explanations. First, the mass region between the largest c/z ion and the charge reduced precursor ion typically contains many fragment ion peaks originating from side chain losses and multiple neutral losses due to the fact that ECD fragmentation originates from the formation of a free radical.[67] Therefore, the apparent $(M+2H)^{+\cdot}$-60 fragment ion in the ECD spectrum of the first HPLC peak may be a combination of neutral losses that overlap in this particular mass region. In particular, a 59.048 Da loss is common from an arginine containing peptide and a 61.016 Da loss corresponding to loss of NH_3 and CO_2 is frequently observed. A second possibility is that the separation may not have been complete resulting in contamination of the first HPLC peak with the Asp form of the peptide.

4.3.3 ECD of a Tryptic Peptide from Reduced and Alkylated Ribonuclease A

This experiment was intended to determine the presence of the isoAsp/Asp diagnostic ions from a protein that deamidates before digestion. Reduced and unfolded ribonuclease A was incubated at pH 7.9 and 37°C for 4 days in order to facilitate the deamidation of Asn67. This Asn residue has been shown to have an accelerated deamidation rate for the unfolded protein (∼0.96 days

at pH 7.9)[129] compared to the highly folded native protein which normally contains 4 disulfide bonds (∼67 days at pH 7.4).[102] Therefore, Asn67 of unfolded ribonuclease A should be ∼95% deamidated under these experimental conditions. The mass spectrum of a tryptic digest peptide mixture from unfolded and aged ribonuclease A showed a tryptic peptide corresponding in mass to the deamidated form of residues 62-85, (^{62}NVACKNGQTNCYQSYSTMSITDCR$_{85}$). Donato and coworkers have shown that Asn67 of this peptide should be primarily (∼80%) isoAsp, suggesting that tryptic cleavage at Lys66 is inhibited by the extra methyl group inserted into the peptide backbone.[113] Therefore, the $c_5\cdot$+57/z_{19}-57 ion intensities should be effectively enhanced compared to the $(M+3H)^{2+\cdot}$-60 fragment ion intensity. The triply charged peptide was isolated by Q1 and irradiated with low energy electrons to produce c and z fragment ions representing 21 out of the possible 23 inter-residue cleavages (figure 4·5). Breuker and co-workers have shown that missed cleavages may be due to hydrogen bonding between fragments, as a result of gas phase folding, that remain after the ECD event thus preventing these fragments from being detected.[66] Also, ions from the N–C_α cleavage between ^{73}Y-Q_{74} may have not been detectable because they overlap with the charge reduced 2+ ion peak, which is of very large intensity. Nonetheless, ∼90% of the inter-residue cleavages with an average fragment mass accuracy of < 2 ppm confirm that it is the deamidated peptide of interest. The $c_5\cdot$+57 ($m/z = 647.306$) was found in the spectrum with ∼1 ppm mass accuracy (figure 4·5, inset). The $z_5\cdot$ fragment overlapped with the A+1 isotope of $c_5\cdot$+57 but the two fragment ions were resolved from one another (figure 4·5, inset). The complimentary ion z_{19}-57 ($m/z = 2213.894$) was also found with < 2 ppm accuracy but overlaps with the $c_{19}\cdot/c_{19}$ fragment ions (figure 4·5, inset). Peak fitting using the theoretical isotopic distributions of the three different species ($c_{19}\cdot$:c_{19}:z_{19}-57) show that the distribution is approximately 37:16:47 based on peak heights. Detection of both the $c_5\cdot$+58 and z_{19}-57 compliment fragment ions indicates the presence and position of the isoAsp residue at position 67 of ribonuclease A. The $(M+3H)^{2+\cdot}$-60 ion was detected in very low abundance, however, Asp85 contributes to the abundance of this fragment as well so that this peak is therefore an ineffective indicator of Asp at position 67. No evidence of Asp83 isomerization or Asn71 deamidation was found in the spectrum; predicted m/z positions for these peaks are noted in figure 4·5 by arrows beneath the baseline. The –NG– sequence in linear, random coil peptides is well known to be the susceptible to deamidation with a typical

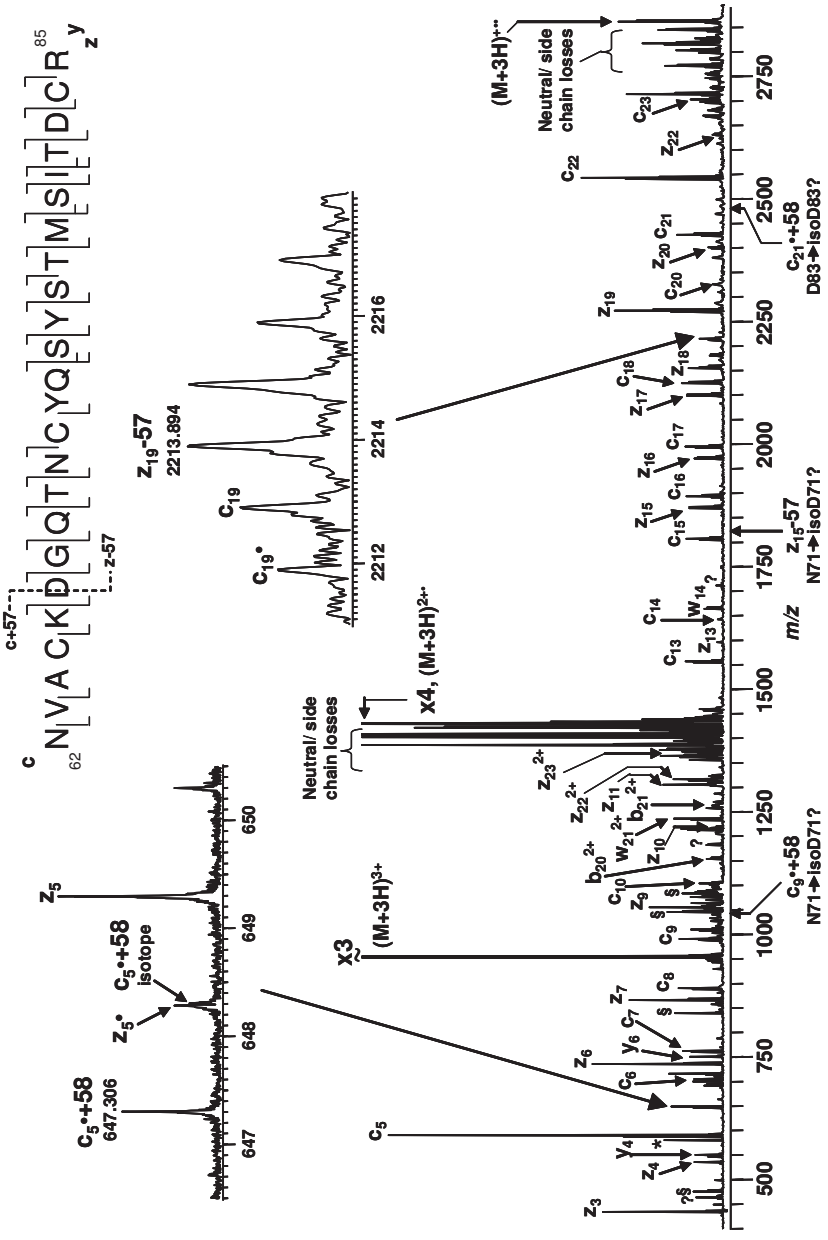

Figure 4·5: ECD spectrum of ^{62}NVAC'K(D_α/D_β)GQTNC'YQSYST-MSITDC'$_{85}$ from unfolded and deamidated ribonuclease A (C', carbamidomethylated cysteine). Insets are zoomed in mass ranges where the z_{19}-57 and c_5·+57 would occur. Arrows under baseline indicate mass ranges where c_{n-1}·+57/z_{l-n-1}-57 would occur if Asn71 or Asp83 were isoAsp. § indicates contamination from imperfect isolation, * indicates electronic noise, and ? indicates an unidentified isotopic pattern.

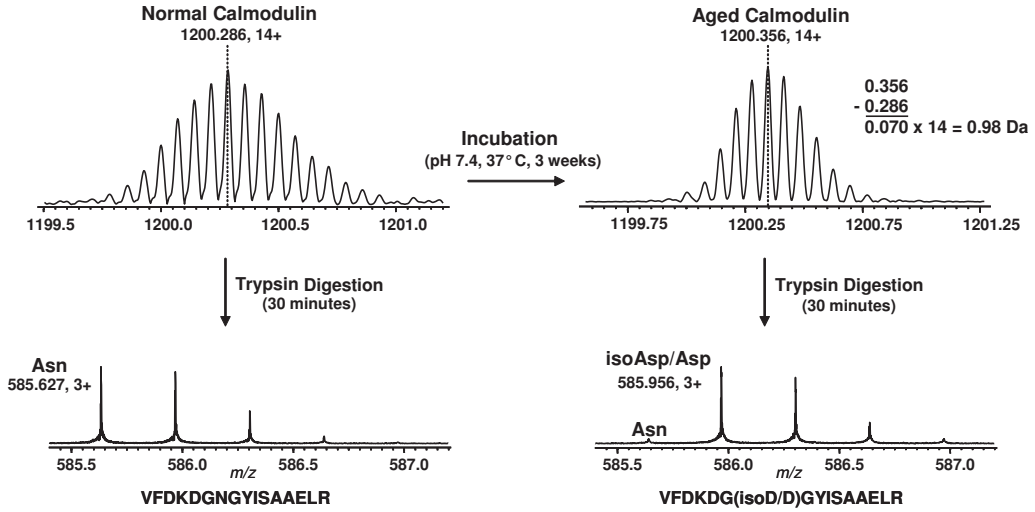

Figure 4·6: Comparison of the 14+ charge states for aged and normal calmodulin and their peptide residues 91-106 from trypsin digest. The 0.071 Da shift in the mass spectra corresponds to +∼0.98 Da which is conversion of one $-NH_2$ to –OH.

$t_{1/2}$ of ∼1 day compared to a $t_{1/2}$ of 53 days for –NC–.

4.3.4 Detection of isoAsp from Native State Calmodulin

Finally, in order to show the use of the isoAsp/Asp diagnostic ions in a protein deamidated in physiological buffers, calmodulin, a protein that easily deamidates in its native state, was analyzed. The –NG– sequence in the active site of calmodulin is available to the solvent and readily deamidates under physiological conditions in the absence of calcium. Extended incubation under near-physiological conditions (tris buffer at pH 7.4, 37°C, 3 weeks) followed by ESI–FT–ICR–MS analysis showed a mass shift of ∼0.98 Da in the 14+ calmodulin isotopic distribution indicating one site of deamidation on the protein (figure 4·6) (internally calibrated using ubiquitin as the internal standard), a trend previously shown for deamidated ribonuclease A.[156] Tryptic digestion of deamidated calmodulin localized the deamidation site to be in one of the active calcium binding sites corresponding to peptide ^{91}VFDKDGNGYISAAELR$_{106}$ which showed a mass shift of +0.329 Da for the 3+ charge state. Calmodulin stored at -80°C and digested with trypsin under the same conditions showed only the non-deamidated peptide indicating that deamidation was not an artifact of digestion. The deamidated peptide was isolated by SWIFT[203] then subjected to ECD (figure 4·7). The ECD spectrum showed 14 out

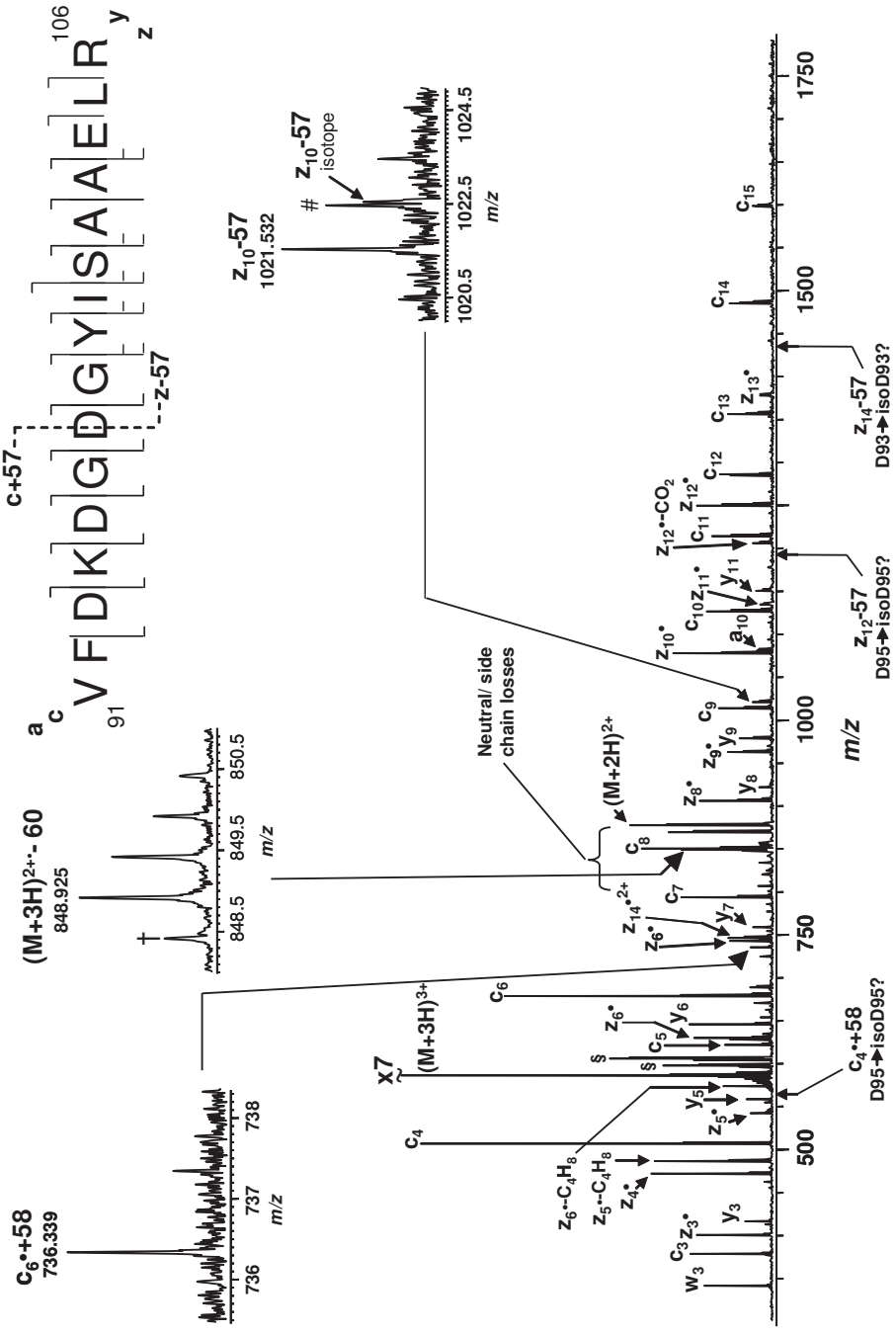

Figure 4·7: ECD spectrum of ^{91}VFDKDG(D_α/D_β)GYISAAELR$_{106}$ from deamidated calmodulin. Insets show z_{10}-57, c_6·+57, and $(M+2H)^{+\cdot}$-60 fragments ions. † indicates loss of NH_3 and CO_2 from $(M+3H)^{2+\cdot}$, and # is z_8·-leucine side chain (C_4H_8). Arrows under baseline indicate mass ranges where c_{n-1}·+57/z_{l-n-1}-57 would occur if Asp95 or Asp93 were isoAsp. § indicates contamination from imperfect isolation.

15 inter-residue cleavages represented by c, z, a and y ions confirming that it is the deamidated peptide of interest. Both complimentary diagnostic ions c_6·+57 and z_{10}-57 were detected with ∼1 ppm accuracy (internally calibrated) indicating the presence and position of an isoAsp substituted for Asn97 (figure 4·7, inset). Both ions were detected because of the fortuitous positioning of the lysine and arginine residue. An intense peak corresponding to $(M+3H)^{2+\cdot}$-60 was also detected; however two Asp residues were already present in the peptide, so that information about the presence of an Asp residue in place of the Asn residue is of lesser value in this case. No isoAsp diagnostic ions were detected for Asp93 or Asp95 suggesting that these were not isomerized during the aging of calmodulin. The isomerization rate of –DG– should be ∼40 times slower than the deamidation of -NG- therefore any isoAsp at position 93 and/or 95 is below the detection limits in this experiment.

4.3.5 Structure Stability of the isoAsp Diagnostic Ions Found in ECD Spectra

ECD fragmentation (figure 1·7) produces EE c ions and OE z ions, however, their isotopic patterns are often distorted due to varying abundances of their hydrogen transfer counterparts (OE c and EE z ions) that differ by the mass of one hydrogen atom (∼1.0078 Da). These isotopic patterns suggest that radical stability plays an important part in governing the relative abundance of each form of the c and z fragment ions that result from ECD processes. The major products of ECD are the EE c and OE z ions as depicted in figure 1·7; the z ion stabilizes the radical on the Cα, which can achieve a planar structure. The Cα positions of the OE c ions most likely retain the radical since these positions have been shown to provide as much as 0.7 eV of stability to radicals compared to their alkyl counterparts due to the captodative effect.[177,178,186] The c_{n-1}·+57 and z_{l-n-1}-57 isoAsp ions in the ECD spectra of the three peptides discussed above show no hydrogen transfer fragment ions and exist solely as OE and EE species, respectively. This is most likely due to the stabilization of the radical of the glycyl-like position on the c_{n-1}·+57 ion. Therefore, as opposed to typical c and z ion formation where intramolecular hydrogen transfer may proceed yielding a mixture of OE and EE populations, the radical is immediately stabilized during the ECD process at isoAsp positions producing only the OE c_{n-1}·+57 and EE z_{l-n-1}-57 fragment ions. Impedance of divergent OE and EE populations may account for the large abundances of the diagnostic isoAsp ions found

in ECD spectra.

4.3.6 Advantages of Using ECD to Analyze Deamidation

The ECD data of the three deamidated peptides derived from cytochrome *c*, ribonuclease A, and calmodulin show that the presence and position of an isoAsp residue can be determined with confidence using the ECD diagnostic ions, therefore showing the method's applicability to routine protein analysis. Diagnosis of the presence and position of isoAsp residues requires 1) accurate assignment of the isoAsp containing peptide, 2) an abundant multiply charged ion for this peptide, and 3) detection of the c_{n-1}·+57 and/or z_{l-n-1}-57 diagnostic ions.

In the ECD spectra, the isoAsp/Asp diagnostic ions frequently overlapped with other fragment ions, such as backbone cleavages and neutral and side chain losses, which are routinely found in ECD spectra. However, internal calibration with the precursor ion and its charge reduced form and the high resolving power offered by FT–ICR–MS typically generates mass accuracy for fragments in the 1-2 ppm range for ECD spectra. Therefore, accurate assignment of fragment ions such as the leucine side chain loss (-56.063 Da) that often overlaps with the z_{l-n}-57 isoAsp ion is readily achieved. The analysis capability of FT–ICR–MS–ECD offers unambiguous identification of an isoAsp residue's presence and position.

Although trypsin was used to generate all the peptides subjected to ECD, theoretically any proteolytic enzyme can be used to obtain the peptides containing possible isoAsp residues. However, ECD requires a multiply charged precursor ion in order to detect fragment ions. Trypsin provides an arginine or lysine residue on the C–terminus so that the z_{l-n-1}-57 isoAsp ion is easily detected. This is illustrated in the cytochrome *c* peptide ECD spectrum where only the z_8-57 was detected. Both diagnostic ions were detected for the peptides from ribonuclease A and calmodulin which contained histidine and lysine, respectively, close to the N–terminus. Detection of both diagnostic ions yields complimentary information and thus greater confidence in the assignment. In some cases, ESI of a limited digestion may be necessary in order to generate higher charged peptides so that both c_{n-1}·+57 and z_{l-n-1}-57 diagnostic ions can be detected.

Finally, the data shows that the presence and position of an isoAsp residue can be determined with confidence using the ECD diagnostic ions but only the presence of the Asp residue may be

determined from the $(M+nH)^{(n-1)+\cdot}$-60 peak; its position must be inferred from backbone c/z cleavages and from the lack of the isoAsp diagnostic ions. If other Asp residues are present in the peptide the Asp diagnostic ion becomes less useful. However, the comprehensive inter-residue cleavage pattern provided by ECD already shows that an Asp residue is present, regardless of iso-form. Therefore, ECD changes the question from "is it isoAsp or Asp" to "is isoAsp present and where is it?".

Most analytical methods used for isoAsp residue detection, such as the immunological,[89] and radioactive assay using the PIMT enzyme,[194] are qualitative in nature and do not reveal the relative amount of isoAsp to Asp residues, which can only be determined when coupled with separation techniques such as HPLC. The results shown here demonstrate that ECD detection of isoAsp residues offers a similar analysis except that it is much faster than the previous mentioned methods and when coupled with HPLC, can easily localize and determine the relative amounts of isoAsp/Asp found in a deamidated protein. Furthermore, while it hasn't yet been systematically studied, mass spectrometric methods suggest the ability to detect the presence and position of isoAsp in proteins at physiologically relevant concentrations.

4.4 Conclusions

The isoAsp ($c_{n-1}\cdot$+57/z_{l-n-1}-57) and Asp ($(M+nH)^{(n-1)+\cdot}$-60) ECD diagnostic ions previously used to differentiate the two isomers in synthetic peptides were reproduced in a deamidated tryptic peptide, a tryptic peptide from an unfolded deamidated protein and in a tryptic peptide from a protein deamidated in its native state therefore clearly showing that the previously developed method is applicable to whole protein analysis. Also, ECD was able to differentiate the HPLC separated isoAsp and Asp forms of the deamidated tryptic peptide using the diagnostic ions unique to each form. While the $c_{n-1}\cdot$+57/z_{l-n-1}-57 fragment ions appear to be very reliable indicators of the presence and position of an isoAsp residue, the $(M+nH)^{(n-1)+\cdot}$-60 fragment ion can only indicate the presence of an Asp residue and position must be inferred from the lack of the isoAsp diagnostic ions. Therefore, complete amino acid sequencing with simultaneous detection of isoAsp residues using ECD will provide additional information for study of the effects of deamidation on protein structure and function.

Chapter 5

Quantitating the Relative Abundance of Isoaspartyl Residues in Deamidated Proteins

5.1 Introduction

5.1.1 Biological Importance of Detecting and Quantitating Deamidation Products in Proteins

In peptides and proteins, deamidation of asparaginyl and isomerization of Asp residues can occur spontaneously to form a mixture of isoAsp and Asp residues (see section 1.3),[2,4,96] a process believed to be a common in vivo degenerative pathway for proteins that affects their structure[124,131,205] and activity.[107,108,206] The rate of deamidation is influenced by steric effects from the C–terminal amino acid neighbor to asparagine[97] and local three-dimensional structure.[100] For example, under physiological conditions, linear, random coil peptides with –NI– were shown to have a deamidation half-life of 300 days as opposed to peptides with –NG– that had a half-life of 1 day.[97] Asp isomerization is also possible (figure 1·10), but occurs ∼40 times slower than deamidation[96] and is therefore a less prevalent modification. The isoAsp form has the C_β originally of the side chain inserted into the backbone, along with shortening of the side chain by the sane amount, altering the fundamental protein structure and is believed to contribute to disruption of protein structure and function more than the Asp form.[127] Hydrolysis of the succinimide intermediate in linear peptides typically results in an approximate 3:1 ratio of products favoring the isoAsp form,[3,110,125,132,151,207] but ratios from succinimide hydrolysis within a structurally restricted environment, such as within a protein's tertiary structure, can deviate from this ratio.[103] For example, N67 of ribonuclease A ultimately deamidated to a

[1]This chapter has been partially/entirely reproduced from
J. J. Cournoyer, C. Lin, M. J. Bowman, and P. B. O'Connor. Quantitating the relative abundance of isoaspartyl residues in deamidated proteins by electron capture dissociation. *Journal of the American Society for Mass Spectrometry*, 18: 48-56, 2007.

3:2 ratio in favor of the Asp form due to the restricted flexibility of the region by two flanking disulfide bonds.[128] Therefore, a method that determines the relative abundance of the products is necessary for complete characterization of asparaginyl deamidation and Asp isomerization that is suspected to affect a protein's structure and function.

5.1.2 Analytical Methods for Detection and Quantitation of Isoaspartyl Resid-ues

Analytical techniques spearheading the analysis of asparaginyl deamidation include radiolabeling, IEF gel electrophoresis, ion exchange and RP–HPLC, Edman degradation, and MS (see section 1.3.4 and 1.3.5). Radioactive methods utilize the PIMT enzyme to selectively methylate isoAsp residues in peptides and proteins with isotopically labeled methyl groups, thus detecting deamidation, but not localizing the site or determining the relative abundance of the products.[154,194]. Separation of proteins from their deamidated counterparts can be done by ion exchange HPLC[113,122,128] or IEF gel electrophoresis[127,134] because there is a net change in the isoelectric point with deamidation. However, the methods are not used for differentiation and relative quantitation of the deamidation products because the acidity constants of the isomers are so similar; isoAsp and Asp were shown to have a difference of only 0.7 pKa units.[132] Deamidated proteins are often digested to localize the deamidation site and determine the ratio of products by RP–HPLC,[110,122,123] but separation of the isomers can be challenging.

Several difficulties are encountered when separating Asp/isoAsp peptides by RP–HPLC; customized separation for each peptide mixture, increased analysis time and sample consumption, and interference from other peptides. The slight structural differences between isoAsp and Asp residues in peptides can make their separation challenging so shallow gradients and long run times are often necessary for baseline separation. For example, a gradient of 15-19% organic mobile phase in 60 minutes was required to achieve baseline separation of isoAsp/Asp peptides from a tryptic digest (see section 4.3.2). Furthermore, larger peptides reduce the influence of the structural difference (isoAsp versus Asp) that is critical for separation and may render these mixtures inseparable. Many HPLC runs are often required before adequate separation is achieved thus increasing total analysis time and sample consumption. Finally, isomers existing in a complex mixture, such as a protein digest, may have retention times similar to other species making their relative quantitation more problematic.

5.1.3 MS Analysis of Asp/isoAsp Residues

Once separation is completed, Edman degradation or MS can differentiate the isomers. Edman degradation, which is blocked by isoAsp residues,[139] requires both chemical and HPLC procedures for sequence determination, thus lengthening analysis time. Substituting Edman degradation for MS can shorten analysis time but differentiation is difficult because there is no mass difference between the isomers. Differences in the fragment mass spectra of the isomers are therefore required for differentiation.

CAD[208,209] in MS can differentiate Asp from isoAsp residues using fragmentation patterns particular to each form but peptide standards are necessary because the method relies on the relative intensity of fragments for differentiation.[161,163,165,195] ECD[1] in an FT–ICR–MS (chapters 3 and 4) or ETD in an ion trap[210] can differentiate the two forms using a diagnostic ion unique to the isoAsp form without the need for peptide standards.

ECD is a sequencing tool that involves the reaction of electrons with gas-phase multiply charged peptide and protein cations. The captured electron initiates N-C_α bond cleavage producing c and z$\cdot$ type fragment ions (N– and C–terminal fragments, respectively) and can preserve PTMs linked to the fragments.[65,201] ECD can also cleave bonds in amino acid side chains such as the C_α-C_β bond.[74] For Asp residues, this results in $M^{+\cdot}$-60, but for isoAsp residues, cleavage of the C_α-C_β backbone bond by ECD generates $c_{n-1}\cdot$+57 and z_{n-l-1}-57 (n is isoAsp, l is length of the peptide) fragment ions thus detecting and localizing the isoAsp residue (figure 4·1).[211] Analysis of deamidated peptides from proteins with HPLC and ECD (section 4.3.2) demonstrated that the combined technique easily differentiates and determines the relative abundance of products but the method is still subject to the limitations associated with HPLC method development described above.

Relative quantitation of isomers with MS alone using fragmentation patterns unique to each form determined the relative abundances of sulfated disaccharides released from digestion of chondroitin,[212,213] suggesting that an analogous method could be developed for relative isoAsp/Asp quantitation. The possible sulfate positions in disaccharides from chondroitin are few compared to the possible amino acid sequences obtained from proteins so a fragmentation trend reproducible for all peptides from proteins is ideal. In this study, ECD spectra of three synthetic peptides sets mixed at different percent isoAsp/Asp compositions showed a repro-

ducible correlation between the relative abundance of the isoAsp diagnostic ion and mixture composition. A method is then suggested using this relationship for complete characterization of asparagine deamidation in a protein and demonstrated using cytochrome *c* as a model.

5.2 Methods and Materials

5.2.1 Materials

Rink resin (1.2 mmol/g loading), *O*-(benzotriazol-1-yl)-*N,N,N,N'*-tetramethyluronium hexafluorophosphate (HBTU) and the N-α-(9-fluorenylmethoxycarbonyl)(FMOC)–protected amino acids glutamic acid, glutamine, isoleucine, histidine, tyrosine, and threonine were purchased from Advanced Chemtech (Louisville, KY). FMOC-protected isoAsp was purchased from NovaBiochem (La Jolla, CA). Trypsin was purchased from Roche chemicals (Indianapolis, IN). All other chemicals were purchased from Sigma Aldrich (St. Louis, MO).

5.2.2 Peptide Synthesis and Purification

The peptides in table 5.1 were synthesized by a standard manual solid phase peptide synthetic method in 1 mL polypropylene syringe barrels (Supelco, St. Louis, MO) utilizing a polyethylene frit (0.2 μm). For each step, 500 μL of the appropriate wash or reaction solution was added to the tube, sealed on both ends with stoppers, mixed on a rotisserie shaker for the specified amount of time and the remaining solution was removed by vacuum filtration (the terms '(X x Y min)' means mixing for Y minutes followed by filtration, done X times). In a typical reaction sequence: resin was pretreated with DMF (3 x 1 min); treated with 20 piperidine solution in DMF (1 x 1 min, 1 x 20 min) to remove the FMOC protecting group; washed to provide the free amine [DMF (3 x 1 min), dichloromethane (DCM) (3 x 1 min), ethanol (3 x 1 min), DCM (3 x 1 min), and DMF (3x 1 min)]; reacted with a 600 μL mixture of the appropriate amino acid solution (2 equivalents of FMOC-amino acid, HBTU and N-ethyldiisopropylethanolamine in DMF preactivated by mixing for 5-8 min) for 2 hours; washed to remove residual reactants [DMF (3 x 1 min), DCM (3 x 1 min)]; dried and stored under vacuum or the cycle was repeated for the next amino acid. About two residues per day were added making total synthesis time 3 weeks for three sets of unpurified peptides. When peptide synthesis was complete, pretreatment with DMF, deprotection and washing with ethanol was completed and the resin was dried under

vacuum overnight. Cleavage of the peptide from the resin was done using a 1 mL solution of TFA:DCM:triisopropylsilane:water (45:45:5:5) with mixing for 2 hours under nitrogen followed by precipitation in cold ether. All peptides (table 5.1) were purified using RP–HPLC with single wavelength detection at 278 nm using a mobile phase system of 5% acetonitrile in water

Table 5.1: Peptides Synthesized

Sequence	Molecular Weight
YWQHTAD$_\alpha$QFR-NH$_2$	1349.6265
YWQHTAD$_\beta$QFR-NH$_2$	1349.6265
YD$_\alpha$FIEYVR-NH$_2$	1102.5448
YD$_\beta$FIEYVR-NH$_2$	1102.5448
WAFD$_\alpha$SAVAWR-NH$_2$	1206.5934
WAFD$_\beta$SAVAWR-NH$_2$	1206.5934

with 0.05% TFA (mobile phase A) and 100% acetonitrile with 0.035% TFA (mobile phase B).

YWQHTA(D$_\alpha$/D$_\beta$)QFR-NH$_2$ were purified by a gradient of 7–15% B in 30 minutes on a 4.6 mm ID x 250 mm C$_{18}$ column (Vydac, Hesperia, CA) at 0.5 mL/min using a System Gold 125 pump and 166 detector (Beckman Coulter, Fullerton, CA). Y(D$_\alpha$/D$_\beta$)FIEYVR-NH$_2$ and WAF(D$_\alpha$/D$_\beta$)SAVAWR-NH$_2$ were purified using gradients of 15–20% B in 23 minutes and 15-25% B in 50 minutes, respectively, on a 10 mm ID x 250 mm C$_{18}$ column (Vydac, Hesperia, CA) at 4 mL/min using Waters 510 HPLC pumps with gradient controller and model 490 wavelength detector (Millipore, Billerica, MA). Peptide sequences were confirmed by FT–ICR–MS–ECD analysis. Stock solutions ranging from 0–100% isoAsp (10% increments) for each set of isomeric peptides were prepared and diluted for FT–ICR–MS–ECD analysis.

5.2.3 Protein Digestion and Aging

Cytochrome *c* was digested with trypsin (100:1, substrate:enzyme, w/w) in 0.1 M AB for 5 hours at 37 °C. The digest was dried to remove the buffer, 5 μL 20% AH (pH 12) was added, and the peptide solution was incubated overnight at 80 °C to completely deamidate N31 of ^{28}TGPNLHGLFGR$_{38}$ to the isoAsp/Asp mixture. The solution was dried under vacuum centrifugation to remove ammonia and then analyzed by FT–ICR–MS–ECD as described below. The peptide ^{28}TGPDLHGLFGR$_{38}$ and its isoAsp counterpart from cytochrome *c* used as cali-

bration samples were previously separated as described in section 4.3.2.

5.2.4 Mass Spectrometry

ECD experiments were performed on a custom-built FT–ICR–MS instrument previously described (see section 1.2.4).[83,214] Peptide solutions were prepared at ∼5-10 μM from stock solutions in a 49.5:49.5:1 water:methanol:formic acid solution and 5 μL was loaded into a glass capillary with 1 μm orifice made using mechanical tip puller (Sutter Instruments, Novato, CA). Applying 1.2 kV to the solution generated positively charged ions used for FT–ICR–MS–ECD analysis. For each experiment, the $(M+2H)^{2+}$ species was isolated by Q1, accumulated in Q2 for 100-1000 ms, transferred to the ICR cell by gated trapping, and then irradiated with electrons at ∼0.2 eV for 50-200 ms. ECD fragments were detected using a typical excitation/detection sequence with 20 scan signal averaging. Accumulation times for $(M+2H)^{2+}$ were optimized to achieve a signal/noise ratio of 500. All analyses were performed in triplicate in order to generate some understanding of abundance variance upon ECD.

5.3 Results and Discussion

5.3.1 ECD of Synthetic Peptides Mixtures

ECD of all isoAsp peptides generated the z_{l-n-1}-57 diagnostic fragment ion that was not found in corresponding Asp ECD spectra (*e.g.* YWQHTAD$_\alpha$QFR-NH_2, figure 5·1). All mixtures showed increasing z_{l-n-1}-57 abundance with increasing isoAsp content. For example, figure 5·2 shows the z_8-57 ion from YWQHTADQFR-NH_2 at different Asp/isoAsp ratios, clearly showing the changes in relative abundance of this ion. Also, the fragment abundance due to loss of CO_2 from z_4 of YWQHTADQFR-NH_2, z_7 of WAFDSAVAWR-NH_2 and z_7 from YDFIEYVR increases with increasing percentage of the Asp form of the peptides. Although they are indicators of Asp, these neutral loses are secondary fragment ions and thus their abundances are dependent upon the energy deposited on the molecule as a result of electron capture and not due to radical rearrangement (*e.g.* c, z and z_{l-n-1}-57 fragment ions). Therefore, CO_2 loss from fragment ions vary (and sometimes do not occur at all) and are not reliable diagnostic ions.

Relative abundance of the z_{l-n-1}-57 fragment (Rel[z_{l-n-1}-57]) with respect to all backbone fragments found in the spectra (y, z, c and their neutral losses) was calculated and plotted

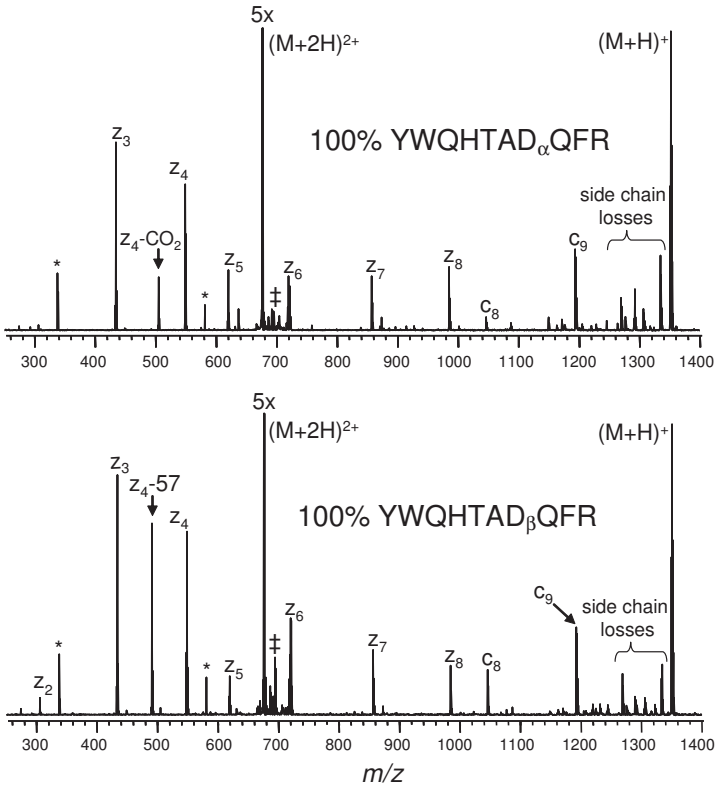

Figure 5·1: ECD fragment spectra of YWQHTA$_\alpha$QFR-NH_2 and YWQHTAD$_\beta$QFR-NH_2. ‡ represent ions from incomplete isolation and * represent electronic noise or harmonics.

against % isoAsp content for all peptide mixtures (figure 5·3). All plots exhibited a near linear relationship with R^2 values greater than 0.98 but with different slopes.

For all three peptide mixtures, particular backbone fragment ion abundances change when the Asp or isoAsp residues are interchanged. The increasing or decreasing fraction of gas-phase structure belonging to one form versus another may account for these trends since intramolecular hydrogen bonding has been shown to remain after ECD cleavage (see section 2.3.2).[66] For the peptide WAFDSAVAWR-NH_2, no fragments that account for at least 5% of the total fragment abundance (excluding cleavage on either side of isoAsp/Asp) change more than 50% suggesting only a minor change in gas phase structure with isoAsp substitution. However, the same comparison for YWQHTADQFR-NH_2 and YDFIEYVR-NH_2 show 60% and 33% of the fragment abundances' experience a 50% change or more with isoAsp substitution. This is probably due to the glutamic acid in Y(D$_\alpha$/D$_\beta$)FIEYVR-NH_2 and two glutamines and histidine residues in YWQHTA(D$_\alpha$/D$_\beta$)QFR-NH_2. Hydrogen bonding involving these residues may be

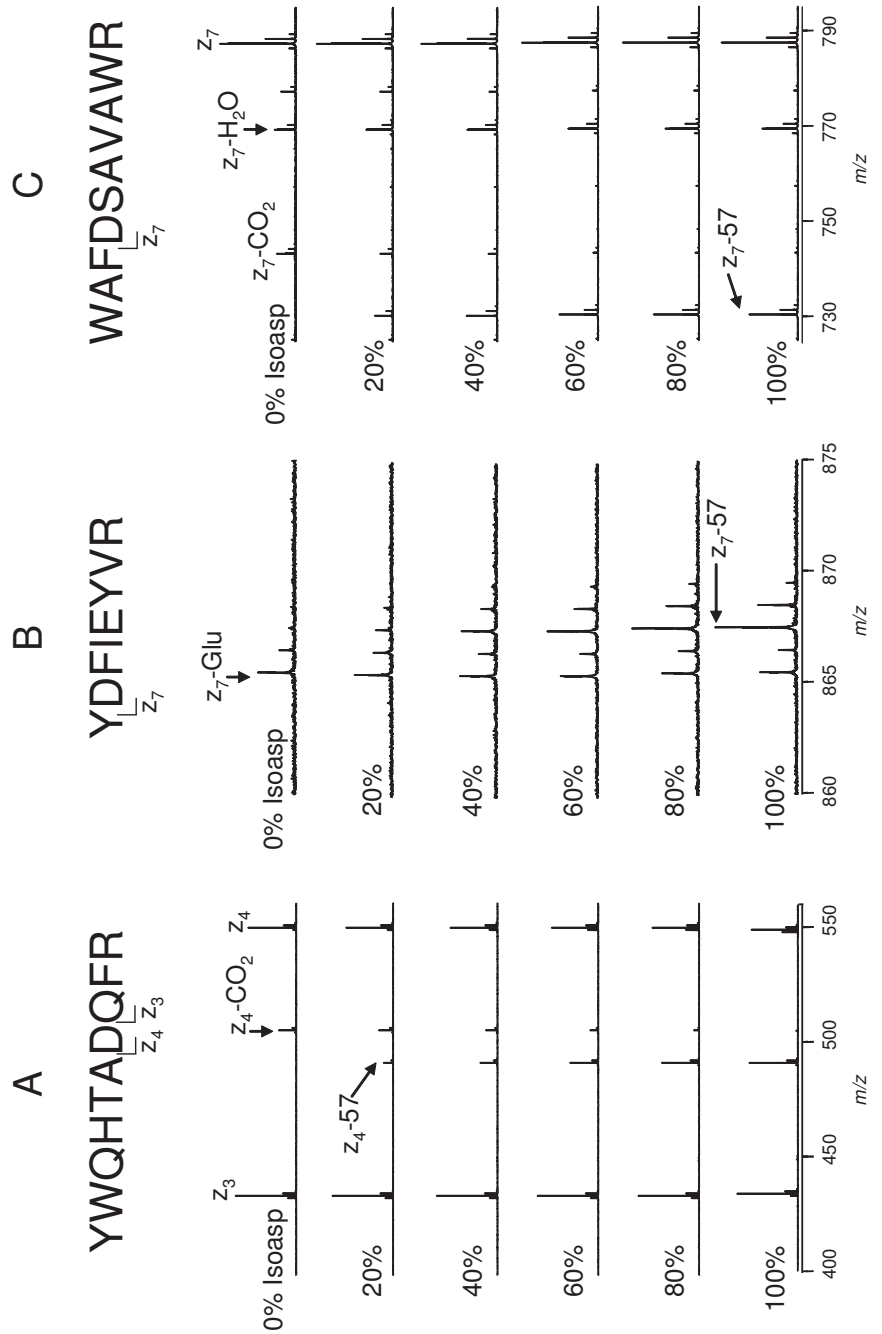

Figure 5·2: (A) The 400-560 m/z region from the ECD fragment spectra of YWQHTA(D_α/D_β)QFR-NH_2 mixtures. (B) The 860–875 m/z region from the ECD fragment spectra of Y(D_α/D_β)FIEYVR-NH_2 mixtures. (C) The 725–795 m/z region from the ECD fragment spectra of WAF(D_α/D_β)SAVAWR-NH_2 mixtures.

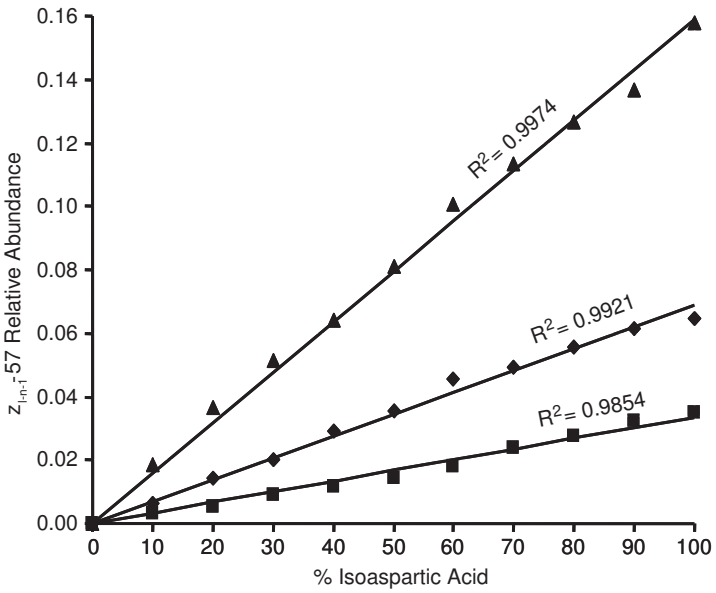

Figure 5·3: Plots of the z_{l-n-1}-57 relative abundance versus % isoAsp content for; [filled triangle], YWQHTADQFR-NH_2; [filled diamond], WAFDSAVAWR-NH_2; [filled square], YDFIEYVR-NH_2.

hindered or favored when interchanging Asp and isoAsp residues. Therefore, determining % isoAsp content using the relative intensities of z_{l-n-1}-57 and any other particular backbone fragment that unknowingly varies may generate erroneous results. Despite the fluctuations in ion abundances, the data demonstrates the trend found between Rel[z_{l-n-1}-57] and % isoAsp content is linear indicating that total fragment ion abundance remains fairly constant even if particular ions show substantial abundance variation. Furthermore, the linearity of these plots appears to be sequence independent but that relationship itself (the slope) is peptide dependent. Similar trends may be observed for CAD spectra since fragments resulting from cleavages adjacent to Asp residues change in abundance upon isoAsp substitution.[161,163,165,195] However, detection alone by CAD relies on discerning the relative intensities of fragments whose formation are collision energy dependent so careful control over experiment parameters are probably necessary to generate useful calibration curves. The isoAsp diagnostic ion from ECD spectra offers unambiguous detection and calibration plots that pass through the origin offering a more straightforward procedure over CAD. Despite the advantage of using ECD, relative quantitation of asparaginyl deamidation or Asp isomerization products by either technique requires synthetic peptides for generating calibration curves.

5.3.2 Relative Quantitation of Deamidation Sites in Proteins without Peptide Standards

Since random coil peptides typically produce a 3:1 ratio of isoAsp:Asp upon asparagine deamidation, the enzymatic digest peptide from the protein itself can potentially be used to generate a standard for quantitation. Clarke,[96] Aswad,[4] Capasso,[132] and others have shown asparagine deamidation in linear peptides to produce mixtures ranging from 70% to 80% in favor of the isoAsp form. Considering these data, rapid aging of a peptide with an asparagine residue released from a protein by enzyme digestion should produce the ∼75 % isoAsp mixture that can be used for calibration. A two point calibration line generated connecting the Rel[z_{l-n-1}-57] (75 % point) from the peptide ECD spectrum and the point of origin can then be used to quantify the relative abundance of products from the *in vivo* or *in vitro* deamidation of the protein (figure 5·4).

Cytochrome *c* was chosen to test this method in a real protein. The tryptic peptide, ^{28}TGPNLHGLFGR$_{38}$, was previously deamidated and its isoforms were separated by HPLC (see section 4.3.2). A two-point calibration equation therefore already exists (y = 0.0259x) using the ECD spectra of the 100% Asp and 100% isoAsp peptide and was used to test whether a ∼75 % isoAsp mixture is generated by this method (figure 5·5). A 5-hr trypsin digestion of cytochrome c produced the peptide ^{28}TGPNLHGLFGR$_{38}$ (m/z = 584.815, 2+) that was to be deamidated. Leucine on the C–terminal side of asparagine is believed to sterically hinder deamidation ($t_{1/2}$ ∼128 days at pH 7.4 and 37 °C)[97] so harsh aging conditions were used to deamidate the peptide. FT–ICR–MS analysis of the tryptic digest after a 16-hr incubation at pH 12 and 80 °C showed complete deamidation indicated by a +0.984 Da shift in its isotopic pattern (*m/z* = 585.307, 2+). The ECD spectrum of the peptide confirmed the sequence was a mixture as revealed by presence of the z_8-57 fragment ion and a peak corresponding to the loss of an Asp side chain ($(M+2H)^{+\cdot}$-60 Da). A value of 0.0192±0.0007 for the Rel[z_8-57] calculated from the ECD spectra corresponds to 74%±4% isoAsp content which falls near the expected 75 % value (figure 5·5). This supports the hypothesis from the procedure presented that a two-point calibration based on the 75 % point (% unknown isoAsp = Rel[isoAsp(unknown)]/Rel[isoAsp(75 % point)] x 75 %) can be used to determine the relative abundance of deamidation products from a protein without the need for synthetic peptides.

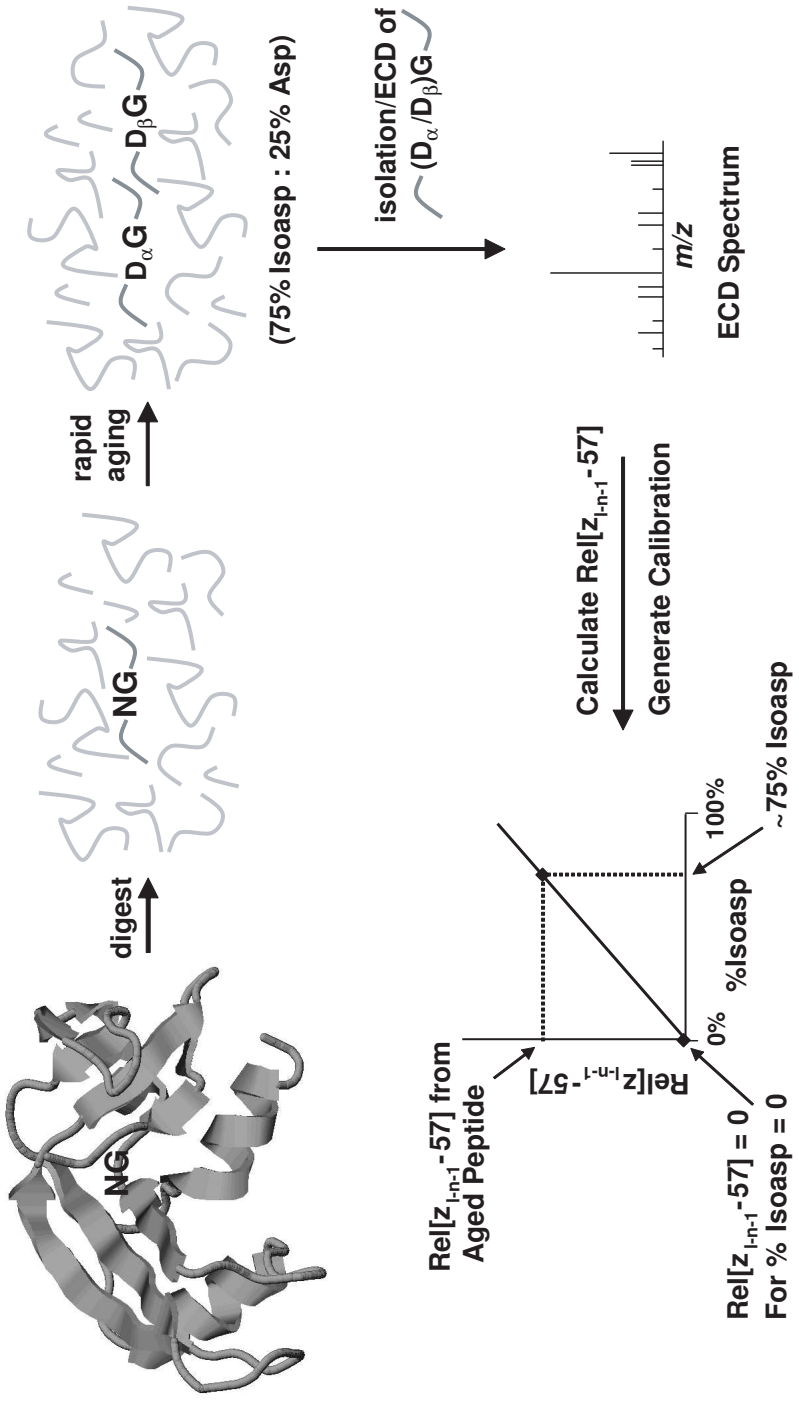

Figure 5·4: Scheme for generating a two-point calibration from a deamidated peptide from a protein digest.

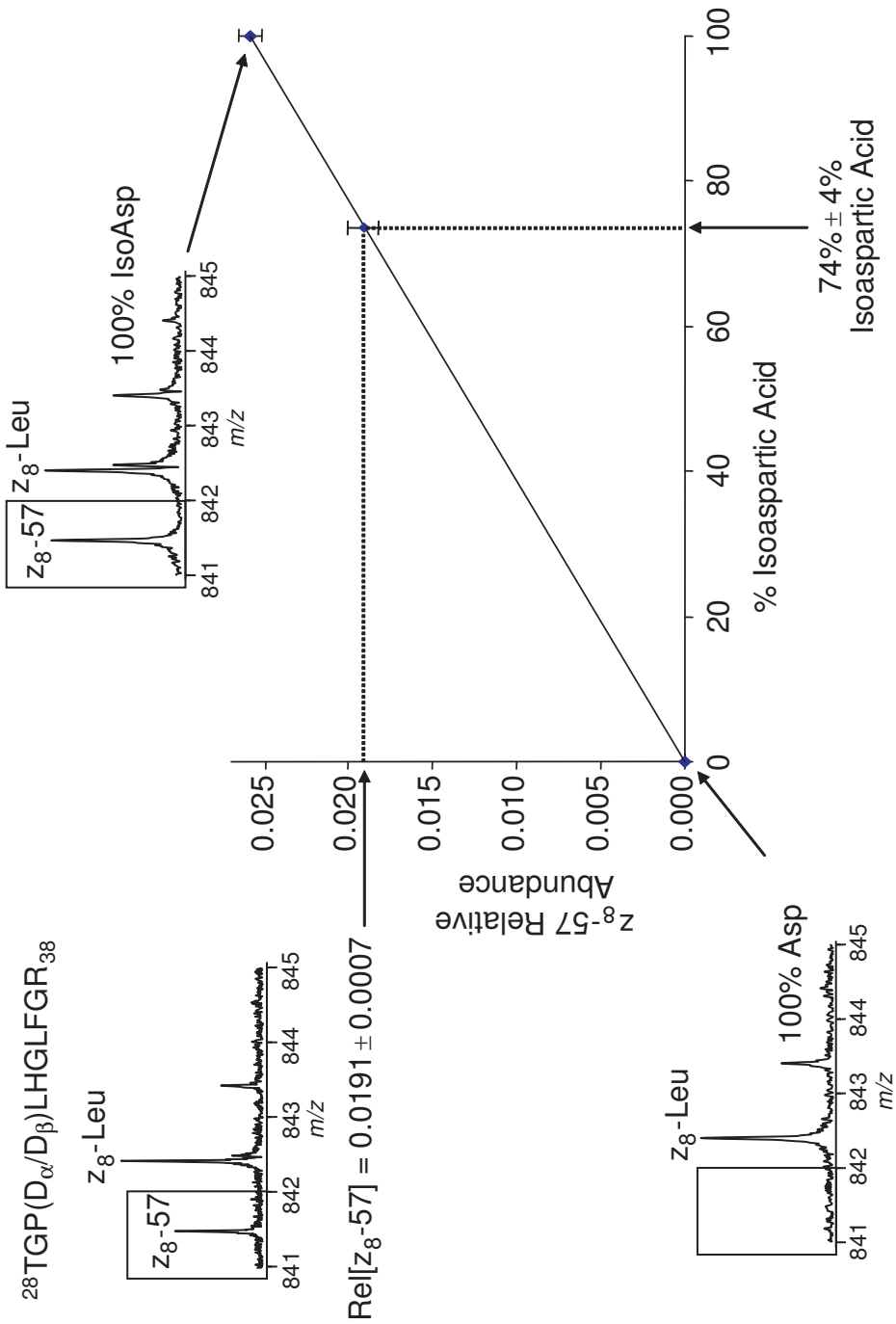

Figure 5·5: Rel[z_8-57] from the ECD spectra of deamidated TGPNLHGLFGR corresponds to 74%±4% using the plot of % isoAsp content versus Rel[z_8-57] constructed from the ECD fragment spectra of TGPD$_\alpha$LHGLFGR and TGPD$_\beta$LHGLFGR, previously separated.

5.3.3 Application of Method to Aspartyl Isomerization

Determining the relative abundance if isoAsp residues resulting from Asp isomerization using the procedure may be possible, but there is no mass change with isomerization, and the point at which the ratio remains constant represents complete Asp isomerization. Peptides containing the –DG– sequence were shown to produce 3:1 (isoAsp:Asp) ratio at equilibrium when incubated in a basic environment (pH $>$ 7),[132] suggesting that the method described above could be applied to Asp isomerization. However, the rate of Asp isomerization is ∼40 times slower than deamidation,[96] so longer and harsher conditions than those typically used for deamidation may be required to force complete isomerization, and such conditions may affect the 3:1 predicted ratio. For example, direct hydrolysis of the side chain amide group to a carboxyl group is promoted when succinimide formation is hindered.[2] This situation would shift the ratio of products away from the expected 3:1 ratio and even more so if the C–terminal neighbor to Asp is a bulky residue. Therefore, additional data may be necessary to confidently say the method proposed above is applicable to Asp isomerization and synthetic standards may be necessary for quantitating the ratio.

5.3.4 Practical Considerations for Using Quantitation Method

All peptides for this study were synthesized with C–terminal arginines to simulate tryptic peptides and their sequences were varied in number of polar/nonpolar residues and position of the isoAsp residue to better represent the sequence diversity found in proteins. The reproducibility of the linear relationship among the four peptides shown strengthens the claim that this method is a useful tool for relative isoAsp/Asp quantitation from asparagine deamidation but only when trypsin is used for protein digestion. The sequence diversity of peptides generated using other enzymes (*e.g.* Glu-C, Lys-C) should statistically be similar to trypsin although their size may be larger. This suggests the applicability of using the isoAsp quantitation method to those employing an enzyme other than trypsin, although additional experiments should be conducted to test this claim.

The procedure for isoAsp quantiation by ECD assumes that a peptide, when harshly deamidated with high temperature, will always achieve a 3:1 molar ratio. While this assumption is clearly true in the case studied here, it may not be true for all peptides. For example, the

competing pathway of direct hydrolysis could alter the ratio when C–terminal neighbors to asparagine are those that greatly reduce the rate of deamidation (*e.g.* valine, isoleucine).[2] Also, Asp and isoAsp could reform the succinimide intermediate when longer incubation periods are required for complete deamidation. Therefore, in cases where more accurate numbers are needed, full calibration plots will have to be generated using pure isoAsp and Asp peptides either from HPLC fractionation, as shown with cytochrome *c*, or synthetically produced, as with the other peptides. Nevertheless, the 3:1 mole ratio from the method presented does generate a good starting point and accurate relative estimates.

Finally, in order to successfully quantitate isoaspartyl residues, a suitable peptide must be obtained that contains the deamidation site and that generates an ECD spectrum with the isoAsp diagnostic ion. Some practical obstacles therefore may be encountered when employing the method such as procuring enough protein for the procedure, isolating a peptide with the deamidation site in the mass spectrometer and generating a useful ECD spectrum from that peptide for quantitation. First, the low-level amount of proteins typically obtained from biological samples is a practical limit to this and most quantitation methods and may prohibit the use of the method entirely or require extensive chromatographic cleanup procedures. Other methods may be necessary, such as immunological[89] or radioactive methods,[154] but these methods can only detect isoAsp residues, and cannot not localize or quantitate the relative abundance of deamidation products. Second, as proteins become larger, their digestion mixtures become more complex. This may result in overlapping species in the broadband ESI spectrum making isolation of the peptide of interest difficult or impossible. Fractionation of the digest therefore may be necessary to reduce the complexity of the mixture, but not as rigorous a separation as one required to differentiate isoAsp from Asp containing peptides. Finally, the peptides used in the experiments were relatively small ($< \sim$1500 Da) and the ECD spectrum of the 2+ charge state for each peptide fortunately showed all inter-residue cleavages including the isoaspartyl diagnostic ion. Therefore, it is important to use a peptide that is favorable for ECD analysis. There are several factors that affect the ECD process such as; the increase in capture cross-section with charge,[62] the hydrogen bonding between fragments that remain after the ECD event,[66] and the distance between the charges and cleavage sites.[211] Because of these factors, a multiply protonated peptide whose charges are uniformly distributed is preferred to facilitate

a complete cleavage pattern and ensure detection of a possible isoaspartyl residue, but it is not always necessary. For example, in section 4.3.3, ECD of the 3+ charge state of a ∼2850 Da tryptic fragment from ribonuclease A showed the diagnostic isoAsp fragment ion but failed to produce fragments representing all inter-residue cleavages. Despite all the possible hurdles discussed, the procedure presented should provide a convenient, MS-based method for relative isoAsp quantitation although additional steps may be necessary to obtain the necessary peptide and generate an adequate ECD spectrum for calculating Rel[z_{l-n-1}-57].

5.4 Conclusion

The plots of Rel[z_{l-n-1}-57] versus % isoAsp content for three sets of synthetic peptides suggest that the linear relationship found is peptide independent but that the slopes are sequence dependent and synthetic standards of each form (isoAsp and Asp) are required to generate calibration curves. However, a method is suggested for determining the relative amounts of protein deamidation products from *in vivo* or *in vitro* experiments without the need to synthetic standards. The procedure involves rapid and harsh aging of the proteolytic peptide containing the deamidation site that can be used to generate a standard mixture for calibration, assuming that the often observed 3:1 (isoAsp:Asp) molar ratio holds true for the peptide of interest, for determining the relative amounts of protein deamidation products. This assumption was tested for cytochrome *c* and appears to be valid. Two important attributes of using ECD to quantitate the relative abundance of isoAsp residues are the elimination of both the need for HPLC separation and the necessity of peptide standards for relative quantitation. Elimination of the HPLC step is beneficial because it dramatically shortens experiment time and decreases sample consumption. This is important considering the amount of protein obtained from typical proteomic experiments. Peptide synthesizers remove tedious manual peptide synthesis but steps such as cleanup procedures and peptide characterization are still required so obtaining the standard directly from the protein is not only facile but also economical. In conclusion, the method presented should be a practical approach for studies involving proteins that have been determined to deamidate but for which the relative abundances of their Asp and isoAsp products are still unknown.

Chapter 6

Probing the gas phase folding kinetics of peptide ions by IR activated DR-ECD

6.1 Introduction

One of the major challenges of modern structural biology is to understand the process of *in vivo* folding of a protein into a well-defined, biologically active structure.[215,216] The effects of aqueous solvation and the intrinsic intramolecular interactions may be better revealed by studying the protein conformation in the gas phase in the absence of solvents. Making use of the soft ionization method of ESI,[10] a number of MS based methods have been applied to investigate the protein conformation in the gas phase, including the ESI charge state distribution to determine the availability of ionization basic sites,[217,218] H/D exchange to identify the exposed region of the conformation,[219–221] drift tube ion mobility spectrometry to measure the conformational cross section,[220,222–224] high-field asymmetric waveform ion mobility spectrometry to separate different conformers,[220,224,225] infrared photodissociation spectroscopy to probe the hydrogen bonding,[226–228] and ECD[1,67] to locate the noncovalent tertiary bonding.[62,66,72,229] Particularly, ECD based methods have been used to study the gas phase unfolding and refolding kinetics of protein ions.[66,72]

ECD in FT–ICR–MS[23] has quickly found wide application in both top-down and bottom-up proteomics,[1,230,231] as well as in identifying and locating PTMs.[171,232,233] As a non-threshold dissociation method, the ECD fragment ion yield of a protein ion is not only affected by its sequence, but also by its higher order structures.[1,225,229] This is the basis of studying protein conformation and folding process by ECD. Noncovalent intramolecular interactions of protein

[1]This chapter has been partially/entirely reproduced from
C. Lin, J. J. Cournoyer, and P. B. O'Connor. Probing the Gas Phase Folding Kinetics of Peptide Ions by IR Activated DR–ECD. *Journal of the American Society for Mass Spectrometry*, accepted, 2008. Copyright 2008 Elsevier

ions may prevent fragment ion separation, leading to decreased product ion yield and poor sequence coverage, both of which can be improved in activated ion (AI)–ECD, where protein ions are unfolded.[234–237] Ion activation is typically done by collisions with background gas molecules,[234,235] raising the ambient temperature,[226] or IR laser irradiation.[236,237] Efficient energy transfer via multiple collisions with gas molecules requires the cell pressure to be increased to the 10^{-6} Torr range, which in turn requires a long pump-down time ($\sim$10 seconds typically) before the pressure is suitable for trapped ion excitation and detection with a sufficiently long transient for good resolving power, making it unattractive for high-throughput analysis or signal averaging when the sample comes in limited amount. Moreover, SORI–CAD[32] of precursor ions is complicated by tuning of optimal conditions for each individual ion, while "in-beam" activation (as in in-beam ECD[234] or plasma ECD experiments[235]) has the limitation of not being able to isolate the precursor ions. Raising the temperature to and keeping it at a well defined value in the ICR cell is not always possible with every FT-ICR mass spectrometer.[44,238] Even when it is possible, it is still inconvenient in that it takes time to heat up the cell before AI–ECD experiments and to cool the cell back down for normal operation afterwards. Furthermore, heating also usually results in an undesirable increase in cell pressure. IR irradiation, on the other hand, is fast, easy to implement, allows precursor ion isolation, and does not result in cell pressure increase, making it the preferred method for ion activation in AI–ECD experiments.

Simultaneous introduction of IR laser and electron beam to intersect the ion cloud in the center of the ICR cell has been previously done by either bringing in one beam off-axis while keeping the other on-axis,[236] or introducing the IR beam through a hollow electron gun mounted on-axis and letting the ring-shaped electron beam be compressed by the magnetic field gradient.[237] It has been shown extensively that ion activation by IR laser absorption lead to enhanced fragmentation in protein ion ECD. The heated, unfolded protein ion can also cool and refold in the gas phase, and ECD fragment ion yield with ECD conducted at various delays after the IR irradiation should provide a measure of the extent of protein refolding.[66]

It should be noted that the increased product ion formation results from the breakdown of the initially formed long-lived fragment ion complexes that stay unseparated during the excitation/detection event in absence of ion activation. Unlike larger protein ions, intramolecular noncovalent interactions in peptide ions are not as numerous. Thus, the resulting fragment ion

complexes in ECD are often short lived, and easily separate to generate individual product ions before ion detection. Consequently, little enhancement in fragment ion yields were expected in AI–ECD of smaller peptide ions. Nonetheless, the existence of these ion complexes in peptide ECD is evident, as suggested by a number of experiments. Deuterium scrambling in ECD of a selectively deuterated linear peptide was readily present, most likely due to intermolecular H/D exchange in the fragment ion complexes (see section 2.3.1). Formation of radical c· ions and even-electron z ions is often observed in peptide ECD experiments, postulated to be the result of H· atom abstraction from the c–ion backbone or side chains by the C_α radical on the z· ion.[239,240] This hypothesis correlates well with the observation of the decreased c·/c ratio and the increased z·/z ratio upon ion activation,[239] when c/z ion separation rate is comparable to that of the H· atom transfer. The knowledge that the c·/c ratio decreases and the z·/z ratio increases upon ion activation has been utilized to distinguish the type of ions formed in ECD.[239] Finally, in DR–ECD experiments, resonant ejection of the charge reduced species and the isobaric fragment ion complexes resulted in abundance decreases of many ECD fragments from peptide ions, thus directly showing that formation of these ECD fragment ions proceeds via radical complex intermediates that have a lifetime at least comparable to that of the ejection time, typically in milliseconds (see section 2.3.2).

6.2 Experimental

6.2.1 Materials and FT–ICR–MS Experiments

Experiments were carried out on a custom-built qQq–FT–ICR–MS with an external electrospray ionization source.[83,214] All peptide were purchased from Sigma Aldrich (St. Louis, MO), and used without further purification. The samples were diluted to ∼5 pmol/μL in 49.5:49.5:1 H_2O:CH_3OH:HCOOH solution, and electrosprayed from glass capillary nanospray tips to generate multiply charged ions. Ions of interest were isolated and accumulated in the front end quadrupoles before entering the cell, where they were subjected to ∼100 ms low energy electron irradiation from an on-axis indirectly heated dispenser cathode (model STD200, Heatwave, Watsonville, CA). In double resonance experiments, the charge reduced molecular ions were resonantly ejected from the cell by applying a single frequency excitation waveform with a V_{p-p} of 2.5 to 40 V during the electron irradiation period.

6.2.2 Implementation of IR Laser for IR–ECD and IR–DR–ECD Experiments

IR light (10.6 μm) from a CO_2 laser (Synrad, Mukilteo, WA) was introduced into the ICR cell through a BaF_2 window, $\sim$ 0.87 inch off center (figure 6·1). The IR laser beam traveled parallel to the magnetic field axis towards a mirror mounted on the cell end trapping plate, with the mirror tilted at $\sim$4.2° such that the reflected beam passed through the center of the

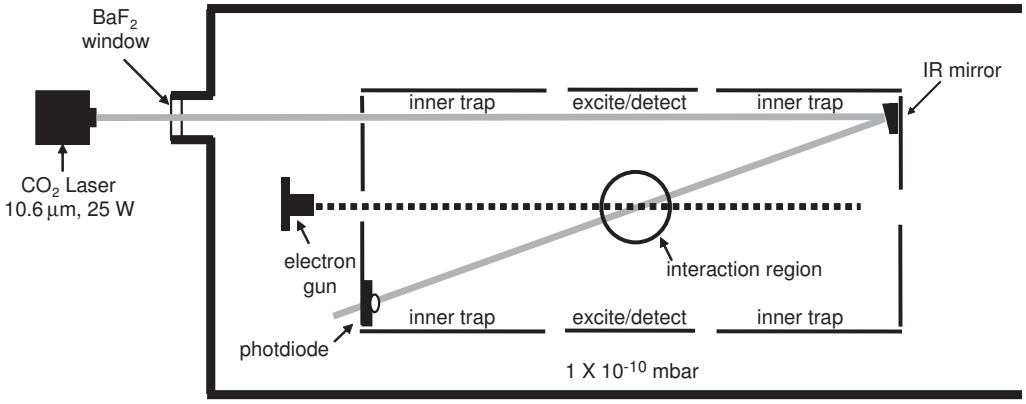

Figure 6·1: Arrangement of the CO_2 laser and electron gun in the ICR region of the FTMS instrument used for IR–ECD experiments. Gray and dashed lines represent IR and electron beam paths, respectively. Circle indicates the region where the ion cloud interacts with both the electron and IR beams.

cell. For initial alignment, a photodiode was installed on the other cell trapping plate, located diagonally from the mirror, also $\sim$ 0.87 inch off center. Overlap of the reflected beam from an alignment diode laser (590 nm) mounted just outside of the laser exit and the photodiode was optimized by maximizing the photoconductivity of the photodiode. The laser beam path was then constructed and defined by insertion and locking of two irises around the beam, and the photodiode was removed as it was not UHV compatible. Final alignment was achieved by maximizing the fragmentation of ubiquitin ions by the 10.6 μm laser. With the IR beam intersecting the ion cloud at an angle, higher fragmentation yield may be achieved by increasing the trapping voltage to squeeze ion cloud axially. However, such was not implemented in IR–DR–ECD experiments, as the objective was merely to heat up the ions gently rather than to achieve maximum fragmentation. The IR irradiation time was adjusted to achieve maximum ion activation without fragmentation.

6.2.3 Data Collection and Processing

A typical spectrum was the sum of 10 scans, acquired at 1 MHz sampling rate and with 512 k point buffer size, corresponding to a 0.524 second transient. The digitized transients were zerofilled twice and fast Fourier transformed without apodization to produce the magnitude mode mass spectra. Because all fragment ions were singly charged, their abundances were calculated directly from peak heights without the need of charge correction to account for ICR response. With the theoretical Fourier-transform limit mass resolving power (f*t/2) being a mere 28,134 at m/z 1000, it was not possible to separate the A+1 isotopic peak of c· or z· ions from the monoisotopic peak of the corresponding c or z ions. Thus, when interference existed, the theoretical A+1 contribution from the OE species was subtracted to give the correct ion abundance of the monoisotopic EE species.

6.3 Results and Discussion

6.3.1 Effects of IR Heating on ECD Pattern of Substance P

As a first example to show the effects of IR heating on ECD pattern of peptide ions, the ECD spectra of substance P (RPKPQQFFGLM-NH_2) both without (figure 6·2–A) and with IR heating (200 ms duration) before (figure 6·2–B) and after (figure 6·2–C) electron irradiation were acquired. Since both basic residues are located near the N–terminus, it is of no surprise that ECD of substance P produced mostly c–type ions, with the only z–type ion being the z_9 that contains the lysine residue. The c_2 ion is not present in the spectrum, even though its *m/z* (273.2) is well above the Nyquist frequency limit used (corresponding to *m/z* ∼215). Post-heating the ion cloud with 200 ms IR irradiation did not change the ECD pattern significantly, with the c_2 ion still missing from the spectrum (figure 6·2–C). Therefore, the absence of c_2 cannot solely be the result of intra-complex noncovalent bonding holding the fragment ion pair together. It has been reported that at 86 K, ECD of substance P generated only two c ions (c_7 and c_{10}), which was proposed to be the result of reduced conformational heterogeneity at lower temperature.[241] The calculated low-energy gas-phase structures of doubly charged substance P involve solvation of the protonated Lys3 away from the N–terminus[242]; thus, even at room temperature, the formation of c_2 is disfavored. The addition of a third charge by either adding a proton or replacing a proton with a divalent metal ion significantly changed the gas phase

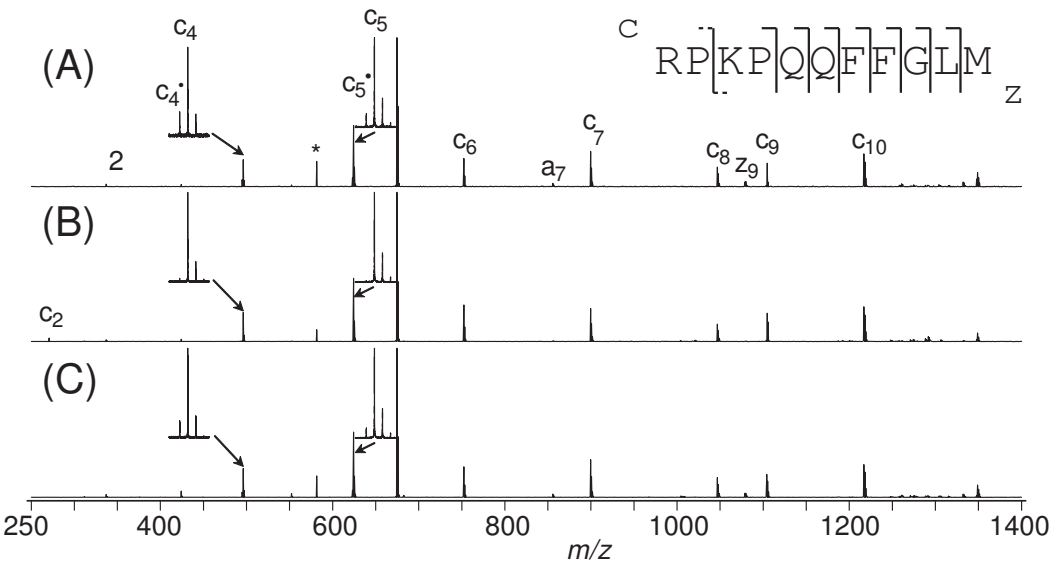

Figure 6·2: ECD spectra of substance P with 150 ms electron irradiation and (A) no IR irradiation, (B) 200 ms IR irradiation immediately before the ECD event and (C) 200 ms IR irradiation immediately after the ECD event. * marks electronic noise.

conformation of substance P, particularly the solvation of the Lys3 proton, as evidenced by the abundant c_2 ion formation.[243] In accordance with these results, preheating the precursor ions with IR also led to the formation of c_2 (figure 6·2–B), likely due to the increased internal energy of the precursor ions by IR heating allowing the protonated Lys3 to be solvated near the N–terminus. The conformational change also led to the disappearance of the z_9 ion, as c_2 formation requires the protonated Lys3 side chain to be hydrogen bonded to the Pro2 carbonyl and neutralized during electron capture, preventing the Arg1 side chain from binding there, which was necessary for z_2 formation. The disappearance of z_2 ions with IR heating may also be the result of secondary fragmentation, although this is unlikely because neither smaller z_n ions nor internal fragment ions were observed. Since the conformational change had to take place before ECD to direct the formation of product ions/neutrals, post-heating the ions would not have similar effects.

In addition to the commonly formed c and z· type ions, ECD of substance P also produced some c· type ions (c_4· and c_5· as shown in the insets of figure 6·2), which disappeared completely when the precursor ions were heated with IR irradiation before ECD. It is generally believed that ECD produces c and z· type ions first and the formation of c· and z ions is the result of

intra-complex hydrogen radical transfer, the extent of which depends on the stability of the z· radical as well as the lifetime of the initially formed c/z· ion pair (see sections 2.3.1 and 2.3.2). [240] IR heating before ECD can disrupt the intramolecular interactions that hold the c/z· ion pair together, leading to shortened lifetime and less c· and z ion formation. On the other hand, post-ECD IR heating appeared to have very little effect, presumably because the intramolecular H· transfer is a fast process that completed before the ion pair complex was heated sufficiently for dissociation. It is also interesting to note that c_4 and c_5 were the only two N–terminal fragment

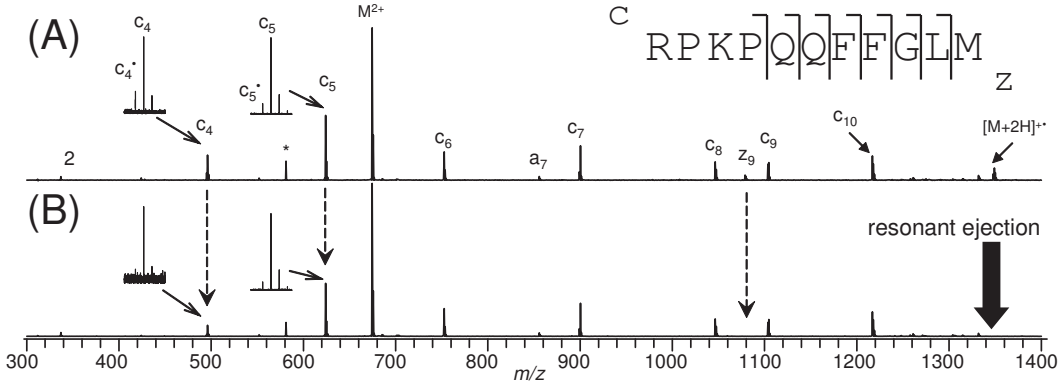

Figure 6·3: ECD (A) and DR–ECD (B) spectra of substance P. * marks electronic noise.

ions showing a significant drop in ion abundances in the DR–ECD experiment (figure 6·3), further suggesting that c· ion formation requires a long-lived ion pair complex. Although the abundances of c_4· and c_5· dropped significantly in DR–ECD, a substantial amount of c· ions remained. Thus, the intra-complex hydrogen radical transfer must have taken place on a timescale at least comparable to that of ion ejection, *i.e.* in sub-milliseconds.

6.3.2 Enhanced Fragment Ion Yield in IR-ECD

While fragment ion yield enhancement and improved sequence coverage in AI–ECD of protein ions were largely attributed to the breaking of noncovalent interactions to facilitate the fragment ion separation and detection, it is clear from the previous example that increased conformational heterogeneity may also play an important role. In IR–ECD of substance P, this resulted in c_2 ion formation and z_9 disappearance with no other significant change in the ECD pattern. A more drastic change in the ECD pattern with IR heating was observed in IR–ECD of fibrinopeptide B (EGVNDNEEGFFSAR), as shown in figure 6·4. ECD of fibrinopeptide B generates mostly z

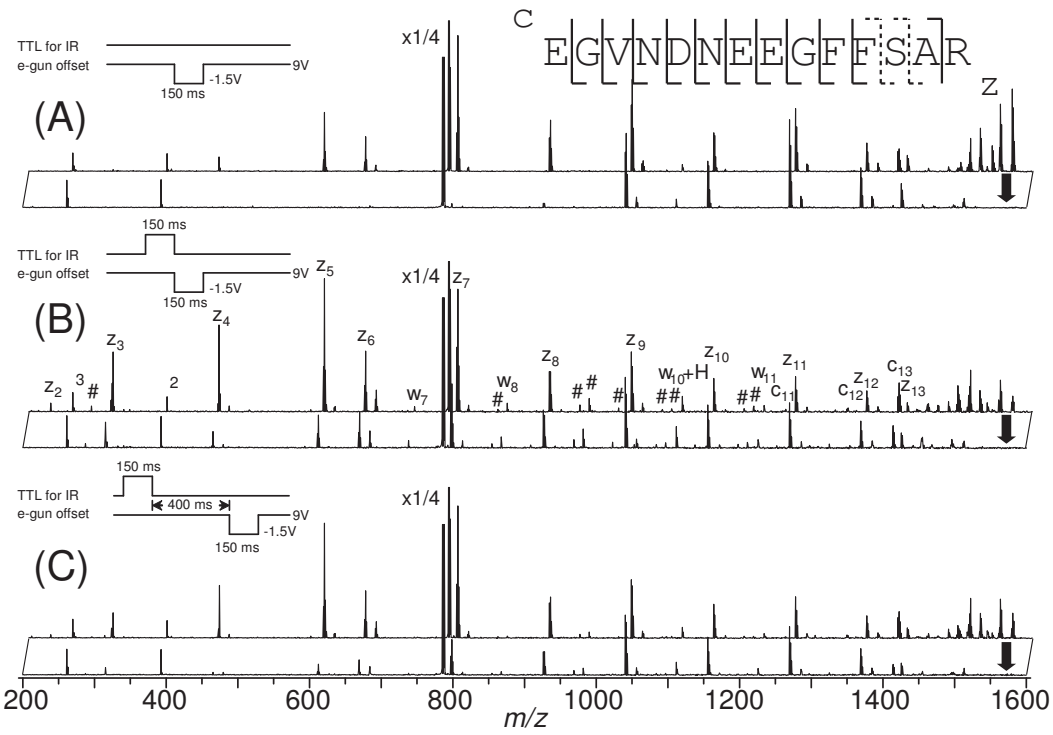

Figure 6·4: ECD (upper) and DR–ECD (lower) spectra of fibrinopeptide B with 150 ms electron irradiation and (A) no IR irradiation, (B) 150 ms IR irradiation immediately before the ECD event, and (C) 150 ms IR irradiation, followed by a 400 ms delay, before the ECD event. Insets illustrate the pulse sequence used in each experiment. For clarity, only c, z and w type ions are labeled, and # indicates secondary fragments corresponding to additional side chain losses from z–type ions. Dashed cleavages are observed in AI–ECD only.

type ions due to charge retention on the C–terminal arginine side chain upon electron capture, with a small peak corresponding to the c_{13} ion (upper spectrum, figure 6·4–A). $z_2\cdot$ ($m/z \sim$230) was missing from the spectrum, and $z_3\cdot$ was barely observable. 150 ms IR irradiation before ECD (upper spectrum, figure 6·4–B) led to formation of the z_2 ion, and a large abundance increase for many small z ions (z_3 to z_6) as well as c_{11} and c_{13} ions. In the DR–ECD experiment, z–ions up to z_8 showed appreciable abundance drop upon resonant ejection of the charge reduced molecular ion (at $m/z \sim$1571) during the ECD event (upper spectrum, figure 6·4–A), suggesting that the C–terminal arginine side chain was hydrogen bonded to the side chains of Asn4 to Glu8 at room temperature, which is highly likely since this sequence contains three acidic residues. The folded structure may also sterically restrict the access of the N–terminal -NH_3^+ group (or other charge sites) to the carbonyls of Gly9 through Ala13, thus minimizing ECD near this region.

Such steric restriction would be removed and the conformation heterogeneity increased when the peptide was unfolded by IR heating prior to electron irradiation, resulting in the fragment ion yield increase as observed. In order to open up new fragmentation channels, the unfolding and the conformational change have to take place before the dissociation event. IR irradiation after ECD did not change the ECD pattern significantly (spectrum not shown). Once again, it shows that the increased fragment ion yield in AI–ECD of small peptide ions is more likely to be the result of conformational change than the ease of fragment ion separation.

6.3.3 Secondary Fragment Ion Formation in IR-ECD of Fibrinopeptide B

ECD of a multiply charged peptide ion produces an EE fragment (c ion) and an OE fragment (z· ion). The radical site on the OE fragment can initiate further reactions such as intra-complex hydrogen radical transfer which leads to the formation of c· and z ions,[240] or secondary fragmentation with little or no activation barrier.[67,69,78,198] Secondary side chain fragmentation leading to the formation of d– and w– type ions is well documented in the ECD literature, and has found application in *de novo* sequencing for its ability to distinguish between Leu and Ile residues.[76,78,204,237] Abundant w ion formation was apparent in the IR–ECD experiment (figure 6·4–B), in accord with previous observations in hot ECD and AI–ECD, where extra energy seem to enhance the w ion formation. Many other secondary fragment ions (peaks marked with # in figure 6·4–B) were also present in the IR–ECD spectrum, corresponding mostly to side chain losses from the z–ions. It is important to heat up the precursor ion before ECD, instead of the fragment ions after ECD, as post-ECD IR irradiation generates little secondary fragment ions. This might be due to rapid radical stabilization (see section 2.3.3)[244,245] via radical rearrangement, such as intra-complex H· transfer, proline ring opening, or radical trapping near the aromatic group, before IR heating. Secondary backbone fragmentations dominated the ECD spectra of cyclic peptides,[67] but no internal fragment ions were found in the IR–ECD spectrum of fibrinopeptide B, presumably because of the charge locations at the termini.

6.3.4 Unfolding and Refolding of Peptide Ion by IR Irradiation

AI–ECD has been used to study protein folding in the gas phase, by monitoring the fragment ion yield, which often increases with ion activation, due to breaking of intramolecular hydrogen

bonds that prevent fragment ion separation.[66,72] The challenge of extending this method to peptide folding studies is that the lifetime of the fragment ion complexes from peptide ion ECD is often much shorter than the delay between the ECD event and ion excitation/detection, and as the result, nearly all fragment ions are readily detected, with or without ion activation. This difficulty may be circumvented by applying the DR–ECD method, where resonant ejection of the fragment ion complexes during ECD can reduce the fragment ion abundance (see section 2.3.2). Because of the rapid ejection time, even fragment ions from intermediates of millisecond lifetime, as is typical in peptide ion ECD, can experience significant abundance drop in DR–ECD, and the subsequent increase when IR irradiation is applied to unfold the precursor ions.

A greater abundance drop in DR–ECD indicates a longer lifetime of the intermediate through which the product ions are formed, as the result of a more folded structure of the precursor ion. Compared to the sharp abundance drop in DR–ECD of room temperature fibrinopeptide B (upper spectrum, figure 6·4–A), many small z ions experienced only moderate to little drop in abundance with pre-ECD IR irradiation (lower spectrum, figure 6·4–B), suggesting that most of the intramolecular hydrogen bonds were already broken. The lifetime of the intermediate can be calculated by assuming that separation of a fragment ion pair follows first–order unimolecular dissociation kinetics (see section 2.3.2). Figure 6·5 plots the abundance

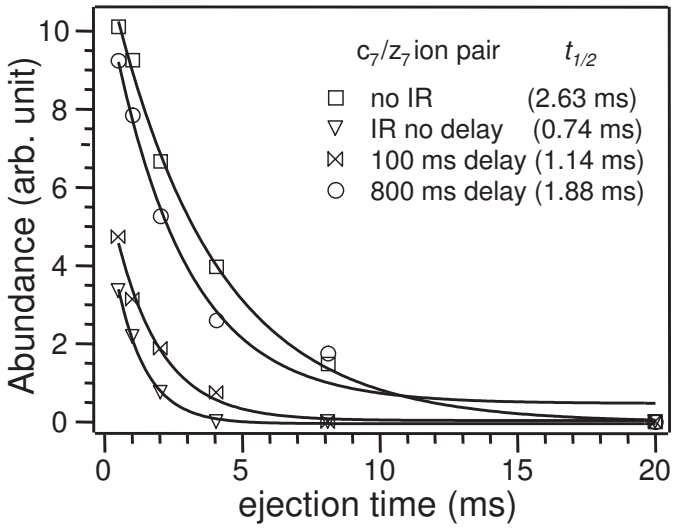

Figure 6·5: First order decays of the intact c_7/z_7 ion pair abundance as a function of ejection time when ECD of fibrinopeptide B was carried out at various delays after the IR irradiation. Solid lines are single exponential fits.

of the intact c_7/z_7 pair, which is calculated as the difference between the abundance of z_7 ion

in normal ECD and that in DR–ECD, against the ejection time with DR–ECD taking place at various time delays after the IR irradiation (or without IR irradiation). The single exponential decay fit gives the lifetime of the c_7/z_7 ion pair complex of ∼2.6 ms without pre-ECD IR heating, and ∼0.7 ms when ECD was performed immediately after the IR irradiation. When there was a delay between the IR and the DR–ECD event (figure 6·4–C), the lifetime of the intermediate increased to ∼1.1 ms with a 100 ms delay, and ∼1.9 ms with a 800 ms delay. Clearly, the unfolded peptide ion can cool and refold back to a more compact structure, particularly in absence of solvent molecules in the gas phase. The refolding process took place in several hundred milliseconds to a few seconds, but a more quantitative assessment of the refolding time constant would require a properly constructed kinetic model.

6.3.5 Refolding Kinetics of Fibrinopeptide B Probed by the Fragment Ion Yield in DR-ECD

A simple two–state model was used to study the refolding kinetics, which assumes that a peptide ion can only exist in one of the two states: a folded state, or an unfolded state. All c/z ion pairs from an unfolded peptide ion will break before ejection, but only a fraction (x) of these ion complexes from a folded peptide ion will break before ejection. The value of x depends on both the amplitude of the resonant ejection waveform and the lifetime of the intermediate, and it can be obtained from the DR–ECD experiment without IR heating, assuming that all peptide ions are folded to start with. If DR–ECD is performed at a delay of t after the IR irradiation, then the ratio (r) of the fragment ion abundance with resonant ejection to the one without resonant ejection can be expressed as;

$$r = y + (1 - y) * x \tag{6.1}$$

where y is the fraction of the peptide ions remaining unfolded at time delay t. This ratio (r) should drop as the delay t increases and the peptide ions refold. Since r can be obtained experimentally, and x is just r without IR irradiation, the fraction of the unfolded peptide ions, y, at any given delay after the IR irradiation can be calculated according to equation 6.1. Assuming first order refolding kinetics, one can obtain the refolding time constant k_{refold} by fitting y as a function of t to a single exponential decay. Figure 6·6 shows one such plot using the

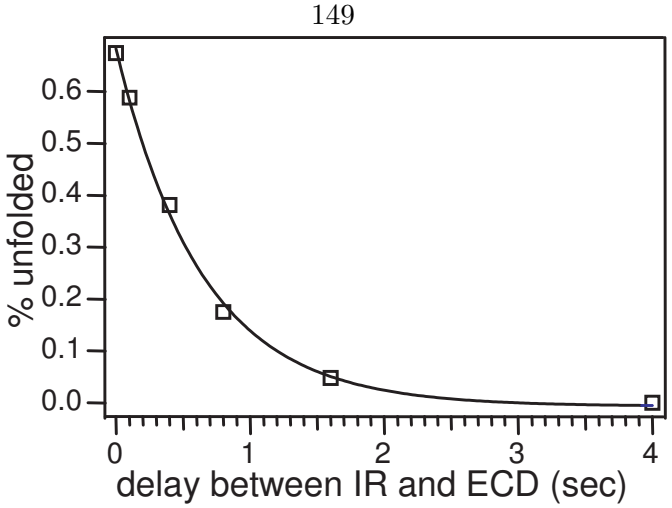

Figure 6·6: Percentage of the fibrinopeptide B ions that remained unfolded (as calculated from the DR-ECD experiment) at various time delays after the IR irradiation was turned off. Solid line is the single exponential fit.

z_7 yield in DR–ECD with 20 V_{p-p} ejection voltage as the probe for precursor ion folding state. Abundances from both the odd and even electron z_7 ions are included, because the formation of either results from the breaking of the same initially formed $c_7/z_7\cdot$ complex. The best fit gives a k_{refold} of 1.55 ± 0.10 s^{-1}, corresponding to a half-life of 0.45 s, which correlates well with figure 6·4–C. This is much faster than that for protein ions, which typically take minutes to refold in the gas phase.[72] Presumably, the reduced dimension of the potential energy surface of the smaller peptide ion makes it faster to find its low energy structures than its protein counterparts.

6.3.6 Refolding Kinetics of Fibrinopeptide B Probed by the Intra-Complex Hydrogen Transfer

The key to the study of gas phase peptide folding by AI–ECD is to find a suitable property that varies with folding states, such as the fragment ion yield in DR–ECD experiment (*vide infra*). Figure 6·7–A shows that even though the total abundance of the z_7 ions in ECD did not change much with the IR heating, the ratio of z to z· ion abundance increased as the delay between IR and ECD increased. This should come as no surprise, as EE z ions are the products of intra-complex hydrogen radical transfer, which should decrease as the IR heating unfolds the peptide, leaving the product ion complex too short-lived to complete the H· transfer. The same two–state model can be used to study the peptide ion refolding, with a slightly different

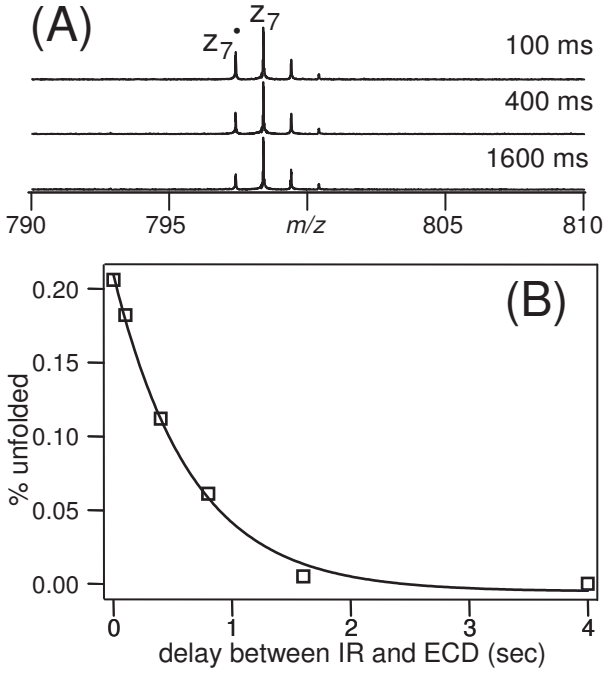

Figure 6·7: (A) Expanded regions of the ECD spectra of fibrinopeptide B showing that the percentage of the hydrogen transfer product (z_7) increased as the delay between the IR and ECD events increased. (B) Percentage of the fibrinopeptide B ions that remained unfolded (as calculated from the ratio of $z_7\cdot$ and z_7 abundances) at various time delays after the IR irradiation was turned off. Solid line is the single exponential fit.

definition for folding and unfolding states. An unfolded peptide should only produce z· ions, as there is nothing to hold the fragment ion pair together for H· transfer to take place. If a peptide is folded, however, a fraction (x) of the z· ions can abstract a hydrogen atom to form z ions, and the value of x can be obtained from the ECD experiment without IR heating, assuming all peptide ions are unfolded before IR irradiation. If y is the fraction of peptide ions remaining unfolded at a delay of t after IR, we have:

$$\frac{[z]_t}{[z]_t + [z\cdot]_t} = (1 - y) * x \tag{6.2}$$

Since the fraction of the even-electron z ions in the total z ion population can be directly measured in the ECD spectrum, y can be calculated for any given delay t. Once again, plotting y as a function of t should give a single exponential decay if the refolding process follows first order kinetics. Figure 6·7–B plots the percentage of the unfolded peptide ions against delay t, using the $[z_7]/([z_7]+[z_7\cdot])$ to calculate y. The best fit gives k_{refold} of 1.52 ± 0.14 s^{-1},

corresponding to a 0.45 s refolding time, nearly the same as that obtained in the IR–DR–ECD approach (section 6.3.5).

Furthermore, it is also possible to estimate the intra-complex H· transfer rate based on the abundance ratio of the EE and OE fragment ions and the fragment ion pair separation rate measured in the DR–ECD experiments. Figure 6·8 illustrates the formation of c· and z ions as the result of intra-complex H· transfer.

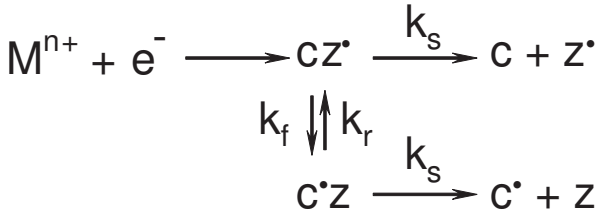

Figure 6·8: Electron capture of a multiply protonated species cleaves an N–C_α bond generating a c/z· pair that are bound by an intramolecular interaction(s). H· transfer between the fragments is reversible process with the rate constants k_f and k_r. Both sets of products can dissociate at a rate k_s to form separate c and z fragments.

The rate equations for relevant species in scheme 1 are shown in equations 6.3;

$$\begin{aligned}
\frac{d[cz\cdot]}{dt} &= -k_s[cz\cdot] - k_f[cz\cdot] + k_r[c\cdot z] \\
\frac{d[c\cdot z]}{dt} &= -k_s[c\cdot z] + k_f[cz\cdot] - k_r[c\cdot z] \\
\frac{d[z\cdot]}{dt} &= k_s[cz\cdot] \\
\frac{d[z]}{dt} &= k_s[c\cdot z]
\end{aligned} \tag{6.3}$$

Equation set 6.3 can be solved analytically, giving;

$$\begin{aligned}
[cz\cdot]_t &= \frac{[cz\cdot]_0}{k_f + k_r}[(k_r e^{-k_s t} + k_f e^{-k_f+k_r+k_s)t}] \\
[c\cdot z]_t &= \frac{[cz\cdot]_0}{k_f + k_r}[(k_f e^{-k_s t} - k_f e^{-k_f+k_r+k_s)t}] \\
[z\cdot]_t &= \frac{[cz\cdot]_0}{k_f + k_r}\left(k_r[1 - e^{-k_s t}] + \frac{k_s k_f}{k_f + k_r + k_s}[1 - e^{-(k_f+k_r+k_s)t}]\right) \\
[z]_t &= \frac{[cz\cdot]_0}{k_f + k_r}\left(k_r[1 - e^{-k_s t}] - \frac{k_s k_f}{k_f + k_r + k_s}[1 - e^{-(k_f+k_r+k_s)t}]\right)
\end{aligned} \tag{6.4}$$

As stated earlier, for most peptide ECD experiments, when the excite/detect event happens,

nearly all fragment ion pairs have already fallen apart. In other words, t in the above solution at the time of detection can be approximated as infinity when considering the product branching ratio, giving:

$$\frac{z\cdot}{z} = \frac{k_r + k_s}{k_f} \tag{6.5}$$

In the extreme case where the separation of product ions is much slower than the intra-complex hydrogen transfer, *i.e.*, $k_s << k_r$, the ratio is governed primarily by thermodynamics, giving the equilibrium constant between the c/z· and c·/z ion pairs. In the other extreme case where the separation of product ions is much faster than the intra-complex hydrogen transfer, *i.e.*, $k_s >> k_r$, the ratio is kinetically controlled, with the equation 6.5 reduced to the familiar form of $[z\cdot]/[z] = k_s/k_f$, giving the branching ratio of a parallel or competitive reactions.

Equation 6.5 can be rearranged as;

$$\frac{z\cdot}{z} = \frac{k_r}{k_f} + \frac{1}{k_f}k_s \tag{6.6}$$

With different delays between IR and ECD events, a set of [z·]/[z] values can be obtained, with the corresponding k_s calculated from the DR–ECD experiment, and fit into a straight line. Figure 6·9 shows one such plot for fibrinopeptide B, using the ratio of [z7·]/[z7] and

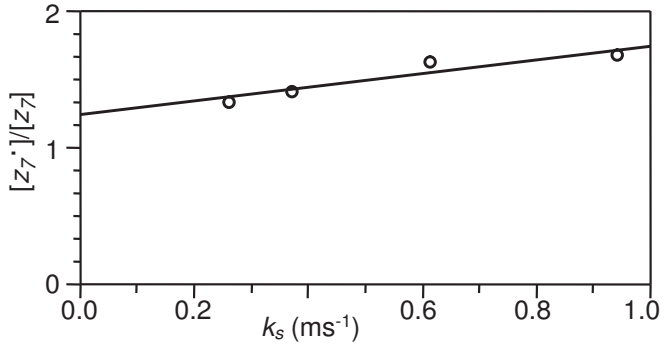

Figure 6·9: Linear fit of the ratio of the $z_7\cdot$ and z_7 abundances as a function of the ion separation rate constant as calculated from the DR-ECD experiments.

the k_s values from figure 6·5. The linear regression fit gives a k_f of 2.0 ms^{-1} and a k_r of 2.4 ms^{-1}. The quality of the fit is only moderate, with a 0.94 correlation coefficient, likely because of the assumption that k_f and k_r are independent of the folding state. Nevertheless, the obtained hydrogen transfer rates are nearly an order of magnitude higher than the rate

of product ion pair separation under normal ECD conditions. It is thus of no surprise that c· and z type ions are commonly observed in peptide ion ECD, as the initially formed c/z· ion pairs have plenty of time to undergo intra-complex hydrogen transfer before they separate to produce individual fragment ions. Despite this fast intra-complex hydrogen transfer rate, c· and z type ions are rarely observed in protein ion ECD experiments. Columbic repulsion between positively charged c and z· counterparts, which are not present in the ECD products of doubly charged tryptic peptide ions, may lead to faster product ion separation in protein ion ECD, contributing to this lack of H· transfer products. However, such is not always the case as demonstrated in the DR–ECD experiment of bovine ubiquitin, where many product ions displayed significant abundance drop upon resonant ejection of the charge reduced molecular ion, indicating millisecond lifetimes (at least) of the fragment ion complexes (see section 2.3.2). Presumably, the much more extensive noncovalent interactions in protein ions outweigh the columbic repulsion in determining the lifetime of intermediates. Most likely, in protein ion ECD, H· transfer still occurs extensively before product ion separation, but somehow preferentially within the z· fragment itself leading to radical stabilization, possibly due to the tertiary structure of the gas phase protein ion.

The percentage of the unfolded peptide ions at any given time delay t is very different for figure 6·6 and figure 6·7, because of different definitions of an unfolded peptide in two methods. For the DR–ECD approach, fragment ion pair complexes from an unfolded peptide cannot have a lifetime longer than the ejection time, while for the H· transfer method, they cannot undergo any (observable) intra-complex H· transfer before they break apart to produce c and z· ions. Since $t_{1/2}$ of H· transfer is much shorter than the ejection time applied in DR–ECD studies, a significant amount of ion complexes from "unfolded" peptide ions in the DR–ECD approach may still live long enough to generate H· transfer products, and are therefore considered "folded" peptides in the H· transfer method. Regardless, despite different ways to probe the folding state of the peptide ions, these two methods give similar refolding time constants. When there are abundant c· or z type ions, the H· transfer approach is convenient, and has the potential of probing folded state that produces fragment ion pairs shorter lived than that can be probed by the IR–DR–ECD approach, as the typical half-life for H· transfer is only a fraction of the ejection time commonly applied. However, not all peptide ions produce appreciable amount of c·

or z type ions, and when this is the result of intra-fragment ion radical stabilization rather than ultra-fast fragment ion pair separation, the IR–DR–ECD method should provide an excellent way to study the folding kinetics.

6.4 Conclusion

The effect of IR irradiation on the ECD fragmentation pattern of peptide ions was investigated using two model peptides, substance P and fibrinopeptide B. The increased internal energy of the precursor ions often led to amplified secondary fragmentation in IR–ECD. Ion activation was accompanied by increased conformational heterogeneity and weakened non-covalent intramolecular interactions. Improved sequence coverage was observed in both peptide ions, likely the result of the conformational change, rather than faster fragment ion separation, as suggested by the lack of sequence coverage improvement when IR irradiation was introduced after the ECD event. Weakening of noncovalent interactions did not lead to appreciable enhancement of fragment ion yield, because even at ambient temperature, fragment ion pair separation from small peptide ECD was nearly complete before ion excitation and detection, making IR–ECD unsuitable for probing gas phase peptide ion folding states. However, IR unfolding of peptide ions did lead to increased c/c· and decreased z/z· ratios, which can be utilized to study the peptide refolding process. The refolding rate constant for fibrinopeptide B was measured to be $\sim$1.5 s^{-1}, much faster than that of protein ions. Linear regression fit based on a simplified kinetic model of intra-complex hydrogen transfer gave the H· transfer rate constant of $\sim$2 ms^{-1}, about an order of magnitude faster than the separation rate of the long-lived c/z ion pair, explaining the ubiquitous presence of c· and z type ions in peptide ion ECD spectra. Alternatively, the folding kinetics of peptide ions can be studied by the IR–DR–ECD method. Rapid resonant ejection of the charge reduced species during ECD can lead to difference in fragment ion yields for folded and unfolded peptide ions, which were indistinguishable under normal ECD conditions, thus making it a suitable probe for folding studies. This approach gave very similar folding time as that obtained by monitoring the extent of hydrogen transfer, and can be especially useful when no appreciable c· and z type ions are present in the ECD spectrum.

Chapter 7

Gas-phase Structure Dissimilarity of Isoasaprtyl and Aspartyl Peptides Revealed by IR-Activated DR-ECD

7.1 Introduction

7.1.1 Using Mass Spectrometry to Probe the Higher-Order Structure of Peptides and Peptides

The combination of soft ionization techniques such as ESI[10] and the high mass accuracy provided by FT–ICR–MS[23] has expanded the ability to study intact biological complexes[218,246,247] therefore becoming complementary to other methods such as chromatographic techniques for binding stoichiometry[248] and NMR for binding sites.[249] However, the verity of the analysis depends heavily on how the complexes (*e.g.* protein-protein, protein-ligand) contend with the transition from the solution to gas-phase in MS, especially for those sprayed from a buffered solution necessary for complex formation.[246] In particular, do these in vacuo complexes and constituent proteins reflect the native solution conformation, and if not, how greatly does the gas phase structure distort the validity of the data obtained from such experiments? To answer these questions, it becomes increasingly important to understand the rules governing the gas-phase structures of these biologically relevant molecules.

Several MS based methods can be used to gain an understanding of the higher-order structure of proteins and other biologically significant molecules in the gas phase such as H/D exchange,[250–252] ion mobility spectrometry[222,253] and ECD.[1,66,72,254] MS analysis of proteins subjected to H/D exchange in solution and gas-phase helps elucidate structural discrepancies of proteins and peptides between the two phases by providing information on exchangeable hydrogens.[247,250–252] IMS provides cross-sectional information on gas-phase structures relative to the predicted structures. Electrosprayed and isolated proteins of the same mass but different

conformations drift through an electric field and a pressurized region at dissimilar velocities providing some comparative information on gas-phase structure.[222] For example, IMS was able to resolve two conformers for the 9+ charge state of ubiquitin since their cross sections were different by 10%.[220]

Finally, ECD can be used to probe both the primary structure and gas-phase conformation of peptides and proteins since weak intramolecular interactions such as hydrogen bonding, vital for supporting higher order structure in the gas-phase, are preserved after dissociation.[72] For sequencing, ECD typically provides a more thorough cleavage pattern[62] and, because the cleavages result from radical rearrangement (also see chapter 2),[67] the mild excitation often preserves important but labile PTMs[65,71,201] (*e.g.* phosphorylation, glycosylation, and sulfation) contrary to cleavages caused by vibrational excitation methods (*e.g.* CAD,[255,256] IRMPD [51]) which typically cause the loss of such modifications. The backbone-directed nature of ECD preserves intramolecular hydrogen bonding occurring in the gas-phase so that the higher-order structure of proteins and peptides can be inferred from the fragmentation spectra. Temperature perturbation inside the ICR cell of the FT–ICR–MS has revealed gas-phase structural information on cytochrome c[72] and ubiquitin[66] in addition to the *in vacuo* unfolding dynamics of the latter. Also, several experiments have used temperature change to study the higher-order structure of peptides. Unfolding caused by increasing the temperature at the ion source followed by ECD allowed partial elucidation of the secondary structure of a peptide.[254] Also, ECD of substance P performed at low temperatures demonstrated fewer cleavages indicating a decrease in the structural heterogeneity at 86 K and/or increase in the stability of the resultant hydrogen bonded complex after the initial cleavage (the reduced molecular ion was present in the spectrum).[241] All of the examples mentioned extracted conformational information from changes in ECD fragmentation pattern with temperature based on the hypothesis that intramolecular interactions were disrupted with increasing ion temperature.

7.1.2 Using DR-ECD to Probe the Effect of Deamidation on Peptide Structure

In section 2.3.2, resonance ejection of the charge reduced precursor ion during ECD (DR–ECD) showed a decrease in some fragment ion populations since the ejected species are sequence complement fragments linked by preserved noncovalent bonds, *i.e.* hydrogen bonds (see chapter

6). Some gas-phase structure information could be extracted from the data based on which fragments experience a change in abundance, specifically, those fragments whose abundances are reduced are involved in noncovalent interactions and fragment. In this study, similar DR–ECD experiments were performed but at different ion temperatures afforded by an IR laser in order to calculate the enthalpy and entropy of peptide unfolding for two isomeric 10-mer peptides, one with Asp and one with isoAsp.

7.1.3 Sample Preparation

Materials

The peptides YWQHTAD$_\alpha$QFR-NH$_2$ and YWQHTAD$_\beta$QFR-NH$_2$ were synthesized by a standard solid-phase peptide synthesis procedure previously described in section 5.2.2. Substance P, ubiquitin, fibrinopeptide B, and formic acid were purchased from Sigma Aldrich (St. Louis, MO) and RAAAGADGDGAGADAR was purchased from Anaspec (San Jose, CA). All other chemicals were purchased from Fisher Scientific (Fairlawn, NJ). Peptides were dissolved in 49.5:49.5:1 methanol:water:formic acid at $\sim 10^{-5}$ M.

7.1.4 IRMPD Setup

In order to use the on-axis solid cathode (electron gun), an off-axis CW IR laser was installed for IR–ECD experiments and described previously in section 6.2.2.

7.1.5 Mass Spectrometry

FT–ICR–MS Experiments

All experiments were performed on a custom qQq–FT–ICR–MS (FT–ICR–MS with mass filtering front-end quadrupole and collision cell) equipped with a nano-spray source and a 7 T actively shielded magnet previously described (section 1.2.4).[83,214] For each experiment, 10 μL of peptide or protein solution was sprayed from a pulled glass capillary nanospray tip (1 μm orifice) with a platinum electrode inserted into the back end and biased to 1200 V to generate positively charged ions. The multiply charged precursor ions were isolated in Q1, accumulated in Q2, and then transmitted to the ICR cell. Proteins or peptides were irradiated with 10.6 μm light from an off-axis CO_2 IR laser (Synrad, Mukilteo, WA) (*vide supra*) for precursor ion heating. An on-axis, indirectly heated cathode dispenser (Heatwave, Watsonville, CA) was pulsed

to a negative voltage to emit low energy electrons for ECD, and the voltage bias was kept at +10 V at all other times. The grid voltage was set to 7 V. The IR–ECD experiments were performed using an IR laser pulse followed by an ECD pulse with a short delay between the two events (5 to 10 ms). The IR irradiation period was adjusted until minimum fragmentation from slow heating dissociation was achieved at 100% laser power, which ranged from 100–300 ms. The laser power was then attenuated to demonstrate peptide unfolding by 10.6 μm light followed by an ECD pulse that typically ranged 50–100 ms.

Thermodynamic calculations were based on IR–DR–ECD experiments that were performed in a similar way to IR–ECD experiments except with constant ejection of the reduced molecular ion ($(M+2H)^{+\cdot}$, m/z = 1351.6) during the ECD event for YWQHTAD$_\alpha$QFR-NH$_2$ and YWQHTAD$_\beta$QFR-NH$_2$. The length of the ECD event was 25 ms to mitigate multiple electron capture. To ensure total ejection of $(M+2H)^{+\cdot}$ during ECD, the resonance pulse (20 V_{p-p}) was applied for a duration of 35 ms, a time period that overlapped before and after the electron irradiation event by 5 ms. All IR–DR–ECD spectra were the sum of 20–25 scans and performed in triplicate.

BIRD–ECD Experiments

A thermocouple was mounted inside the ICR cell to perform black-body infrared radiative dissociation (BIRD)[42]–ECD experiments so that ion temperature could be calibrated to the laser irradiation. The thermocouple (Omega, Stamford, CT) was calibrated by baking the chamber containing the ICR cell at specific temperatures. The chamber was allowed to come into equilibrium overnight for each temperature point and a calibration curve of voltage versus temperature was constructed. For BIRD–ECD experiments, cations were stored in the ICR cell for specific times before the ECD pulse (10, 1000, 2000, 4000 milliseconds for substance P and 5, 500, 1000, 2000, 3000 milliseconds for YWQHTAD$_\alpha$QFR-NH$_2$ and YWQHTAD$_\beta$QFR-NH$_2$.

7.2 Experimental Results

7.2.1 Peptide Unfolding and Intra-complex H$_{\mathrm{cot}}$ Transfer

The shift of c$\cdot$/z ions to their corresponding c/z$\cdot$ ions has been shown to occur as a result of peptide heating by IR light[239,240] and ejection of the reduced species during ECD (DR–ECD)(see

section 2.3.2 and chapter 6) suggesting that H· transfer occurs primarily between spatially adjacent regions of the peptide within the post-ECD hydrogen-bonded complex (figure 2·6). The peptide regions that neighbor one another are supported by intramolecular interactions that sustain the higher-order structure. In the case of multiply protonated gas phase peptides, the most likely interactions are hydrogen bonds between the protonation site and neighboring polar groups such as backbone carbonyl groups and amino acid side chain groups,[240,242,254,257] although other interactions, such as salt bridges, are also possible. Heating the peptide via blackbody irradiation or IR light ruptures these interactions thus unfolding the peptide and separating the previously neighboring regions. ECD is a useful tool for monitoring this process because it simultaneously preserves these labile interactions during unfolding and provides a gauge by which to measure the process, the H· transfer products (c·/z ions). Therefore, unfolding of a peptide in the gas-phase can be described as a transition between two states that are designated by what ECD fragments they generate; a folded state that generates a mixture of c/c· and z·/z ions and an unfolded one that generates only c and z· fragments. To illustrate this correlation, several gas-phase peptides were unfolded by IR light and the extent of H· transfer for their ECD fragments were examined.

Fibrinopeptide B, substance P, and RAAAGADGDGAGADAR all show shifts to a higher population of EE c and OE z ions with IR heating (figure 7·1). The laser power was adjusted rather than irradiation times to avoid complications regarding electron beam-ion cloud overlap caused by magnetron motion.[86] Since the heated peptide ions will cool off once the IR irradiation is turned off, it is important to keep the delay between the end of the IR event and the start of the ECD event constant so that the equivalent internal temperature of the ions will remain the same between all experiments with the same laser power. Peptide refolding induction times are generally greater than 100 ms (see section 6.3.5), therefore the ECD event must occur within at least 100 ms of IR irradiation so that the fragmentation spectrum accurately reflects the distribution of unfolded states at a specific laser power. Short irradiation periods (<100 ms) with 10.6 μm light typically increases the internal energy of the peptide disrupting weaker intramolecular forces (*e.g.* hydrogen bonding) resulting in a reduced fraction of the folded species in the total ion population. As a result, intra-complex H· transfer decreases because interacting regions are no longer adjacent to one another, *i.e.* peptides are unfolded.

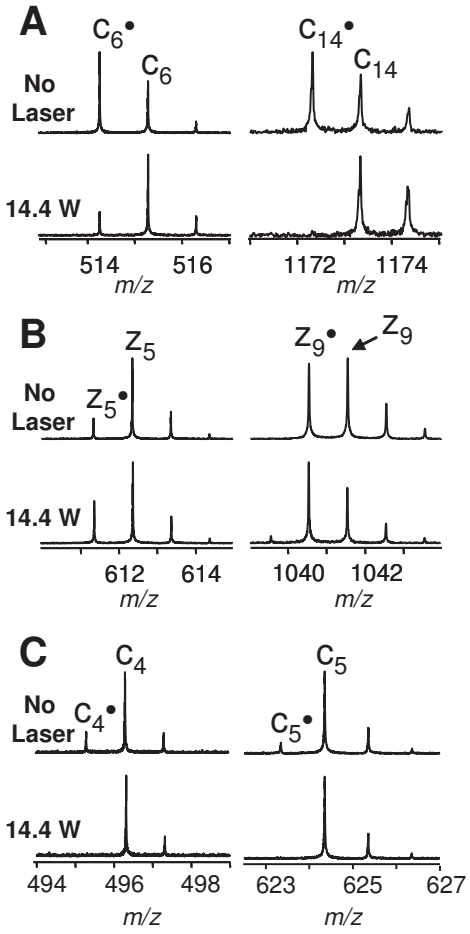

Figure 7·1: Particular fragment isotopic distributions from the ECD spectra of (A) RAAAGADGDGAGADAR, (B) EGVNDNEEGFFSAR, and (C) RPKPQQFFGLM. Decrease in c·/c and z/z· occurs with prior heating using 14.4 W of CO_2 laser power for each fragment isotopic distribution.

In figure 7·1–C, hydrogen atom transfer involving c_4 and c_5 in the ECD spectrum of substance P was eliminated with 180 ms of 14.4 W IR light while similar conditions for RAAAGADGDGAGADAR (figure 7·1–A) showed a complete shift to even electron ions only for c_{14} and c_{15} (not shown). Incomplete conversion is probably due to the retention of some intramolecular forces indicating a mixture of unfolded and folded states that exhibits some H· transfer.

7.2.2 Ion Temperature and H· Transfer

Since the intra-complex H· transfer is affected by the elevated ion temperature, which can be achieved by either thermal heating or IR irradiation, it was possible to correlate the laser irradiation to the effective ion temperature via BIRD–ECD studies by measuring the extent

in the shift of the c·/c or z/z· ratios. To this end, a thermocouple was installed in the ICR

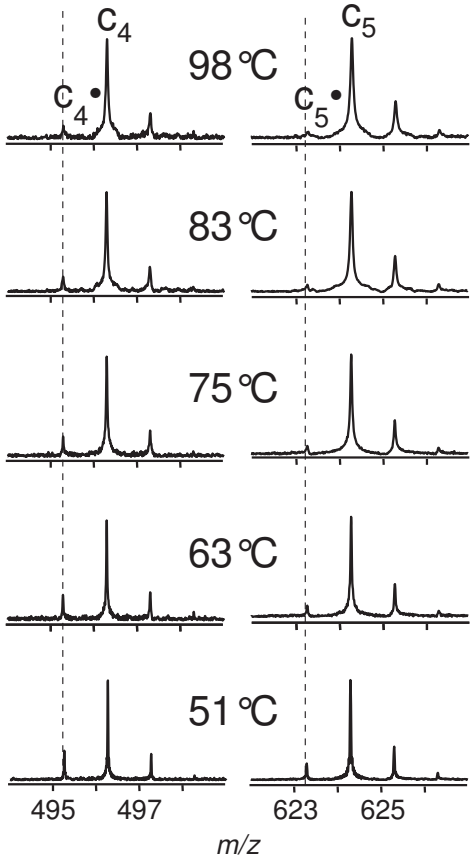

Figure 7·2: Expanded views of c_4 and c_5 from the ECD spectra of substance P in the ICR cell heated to different temperatures. Dashed lines indicate position of the hydrogen transfer c ion (c· ion).

cell to measure the temperature. Figure 7·2 shows the increase in c·/c ratios for c_4 and c_5 of substance P corresponding to the folding of the peptide with decreasing cell temperature. In order for the ratios to truly reflect the ion temperature, the precursor cations were equilibrated to the cell temperature before ECD. Temperature equilibrium was assumed to be reached when, at a specific temperature, the extent of H· transfer stabilized amongst the fragments. Plots of c/c· and/or z·/z ratios versus temperature converged upon one another (*i.e.* reached temperature equilibrium) as the incubation period was increased beyond 2 s for substance P, YWQHTAD$_\alpha$QFR-NH$_2$ (figure 7·3) and YWQHTAD$_\beta$QFR-NH$_2$ (data not shown). Since a steady state internal energy distribution of gaseous peptides can be achieved using monochromatic light that is nearly identical to blackbody irradiation, calibration curves relating laser

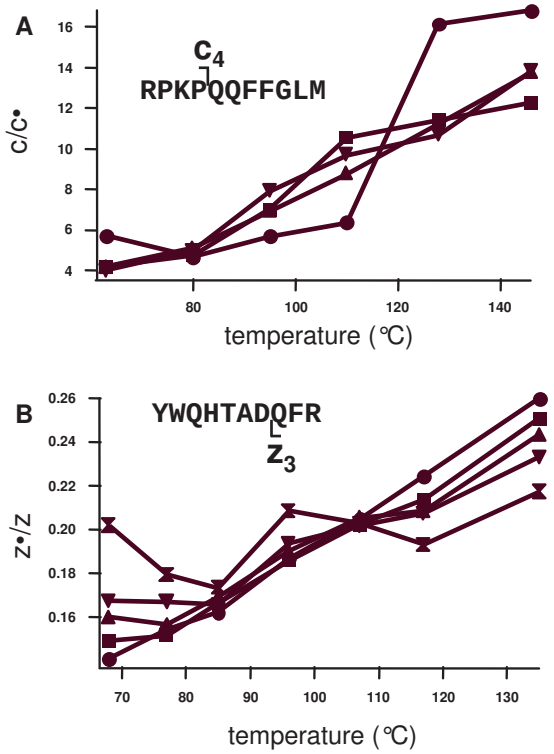

Figure 7·3: Incubation time in heated ICR before ECD versus fragment ion ratio (c/c· or z·/z). (A) c_4 of substance P at 10 ms, filled ∘, 100 ms, filled □, 2000 ms, filled ▽, 4000 ms, filled △. (B) z_4 of YWQHTAD$_\alpha$QFR-NH$_2$ at 5 ms, filled ▷, 500 ms, filled ▽, 1000 ms, filled △, 2000 ms, filled □, 3000 ms, filled ∘.

power and ion temperature can be generated.[42,258] The $c_9/c_9\cdot$ ratio was used for temperature calibration of YWQHTA(D$_\alpha$/D$_\beta$)QFR-NH$_2$ since the abundance of this fragment ion was of large and stable abundance (*i.e.* total abundance did not vary with temperature) in all ECD spectra. Figure 7·4–A is the plot of the $c_9/c_9\cdot$ ratio versus cell temperature where the solid line is a three-parameter polynomial fit. For IR–ECD experiments, the effective ion temperature for each laser power was obtained by finding the corresponding value on the polynomial fit curve (figure 7·4–B) based on the $c_9/c_9\cdot$ ratio. A set of IR power versus effective ion temperature values are plotted in figure 7·4–B, which displays a linear correlation as expected. This linear relationship was used to extrapolate to higher ion temperatures that can be achieved using IR radiation (>130 °C). Plots are peptide dependent and, most likely, reliant on instrument parameters and should be re-generated over time due to electronic fluctuations and drift in laser alignment.

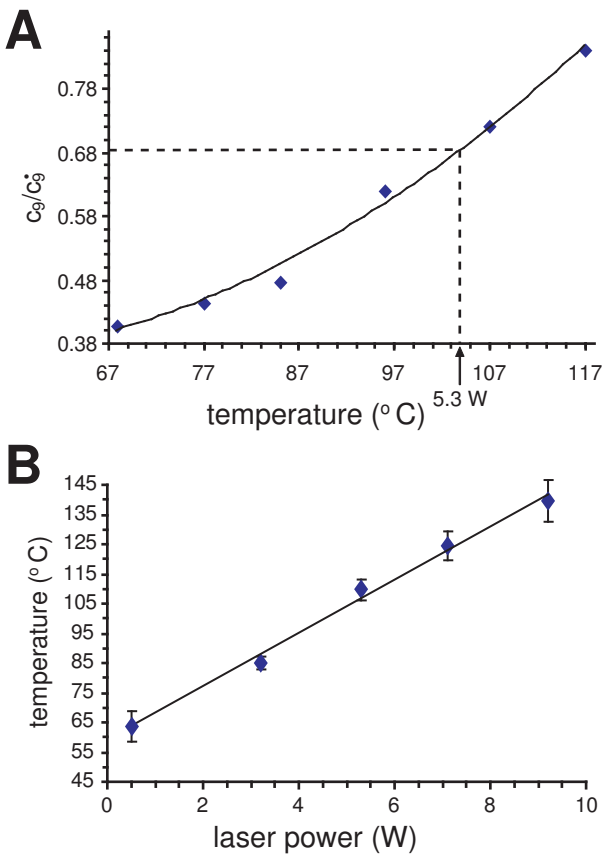

Figure 7·4: (A) Plot of $c_9/c_{9\cdot}$ ratio versus cell temperature fitted with a 2^{nd} order polynomial. (B) Linear plot ($R^2 = 0.9937$) of laser power versus ion temperature of YWQHTADQFR-NH_2 using the $c_9/c_{9\cdot}$ ratio from the ECD spectra. Arrow indicates temperature that corresponds to a laser power of 5. 3 W for a $c_9/c_{9\cdot}$ ratio of 0.685.

7.2.3 Thermodynamic Model

Since ion temperature can be correlated to laser power, DR–ECD of multiply protonated peptides equilibrated to known temperatures by IR light should provide thermodynamic information on the noncovalent interactions that support the higher-order structure once the proper thermodynamic model is established. The two-state model described in figure 7·5 shows that a change in temperature shifts the ion population between the unfolded and folded states. The folded state is preserved using ECD in the form of the reduced molecular ion ($(M+nH)^{(n-1)+\cdot}$) which is composed of the N– and C–terminal fragments still bound to one another by intracomplex interactions with survival lifetimes greater than several milliseconds (see secion 6.3.5), while the unfolded state results in c and z ions. There is a possibility that the ion would

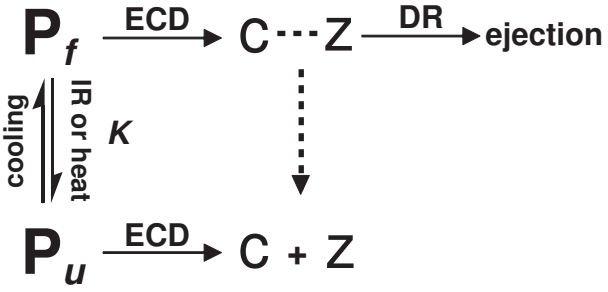

Figure 7·5: The shifting between a folded state (P_f) and an unfolded state (P_u) of a gas-phase peptide ion can be accomplished using heat or an IR laser for unfolding or by allowing the activated peptides to undergo radiative cooling for folding. ECD of unfolded peptides should generate only c/z ions while the folded states generate only $(M+nH)^{(n-1)+\cdot}$, which are the N– and C–terminal fragments still bound by noncovalent interactions. DR ejection of $(M+nH)^{(n-1)+\cdot}$ during ECD should eliminate all fragments generated from the dissociation of the bonded fragments. The dashed arrow represents the portion of the folded state that dissociate during or before ejection as described in the text.

capture an electron and not cause a backbone cleavage but instead result in side chain, small molecule, proline cleavage and H· losses. Breuker *et al.* showed that H· loss is a significant pathway only for larger molecules (>20 kDa)[66] and therefore is negligible in these experiments. Close examination of the spectra shows that IR–DR–ECD does not affect the abundance of side chain losses so these rearrangements either happen faster than ejection ($< \sim$1–2 ms) or are not dependent on the higher-order structure of the gas-phase peptide. Furthermore, no information is drawn from the reduced molecular ion and its abundance is not therefore does not affect the calculations.

A portion of the bound complexes can also dissociate into separate fragments before the excitation/detection event which are detected as c and z ions, thus their origin, from the unfolded or unfolded state, cannot be determined. However, DR ejection of $(M+2H)^{+\cdot}$ during the ECD event will eliminate all fragments derived from the radical complex since resonance ejection occurs on a time scale faster than dissociation of the complex. Therefore, by measuring the change in fragment abundances from DR–ECD spectra with ion temperature, thermodynamic information, such as the energy of interaction that maintains the higher-order structure of peptide preserved by ECD, can be determined from the fragment spectra. This method is different than that used to calculate the thermodynamics of ubiquitin unfolding where the

abundance of the unfolded protein was calculated as the sum of the ECD fragment abundances, while the abundance of the folded protein was the sum of the reduced molecular ion and the small molecule losses thereof.[66] These abundances were found to vary with temperature and their changing ratio was used to calculate the unfolding constant for the protein. For peptide ions, this approach is not always applicable because the post-ECD complex is often a transient species. The reduced molecular ion for a peptide is sustained by fewer intramolecular interactions than a protein ion and the complex could dissociate in the several hundred milliseconds between electron irradiation and subsequent detection. DR–ECD eliminates the delay by ejecting the reduced molecular ion immediately after ECD cleavage, therefore, providing a snapshot of the abundance of the unfolded peptide ion population. The change in abundance of the fragments with ion temperature can then be used to calculate the equilibrium constant without relying on the detection of the reduced molecular ion.

In this study, the change in fragment abundances are used to estimate the fraction of the peptide ion population that is unfolded so that the equilibrium constant ($K = P_{unfolded}/P_{folded}$ or P_u/P_f), and finally the ΔH° and ΔS° of unfolding, can be calculated using the van't Hoff equation. This method is analogous to a method employed by Breuker *et al.* to measure the enthalpy and entropy of unfolding of several charge states of gas-phase ubiquitin ions.[66] Ions are assumed to be in thermal equilibrium when heated by IR light until photon emission and ion cooling results in peptide refolding ($\sim$<200 ms, section 6.3.5); for these experiments, the DR–ECD pulses are within 100 ms of the IR irradiation event.

The initial state of the ions is assumed to be a fully folded (P_f) state when the ions are not irradiated with IR light and only experience radiative heating via the electron gun ($\sim$70 °C) (figure 7·5). Under these conditions, the abundance A for a specific fragment ion population occurring from ECD without DR decreases to B when the same experiment is performed with DR ejection of $(M+2H)^{+\cdot}$ during electron irradiation (figure 7·6–A versus 7·6–B). Therefore, fragments that decrease in abundance are assumed to be from the folded state and still bound to one another in the form of the reduced molecular ion. As the ion temperature increases with increasing laser power, the unfolded population (P_u) increases so that the abundance of the post-ECD radical complex decreases, which leads to a decrease in the difference between ECD fragment abundances without, C, and with, D, DR ejection (figure 7·6–C versus 7·6–D). The

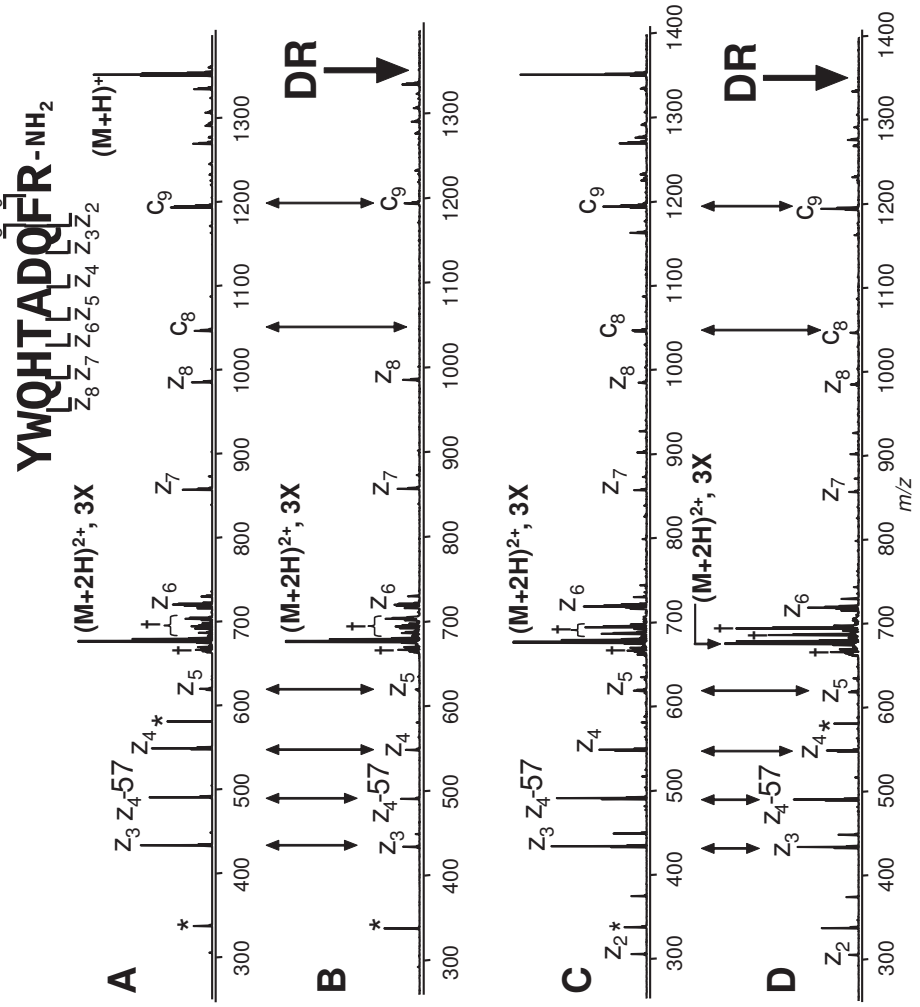

Figure 7·6: The top two are the ECD (A) and DR–ECD (B) spectra of YWQHTAD$_\alpha$QFR-NH$_2$ without IR activation (ion temperature ∼70 °C). Arrows indicate fragments that change with resonant ejection of the reduced molecular ion during the electron irradiation event. Large arrow represents m/z region where DR pulse occurs. The bottom two are the ECD (C) and DR–ECD (D) spectra of YWQHTAD$_\alpha$QFR-NH$_2$ except with prior IR heating (ion temperature at ∼250 °C). Electronic noise is represented by * and ions resulting from incomplete isolation of the precursor ion are represented by †.

abundance D of a specific fragment can be calculated from the equation,

$$D = P_U * C + P_F * C * (B/A). \tag{7.1}$$

where the first term is the contribution from the unfolded peptide ions. The second term is a correction to abundance D due to contributions that result from dissociation of the complex occurring before and during resonance ejection of $(M+2H)^{\cdot+}$. DR ejection of the complex under initial temperature conditions (*vide supra*) should theoretically eliminate all fragments involved in intramolecular interactions that form the post-ECD complex assuming that the peptide is completely folded at this temperature. For example, c_8 in figure 7·6–A is completely gone in figure figure 7·6–B with resonance ejection. However, some fragments decrease drastically but are not completely eliminated (*e.g.* z_3 and z_4 in figure figure 7·6–A and figure 7·6–B) and must originate from dissociation of the complex that occurs during and before resonance ejection (this event is denoted as the dashed arrow in figure 7·5). Therefore, a fraction (B/A) of the fragment ions from DR–ECD of the folded state ($C\mathrm{P}_f$) will contribute to the ion abundance (D) at elevated temperatures. Finally, substitution of $\mathrm{P}_u = 1$ - P_f and subsequent rearrangement of equation gives the fraction of the ion population that is in the folded state,

$$P_F = [1 - (D/C)]/[1 - (B/A)] \tag{7.2}$$

which can then be used to calculate K. Van't Hoff plots (lnK versus 1/T) allow the enthalpy and entropy of the unfolding of the peptide to be calculated (see example in figure 7·7 for z_4). Complexes are expressed in the form $c_n(+)/z_{l-n}(+)$ (n is amino acid number and l is the length of the peptide), where c and z ions are complement fragments with one retaining the positive charge and the other being neutral remaining undetected. For example, the increase in the abundance of z_4 reflects dissociation of the complex c_6/z_4+ in which c_6 is the neutral complement fragment

7.2.4 ΔH° and ΔS° values for the decapeptides YWQHTAD$_\alpha$QFR-NH$_2$ and YWQHTAD$_\beta$QFR-NH$_2$

Of the 9 inter-residue cleavages possible, 8 were detected (z_3–z_8, c_8, c_9) in the ECD spectrum of doubly protonated YWQHTADQFR-NH_2 and the isoAsp counterpart decapeptide (figure 7·6).

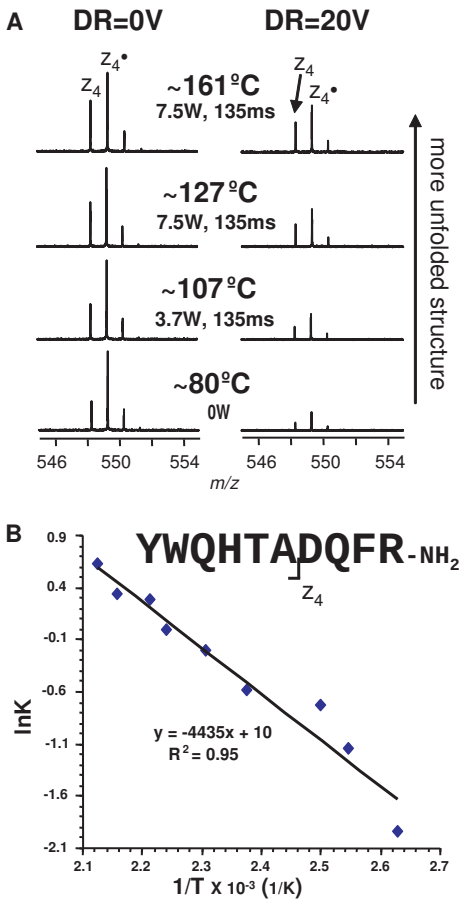

Figure 7·7: (A) Effect of double resonance ejection of the reduced molecular ion at 0 V (no DR pulse) and 20 V on the abundance of z_4 from the ECD spectra of YWQHTAD$_\alpha$QFR-NH_2 at different temperatures. (B) Vant Hoff plot (ln(K) versus 1/T) of the dissociation of z_4+/c_6.

The most likely sites of protonation are the guanidine group of arginine and the N–terminal amine, which have the highest proton affinity and would have minimal columbic interaction, with the most likely site of electron capture being the N–terminal amine since it is less basic than the guanidine group.[69] However, since c_8 and c_9 are detected, a small fraction of the population could capture an electron at arginine, so that some of the N–terminal fragments can retain the charge most likely at the histidine residue or the N–terminal amine. Only the fragment ions z_3–z_6, c_8, and c_9 showed both change in abundance with DR ejection of $(M+2H)^{+\cdot}$ and H· transfer suggesting that these fragments are part of the radical complex while z_7 and z_8 remained exclusively odd electron fragments and experienced no change with resonance ejection. The fragment ions z_3–z_5, c_8, and c_9 show positive ΔH° and ΔS° values (tables 7.1 and 7.2) indicating

that unfolding of all investigated bonded fragments are endothermic processes accompanied with an increase in disorder of the systems. Enthalpy values fall within the expected range for ionic and neutral hydrogen bonding (17-126 kJ/mol).[259] Entropy values are also within the expected range for the dissociation of hydrogen bonded structures (84-125 J/molK)[259] although errors are probably underestimated since values are based on intercepts. Although the z_6 showed some change with DR ejection and H· transfer, no reasonable van't Hoff plot could be constructed due to large uncertainties.

Table 7.1: Thermodynamic Values for YWQHTAD$_\beta$QFR-NH$_2$

fragment	enthalpy (kJ/mol)	entropy (J/mol·K)	melting temperature (°C)
c_9	52.9±6.5	132.1±19.2	127±24
c_8	48.0±10.1	105.6±19.3	182±51
z_3	40.0±10.4	91.6±25.4	164±62
z_4	37.4±7.2	88.1±20.9	152±47
z_5	35.6±7.9	88.2±21.4	130±43

Table 7.2: Thermodynamic Values for YWQHTAD$_\alpha$QFR-NH$_2$

fragment	enthalpy (kJ/mol)	entropy (J/mol·K)	melting temperature (°C)
c_9	57.3±12.3	144.5±37.9	124±42
c_8	53.0±10.3	119.3±22.6	172±47
z_3	43.3±4.9	106.7±12.6	133±22
z_4	53.4±11.6	133.2±30.2	128±40
z_5	68.7±10.8	169.2±28.0	133±30

7.2.5 Activated ion–DR–ECD of YWQHTAD$_\alpha$QFR-NH$_2$ versus YWQHTAD$_\beta$QFR-NH$_2$

IsoAsp residues are β-amino acids with the C_β inserted into the peptide backbone resulting in both an extension of the backbone and shortening of the side chain by one methylene unit (figure 7·8). In general, the Asp decapeptide has larger ΔH° and ΔS° values than those of the isoAsp counterpart suggesting that the substitution with isoAsp residue weakens intramolecular bonding and destabilizes the higher-ordered structure of the gas-phase peptide.

For both peptides, ΔH° values for c_9, c_8, and z_3 are similar and decrease concomitantly (tables 7.1 and 7.2). Assuming hydrogen bonding is occurring between the guanidine group of the C–terminal arginine and adjacent carbonyl groups, as suggested by Iavarone *et al.*,[211]

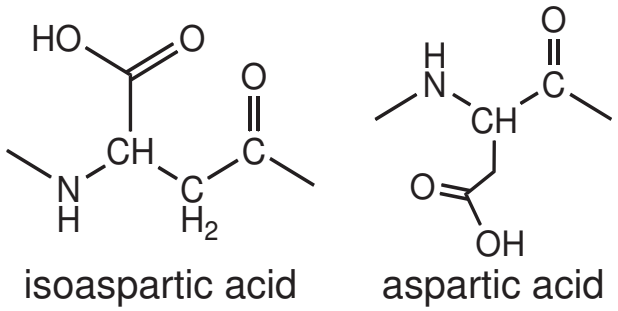

Figure 7·8: IsoAsp (left) has the C_β inserted into the backbone lengthening it by one methylene unit and as well as shortening the side chain by the same amount compared to traditional Asp form (right).

decreasing enthalpies of unfolding correlates with the increasing size of the detected fragments and decrease in the number of noncovalent interactions between complement fragments. For example, the unfolding enthalpy of c_9+/z_1 is larger than that of c_8+/z_2 because the former

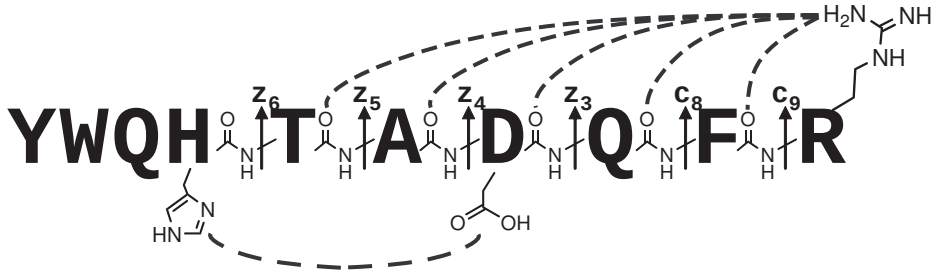

Figure 7·9: Proposed structure for YWQHTAD$_\alpha$QFR-NH_2. Dashed lined represent non-covalent interactions. Guanidine-carbonyl interactions are hydrogen bonds while the carboxyl-imidizole interaction is a salt-bridge.

interacts with one more backbone carbonyl group than c_8+/z_2 (figure 7·9). This value is in good agreement with peptide studies that demonstrates a stepwise increase in stability with the addition of each hydrogen bond to the empirical hydrogen bond.[260,261]

For the Asp peptide, the average ΔH° values for c_6/z_4+ and c_5/z_5+ are higher than the average for other three complexes (c_7/z_3+, c_8+/z_2, c_9+/z_1) while the isoAsp peptide shows no such abnormality (tables 7.1 and 7.2). The structural difference between these two sets of complexes is the repositioning of Asp (or isoAsp) to the fragment containing arginine suggesting that the Asp side chain may be interacting with the N–terminal region of the peptide (YWQHT–). One possible interaction is a salt-bridge between the negatively charged carboxyl side chain and a nearby protonated site; loss of CO_2 from z_4 found in the ECD spectra of the Asp

peptide indicates that the Asp side chain may be negatively charged.[257] The peptides studied here contain a motif similar to bradykinin which has shown that the carboxylate group can interact with two sites of protonation to form a salt-bridge.[262] The three most likely sites of protonation would then be the histidine, arginine and the N–terminal amine resulting in a doubly protonated peptide when the carboxylate group is taken into account. No change in abundance or H· transfer occurs for z_7 and z_8, fragments that include histidine, suggesting that a protonated imidazole could be a contributor to a salt bridge rather than the N–terminal amine (figure 7·9). Since the extension of the backbone occurs on the C–terminal side of the Asp residue, it should not affect the strength of the interaction between protonated histidine and Asp. Therefore, the weakening effect when the Asp residue is substituted with isoAsp as evidenced by the large decrease in ΔH° values for c_6/z_4+ and c_5/z_5+ should mostly arise from the shortening of the side chain rather than the lengthening of the backbone.

7.2.6 IsoAsp Substitution Effects H· Transfer

The decrease in enthalpy values for c_5/z_5+ and c_6/z_4+ with isoAsp substitution are accompanied with a decrease in H· transfer within these complexes. Larger enthalpy values for Asp suggest that the two complement fragments are closer in proximity to one another, enhancing H· transfer to z_5 and z_4 and vice versa for the isoAsp version. Another possibility is that isoAsp residues have a smaller affinity for H· than Asp residues. Based on the ECD spectra of 1500 peptides, Savitski *et al.* have shown that an average of 60% of fragments from cleavage on the C–terminal side of Asp residues exist as even electron fragments.[240] The magnitude of H· transfer for isoAsp residues has not been studied but the possibility that the isomeric form may exhibit more transfer over the Asp form cannot be disregarded. The difference in z_4 between the two forms is the placement of the radical; the radical is deposited on the C_β for isoAsp versus the C_α for Asp residue after cleavage by ECD. The C_β radical is fairly reactive under elevated temperatures causing loss of glutamine side chain from z_4 generating a terminal γ-lactam similar to a rearrangement generating u ions in the high-energy ECD spectra of peptides,[204] a loss that was not detected for the Asp version. Heightened reactivity of the radical N–terminal to isoAsp could support the idea that more H· transfer is expected than from the Asp form, however z_5 also experiences less intra-complex hydrogen atom transfer for the isoAsp form.

According to Savitski's study, variability of the neighboring residues adjacent to the cleavage site (*i.e.* n+1 and n-1 where n is the cleavage site) has an almost negligible affect on the extent of H· transfer.[240] Therefore, the significant increase in H· transfer for Asp z_5, and hence z_4, is most likely due to a more folded structure for Asp than the isoAsp form.

7.2.7 IsoAsp versus Asp: Impact on Peptide Structure

Asparagine deamidation to a mixture of isoAsp and Asp residues is believed to be one pathway for protein aging, wherein the impact of isoaAsp formation, an abnormal amino acid residue structure, is more damaging to protein and peptide structure and function than that of Asp formation (see section 1.3).[2,96,97] The data presented here shows that the difference in the thermodynamics of gas-phase unfolding between the two forms demonstrates a significant structural impact when isoAsp and Asp are interchanged. The data suggests that, in this peptides studied here, shortening the side chain by one methylene group influences the gas-phase structure more so than lengthening the peptide backbone with isoAsp substitution; the length of the side chain, and hence interactions involving the carboxyl group, are important to sustaining the secondary structure of the Asp peptide. Although the structural implications of the data are in regard to the gaseous structure, the hydrogen bonding studied here is strengthened in the gas-phase, and therefore the possible interactions proposed should hold some correlation to solution-phase structure. Nonetheless, the differences in enthalpy values should shed some light on the effects of isoAsp substitution and asparagine deamidation on peptide and protein structure.

7.3 Conclusions

Experiments involving IR–DR–ECD provides information on the gas-phase structure of peptides; peptide unfolding by IR irradiation can be observed by monitoring the decrease in intracomplex hydrogen atom transfer and the thermodynamics of noncovalent, intramolecular binding forces can be explored by measuring the decrease in fragment abundances by resonantly ejecting the reduced molecular ion during electron irradiation. A common intramolecular, noncovalent interaction that supports peptide secondary structure is the hydrogen bond, an interaction that is strengthened in the gas-phase. The ΔH° and ΔS° values of unfolding obtained from IR–DR–ECD experiments correlate well with the dissociation of a hydrogen bond

that maintains the folded arrangement thus supporting the claim that hydrogen bonding (ionic or neutral) plays an important role in the higher-order structure of gas-phase biomolecules. Furthermore, the data suggests that other non-covalent interactions, such as salt-bridges, provide support to the structure as well. A minor modification of the Asp residue disrupts this interaction as revealed by the decrease in ΔH° values with isoAsp substitution. Also, decrease in H· transfer surrounding the isoAsp region reinforces the idea that the Asp version offers a more tightly bound gas-phase structure. This data demonstrates that IR–DR–ECD could be a convenient probe to study how biologically important modifications affect the gas-phase structure and in turn possibly help understand how these modifications affect the solution phase structure as well, such as those involved in protein deamidation.

Chapter 8

Using FT–ICR–MS and FT–ICR–MS–ECD to Study the Deamidation of rPA

8.1 Introduction

The protective antigen (PA) of *Bacillus anthracis* is an 83 kDa toxin component protein that has emerged as the lead candidate active ingredient for a new subunit vaccine against inhalation anthrax, a biological warfare risk and terrorist threat.[263]. The currently licensed human anthrax vaccine is prepared from precipitated culture supernatant proteins as based on 50 year old technology and is not fully defined. Moreover, it is reactogenic, requires multiple doses with annual boosts to establish and maintain protective immunity, and has a growing record of adverse events. Alternatively, purified recombinant PA (rPA) has proven to be highly effective in animal studies[131,264] and is under clinical study as the next human anthrax vaccine being developed by the Departments of Defense and Homeland Security. Since the Food and Drug Administration (FDA) authorizes its licensing, marketing, and use, rPA protein must be thoroughly characterized in its composition, strength, and potency. In particular, FDA guidance requires that methods be established and documentation be collected which measure and define rPA as a biological drug, including any change in physicochemical structure or biological activity that may occur as a result of use, handling, shipping, and storage. Thus, a detailed understanding of rPA protein structure and stability is critical for its eventual use, not only for prophylaxis and therapy against anthrax, but also as a key component of new cancer treatments.[265,266] In this regard, a long standing mystery about observed charge heterogeneity PA was recently resolved by the discovery and characterization of deamidation at several of its asparagine residues.[263] Deamidation is the spontaneous, nonenzymatic loss of ammonia from asparagine or glutamine side chain amide and among the most frequent type of protein degradation both in vivo and in vitro clarke1987. While partial deamidation observed at its most

labile residues did not correlate with loss of biological activity in vitro[263] or potency as a vaccine immunogen,[131] only 19 % (13 out of 68) of all possible asparagine residues in the protein were confidently measured, leaving uncertainty as to the full extent and effect of deamidation on rPA structure and function. Furthermore, the analytical method employed produced only a cursory description of the potential intermediates and end products of asparagine deamidation. Most notably, the content of isoaspartate within rPA has yet to be adequately defined.

Deamidation of asparagine residues (and to a lesser extent, isomerization of Asp) is a modification of proteins that occurs via a succinimide intermediate to form a mixture of Asp or isoAsp residues (see section 1.3).[2–5,96,97] Formation of the isoAsp residues is believed to cause the inactivation, aggregation and aging of proteins in tissue because the backbone and side chain is lengthened and shortened, respectively, by one methylene unit (–CH_2–).[2,4,87–92] The C–terminal side amino acid neighbor to the asparaginyl residue influences the rate of succinimide formation more so than those on the N–terminal side.[96–98] The rate of deamidation increases for amino acids with less bulky residues (*e.g.* glycine) and highly polar side chains (*e.g.* histidine) as well as with an increase in temperature and pH.[97]

Presence of several deamidations, as in the case of rPA, results in protein charge heterogeneity that can be partially resolved by isoelectric electrophosesis[263] or ion exchange chromatography[131]; multiple deamidations increases the net ionic charge of the protein depending on how many –NH_2 groups are converted to –OH groups. However, neither method can localize each deamidation site in the protein. Bottom-up MS (MS analysis of peptides from protein digestion) can be used to determine which sites are modified, if the peptides are detected in the mass spectrum. Measurement of the extent of deamidation can be performed by isotopic deconvolution as described in section 1.3.5. Using this methodology, individual deamidation sites can be located and measured in order to understand how conversion to Asp and isoAsp residues affect the structure and function of the protein. For rPA, once the deamidation sites are characterized, protein synthesis, isolation and storage can be adjusted to prevent unwanted modification and help preserve its potency.

In an earlier study, seven (out of 68) particular asparagine residues were confirmed to deamidate and many aged at rates that differed substantially from values predicted by a popular algorithm. These residues are (in decreasing order of deamidation rate) N537, N713,

N466 N719, N601, N408, and N602.[263] Their deamidations were previously characterized using LC–MS/MS techniques and the extent of deamidation was determined based on extracted ion chromatograms with manual confirmation of spectra supporting sequence and each modified amino acids. In this study, a similar method is used to replicate the data without using chromatography and rely solely on the high resolution data offered by FT–ICR–MS. Furthermore, ECD analysis is performed to determine if a deamidation site contains an isoAsp acid residue using the ECD diagnostic marker ions (see section 3.3.3).

8.2 Experimental

8.2.1 Materials Supplied by Collaborator

Five groups of rPA samples were studied; 'fresh', 4hr–'fresh', 4hr–'aged', 18hr–'fresh', and 18hr–'aged' which were supplied by Bradford Powell of the USAMRIID. Samples labeled 'fresh' were clinical grade protein supplied by the manufacturer to the collaborator as bulk biological substance in 50 mM ammonium acetate (pH 8.9) maintained at -70 °C in original vials. Bulk substance was 'aged' to promote degradation, *i.e.* deamidation, by two methods to simulate and accelerate what may occur by typical handling prior to enzymatic treatment. These treatments comprised either several freeze-thaw cycles or hold over night at 37 °C. To test whether trypsinolysis itself affects deamidation, protein samples were digested in 4 or 18 hour durations, as noted (trypsin at 1:15-20 enzyme:substrate ratio (w/w), 50 mM Tris at pH 8.0, 37 °CC). In addition, tryptic peptides of rPA were also 'aged' by extended hold at 37 degrees after enzymatic digestion. Trypsin digests were stopped with 4 μL of acetic acid and frozen. Before MS analysis, samples were cleaned (Tris buffer removed) using custom made POROS tips (method described in section 2.2.1) and evaporated using a speedvac with refrigerated vapor trap (Savant RVT 4104, Thermo Electron Corp., Milford, MA) several times in water to remove acid for FT–ICR–MS analysis.

8.2.2 Protein Aging and Digestion

Clinical grade bulk substance product was aged as a whole protein in order to gain an understanding of which asparagine residues age more rapidly in the native state. A 20 μg portion of the whole protein was aged by dissolving it in 20 μL of an AH solution (0.4 % in water, pH

~10.2), sealing with parafilm and incubating at 37°C overnight (~12 hours). The next day, the sample was split into two equal portions and dried to remove solvent. One half was digested with trypsin (0.1 M AB (pH 8.3), 1:5 enzyme:substrate (w/w), 37 °C for 30 minutes) and the other with Glu-C (0.05 M AA (pH 6.5), 1:5 enzyme:substrate (w/w), 37 °C for 30 minutes). For a set of control samples, two 20 μg portions of 'fresh' whole protein were digested as described above. Samples were fractionated using custom made POROS tips (method described in section 2.2.1). To age the proteolytic peptides, half of each digestion of 'fresh' rPA were incubated at pH 10.2 (0.4 % AH in water) overnight at 37 °C. All samples were evaporated using a speedvac with refrigerated vapor trap (Savant RVT 4104, Thermo Electron Corp., Milford, MA) several times in water to remove AH for FT–ICR–MS analysis.

8.2.3 FT–ICR–MS and FT–ICR–MS–ECD Analysis

ECD experiments were performed on a custom-built FT–ICR–MS instrument previously described (see section 1.2.4).[83,214] Peptide solutions were prepared at ~5-10 μM from stock solutions in a 49.5:49.5:1 water:methanol:formic acid solution and 5 μL was loaded into a glass capillary with 1 μm orifice made using mechanical tip puller (Sutter Instruments, Novato, CA). Applying 1.2 kV to the solution generated positively charged ions used for FT–ICR–MS and FT–ICR–MS–ECD analysis. For full mass spectra scans, a routine method was used where by ions were externally accumulated in the CAD cell (Q2), transferred to the ICR cell by gated trapping, and a subsequent excitation/detection was used to generate a mass spectrum. These spectra were used determine which and to what extent each detected peptide was deamidated.

For the FT–ICR–MS–ECD experiment, the $(M+3H)^{3+}$ charge state of ^{526}ALKIAFGFNEPNGNLQYQGKDITE$_{549}$ (from Glu-C digested whole 'fresh' protein sample, 40:60 MeOH:H_2O fraction) was isolated by Q1, accumulated in Q2, transferred to the ICR cell by gated trapping, and then irradiated with electrons at ~0.2 eV for ~50 milliseconds. ECD fragments were detected using a typical excitation/detection sequence with 20-scan signal averaging.

8.3 Results and Discussion

8.3.1 FT–ICR–MS Analysis of Proteolytic Peptides from rPA Aged by Repeated Freeze-Thaw Cycles

Native protein was aged prior to generation of proteolytic peptides to better measure the resultant peptides by high resolution FT–ICR–MS. The measurement of the extent of deamidation in rPA using FT–ICR–MS was first performed on the tryptic peptides and their aged counterparts.[263] To extend these findings, rPA was digested here with trypsin for two specific time intervals, 4 hours and 18 hours, after undergoing consecutive freeze-thaw cycles ('aged' samples) to replicate how a stock of therapeutic protein may be stored and accessed during usage. Measurement of the extent of deamidation is performed by isotopic deconvolution as described in section 1.3.5. Briefly, decrease in the first isotopic peak corresponds in a shift of the isotopic pattern, when compared to the theoretical pattern, by +0.984 Da since the $-NH_2$ group is converting to an –OH group, *i.e.* deamidation. These measurements are peformed on peptides released from digestion and are presumably more flexible and linear than as part of the higher-order structure of the whole protein. Therefore, the rates of deamidation are most likely accelerated compared to those found for the same sites within the native protein. However, FT–ICR–MS analysis of these samples can provide some useful insight on how digestion can affect the deamidation rate when studying a labile protein such as rPA.

Of the seven deamidation sites mentioned in the preliminary study, 6 were found in the tryptic digest of the samples supplied by the collaborator (figure 8·1), and only the tryptic peptide containing N^{466} was not found. After a 4 hour digestion period, only the $N^{537}G$ site showed partial deamidation (peptide ^{529}IAFGFNEPNGNLQYAGK$_{545}$, figure 8·1–B1), which is the site previously reported to be the fastest to deamidate in the whole protein. Furthermore, after the peptides had undergone several freeze-thaw cycles, the same peptide for the 4 hour sample ('aged') was completely deamidated (complete +0.984 Da shift, figure 8·1–B2)). The previous study predicted $N^{713}G$ and $N^{719}G$ to be the sites to deamidate the next fastest after $N^{537}G$, and both sites were located within the tryptic peptide ^{704}ENTIINPSENGDTSTNGIK$_{722}$.[263] Both sites in this peptide deamidate at a slower rate than $N^{537}G$ since no deamidation was detected in the 'fresh' 4 hour sample (figure 8·1–D1). However, the 'aged' 4 hour sample begins to show some deamdiation (figure 8·1–D2), but which site is deamidating at a faster rate cannot be de-

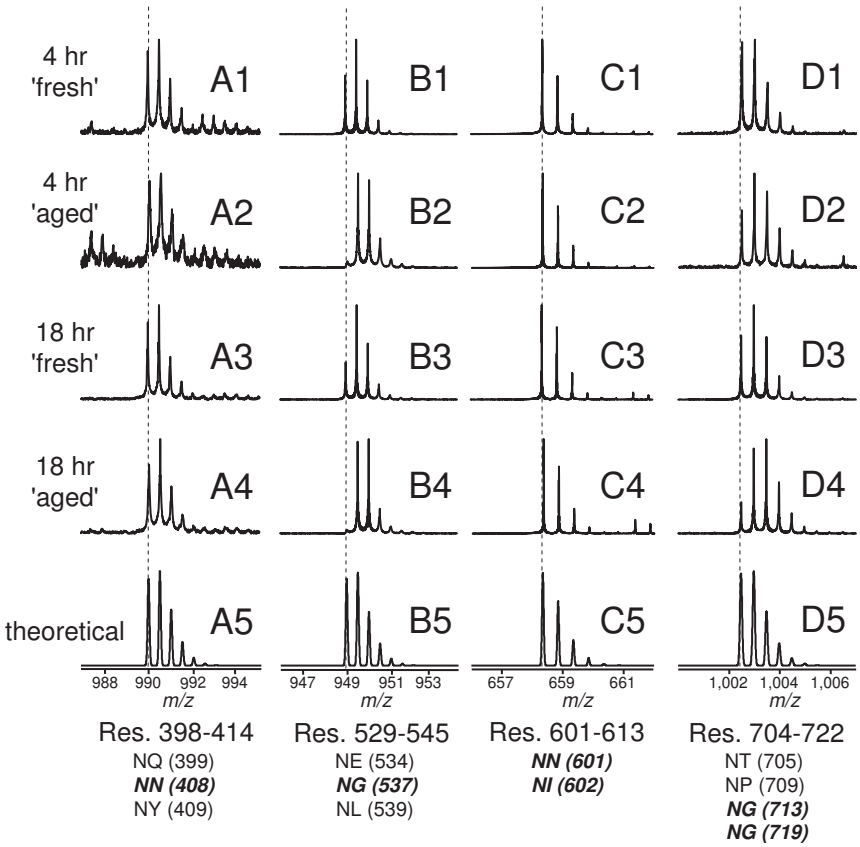

Figure 8·1: FT–ICR–MS spectra of the tryptic peptides (A–C) from rPA that contain the deamidation sites of interest (bold and italicized in the listed sites at the bottom of each column). Each frame is zoomed in spectra from the full-scan FT–ICR–MS spectra; the 4 hour trpytic digest 'fresh' (1) and 'aged' (2) and 18 hour tryptic digest 'fresh' (3) and 'aged' (4). The bottom row (5) is the theoretical isotopic pattern for each peptide.

termined from the spectrum. The sites $N^{408}N$ (from $^{398}ENQLSQILAPNNYYPSK_{414}$), $N^{601}N$ and $N^{602}I$ (from $^{601}NNIAVGADESVVK_{613}$) did not show any evidence of deamidation for the both 'fresh' and 'aged' 4 hour digests (figures 8·1–A1, –A2, –C1, –C2).

Similar results regarding the extent of deamidation were obtained for the peptide containing $N^{537}G$ for the 18 hour samples and their 4 hour counterpart samples (compare figures 8·1–B3 and –B4 with –B1 and –B2, respectively). For $N^{713}G$ and $N^{719}G$, partial deamidation occued after an 18 hour digest (figure 8·1–D3). A subsequent freeze-thaw cycle ('aged' 18 hr) shows that there was partial deamidation at both sites; the peak at m/z 1003.5 became the prominent peak, which corresponds to at least one mole of $–NH_2$ converting to an –OH group in $^{704}ENTIINPSENGDTSTNGIK_{722}$ (figure 8·1–D4). Figure 8·1–A3 and –A4 show that the

peptide containing $N^{408}N$ shows evidence of some deamidation ('aged' > 'fresh' for 18 hour samples) although not to the extent found the two previously discussed peptides. The peptide containing the sites $N^{601}N$ and $N^{602}I$ showed no evidence of aging for two 18 hour samples (figure 8·1–C3 and –C4).

Of the six sites found, the data discussed shows that $N^{537}G$, $N^{713}G$ and $N^{719}G$ are the fastest deamdiating sites where the former is the fastest and the latter two are relatively slower, respectively ($N^{713}G$ and $N^{719}G$ have rates that cannot be differentiated in this experiment). The site $N^{408}N$ showed some deamidation in the peptide after 18 hours of digestion while $N^{601}N$ and $N^{602}I$ still showed no evidence of deamidation even after 18 hours of digestion. According to this data, the deamidation rates for the sites in the tryptic peptides can be ranked in order of decreasing value; $N^{537}G > N^{713}G$, $N^{719}G > N^{408}N > N^{601}N$ and $N^{602}I$. This is not surprising since glycine on the C-terminal side of asparagine is supposed to have the fastest rate. However, these rates are based on peptides released from protein digestion and are more than likely a random coil structure in solution so their deamidation rate is almost certainly greater than if the site was still under the influence of the proteins original higher-order structure.

8.3.2 FT–ICR–MS Analysis of Proteolytic Peptides from rPA Aged by Mild Heat

The characterization of protein deamidation is best understood when the conditions of measurement do not influence the outcome. Therefore precautions should be a taken to prevent artificial deamidation during routine digestion procedures. In the experiment described above, deamidation at $N^{537}G$ may have been influenced by the 4 hour duration of trypsin digestion. To mitigate this, accelerated digestions were employed with greater enzyme-to-substrate ratio (10x higher), reduced duration (30 minutes) and lower buffer pH (~ 6.5)[2] during protein processing. As shown in section 4.3.4, a 30 minute tryptic digestion can prevent deamidation even though the pH is 8.3 and the site of interest in the knowingly labile NG. Therefore, in order to study the *in vitro* deamidation of rPA, protein digestion was performed at pH 8.3 (for trypsin) and 6.5 (for Glu-C) for 30 minutes on both 'aged' (pH 10.2 overnight at 37 °C) and 'fresh' (frozen in buffered solution as delivered by collaborator) to limit any artificial deamidations. FT–ICR–MS scans of each sample was collected and the mass spectra were searched for all peptides containing asparagine residues.

Figures 8·2 and 8·3 show results from the tryptic digest of 'aged' and 'fresh' protein as well as the 'aged' tryptic digest. Of the possible 68 asparagine residues in rPA, 28 were detected within the trytpic peptides (∼41 %). Digestion was performed for 30 minutes in order to limit any artificial deamidation incurred by proteolysis. Only three peptides (figure 8·2 column D and H and figure 8·3 column J) showed evidence of deamidation as indicated by a shift in the isotopic pattern when compared to the theoretical isotopic distribution (bottom row of figures 8·2 and 8·3). Column D of figure 8·2 shows deamidation occurring in the peptide ^{529}IAFGFNEPNGNLQYAGK$_{545}$ which is assumed to be N^{537}G due to the glycine residue that is C-terminal to the asparagine residue. All three isotopic patterns (D1–3) show evidence of deamidation, the most occurring in the aging of the digest which is expected since it should be a linear peptide when aged in this case. Interestingly, both D1 and D3 have similar (D3 is slightly more deamidated than D1) extents of deamidation even though D3 was from the 'aged' protein. This indicates that most of the potential deamidation that could happen at N^{537}G had occurred by freeze/thaw treatment and further 'aging' by holding overnight at 37 °C had an almost negligible affect. rPA protein appeared to be stable as held in 37 °C for at least an over night duration. A similar situation exists for ^{704}ENTIINPSENGDTSTNGIK$_{722}$ which contains the labile asparagines N^{713}G and N^{719}G. The pattern in H2 shows two deamidations when the peptide is aged, as was found in section 8.3.1, but H1 and H3 show similar extents of deamidation suggesting again that deamidation at these sites has occurred by prior treatment before this analysis. Finally, the last deamidating peptide detected was ^{366}YVNTGTAPIYNVLPTTSLVLGK^{387} which contains N^{368}T and N^{376}V (figure 8·3 column J). Deamidation was detected in the aging of the tryptic peptide (J2) and not for the native or 'aged' protein (J1 and J3, respectively). The fact that this peptide deamidates more than others is unexpected; both asparagines are N-terminal to amino acids with relatively bulky side chains, while other peptides, such as ^{618}EVINSSTEGLLLNIDKDIRK$_{636}$ (figure 8·3 column I) which contains N^{621}S, shows no deamidation for the released peptide even though it is predicted that the C-terminal asparagine neighbor serine has a faster deamidation rate than those adjacent to threonine or valine. Therefore, some higher-order structure of the peptide may exist for the peptide that promotes deamidation.

Figures 8·4 and 8·5 show results from the Glu-C digest of 'aged' and 'fresh' protein as

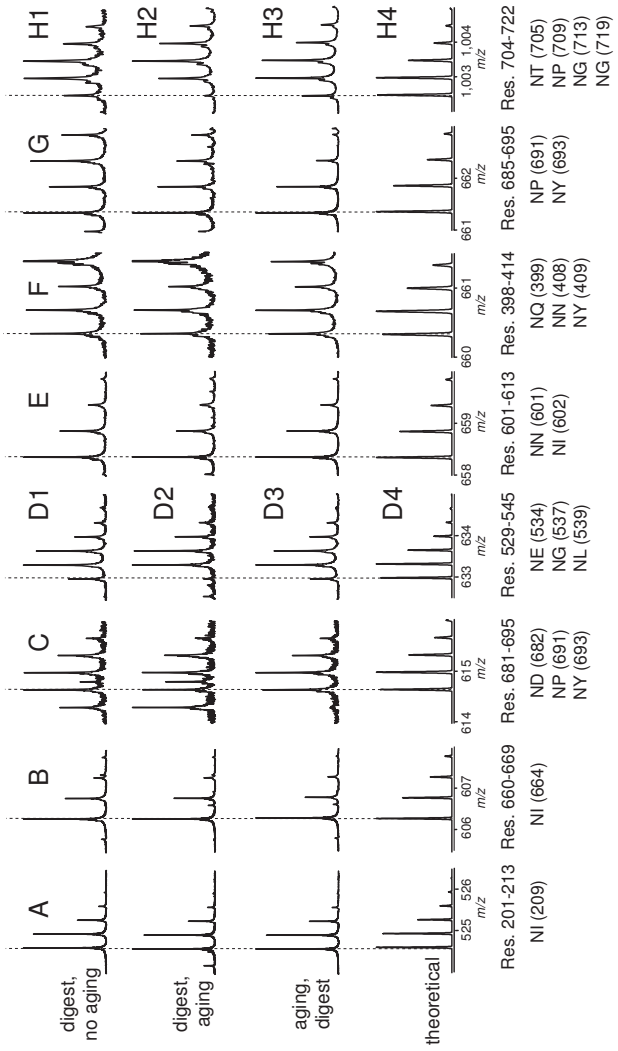

Figure 8·2: FT–ICR–MS spectra of the proteolytic peptides (A–H) from trypsin digest of rPA that contain possible deamidation sites. Each frame is zoomed in spectra from the full-scan FT–ICR–MS spectra: top row, peptides from trypsin digest of 'fresh' rpA; second row, 'aged' tryptic peptides (overnight at 37 °C and pH 10.2); third row, peptides from trypsin digestion of 'aged' rPA (overnight at 37 °C and pH 10.2); fourth row, theoretical isotopic pattern for the detected peptide and charge state. Below the spectra are the peptide residues and the possible deamidating asparagine residues.

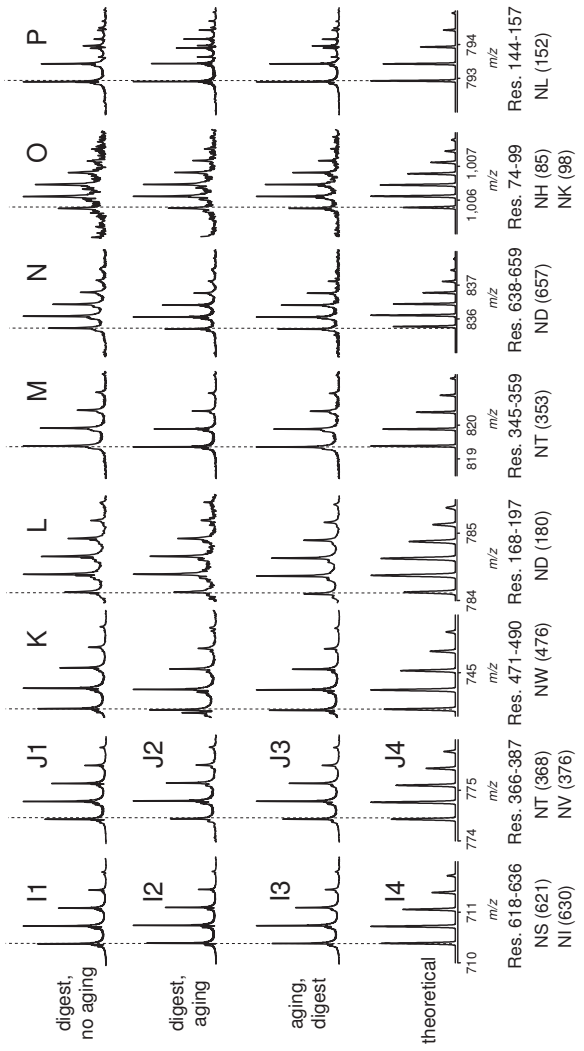

Figure 8·3: FT–ICR–MS spectra of the proteolytic peptides (I–P) from trypsin digest of rPA that contain possible deamidation sites. Each frame is zoomed in spectra from the full-scan FT–ICR–MS spectra: top row, peptides from trypsin digest of 'fresh' rpA; second row, 'aged' tryptic peptides (overnight at 37 °C and pH 10.2); third row, peptides from trypsin digestion of 'aged' rPA (overnight at 37 °C and pH 10.2); fourth row, theoretical isotopic pattern for the detected peptide and charge state. Below the spectra are the peptide residues and the possible deamidating asparagine residues.

well as the 'aged' tryptic digest. Of the possible 68 asparagine residues in rPA, 34 were detected within the proteolytic peptides (50 %). For Glu-C digestion, pH 6.5 is used which has demonstrated to be a condition at which deamidation is the slowest.[2] Therefore, under these conditions (30 minutes at pH 6.5), artificial deamidation should be greatly mitigated. Three peptides (figure 8·4 column A, E and G) showed evidence of deamidation. Not surprisingly, these peptides contain the four sites believed to be the sites with the fastest deamidating asparagines, and have C-terminal glyicines: $N^{466}G$, $N^{713}G$, $N^{719}G$ and $N^{537}G$. So far, $N^{466}G$ has only been detected in the Glu-C digest and not in the tryptic digests of rPA. Only $N^{537}G$ (figures 8·4 column G, ^{526}ALKIAFGFNEPNGNLQYAGKDITE$_{549}$) showed deamidation in the 'fresh' protein digested with Glu-C indicating that the sample was partially deamidated before analysis, which was also found for the same experiment performed with trypsin. Aging of the protein followed by digestion showed that two peptides were deamidating at sites $N^{713}G$, $N^{719}G$ (^{705}NTIINPSENGDTSTNGIKKILIFSKKGYE$_{733}$) and $N^{537}G$. Similar to what was found for trypsin, the peptide from the 'aged' protein sample containing $N^{537}G$ had deamidated to a comparable extent as the same proteolytic peptide from the 'fresh' protein sample (G3 showed a little more deamidation than G1). Again, corroborating our prior finding of little degradation by overnight incubation at 37 °C. The proteolytic peptide from the 'aged' protein containing $N^{713}G$ and $N^{719}G$ also showed some deamidation, although the extent at either site cannot be distinguished in this experiment. Finally, the aging of the digest showed deamidation at $N^{466}G$, $N^{713}G$, $N^{719}G$ and $N^{537}G$ (columns A, E and G, row 2). All these should be random coil peptides in solution during the 'aging' condition applied here and are expected to deamidate at the NG sites under these conditions (overnight at elevated temperature and pH). The peptide containing $N^{537}G$ (G2) was almost completely deamidated as indicated by one complete mass unit shift in the isotopic pattern. Compared to the theoretical pattern, the peptide with $N^{713}G$ and $N^{719}G$ showed more than one deamidation because at least one mole of $-NH_2$ converted to –OH, although, to what extent at which site cannot be determined. Of the four sites mentioned, $N^{466}G$ only deamidates when it is in a proteolytic peptide and must be protected to some extent in the higher-order structure of the protein.

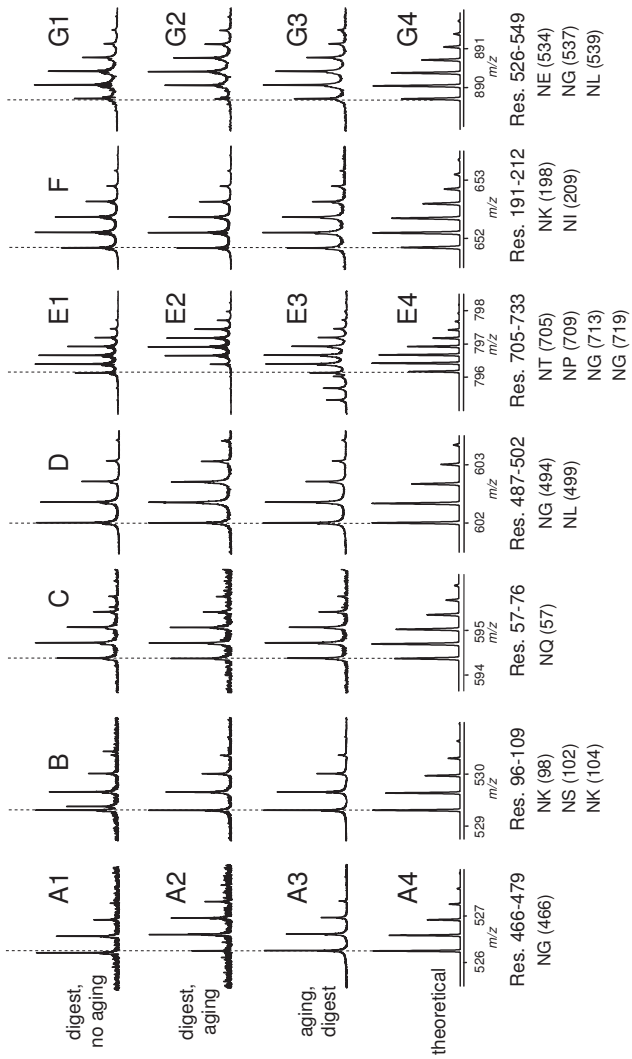

Figure 8·4: FT–ICR–MS spectra of the proteolytic peptides (A–G) from Glu-C digest of rPA that contain possible deamidation sites. Each frame is zoomed in spectra from the full-scan FT–ICR–MS spectra: top row, peptides from Glu-C digest of 'fresh' rpA; second row, 'aged' Glu-C proteolytic peptides (overnight at 37 °C and pH 10.2); third row, peptides from Glu-C digestion of 'aged' rPA (overnight at 37 °C and pH 10.2); fourth row, theoretical isotopic pattern for the detected peptide and charge state. Below the spectra are the peptide residues and the possible deamidating asparagine residues.

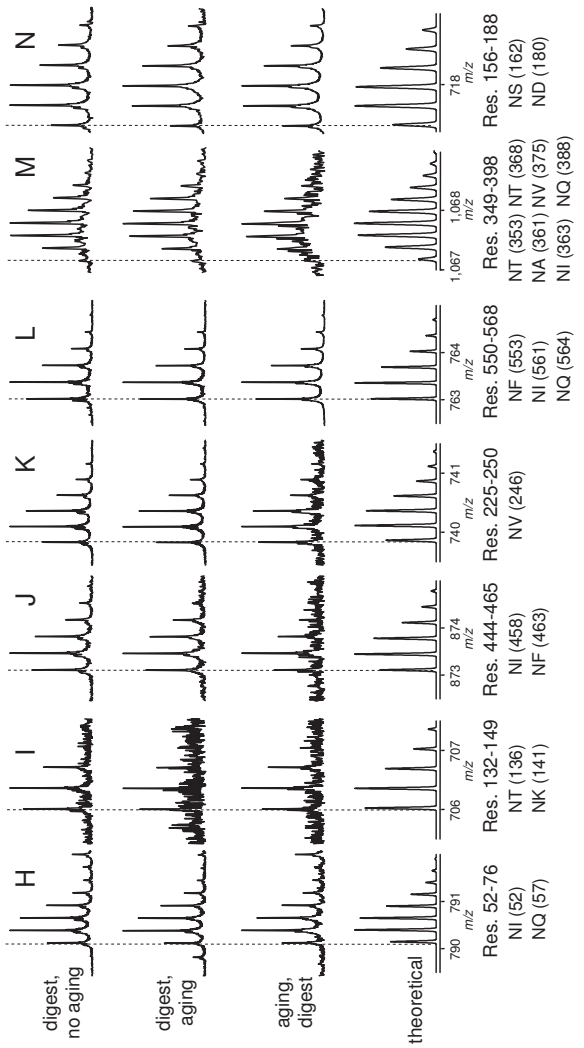

Figure 8·5: FT–ICR–MS spectra of the proteolytic peptides (H–N) from Glu-C digest of rPA that contain possible deamidation sites. Each frame is zoomed in spectra from the full-scan FT–ICR–MS spectra: top row, peptides from Glu-C digest of 'fresh' rpA; second row, 'aged' Glu-C proteolytic peptides (overnight at 37 °C and pH 10.2); third row, peptides from Glu-C digestion of 'aged' rPA (overnight at 37 °C and pH 10.2); fourth row, theoretical isotopic pattern for the detected peptide and charge state. Below the spectra are the peptide residues and the possible deamidating asparagine residues.

8.3.3 FT–ICR–MS–ECD Detection of an IsoAsp Residue in Deamidated rPA

According to these findings, the site $N^{537}G$ of rPA was partially deamidated before any analysis was performed and must have occurred during production, packaging or storage of the protein. This peptide was determined to be ∼13 % deamidated which was determined using the least squares method and the isotopic patterns for the asparagine and Asp versions. The 3+ charge state of peptide ^{526}ALKIAFGFNEPNGNLQYAGKDITE$_{549}$ from the Glu-C digest of 'fresh' rPA (figure 8·4–G1) was selected for ECD analysis and the spectra is shown in figure 8·6. Fragments resulting from 16 out of the 22 possible inter-residue cleavages were detected (cleavage on the N-terminal side of proline cannot be cleaved by ECD and was not counted as a possible cleavage site). The two complement isoAsp diagnostic fragments, c_{11}+57 and z_{13}-57 (with ∼1 ppm accuracy), were detected thus localizing the isoAsp residue to position 537 of the peptide (position of the asparagine residue). Since only ∼13 % of the peptide is deamidated, there is possibly a mixture of three residues at position 537; isoAsp, Asp, and asparagine. Loss of the Asp side chain from the reduced molecular ion ($(M+3H)^{2+\cdot}$ - 60 Da) could not be used to determine the presence of Asp at position 537 since there exists an Asp residue at position 546. Therefore, in order to determine how much of each form is present, HPLC must be used to determine the relative abundance of the three forms. However, the results demonstrate that isoAsp is being formed in the protein that could occur during synthesis, isolation and storage which could affect the overall activity and stability of the protein.

8.4 Conclusion

Protein digestion followed by FT–ICR–MS allowed the localization of several deamidation sites and determination of their extent of deamidation under various conditions. According to the MS data that was collected without the aid of chromatography, all deamidation sites previously found to deamidate were detected in the trypsin and Glu-C digestions and their relative rates of deamidation were roughly estimated; (in decreasing order of deamidation rate) $N^{537}G > N^{713}G$, $N^{719}G > N^{408}N > N^{601}N$ and $N^{602}I$. The next step would be to perform MS/MS in order to distinguish which location and timing as to which sites were actually modified. For example, MS/MS of ^{704}ENTIINPSENGDTSTNGIK$_{722}$ would help determine the extent of deamidation at $N^{713}G$ or $N^{719}G$ based on the isotopic pattern of the fragments. Furthermore, $N^{537}G$ was

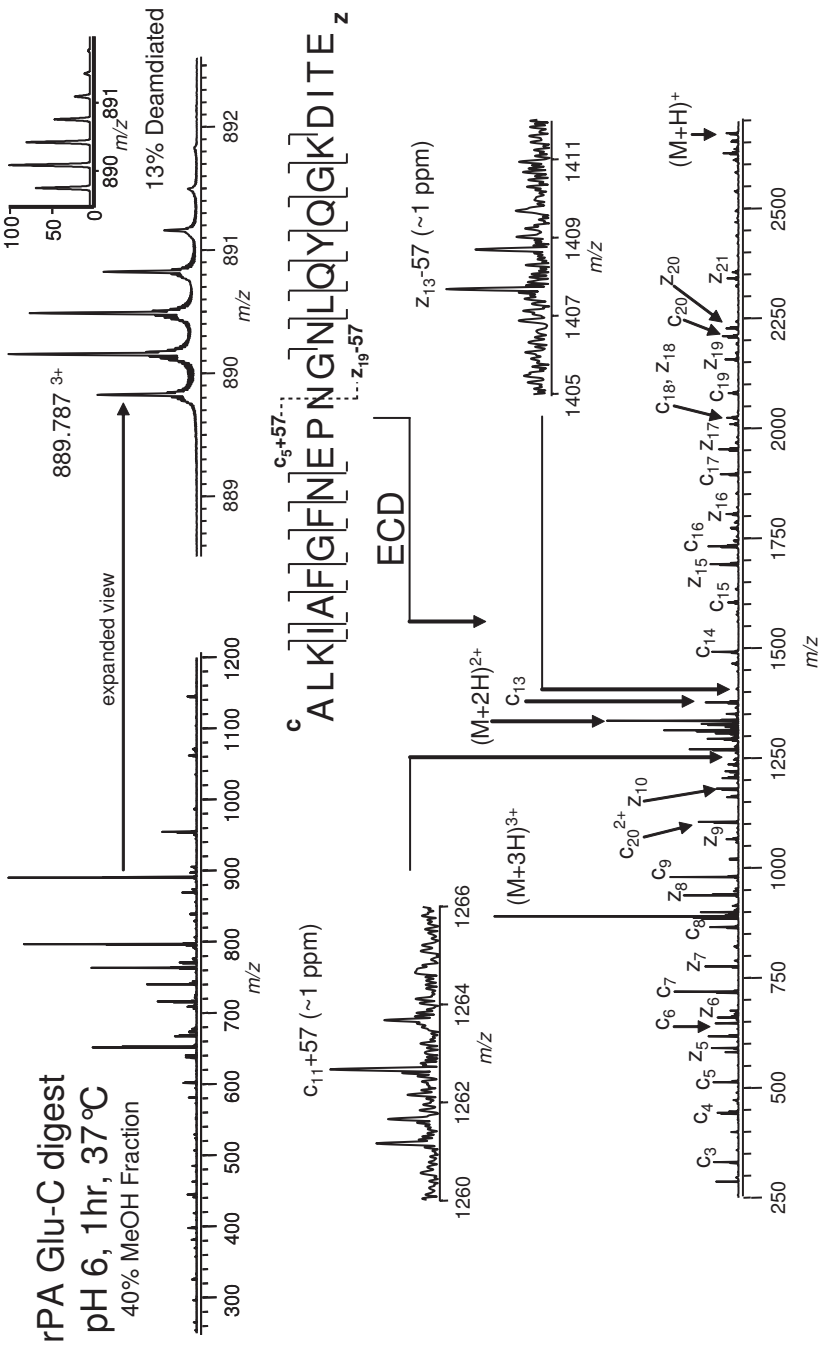

Figure 8·6: ECD of a peptide from the Glu-C digestion of rPA. Digested rPA was fractionated using POROS and the 40 % methanol (60 % water) fraction was found to contain the partially deamidated (∼13 %, inset is the theoretical isotopic pattern) peptide ^{526}ALKIAFGFNEPNGNLQYAGKDITE$_{549}$ (3+ charge state) which was then subjected to ECD. Insets are zoomed regions of the ECD spectrum indicating the presence of the isoAsp diagnostic ions.

found to be partially ($\sim$ 13 %) deamidated before shipment. ECD of the partially aged peptide reveals the presence of isoAsp due to deamidation which could contribute to the instability and resultant loss of function for rPA. To conclude, FT–ICR–MS and FT–ICR–MS–ECD can be used to efficiently characterize deamidation sites in proteins in terms of the localization and extent of the conversion and whether an isoAsp acid residue has formed. This work establishes FT–ICR–MS as a useful tool for the analysis of protein deamidation. The method presented here is more rapid and more sensitive than prior methods reported for the characterization of anthrax protective antigen protein.

References

[1] R. A. Zubarev, N. L. Kelleher, and F. W. McLafferty. Electron capture dissociation of multiply charged protein cations. A nonergodic process. *Journal of the American Chemical Society*, 120(13):3265–3266, 1998.

[2] A. B. Robinson and N. E. Robinson. *Molecular Clocks: Deamidation of Asparaginyl and Glutaminyl Residues in Peptides and Proteins*. Althouse Press, Cave Junction, OR, 2004.

[3] T. Geiger and S. Clarke. Deamidation, isomerization, and racemization at asparaginyl and aspartyl residues in peptides. *Journal of Biological Chemistry*, 262(2):785–795, 1987.

[4] D. W. Aswad, M. V. Paranandi, and B. T. Schurter. Isoaspartate in peptides and proteins: formation, significance, and analysis. *Journal of Pharmaceutical and Biomedical Analysis*, 21:1129–1136, 2000.

[5] J. L. Radkiewicz, H. Zipse, S. Clarke, and K. N. Houk. Accelerated racemization of aspartic acid and asparagine residues via succinimide intermediates: An ab initio theoretical exploration of mechanism. *Journal of the American Chemical Society*, 118(38):9148–9155, 1996.

[6] J. T. Watson. *Introduction to Mass Spectrometry*. Lippincott-Raven, New York, NY, 1997.

[7] J. R. Chapman. *Practical Organic Mass Spectrometry, 2nd Edition*. Wiley, West Sussex, England, 1997.

[8] K. B. Tomer. The development of fast atom bombardment combined with tandem mass spectrometry for the determination of biomolecules. *Mass Spectrometry Reviews*, 8:445–482, 1989.

[9] J. Sunner. Ionization in liquid secondary-ion mass-spectrometry (LSIMS). *Organic Mass Spectrometry*, 28(8):805–823, 1993.

[10] J. B. Fenn, M. Mann, C. K. Meng, S. F. Wong, and C. M. Whitehouse. Electrospray ionization for mass spectrometry of large biomolecules. *Science*, 246(4926):64–71, 1989.

[11] M. Karas, D. Bachman, U. Bahr, and F. Hillenkamp. Matrix-assisted ultraviolet laser desorption of non-volatile compounds. *International Journal of Mass Spectrometry and Ion Processes*, 78:53–68, 1987.

[12] G. C. Thorne, K. D. Ballard, and S. J. Gaskell. Metastable decomposition of peptide (M+H)+ ions via rearrangement involving loss of the C-terminal amino acid residue. *Journal of the American Society for Mass Spectrometry*, 1:249–257, 1990.

[13] I. A. Papayannopoulos and K. Biemann. Fast-atom-bombardment and tandem mass-spectrometry of synthetic peptides and by-products. *Peptide Research*, 5(2):83–90, 1992.

[14] K. Strupat, M. Karas, and F. Hillenkamp. 2,5-dihydroxybenzoic acid: a new matrix for laser desorption-ionization mass spectrometry. *International Journal of Mass Spectrometry and Ion Processes*, 72(111):89–102, 1991.

[15] R. C. Beavis and B. T. Chait. Cinnamic acid derivatives as matrices for ultraviolet laser desorption mass spectrometry of proteins. *Rapid Communications in Mass Spectrometry*, 3(12):432–435, 1989.

[16] P. Kebarle. A brief overview of the present status of the mechanisms involved in electrospray mass spetrometry. *Journal of Mass Spectrometry*, 35(7):804–817, 2000.

[17] N. V. Konenkov, M. Sudakov, and D. J. Douglas. Matrix methods for the calculation of stability diagrams in quadrupole mass spectrometry. *Journal of the American Society for Mass Spectrometry*, 13(6):597–613, 2002.

[18] G. C. Stafford. Ion trap mass spectrometry: a personal perspective. *Journal of the American Society for Mass Spectrometry*, 13(6):587–588, 2002.

[19] G. C. Stafford, P. E. Kelley, J. E. P. Syka, and J. F. J. Reynolds, W. E. Todd. Recent improvements in and analytical applications of advanced ion trap technology. *International Journal Mass Spectrometry and Ion Processes*, 60:85–98, 1984.

[20] M. Guilhaus. Principles and intstrumentation in TOF-MS. *Journal of Mass Spectrometry*, 30:1519–1532, 1995.

[21] H. Wollnik. TOF-MS. *Mass Spectrometry Reviews*, 12:89–114, 1993.

[22] W. C. Wiley and I. H. McLaren. TOF-S with improved resolution. *Review of Scientific Instruments*, 26:1150–1157, 1955.

[23] M. B. Comisarow and A. G. Marshall. Fourier transform ion cyclotron mass spectroscopy. *Chemical Physics Letters*, 25:282–283, 1974.

[24] A. G. Alan G. Marshall, C. L. Hendrickson, and G. S. Jackson. Fourier transform ion cyclotron resonance mass spectrometry: A primer. *Mass Spectrometry Reviews*, 17:1–35, 1998.

[25] M. B. Comisarow. Cubic trapped-ion cell for ion cyclotron resonance. *International Journal of Mass Spectrometry and Ion Physics*, 37:251–257, 1981.

[26] S. C. Beu and D. A. Laude. Open trapped ion cell geometries for Fourier transform ion cyclotron resonance mass spectrometry. *International Journal of Mass Spectrometry and Ion Processes*, 112:215–230, 1992.

[27] S. C. Beu and D. A. Laude. Elimination of axial ejection during excitation with a capacitively coupled open trapped-ion cell for Fourier transform ion cyclotron resonance mass spectrometry. *Analytical Chemistry*, 64:177–180, 1992.

[28] I. J. Amster. Fourier Transform Mass Spectrometry. *International Journal of Mass Spectrometry*, 31:1325–1337, 1996.

[29] N.K. Kaiser and J.E. Bruce. Observation of increased ion cyclotron resonance signal duration through electric field perturbations. *Analytical Chemistry*, 77:5973–5981, 2005.

[30] N.K. Kaiser and J.E. Bruce. Reduction of ion magnetron motion and space charge using radial electric field modulation. *International Journal of Mass Spectrometry*, 265:271–280, 2007.

[31] L. Zhang, D. Rempel, B. N. Pramanik, and M. L. Gross. Accurate mass measurements by Fourier transform mass spectrometry. *Mass Spectrometry Reviews*, 24:286–309, 2005.

[32] J. W. Gauthier, T. R. Trautman, and D. B. Jacobson. Sustained off-resonance irradiation for collision-activated dissociation involving Fourier-transform mass-spectrometry - collision-activated dissociation technique that emulates infrared multiphoton dissociation. *Analytica Chimica Acta*, 246(1):211–225, 1991.

[33] P. Roepstorff and J. Fohlman. Proposal for a common nomenclature for sequence ions in mass spectra of peptides. *Biomedical Mass Spectrometry*, 11(11):601, 1984.

[34] W. F. Haddon and F. W. McLafferty. Metastable ion characteristics. VII. collision-induced metastables. *Journal of the American Chemical Society*, 90:4745, 1968.

[35] K. Biemann and S. A. Martin. Mass spectrometruic determination of the amino acid sequence of peptides and proteins. *Mass Spectrometry Reviews*, 6:1–75, 1987.

[36] D. F. Hunt, J. R. Yates, J. Shabanowitz, J. Winston, and C. R. Hauer. Protein sequencing by tandem mass spectormetry. *Proceedings of the National Academy of Science*, 83:6233–6237, 1986.

[37] S. A. McLuckey and D. E. Goeringer. Slow heating methods in tandem mass spectrometry. *Journal of Mass Spectrometry*, 32:461–474, 1997.

[38] R. A O'Hair. The role of nucleophile-electrophile interactions in the unimolecular and bimolecular gas-phase ion chemistry of peptides and related systems. *Journal of Mass Spectrometry*, 35:1377–1381, 2000.

[39] M. J. Polce, D. Ren, and C. J. Wesdemiotis. Dissociation of the peptide bond in protonated peptides. *Journal of Mass Spectrometry*, 35:1391, 200.

[40] A. Schlosser and W. D. Lehmann. Five-membered ring formation in unimolecular reactions of peptides: a key structural element controlling low-energy collision-induced dissociation of peptides. *Journal of Mass Spectrometry*, 35:1382–1390, 2000.

[41] V. H. Wysocki, G. Tsaprailis, L. L. Smith, and L. A. Breci. Mobile and localized protone: a framework for understanding peptide dissociation. *Journal of Mass Spectrometry*, 35:1399–1406, 2000.

[42] R. C. Dunbar. BIRD (blackbody infrared radiative dissociation): Evolution, principles, and applications. *Mass Spectrometry Reviews*, 23(2):127–158, 2004.

[43] J. Perrin. *Annals of Physics*, 11:1–5, 1919.

[44] W. D. Price, P. D. Schnier, and E. R. Williams. Tandem mass spectrometry of large biomolecule ions by blackbody infrared radiative dissociation. *Analytical Chemistry*, 68:859–866, 1996.

[45] W. D. Price, P. D. Schnier, R. A. Jockusch, E. F. Strittmatter, and E. R. Williams. Unimolecular reaction kinetics in the high-pressure limit without collisions. *Journal of the American Chemical Society*, 118:10640–10644, 1996.

[46] D. S. Gross, Y. Zhao, and E. R. Williams. Dissociation of heme-globin complexes by blackbody infrared radiative dissociation: Molecular specificity in the gas phase? *Journal of the American Society for Mass Spectrometry*, 8:519–524, 1997.

[47] J. S. Klassen, P. D. Schnier, and E. R. Williams. Blackbody infrared radiative dissociation of oligonucleotide anions. *Journal of the American Society for Mass Spectrometry*, 9:1117–1124, 1998.

[48] N. Felitsyn, E. N Kitova, and Klassen J. S. Thermal decomposition of a gaseous multiprotein complex studied by blackbody infrared radiative dissociation. investigating the origin of the asymmetric dissociation behavior. *Analytical Chemistry*, 73:4647–4661, 2001.

[49] R. B. Cody, R. C. Burnier, and B. S. Frelser. Collision-induced dissociation with Fourier transform mass spectrometry. *Analytical Chemistry*, 54:96–101, 1982.

[50] R. L. Woodin, D. S. Bomse, and J. L. Beauchamp. Multiphoton dissociation of molecules with low power continuous wave infrared laser radiation. *Journal of the American Chemical Society*, 100:3248–3250, 1978.

[51] D. P. Little, J. P. Speir, M. W. Senko, P. B. Oconnor, and F. W. McLafferty. Infrared multiphoton dissociation of large multiply-charged ions for biomolecule sequencing. *Analytical Chemistry*, 66(18):2809–2815, 1994.

[52] J. L. Stephenson, M. M. Booth, J. A. Shalosky, J. R. Eyler, and R. A. Yost. Infrared multiple-photon dissociation in the quadrupole ion-trap a multipass optical arrangement. *Journal of the American Society for Mass Spectrometry*, 5:886, 1994.

[53] R. C. Dunbar. Kinetics of low-intensity infrared laser photodissociation. the thermal model and application of the Tolman theorem. *Journal of Chemical Physics*, 95:2537–2548, 1991.

[54] M. C. Crowea and J. S. Brodbelt. Infrared multiphoton dissociation (IRMPD) and collisionally activated dissociationof peptides in a quadrupole ion trapwith selective IRMPD of phosphopeptides. *Journal of the American Society of Mass Spectrometry*, 15:1581–1592, 2004.

[55] W. D. Bowers, S. Delbert, R. L. Hunter, and R. T. McIver. Fragmentation of oligopeptide ions using ultraviolet laser radiation and Fourier transform mass spectrometry. *Journal of the American Chemical Society*, 106:7289–7291, 1984.

[56] E. R. Williams, J. J. P. Furlong, and F. W. McLafferty. Efficiency of collisionally-activated dissociation and 193-nm photodissociation of peptide ions in fourier transform mass spectrometry. *Journal of the American Society for Mass Spectrometry*, 1:288–294, 1990.

[57] C. B. Lebrilla, D. T. Wang, T. J. Mizoguchi, and R. T. McIver. Comparison of the fragmentation produced by fast atom bombardment and photodissociation of peptides. *Journal of the American Chemical Society*, 111:8593–8598, 1989.

[58] G. S. Gorman and I. J. Amster. Photodissociation studies of small peptide ions by Fourier transform mass spectrometry. *Organic Mass Spectrometry*, 28:437–444, 1993.

[59] T. Tabarin, R Antoine, M Broyer, and P. Dugourd. Specific photodissociation of peptides with multi-stage mass spectrometry. *Rapid Communications in Mass Spectrometry*, 19:2883–2892, 2005.

[60] T. Y. Kim, M. S. Thompson, and J. P. Reilly. Peptide photodissociation at 157 nm in a linear ion trap mass spectrometer. *Rapid Communications in Mass Spectroemtry*, 19:1657–1665, 2005.

[61] M. E. Gimon-Kinsel, G. R. Kinsel, R. D. Edmondson, and D. H. Russell. Photodissociation of high molecular weight peptides and proteins in a two-stage linear time-of-flight mass spectrometer. *Journal of the American Society for Mass Spectrometry*, 6:578–587, 1995.

[62] R. A. Zubarev, D. M. Horn, E. K. Fridriksson, N. L. Kelleher, N. A. Kruger, M. A. Lewis, B. K. Carpenter, and F. W. McLafferty. Electron capture dissociation for structural characterization of multiply charged protein cations. *Analytical Chemistry*, 72(3):563–573, 2000.

[63] E. A. Syrstad and F. Turecek. Toward a general mechanism of electron capture dissociation. *Journal of the American Society for Mass Spectrometry*, 16:208–224, 2005.

[64] N. A. Kruger, R. A. Zubarev, B. K. Carpenter, N. L. Kelleher, D. M. Horn, and F. W. McLafferty. Electron capture versus energetic dissociation of protein ions. *International Journal of Mass Spectrometry*, 183:1–5, 1999.

[65] E. Mirgorodskaya, P. Roepstorff, and R. A. Zubarev. Localization of O-glycosylation sites in peptides by electron capture dissociation in a Fourier transform mass spectrometer. *Analytical Chemistry*, 71(20):4431–4436, 1999.

[66] K. Breuker, H. B. Oh, B. A. Cerda, D. M. Horn, and F. W. McLafferty. Hydrogen atom loss in electron-capture dissociation: a Fourier transform-ion cyclotron resonance study with single isotopomeric ubiquitin ions. *European Journal of Mass Spectrometry*, 8:177–180, 2002.

[67] N. Leymarie, C. E. Costello, and P. B. O'Connor. Electron capture dissociation initiates a free radical reaction cascade. *Journal of the American Chemical Society*, 125(29):8949–8958, 2003.

[68] S. D. H. Shi, M. E. Hemling, S. A. Carr, D. M. Horn, I. Lindh, and F. W. McLafferty. Phosphopeptide/phosphoprotein mapping by electron capture dissociation mass spectrometry. *Analytical Chemistry*, 73(1):19–22, 2001.

[69] R. A. Zubarev. Reactions of polypeptide ions with electrons in the gas phase. *Mass Spectrometry Reviews*, 22(1):57–77, 2003.

[70] K. Hakansson, H. J. Cooper, M. R. Emmett, C. E. Costello, A. G. Marshall, and C. L. Nilsson. Electron capture dissociation and infrared multiphoton dissociation MS/MS of an N-glycosylated tryptic peptide to yield complementary sequence information. *Analytical Chemistry*, 73(18):4530–4536, 2001.

[71] R. L. Kelleher, R. A. Zubarev, K. Bush, B. Furie, B. C. Furie, F. W. McLafferty, and C. T. Walsh. Localization of labile posttranslational modifications by electron capture dissociation: The case of γ-carboxyglutamic acid. *Analytical Chemistry*, 71(19):4250–4253, 1999.

[72] D. M. Horn, K. Breuker, A. J. Frank, and F. W. McLafferty. Kinetic intermediates in the folding of gaseous protein ions characterized by electron capture dissociation mass spectrometry. *Journal of the American Chemical Society*, 123(40):9792–9799, 2001.

[73] K. F. Haselmann, T. J. D. Jrgensen, B. A. Budnik, F. Jensen, and R. A. Zubarev. Electron capture dissociation of weakly-bound polypeptide polycationic complexes. *Rapid Communications in Mass Spectrometry*, 16:2260–2265, 2002.

[74] H. J. Cooper, R. R. Hudgins, K. Hakansson, and A. G. Marshall. Characterization of amino acid side chain losses in electron capture dissociation. *Journal of the American Society for Mass Spectrometry*, 13(3):241–249, 2002.

[75] K. F. Haselmann, B. A. Budnik, F. Kjeldsen, N. C. Polfer, and R. A. Zubarev. Can the (M center dot-X) region in electron capture dissociation provide reliable information on amino acid composition of polypeptides? *European Journal of Mass Spectrometry*, 8(6):461–469, 2002.

[76] F. Kjeldsen, K. F. Haselmann, B. A. Budnik, F. Jensen, and R. A. Zubarev. Dissociative capture of hot (3-13 eV) electrons by polypeptide polycations: an efficient process accompanied by secondary fragmentation. *Chemical Physics Letters*, 356(3-4):201–206, 2002.

[77] F. Kjeldsen, K. F. Haselmann, E. S. Sorensen, and R. A. Zubarev. Distinguishing of Ile/Leu amino acid residues in the PP3 protein by (hot) electron capture dissociation in Fourier transform ion cyclotron resonance mass spectrometry. *Analytical Chemistry*, 75:1267–1724, 2003.

[78] H. J. Cooper, R. R. Hudgins, K. Hakansson, and A. G. Marshall. Secondary fragmentation of linear peptides in electron capture dissociation. *International Journal of Mass Spectrometry*, 228(2-3):723–728, 2003.

[79] K.F. Haselmann, B. A. Budnik, J. V. Olsen, M. L. Nielsen, C.A. Reis, H. Clausen, A. H. Johnson, and R. A. Zubarev. Advantages of external accumulation for electron capture dissociation in Fourier transform mass spectrometry. *Analytical Chemistry*, 73:2998–3005, 2001.

[80] J. E. P. Syka, J. J. Coon, M. J. Schroeder, J. Shabanowitz, and D. F. Hunt. Peptide and protein sequence analysis by electron transfer dissociation mass spectrometry. *Proceedings of the National Academy of Sciences of the United States of America*, 101(26):9528–9533, 2004.

[81] J. J. Coon, B. Ueberheide, J. E. P. Syka, D. D. Dryhurst, J. Ausio, J. Shabanowitz, and D. F. Hunt. Protein identification using sequential ion/ion reactions and tandem mass spectrometry. *Proceedings of the National Academy of Science*, 102:9463–9468, 2005.

[82] H. P. Gunawardena, M. He, P. S. Chrisman, S. J. Pitteri, J. M. Hogan, B. D. M. Hodges, and S. A. McLuckey. Electron transfer versus proton transfer in gas-phase ion/ion reactions of polyprotonated peptides. *Journal of the American Chemical Society*, 127:12627–12639, 2005.

[83] P. B. O'Connor, J. L. Pittman, B. A. Thomson, B. A. Budnik, J. C. Cournoyer, J. Jebanathirajah, C. Lin, S. Moyer, and C. Zhao. A new hybrid electrospray Fourier transform mass spectrometer: design and performance characteristics. *Rapid Communications in Mass Spectrometry*, 20(2):259–266, 2006.

[84] J. L. Pittman and P. B. O'Connor. A minimum thickness gate valve with integrated ion optics for mass spectrometry. *Journal of the American Society for Mass Spectrometry*, 16:441–445, 2005.

[85] Y. O. Tsybin, P. Hakansson, B. A. Budnik, K. F. Haselmann, F. Kjeldsen, M. Gorshkov, and R. A. Zubarev. Improved low-energy electron injection systems for high rate electron capture dissociation in Fourier transform ion cyclotron resonance mass spectrometry. *Rapid Communications in Mass Spectrometry*, 15(19):1849–1854, 2001.

[86] Y. O. Tsybin, C. L. Hendrickson, S. C. Beu, and A. G. Marshall. Impact of ion magnetron motion on electron capture dissociation Fourier transform ion cyclotron resonance mass spectrometry. *International Journal of Mass Spectrometry*, 255:144–149, 2006.

[87] A. E. Roher, J. D. Lowenson, S. Clarke, C. Wolkow, R. Wang, R. J. Cotter, I. M. Reardon, H. A. Zurcherneely, R. L. Heinrikson, M. J. Ball, and B. D. Greenberg. Structural alterations in the peptide backbone of β-amyloid core protein may account for its deposition and stability in Alzheimers disease. *Journal of Biological Chemistry*, 268(5):3072–3083, 1993.

[88] E. Kim, J. D. Lowenson, D. C. MacLaren, S. Clarke, and S. G. Young. Deficiency of a protein-repair enzyme results in the accumulation of altered proteins, retardation of growth, and fatal seizures in mice. *Proceedings of the National Academy of Sciences of the United States of America*, 94(12):6132–6137, 1997.

[89] T. Shimizu, A. Watanabe, M. Ogawara, H. Mori, and T. Shirasawa. Isoaspartate formation and neurodegeneration in Alzheimer's disease. *Archives of Biochemistry and Biophysics*, 381(2):225–234, 2000.

[90] N. E. Robinson and A. B. Robinson. Deamidation of human proteins. *Proceedings of the National Academy of Sciences of the United States of America*, 98(22):12409–12413, 2001.

[91] S. Ritz-Timme and M. J. Collins. Racemization of aspartic acid in human proteins. *Ageing Research Reviews*, 1(1):43–59, 2002.

[92] K. J. Reissner and D. W. Aswad. Deamidation and isoaspartate formation in proteins: unwanted alterations or surreptitious signals? *Cellular and Molecular Life Sciences*, 60(7):1281–1295, 2003.

[93] N. E. Robinson, Z. W. Robinson, B. R. Robinson, A. L. Robinson, J. A. Robinson, M. L. Robinson, and A. B. Robinson. Structure-dependent nonenzymatic deamidation of glutaminyl and asparaginyl pentapeptides. *Journal of Peptide Research*, 63(5):426–436, 2004.

[94] J. A. Thomson and R. C. Augusteyn. Ontogeny of human lens crystallins. *Experimental Eye Research*, 40:393–410, 1985.

[95] L. Takemoto and D. Boyle. Deamidation of specific glutamine residues from α-A crystallin during aging of the human lens. *Biochemistry*, 37(39):13681–13685, 1998.

[96] S. Clarke. Propensity for spontaneous succinimide formation from aspartyl and asparaginyl residues in cellular proteins. *International Journal of Peptide and Protein Research*, 30:808–821, 1987.

[97] N. E. Robinson and A. B. Robinson. Molecular clocks. *Proceedings of the National Academy of Sciences of the United States of America*, 98(3):944–949, 2001.

[98] N. E. Robinson, A. B. Robinson, and R. B. Merrifield. Mass spectrometric evaluation of synthetic peptides as primary structure models for peptide and protein deamidation. *Journal of Peptide Research*, 57(6):483–493, 2001.

[99] S. Capasso, L. Mazzarella, F. Sica, A. Zagari, and S. Salvadori. Kinetics and mechanism of succinimide ring formation in the deamidation process of asparagine residues. *Journal of the Chemical Society-Perkin Transactions 2*, (4):679–682, 1993.

[100] N. E. Robinson and A. B. Robinson. Prediction of protein deamidation rates from primary and three-dimensional structure. *Proceedings of the National Academy of Sciences of the United States of America*, 98(8):4367–4372, 2001.

[101] A. A. Kossiakoff. Tertiary structure is a principal determinant to protein deamidation. *Science*, 240(4849):191–194, 1988.

[102] S. Capasso and S. Salvadori. Effect of the three-dimensional structure on the deamidation reaction of ribonuclease A. *Journal of Peptide Research*, 54(5):377–382, 1999.

[103] L. Athiner, J. Kindrachuk, F. Georges, and S. Napper. The influence of protein structure on the products emerging from succinimide hydrolysis. *Journal of Biological Chemistry*, 277(34):30502–30507, 2002.

[104] K. J. Reissner, M. V. Paranandi, T. M. Luc, H. A. Doyle, M. J. Mamula, J. D. Lowenson, and D. W. Aswad. Synapsin I is a major endogenous substrate for protein L-isoaspartyl methyltransferase in mammalian brain. *Journal of Biological Chemistry*, 281(13):8389–8398, 2006.

[105] B. A. Johnson, E. L. Langmack, and D. W. Aswad. Partial repair of deamidation-damaged calmodulin by protein carboxyl methyltransferase. *Journal of Biological Chemistry*, 262(25):12283–12287, 1987.

[106] D. A. Chavous, F. R. Jackson, and C. M. O'connor. Extension of the drosphilia lifespan by overexpression of a protein repair methyltransferase. *Proceedings of the National Academy of Sciences of the United States of America*, 98(25):14814–14818, 2001.

[107] H. Gershon and D. Gershon. Inactive enzyme molecules in aging mice: Liver aldolase. *Proceedings of the National Academy of Sciences of the United States of America*, 70(3):909–913, 1973.

[108] B. E. Deverman, B. L. Cook, S. R. Manson, R. A. Niederhoff, E. M. Langer, I. Rosova, L. A. Kulans, X. Y. Fu, J. S. Weinberg, J. W. Heinecke, K. A. Roth, and S. J. Weintraub. Bcl-X-L deamidation is a critical switch in the regulation of the response to DNA damage. *Cell*, 111(1):51–62, 2002.

[109] W. Zhang and M. J. Czupryn. Analysis of isoaspartate in a recombinant monoclonal antibody and its charge isoforms. *Journal of Pharmaceutical and Biomedical Analysis*, 30(5):1479–1490, 2003.

[110] D. Chelius, D. S. Rehder, and P. V. Bondarenko. Identification and characterization of deamidation sites in the conserved regions of human immunoglobulin gamma antibodies. *Analytical Chemistry*, 77(18):6004–6011, 2005.

[111] D. Kameoka. A method for the detection of asparagine deamidation and aspartate. *Journal of Biochemistry*, 134(1):129–135, 2003.

[112] A. Di Donato, P. Galletti, and G. D'Alessio. Selective deamidation and enzymatic methylation of seminal ribonuclease. *Biochemistry*, 25:8361–8363, 1986.

[113] D. A. Donato, M. A. Ciardiello, M. de Nigris, R. Piccoli, L. Mazzarella, and G. D'Alessio. Selective deamidation of ribonuclease A - isolation and characterization of the resulting isoaspartyl and asaprtyl derivatives. *Journal of Biological Chemistry*, 268:4745–4751, 1993.

[114] J. P. Tam. Synthetic peptide vaccine design: Synthesis and properties of a high-density multiple antigenic peptide system. *Proceedings of the National Academy of Sciences of the United States of America*, 85:5409–5413, 1988.

[115] T. Shimizu, H. Fukuda, S. Murayama, N. Izumiyama, and T. Shirasawa. Isoaspartate formation at position 23 of amyloid beta peptide enhanced fibril formation and deposited onto senile plaques and vascular amyloids in Alzheimer's disease. *Journal of Neuroscience Research*, 70(3):451–461, 2002.

[116] Y. Shin, H. S. Cho, H. Fukumoto, T. Shimizu, T. Shirasawa, S. M. Greenberg, and G. W. Rebeck. Aβ species, including isoasp23 Aβ, in iowa-type familial cerebral amyloid angiopathy. *Acta Neuropathologica*, 105(3):252–258, 2003.

[117] E. D. Murray and S. Clarke. Synthetic peptide-substrates for the erythrocyte protein carboxyl methyltransferase - detection of a new site of methylation at isomerized L-aspartyl residues. *Journal of Biological Chemistry*, 259(17):722–732, 1984.

[118] P. N. McFadden and S. Clarke. Conversion of isoaspartyl peptides to normal peptides - implications for the cellular repair of damaged proteins. *Proceedings of the National Academy of Sciences of the United States of America*, 84(9):2595–2599, 1987.

[119] T. V. Brennan and S. Clarke. Spontaneous degradation of polypeptides at aspartyl and asparaginyl residues - effects of the solvent dielectric. *Protein Science*, 2(3):331–338, 1993.

[120] B. A. Johnson, E. D. Murray, S. Clarke, D. B. Glass, and D. W. Aswad. Protein carboxyl methyltransferase facilitates conversion of atypical L-isoaspartyl peptides to normal L-aspartyl peptides. *Journal of Biological Chemistry*, 262(12):5622–5629, 1987.

[121] P. T. Jedrzejewski, A. Girod, A. Tholey, N. Konig, S. Thullner, V. Kinzel, and D. Bossemeyer. A conserved deamidation site at Asn 2 in the catalytic subunit of mammalian cAMP-dependent protein kinase detected by capillary LC–MS and tandem mass spectrometry. *Protein Science*, 7(2):457–469, 1998.

[122] L. H. Huang, J. R. Li, V. J. Wroblewski, J. M. Beals, and R. M. Riggin. *In vivo* deamidation characterization of monoclonal antibody by LC/MS/MS. *Analytical Chemistry*, 77(5):1432–1439, 2005.

[123] J. J. Cournoyer, C. Lin, and P. B. O'Connor. Detecting deamidation products in proteins by electron capture dissociation. *Analytical Chemistry*, 78(4):1264–1271, 2006.

[124] M. R. Nilsson, M. Driscoll, and D. P. Raleigh. Low levels of asparagine deamidation can have a dramatic effect on aggregation of amyloidogenic peptides: Implications for the study of amyloid formation. *Protein Science*, 11(2):342–349, 2002.

[125] S. M. Potter, W. J. Henzel, and D. W. Aswad. *In Vitro* aging of calmodulin generates isoaspartate at multiple Asn-Gly and Asp-Gly sites in calcium-binding domain-II, domain-III, and domain-IV. *Protein Science*, 2(10):1648–1663, 1993.

[126] D. W. Aswad. Stoichiometric methylation of porcine adrenocorticotropin by protein carboxyl methyltransferase requires deamidation of asparagine-25 - evidence for methylation at the alpha-carboxyl group of atypical L-isoaspartyl residues. *Journal of Biological Chemistry*, 259(17):714–721, 1984.

[127] Y. R. Hsu, W. C. Chang, E. A. Mendiaz, S. Hara, D. T. Chow, M. B. Mann, K. E. Langley, and H. S. Lu. Selective deamidation of recombinant human stem cell factor during *in vitro* aging: Isolation and characterization of the aspartyl and isoaspartyl homodimers and heterodimers. *Biochemistry*, 37(8):2251–2262, 1998.

[128] S. Capasso and P. Di Cerbo. Kinetic and thermodynamic control on the yeild of deamidation of asparagine and isomerization of aspartic acid residues. *Journal of Peptide Research*, 56:382–387, 2000.

[129] S. J. Wearne and T. E. Creighton. Effect of protein conformation on rate of deamidation - ribonuclease A. *Proteins: Structure, Function, and Genetics*, 5(1):8–12, 1989.

[130] V. N. Lapko, A. G. Purkiss, D. L. Smith, and J. B. Smith. Deamidation in human gamma S-crystallin from cataractous lenses is influenced by surface exposure. *Biochemistry*, 41(27):8638–8648, 2002.

[131] W. J. Ribot, B. S. Powell, B. E. Ivins, S. F. Little, W. M. Johnson, T. A. Hoover, S. L. Norris, J. J. Adamovicz, A. M. Friedlander, and G. P. Andrews. Comparative vaccine efficacy of different isoforms of recombinant protective antigen against *bacillus anthracis* spore challenge in rabbits. *Vaccine*, 24(17):3469–3476, 2006.

[132] S. Capasso. Thermodynamic parameters of the reversible isomerization of aspartic residues via a succinimide derivative. *Thermochimica Acta*, 286(1):41–50, 1996.

[133] G. Zomber, S. Reuveny, N. Garti, A. Shafferman, and E. Elhanany. Effects of spontaneous deamidation on the cytotoxic activity of the *bacillus anthracis* protective antigen. *Journal of Biological Chemistry*, 280(48):39897–39906, 2005.

[134] T. Solstad, R. N. Carvalho, O. A. Andersen, D. Waidelich, and T. Flatmark. Deamidation of labile asparagine residues in the autoregulatory sequence of human phenylalanine hydroxylase - structural and functional implications. *European Journal of Biochemistry*, 270(5):929–938, 2003.

[135] C. Vanbelle, F. Halgand, T. Cedervall, E. Thulin, K. S. Akerfeldt, O. Laprevote, and S. Linse. Deamidation and disulfide bridge formation in human calbindin D-2gk with effects on calcium binding. *Protein Science*, 14(4):968–979, 2005.

[136] W. J. Chazin, J. Kordel, E. Thulin, T. Hofmann, T. Drakenberg, and S. Forsen. Identification of an isoaspartyl linkage formed upon deamidation of bovine calbindin-D9k and structural characterization by 2D H-1-NMR. *Biochemistry*, 28(21):8646–8653, 1989.

[137] M. J. Mamula, R. J. Gee, J. I. Elliott, A. Sette, S. Southwood, P. J. Jones, and P. R. Blier. Isoaspartyl post-translational modification triggers autoimmune responses to self-proteins. *Journal of Biological Chemistry*, 274(32):22321–22327, 1999.

[138] K. Wutrich. *NMR of Proteins and Nucleic Acids*. Wiley, New York, 1986.

[139] D. G. Smyth, W. H. Stein, and S. Moore. On the sequence of residues 11 to 18 in bovine pancreatic ribonuclease. *Journal of Biological Chemistry*, 237(6):1845–1850, 1962.

[140] J. D. Gary and S. Clarke. Purification and characterization of an isoaspartyl dipeptidase from *escherichia coli*. *Journal of Biological Chemistry*, 270(8):4076–4087, 1995.

[141] C. Fledelius, A. H. Johnsen, P. A. C. Cloos, M. Bonde, and P. Qvist. Characterization of urinary degradation products derived from type I collagen - identification of a β-isomerized Asp-Gly sequence within the C-terminal telopeptide (alpha 1) region. *Journal of Biological Chemistry*, 272(15):9755–9763, 1997.

[142] D E. Macfarlane. Inhibitors of cyclic nucleotide phosphodiesterases inhibit protein carboxyl methylation in intact blood platelets. *Journal of Biological Chemistry*, 259(2):1357–1362, 1984.

[143] D. W. Aswad and E. A. Deight. Purification and characterization of two distinct isoozymes of protein carboxymethylase from bovine brain. *Journal of Neurochemistry*, 40:1718–1725, 1983.

[144] C. M. O'Connor. Regulation and subcellular-distribution of a protein methyltransferase and its damaged aspartyl substrate sites in developing *xenopus* oocytes. *Journal of Biological Chemistry*, 262(21):10398–10403, 1987.

[145] J. Kindrachuk, J. Parent, G. F. Davies, M. Dinsmore, S. Attah-Poku, and S. Napper. Overexpression of L-isoaspartate O-methyltransferase in *escherichia coli* increases heat shock survival by a mechanism independent of methyltransferase activity. *Journal of Biological Chemistry*, 278(51):50880–50886, 2003.

[146] D. Ingrosso, S. D'Angelo, A. F. Perna, A. Iolascon, E. Miragali Del Giudice, S. Perrota, V. Zappia, and P. Galletti. Increased membrane-protein methylation in hereditary spherocytosis. a marker of cytoskeletal disarray. *European Journal of Biochemistry*, 228:894–898, 1995.

[147] A. Niewmierzycka and S. Clarke. Do damaged proteins accumulate in *caenorhabditis elegans* L-isoaspartate methyltransferase (pcm-1) deletion mutants? *Archives of Biochemistry and Biophysics*, 364(2):209–218, 1999.

[148] J. D. Lowenson, E. Kim, S. G. Young, and S. Clarke. Limited accumulation of damaged proteins in L-isoaspartyl (D-aspartyl) O-methyltransferase-deficient mice. *Journal of Biological Chemistry*, 276(23):20695–20702, 2001.

[149] M. V. Paranandi, A. W. Guzzetta, W. S. Hancock, and D. W. Aswad. Deamidation and isoaspartate formation during *in vitro* aging of recombinant tissue-plasminogen activator. *Journal of Biological Chemistry*, 269(1):243–253, 1994.

[150] A. L. Young, W. G. Carter, H. A. Doyle, M. J. Mamula, and D. W. Aswad. Structural integrity of histone H2B in vivo requires the activity of protein L-isoaspartate O-methyltransferase, a putative protein repair enzyme. *Journal of Biological Chemistry*, 276(40):37161–37165, 2001.

[151] R. Tyler-Cross and V. Schirch. Effects of amino-acid-sequence, buffers, and ionic-strength on the rate and mechanism of deamidation of asparagine residues in small peptides. *Journal of Biological Chemistry*, 266(33):22549–22556, 1991.

[152] J. R. Barber and S. Clarke. Membrane-protein carboxyl methylation increases with human-erythrocyte age - evidence for an increase in the number of methylatable sites. *Journal of Biological Chemistry*, 258(2):1189–1196, 1983.

[153] G. W. Young, S. A. Hoofring, M. J. Mamula, H. A. Doyle, G. J. Bunick, Y. L. Hu, and D. W. Aswad. Protein L-isoaspartyl methyltransferase catalyzes in vivo racemization of aspartate-25 in mammalian histone H2B. *Journal of Biological Chemistry*, 280(28):26094–26098, 2005.

[154] A. D. Carlson and R. M. Riggin. Development of improved high-performance liquid chromatography conditions for nonisotopic detection of isoaspartic acid to determine the extent of protein deamidation. *Analytical Biochemistry*, 278(2):150–155, 2000.

[155] R. N. Carvalho, T. Solstad, E. Bjorgo, J. F. Barroso, and T. Flatmark. Deamidations in recombinant human phenylalanine hydroxylase - identification of labile asparagine residues and functional characterization of Asn to Asp mutant forms. *Journal of Biological Chemistry*, 278(17):15142–15152, 2003.

[156] V. Zabrouskov, X. M. Han, E. Welker, H. L. Zhai, C. Lin, K. J. van Wijk, H. A. Scheraga, and F. W. McLafferty. Stepwise deamidation of ribonuclease A at five sites determined by top down mass spectrometry. *Biochemistry*, 45(3):987–992, 2006.

[157] N. E. Robinson, V. Zabrouskov, J. Zhang, K. J. Lampi, and A. B. Robinson. Measurement of deamidation of intact proteins by isotopic envelope and mass defect with ion cyclotron resonance Fourier transform mass spectrometry. *Rapid Communications in Mass Spectrometry*, 20(23):3535 – 3541, 2006.

[158] D. G. Schmid, F. von der Mulbe, B. Fleckenstein, T. Weinschenk, and G. Jung. Broadband detection electrospray ionization Fourier transform ion cyclotron resonance mass spectrometry to reveal enzymatically and chemically induced deamidation reactions within peptides. *Analytical Chemistry*, 73:6008–6013, 2001.

[159] N. E. Robinson, K. J. Lampi, R. T. McIver, R. H. Williams, W. C. Muster, G. Kruppa, and A. B. Robinson. Quantitative measurement of deamidation in lens βB2-crystallin and peptides by direct electrospray injection and fragmentation in a Fourier transform mass spectrometer. *Molecular Vision*, 11:1211–1219, 2005.

[160] S. A. Carr, M. E. Hemling, M. F. Bean, and G. D. Roberts. Integration of mass spectrometry in analytical biotechnology. *Analytical Chemistry*, 63(24):2802–2824, 1991.

[161] P. Schindler, D. Muller, W. Marki, H. Grossenbacher, and W. J. Richter. Characterization of a β-asp33 isoform of recombinant hirudin sequence variant 1 by low-energy collision-induced dissociation. *Journal of Mass Spectrometry*, 31(9):967–974, 1996.

[162] K. D. Ballard and S. J. Gaskell. Intermolecular [O-18] isotopic exchange in the gas-phase observed during the tandem mass spectrometric analysis of peptides. *Journal of the American Chemical Society*, 114:64–71, 1992.

[163] L. J. Gonzalez, T. Shimizu, Y. Satomi, L. Betancourt, V. Besada, G. Padron, R. Orlando, T. Shirasawa, Y. Shimonishi, and T. Takao. Differentiating α- and β-aspartic acids by electrospray ionization and low-energy tandem mass spectrometry. *Rapid Communications in Mass Spectrometry*, 14(22):2092–2102, 2000.

[164] J. R. Lloyd, M. L. Cotter, D. Ohori, and D. L. Doyle. Distinction of α-aspartyl and β-aspartyl and α-glutamyl and γ-glutamyl-transferase peptides by fast atom bombardment tandem mass-spectrometry. *Biomedical and Environmental Mass Spectrometry*, 15(7):399–402, 1988.

[165] W. Lehmann, A. Schlosser, G. Erben, R. Pipkorn, D. Bossemeyer, and V. Kinzel. Analysis of isoaspartate in peptides by electrospray tandem mass spectrometry. *Protein Science*, 9(12):2290–2268, 2000.

[166] W. Lehmann and A. Schlosser. Five-membered ring formation in unimolecular reactions of peptides: a key structural element controlling low-energy collision-induced dissociation of peptides. *Journal of Mass Spectrometry*, 35:1382–1390, 2000.

[167] M. J. Harms, P. A. Wilmarth, D. M. Kapfer, E. A. Steel, L. L. David, H. P. Bachinger, and K. J. Lampi. Laser light-scattering evidence for an altered association of β B1-crystallin deamidated in the connecting peptide. *Protein Science*, 13(3):678–686, 2004.

[168] S. N. McAdam, B. Fleckenstein, I. B. Rasmussen, D. G. Schmid, I. Sandlie, B. Bogen, N. J. Viner, and L. M. Sollid. T cell recongnition of the dominant I-ak restricted hen egg lysozyme epitope: Critical role for asparagine deamidation. *Journal of Experimental Medicine*, 193:1239–1246, 2001.

[169] I. A. Popov, S. Kozin, O. N. Kharybin, A. S. Kononikhin, and E. N. Nikolaev. Recognition of individual amino acid isomeric form in peptides by FT-ICR mass spectrometry. application to Alzheimer's disease peptides. In *54th ASMS Conference on Mass Spectrometry and Allied Topics*, Seattle, 2006.

[170] M. F. Bean and S. A. Carr. Differentiation of α- and β-aspartic acids in isomerized peptides by tandem MS. In *The 40th ASMS Conference on Mass Spectrometry and Allied Topics*, 1999.

[171] C. Zhao, M. Sethuraman, N. Clavreul, P. Kaur, R. A. Cohen, and P. B. OConnor. A detailed map of oxidative post-translational modifications of human p21ras using Fourier transform mass spectrometry. *Analytical Chemistry*, 78:5134–5142, 2006.

[172] H. J. Cooper, R. R. Hudgins, and A. G. Marshall. Electron capture dissociation Fourier transform ion cyclotron resonance mass spectrometry of cyclodepsipeptides, branched peptides, and α-peptides. *International Journal of Mass Spectrometry and Ion Porcesses*, 234:23–35, 2004.

[173] R. Hodyss, H. A. Cox, and J. L. Beauchamp. Bioconjugates for tunable peptide fragmentation: Free radical initiated peptide sequencing (FRIPS). *Journal of the American Chemical Society*, 127:12436–12437, 2005.

[174] Y. M. E. Fung and T.-W. D. Chan. Experimental and theoretical investigations of the loss of amino acid side chains in electron capture dissociation of model peptides. *Journal of the American Society for Mass Spectrometry*, 16:1523–1535, 2005.

[175] Y. J. Hu, B. Hadas, M. Davidovitz, B. Balta, and C. Lifshitz. Does IVR take place prior to peptide ion dissociation? *Journal of Physical Chemistry*, 107:6507–6514, 2003.

[176] F. Turecek and E. A. Syrstad. Mechanism and energetics of intramolecular hydrogen transfer in amide and peptide radicals and cation-radicals. *Journal of the American Chemical Society*, 125:3353–3369, 2004.

[177] A. Rauk, D. Yu, and D. A. Armstrong. Oxidative damage to and by cysteine in proteins: An ab initio study of the radical structures, C-H, S-H, and C-C bond dissociation energies, and transition structures for H abstraction by thiyl radicals. *Journal of the American Chemical Society*, 120(34):8848–8855, 1998.

[178] A. Rauk, D. Yu, J. Taylor, G. V. Shustov, D. A. Block, and D. A. Armstrong. Effects of structure on C_α-H bond enthalpies of amino acid residues: Relevance to H transfers in enzyme mechanisms and in protein oxidation. *Biochemistry*, 38(28):9089–9096, 1999.

[179] M. R. Asam and G. L Glish. Determination of the dissociation kinetics of a transient intermediate. *Journal of the American Society for Mass Spectrometry*, 10:119–125, 1991.

[180] A. Pashkova, E. Moskovets, and B. L. Karger. Coumarin tags for improved analysis of peptides by MALDI-TOF MS and MS/MS. *Analytical Chemistry*, 76:4550–4557, 2004.

[181] R. S. Johnson. *Determination of peptide and protein structure by tandem mass spectrometry*. PhD thesis, M. I. T., 1989.

[182] C. Hagman, P. Hakansson, J. Buijs, and K. Hakansson. Inter-molecular migration during collisional activation monitored by hydrogen/deuterium exchange FT–ICR tandem mass spectrometry. *Journal of the American Chemical Society*, 15:639–646, 2004.

[183] J. Buijs, C. Hagman, K. Hakansson, J. H. Richter, and P. Hakansson. Inter- and intra-molecular migration of peptide amide hydrogens during electrospray ionization. *Journal of the American Society for Mass Spectrometry*, 12:410–419, 2001.

[184] G. E. Reid, R. J. Simpson, and R. A. J. OHair. Probing the fragmentation reactions of protonated glycine oligomers via multistage mass spectrometry and gas phase ion molecule hydrogen/deuterium exchange. *International Journal of Mass Spectrometry*, 190/191:209–230, 1999.

[185] J. A. A. Demmers, J. T. S. Rijkers, J. Haverkamp, and A. J. R. Killian, J. A.and Heck. Factors affecting gas-phase deuterium scrambling in peptide ions and their implications for protein structure determination. *Journal of the American Chemical Society*, 124:11191–11198, 2002.

[186] A. Rauk, D. Yu, and D. A. Armstrong. Toward site specificity of oxidative damage in proteins: C-H and C-C bond dissociation energies and reduction potentials of the radicals of alanine, serine, and threonine residues - an ab initio study. *Journal of the American Chemical Society*, 119(1):208–217, 1997.

[187] T. A. Lehman. Isotope effects in the bimolecular reactions of gaseous ions. concepts, techniques, and reactions. *Mass Spectrometry Reviews*, 14:353–382, 1995.

[188] V. G. Anicich, A. D. Sen, W. T. Huntress, and M. J. McEwan. Lifetime measurement of a collision complex using ioncyclotron double-resonance $(H_2C_6N_2)^+$. *Journal of Chemical Physics*, 94:4189–4191, 1991.

[189] M. R. Asam and G. L Glish. Tandem mass spectrometry of alkali cationized polysaccharides in a quadrupole ion trap. *Journal of the American Society for Mass Spectrometry*, 8:987–995, 1997.

[190] M. B. Comisarow, V. Grassi, and G. Parisod. Fourier transform ion cyclotron double resonance. *Chemical Physics Letters*, 57:413–416, 1978.

[191] J. C. Jurchen, D. E. Garcia, and E. R. Williams. Gas-phase dissociation pathways of multiply charged peptide clusters. *Journal of the American Society of Mass Spectrometry*, 14:1373–1386, 2003.

[192] S. A. Shaffer, M. Sadilek, and F. Turecek. Hypervalent ammonium radicals. effects of alkyl groups and aromatic substituents. *Journal of Organic Chemistry*, 61:5234–5245, 1996.

[193] M. M. Savitski, M. L. Nielsen, and R. A. Zubarev. Side chain losses in electron capture dissociation to improve peptide identification. *Analytical Chemistry*, 79:2296–2302, 2007.

[194] T. P. Cirrito, Z. Pu, M. B. Deck, and E. R. Unanue. Deamidation of asparagine in a major histocompatibility complexbound peptide affects T cell recognition but does not explain type B reactivity. *Journal of Experimental Medicine*, 194(8):1165–1170, 2001.

[195] N. C. Luu, S. Robinson, R. Zhao, R. McKean, and D. P. Ridge. Mass spectrometric differentiation of α- and β-aspartic acid in a pseudo-tetrapeptide thrombosis inhibitor and its isomer. *European Journal of Mass Spectrometry*, 10(2):279–287, 2004.

[196] C. J. Easton. alpha-carbon-centered radicals from amino acids and their derivatives. In *Advances in Detailed Reaction Mechanisms*, volume 1, pages 83–129. JAI Press Inc., 1991.

[197] F. W. McLafferty and F Turecek. Interpretation of Mass Spectra. In F. W. McLafferty and F Turecek, editors, *Interpretation of Mass Spectra*, page 72. University Science Books, Sausalito, 4th edition, 1993.

[198] C Yao, E. A. Syrstad, and F. Turecek. Electron transfer to protonated β-alanine N-methylamide in the gas phase: An experimental and computational study of dissociation energetics and mechanisms. *Journal of Physical Chemistry A*, 111:4167–4180, 2007.

[199] N. L. Kelleher, H. Y. Lin, G. A. Valaskovic, D. J. Aaserud, E. K. Fridriksson, and F. W. McLafferty. Top down versus bottom up protein characterization by tandem high-resolution mass spectrometry. *Journal of the American Chemical Society*, 121(4):806–812, 1999.

[200] Y. O. Tsybin, M. Ramstrom, M. Witt, G. Baykut, and P. Hakansson. Peptide and protein charachetrization by high-rate electron capture resonance mass spectrometry. *Journal of Mass Spectrometry*, 39:719–729, 2004.

[201] A. Stensballe, O. N. Jensen, J. V. Olsen, K. F. Haselmann, and R. A. Zubarev. Electron capture dissociation of singly and multiply phosphorylated peptides. *Rapid Communications in Mass Spectrometry*, 14(19):1793–1800, 2000. Article.

[202] N. A. Kruger, R. A. Zubarev, D. M. Horn, and F. W. McLafferty. Electron capture dissociation of multiply charged peptide cations. *International Journal of Mass Spectrometry*, 187:787–793, 1999.

[203] L. Chen, T. C. L. Wang, T. L. Ricca, and A. G. Marshall. Phase-modulated stored waveform inverse Fourier transform excitation for trapped ion mass spectrometry. *Analytical Chemistry*, 59:449–454, 1987.

[204] F. Kjeldsen and R. Zubarev. Secondary losses via γ-lactam formation in hot electron capture dissociation: A missing link to complete *de novo* sequencing of proteins? *Journal of the American Chemical Society*, 125(22):6628–6629, 2003.

[205] S. R. A. Hanson, A. Hasan, D. L. Smith, and J. B. Smith. The major *in vivo* modifications of the human water-insoluble lens crystallins are disulfide bonds, deamidation, methionine oxidation and backbone cleavage. *Experimental Eye Research*, 71(2):195–207, 2000.

[206] A. R. Friedman, A. K. Ichhpurani, D. M. Brown, R. M. Hillman, L. F. Krabill, R. A. Martin, H. A. Zurcherneely, and D. M. Guido. Degradation of growth-hormone releasing-factor analogs in neutral aqueous-solution is related to deamidation of asparagine residues - replacement of asparagine residues by serine stabilizes. *International Journal of Peptide and Protein Research*, 37(1):14–20, 1991.

[207] Y. C. Meinwald, E. R. Stimson, and H. A. Scheraga. Deamidation of the asparaginylglycyl sequence. *International Journal of Peptide and Protein Research*, 28(1):79–84, 1986.

[208] F. W. McLafferty. *Tandem Mass Spectrometry*. Wiley, New York, 1983.

[209] A. K. Shukla and J. H. Futrell. Collisional activation and dissociation of polyatomic ions. *Mass Spectrometry Reviews*, 12(4):211–255, 1993.

[210] P. B. O'Connor, J. J. Cournoyer, S. J. Pitteri, P. A. Chrisman, and S. A. McLuckey. Differentiation of aspartic and isoaspartic acids using electron transfer dissociation. *Journal of the American Society for Mass Spectrometry*, 17(1):15–19, 2006.

[211] A. T. Iavarone, K. Paech, and E. R. Williams. Effects of charge state and cationizing agent on the electron capture dissociation of a peptide. *Analytical Chemistry*, 76(8):2231–2238, 2004.

[212] H. Desaire and J. A. Leary. Detection and quantification of the sulfated disaccharides in chondroitin sulfate by electrospray tendem mass spectrometry. *Journal of the American Society for Mass Spectrometry*, 11(10):916–920, 2000.

[213] A. M. Hitchcock, C. E. Costello, and J. Zaia. Glycoform quantification of chondroitin/dermatan sulfate using a liquid chromatography-tandem mass spectrometry platform. *Biochemistry*, 45(7):2350–2361, 2006.

[214] J. A. Jebanathirajah, J. L. Pittman, B. A. Thomson, B. A. Budnik, P. Kaur, M. Rape, M. Kirschner, C. E. Costello, and P. B. O'Connor. Characterization of a new qQq-FTICR mass spectrometer for post-translational modification analysis and top-down tandem mass spectrometry of whole proteins. *Journal of the American Society for Mass Spectrometry*, 16(12):1985–1999, 2005.

[215] M. J. Gething and J. Sambrook. Protein folding in the cell. *Nature*, 355:33–45, 1992.

[216] C. M. Dobson. Protein folding and misfolding. *Nature*, 426:884–890, 2003.

[217] S. K. Chowdhury, V. Katta, and B. T. Chait. Differences in charge states of electrosprayed native and denatured proteins. *Journal of the American Chemical Society*, 112:9012, 1990.

[218] J. A. Loo. Electrospray ionization mass spectrometry: a technology for studying noncovalent macromolecular complexes. *International Journal of Mass Spectrometry*, 200(1-3):175–186, 2000.

[219] T. Wyttenbach and M. T. Bowers. Gas phase conformations of biological molecules: The hydrogen/deuterium exchange mechanism. *Journal of the American Society of Mass Spectormetry*, 10:9–14, 1999.

[220] E. W. Robinson and E. R. Williams. Multidimensional separations of ubiquitin conformers in the gas phase: Relating ion cross sections to H/D exchange measurements. *Journal of the American Society for Mass Spectrometry*, 16(9):1427–1437, 2005.

[221] M. A. Freitas, C. L. Hendrickson, M. R. Emmett, and A. G. Marshall. Gas-phase bovine ubiquitin cation conformations resolved by gas-phase hydrogen/deuterium exchange rate and extent. *International Journal of Mass Spectrometry*, 187:565–575, 1999.

[222] D. E. Clemmer, R. R. Hudgins, and M. F. Jarrold. Naked protein conformations - cytochrome-*c* in the gas-phase. *Journal of the American Chemical Society*, 117(40):10141–10142, 1995.

[223] M. F. Jarrold. Peptides and proteins in the vapor phase. *Annual Reviews in Physical Chemistry*, 51:179–207, 2000.

[224] R. W. Purves, D. A. Barnett, and R. Guevremont. Separation of protein conformers using electrospray-high field asymmetric waveform ion mobility spectrometry-mass spectrometry. *International Journal Mass Spectrometry*, 197:163–177, 2000.

[225] E. W. Robinson, R. D. Leib, and E. R. Williams. The role of conformation on electron capture dissociation of ubiquitin. *Journal of the American Society for Mass Spectrometry*, 17:1469–1479, 2006.

[226] H. B. Oh, K. Breuker, Siu Kwan Sze, Ying Ge, B. K. Carpenter, and F. W. McLafferty. Secondary and tertiary structures of gaseous protein ions characterized by electron capture dissociation mass spectrometry and photofragment spectroscopy. *Proceedings of the National Academy of Sciences of the United States of America*, 99(25):15863–15868, 2002.

[227] H. B. Oh, C. Lin, H. Y. Hwang, H. L. Zhai, K. Breuker, V. Zabrouskov, B. K. Carpenter, and F. W. McLafferty. Infrared photodissociation spectroscopy of electrosprayed ions in a Fourier transform mass spectrometer. *Journal of the American Chemical Society*, 127:4076–4083, 2005.

[228] J. J. Valle, J. R. Eyler, J. Oomens, D. T. Moore, A. F. G. van der Meer, G. von Helden, G. Meijer, C. L. Hendrickson, A. G. Marshall, and G. T. Blakney. Free electron laser Fourier transform ion cyclotron resonance mass spectrometry facility for obtaining infrared multiphoton dissociation spectra of gaseous ions. *Review if Scientific Instruments*, 76, 2005.

[229] K. Breuker, H. B. Oh, C. Lin, B. K. Carpenter, and F. W. McLafferty. Nonergodic and conformational control of the electron capture dissociation of protein cations. *Proceedings of the National Academy of Sciences of the United States of America*, 101:14011–14016, 2004.

[230] Y. Ge, B. G. Lawhorn, M. ElNaggar, E. Strauss, J. H. Park, T. P. Begley, and F. W. McLafferty. Top down characterization of larger proteins (45 kDa) by electron capture dissociation mass spectrometry. *Journal of the American Chemical Society*, 124:672–678, 2002.

[231] M. M. Savitski, M. L. Nielsen, F. Kjeldsen, and R. A. Zubarev. Proteomics-grade *de novo* sequencing approach. *Journal of Proteome Research*, 4:2348–2354, 2005.

[232] S. K. Sze, Y. Ge, H. Oh, and F. W. McLafferty. Top-down mass spectrometry of a 29-kDa protein for characterization of any posttranslational modification to within one residue. *Proceedings of the National Academy of Sciences of the United States of America*, 99:1774–1779, 2002.

[233] F. Meng, A. J. Forbes, L. M. Miller, and N. L. Kelleher. Detection and localization of protein modifications by high resolution tandem mass spectrometry. *Mass Spectrometry Reviews*, 24:126–134, 2005.

[234] D. M. Horn, Y. Ge, and F. W. McLafferty. Activated ion electron capture dissociation for mass spectral sequencing of larger (42 kDa) proteins. *Analytical Chemistry*, 72(20):4778–4784, 2000.

[235] S. K. Sze, Y. Ge, H. Oh, and F. W. McLafferty. Plasma electron capture characterization of large dissociation for the proteins by top down mass spectrometry. *Analytical Chemistry*, 75:1599–1603, 2003.

[236] K. Hakansson, M. J. Chalmers, J. P. Quinn, M. A. McFarland, C. L. Hendrickson, and A. G. Marshall. Combined electron capture and infrared multiphoton dissociation for multistage MS/MS in a Fourier transform ion cyclotron resonance mass spectrometer. *Analytical Chemistry*, 75:3256–3262, 2001.

[237] Y. O. Tsybin, M. Witt, G. Baykut, F. Kjeldsen, and P. Hakansson. Combined infrared multiphoton dissociation and electron capture dissociation with a hollow electron beam in Fourier transform ion cyclotron resonance mass spectrometry. *Rapid Communications in Mass Spectormetry*, 17:1759–1768, 2006.

[238] R. C. Dunbar and T. B. McMahon. Activation of unimolecular reaction by ambient blackbody radiation. *Science*, 279:194–197, 1998.

[239] Y. O. Tsybin, H. He, M. R. Emmett, C. L. Hendrickson, and A. G. Marshall. Activation in electron capture dissociation to distinguish between N-terminal and C-terminal product ions. *Journal of the American Society of Mass Spectrometry*, 79:7596–7602, 2007.

[240] M. M. Savitski, F. Kjeldsen, M. L. Nielsen, and R. A. Zubarev. Hydrogen rearrangement to and from radical z fragments in electron capture dissociation of peptides. *Journal of the American Society for Mass Spectrometry*, 18(1):113–120, 2007.

[241] R. Mihalca, A. J. Kleinnijenhuis, A. J. R. McDonnell, L. A.and Heck, and R. M. A Heeren. Electron capture dissociation at low temperatures reveals selective dissociations. *Journal of the American Society for Mass Spectrometry*, 15:1869–1873, 2004.

[242] A. C. Gill, K. R. Jennings, T. Wyttenbach, and M. T. Bowers. Conformations of biopolymers in the gas phase: a new mass spectrometric method. *International Journal of Mass Spectrometry*, 196:685–697, 2000.

[243] H. C. Liu and K. Hakansson. Divalent metal ion-peptide interactions probed by electron capture dissociation of trications. *Journal of the American Society of Mass Spectrometry*, 17:1731–1741, 2006.

[244] S. Hayakawa, M. Hashimoto, H. Matsubara, and F. Turecek. Dissecting the proline effect: Dissociations of proline radicals formed by electron transfer to protonated Pro-Gly and Gly-Pro dipeptides in the gas phase. *Journal of the American Chemical Society*, 129:7936–7949, 2007.

[245] J. W. Jones, T. Sasaki, D. R. Goodlett, and F. Turecek. Electron capture in spin-trap capped peptides. an experimental example of ergodic dissociation in peptide cation-radicals. *Journal of the Americna Society of Mass Spectrometry*, 18:432–444, 2007.

[246] B. N. Pramanik, P. L. Bartner, U. A. Mirza, Y. H. Liu, and A. K. Ganguly. Electrospray ionization mass spectrometry for the study of non-covalent complexes: An emerging technology. *Journal of Mass Spectrometry*, 33(10):911–920, 1998.

[247] K. Breuker. New mass spectrometric methods for the quantification of protein-ligand binding in solution. *Angewandte Chemie-International Edition*, 43(1):22–25, 2004.

[248] G. Berger and G. Girault. Macromolecule-ligand binding studied by the Hummel and Dreyer method: current state of the methodology. *Journal of Chromatography B*, 797:51–61, 2003.

[249] J. Cheuring, M. Fischer, M. Cushman, J. Lee, A. Bacher, and H Oschkinat. NMR analysis of site-specific ligand binding in oligomeric proteins. dynamic studies on the interaction of riboflavin synthase with trifluoromethyl-substituted intermediates. *Biochemistry*, 35:9637–9646, 1996.

[250] J. K. Hoerner, H. Xiao, and I. A. Kaltashov. Structural and dynamic characteristics of a partially folded state of ubiquitin revealed by hydrogen exchange mass spectrometry. *Biochemistry*, 44(33):11286–11294, 2005.

[251] T. E. Wales and J. R. Engen. Hydrogen exchange mass spectrometry for the analysis of protein dynamics. *Mass Spectrometry Reviews*, 25(1):158–170, 2006.

[252] S. A. Lorenz, E. P. Maziarz, and T. D. Woods. Using solution phase hydrogen/deuterium (H/D) exchange to determine the origin of non-covalent complexes observed by electrospray ionization mass spectrometry: in solution or *in vacuo*? *Journal of the American Society for Mass Spectrometry*, 12(7):795–804, 2001.

[253] M. K. Green and C. B. Lebrilla. Ion-molecule reactions as probes of gas-phase structures of peptides and proteins. *Mass Spectrometry Reviews*, 16(2):53–71, 1997.

[254] C. M. Adams, B. A. Budnik, K. F. Haselmann, F. Kjeldsen, and R. A. Zubarev. Electron capture dissociation distinguishes a single D-amino acid in a protein andprobes the tertiary strucutre. *Journal of the American Society for Mass Spectrometry*, 15(7):1087–1098, 2004.

[255] M. W. Senko, J. P. Speir, and F. W. McLafferty. Collisional activation of large multiply-charged ions using Fourier transform mass spectrometry. *Analytical Chemistry*, 66(18):2801–2808, 1994.

[256] J. Laskin and J. H. Futrell. Collisional activation of peptide ions in FT-ICR mass spectrometry. *Rapid Communications in Mass Spectrometry*, 17(23):2694–2694, 2003.

[257] F. Kjeldsen, M. M. Savitski, C. M. Adams, and R. A. Zubarev. Determination of the location of positive charges in gas-phase polypeptide polycations by tandem mass spectrometry. *International Journal of Mass Spectrometry*, 252(3):204–212, 2006.

[258] M. A. Freitas, C. L. Hendrickson, and A. G. Marshall. Determination of relative ordering of activation energies for gas-phase ion unimolecular dissociation by infrared radiation for gaseous multiphoton energy transfer. *Journal of the American Chemical Society*, 122(32):7768–7775, 2000.

[259] M. Meot-Ner. The ionic hydrogen bond. *Chemical Reviews*, 105(1):213–284, 2005.

[260] A. R. Fersht. The hydrogen bond in molecular recognition. *Trends in Biochemical Sciences*, 12(8):301–304, 1987.

[261] F. Avbelj, P. Z. Luo, and R. L. Baldwin. Energetics of the interaction between water and the helical peptide group and its role in determining helix propensities. *Proceedings of the National Academy of Sciences of the United States of America*, 97(20):10786–10791, 2000.

[262] P. D. Schnier, W. D. Price, R. A. Jockusch, and E. R. Williams. Blackbody infrared radiative dissociation of bradykinin and its analogues: Energetics, dynamics, and evidence for salt-bridge structures in the gas phase. *Journal of the American Chemical Society*, 118(30):7178–7189, 1996.

[263] B. S. Powell, J. T. Enama, W. J. Ribot, W. Webster, S. Little, T. Hoover, J. J. Adamovicz, and G. P. Andrews. Multiple asparagine deamidation of *bacillus anthracis* protective antigen causes charge isoforms whose complexity correlates with reduced biological acivity. *Proteins: Structure, Function, and Bioinformatics*, 68:458–479, 2007.

[264] P. C. Turnbull. Anthrax vaccines: past, present and future. *Vaccine*, 9:533–539, 1991.

[265] N. Arora and S. H. Leppla. Fusions of anthrax toxin lethal factor with shiga toxin and diphtheria toxin enzymatic domains are toxic to mammalian cells. *Infection and Immunity*, 62:4955–4961, 1994.

[266] S. Liu, H. Aaronson, D. J. Mitola, S. H. Leppla, and T. H. Bugge. Potent antitumor activity of a urokinase-activated engineered anthrax toxin. *Proceedings of the National Academy of Sciences of the United States of America*, 100:657–662, 2003.

CURRICULUM VITAE

Jason Cournoyer

CONTACT INFORMATION

43 Parkton Road
Apartment #1
Jamaica Plain, MA 02130
jasononetwo@hotmail.com

OBJECTIVE: Obtain a position in the biotechnology or pharmaceutical industry.

EDUCATION:

Ph.D., Chemistry, Boston University, Boston MA, anticipated March 2008
Thesis title: "Mechanism of Electron Capture Dissociation and the Application to the Differentiation of Isoaspartic and Aspartic Acid Residues"
Advisor: Professor Peter B. O'Connor

B.S., Chemistry, University of Rhode Island, Kingston RI, 1996
Concentration: Computational Chemistry

EMPLOYMENT HISTORY:

2003–present	Graduate Research Assistant, Boston University School of Medicine
1999–2003	Research Associate II, Discovery Partners International, South San Francisco, CA
1997–1999	Analytical Chemist, Mikart Pharmaceuticals, Atlanta, GA

AWARDS:

1996	Presidents Award, outstanding achievement in chemistry for the academic year
2003	Dean's Fellowship, based undergraduate performance and previous professional experience
2007	Travel Award, invited speaker to the Association of Biological Resource Facilities annual meeting 2007, Tampa, FL

PUBLICATIONS:

M. Irving, J. J. Cournoyer, R. S. Li, C. Santos, and B. Yan. Qualitative and quantitative analyses of resin-bound organic compounds. *Combinatorial Chemistry & High Throughput Screening*, 4:353-362, 2001.

J. J. Cournoyer, T. Kshirsagar, P. P. Fantauzzi, G. M. Figliozzi, T. Makdessian, and B. Yan. Color test for the detection of resin-bound aldehyde in solid-phase combinatorial synthesis. *Journal of Combinatorial Chemistry*, 4:120-124, 2002.

L. Fang, J. J. Cournoyer, M. Demee, J. Zhao, D. Tokushige, and B. Yan. High-throughput liquid chromatography ultraviolet/mass spectrometric analysis of combinatorial libraries using an eight-channel multiplexed electrospray time-of-flight mass spectrometer. *Rapid Communications in Mass Spectrometry*, 16:1440-1447, 2002.

L. Fang, M. Demee, J. Cournoyer, T. Sierra, C. Young, and B. Yan. Parallel high-throughput accurate mass measurement using a nine-channel multiplexed electrospray liquid chromatography ultraviolet time-of-flight mass spectrometry system. *Rapid Communications in Mass Spectrometry*, 17:1425-1432, 2003.

J. J. Cournoyer, C. A. Kreuger, J. V. Wade, and B. Yan. In Analysis and Purification Methods in Combinatorial Chemistry. B. Yan, Ed, John Wiley and Sons: New York; 2004, Chapter 3.

J. J. Cournoyer, J. L. Pittman, V. B. Ivleva, E. Fallows, L. Waskell, C. E. Costello, and P. B. O'Connor. Deamidation: Differentiation of aspartyl from isoaspartyl products in peptides by electron capture dissociation. *Protein Science*, 14:452-463, 2005.

P.B. O'Connor, J. J. Cournoyer, S. J. Pitteri, P. A. Chrisman, and S. A. McLuckey. Differentiation of aspartic and isoaspartic acid residues in peptides using electron transfer dissociation. *Journal of the American Society for Mass Spectrometry*, 17(1):15-19, 2006.

J. J. Cournoyer, C. Lin, and P. B. O'Connor. Detecting Deamidation Products in Proteins by Electron Capture Dissociation. *Analytical Chemistry*, 78(4):1264-1271, 2006.

P. B. O'Connor, J. L. Pittman, B. A. Thomson, B. A. Budnik, J. J. Cournoyer, J. Jebanathirajah, C. Lin, S. Moyer, and C. Zhao. A new hybrid electrospray Fourier transform mass spectrometer: design and performance characteristics. *Rapid Communications in Mass Spectrometry*, 20(2):259-266, 2006.

P. B. O'Connor, C. Lin, J. J. Cournoyer, J. L. Pittman, M. A. Belyayev, and B. A. Budnik. Long-lived electron capture dissociation product ions experience radical migration via hydrogen abstraction. *Journal of the American Society for Mass Spectrometry*, 17(4):576-585, 2006.

M. A. Belyayev, J. J. Cournoyer, C. Lin, and P. B. O'Connor. The Effect of Radical Trap Moieties on Electron Capture Dissociation Spectra of Substance P. *Journal of the American Society for Mass Spectrometry*, 17(10):1429-1437, 2006.

C. Lin, J. J. Cournoyer, and P. B. O'Connor. Use of a double resonance electron capture dissociation experiment to probe fragment intermediate lifetimes. *Journal of the American Society for Mass Spectrometry*, 17(11):1605-1615, 2006.

J. J. Cournoyer, C. Lin, M. J. Bowman, and P. B. O'Connor. Quantitating the relative abundance of isoaspartyl residues in deamidated proteins by electron capture dissociation. *Journal of the American Society for Mass Spectrometry*, 18(1):48-56, 2007.

J. J. Cournoyer, J. J. and P. B. O'Connor. In Post-translational modifications; Whitelegge, J. P., Ed., 2008, in press.

C. Lin, J. J. Cournoyer, and P. B. O'Connor. Probing the Gas Phase Folding Kinetics of Peptide Ions by IR Activated DR–ECD. *Journal of the American Society for Mass Spectrometry*, accepted, 2008.